MAPPING SOIL TRAFFICABILITY BY WAY OF TEMPORAL HYDROLOGY MODELING AND SPATIAL WET-AREAS-MAPPING

by

Marie-France Jones

Master of Science in Forestry, UNB, 2012
Bachelor of Science in Forestry and Environmental Management, UNB, 2009

A DISSERTATION SUBMITTED IN PARTIAL FULFILLMENT OF THE REQUIREMENTS FOR THE DEGREE OF

Doctor of Philosophy

In the Graduate Academic Unit of Forestry and Environmental Management

Supervisor(s): Paul Arp, PhD, Forestry and Environmental Management

Examining Board: Charles Bourque, PhD, Forestry and Environmental Management

Fan Rui Meng, PhD, Forestry and Environmental Management

Bruce Broster, PhD, Earth Sciences

External Examiner: Nicholas Coops, PhD, Faculty of Forestry, UBC

This dissertation is accepted

Dean of Graduate Studies

THE UNIVERSITY OF NEW BRUNSWICK
August, 2019

©Marie-France Jones, 2019

Abstract

Heavy forest operations can lead to extensive soil disturbances in the form of soil compaction and displacement resulting in deep rut formations, and increased erosion. To mitigate these effects through forecasting, this Thesis reports on a Soil Trafficability Model (STRAM) to estimate daily soil moisture, penetrability and potential machine-specific soil rut depths, using the Forest Hydrology Model ForHyM in conjunction with digital high-resolution wet-area and soil property maps. Model development was guided using in-field data for model validation. The data so acquired refer to (i) biweekly year-round observations of soil moisture and penetrability conditions at select sites in Fredericton, (ii) reporting on GPS-tracked wood-forwarding machine clearances in select harvest blocks across northwestern New Brunswick, and (iii) analyzing soil moisture, soil penetrability and rut depths inside and outside some of the wood-forwarding tracks, by harvest block conditions. It was found that, through multivariate regression analysis (MR), 40 to 60 % of the field-determined soil penetrability variations by way of the cone penetrability index (CI) could be related to combined variations in pore space, coarse fragment content and weather-affected variations in soil moisture. The variations in wood-forwarding machine clearances and rut depths followed a similar pattern, but the number of passes over the same track needed to be taken into account as well. Block-specific variations in elevation, forest cover type and time of operation and machine specific variations in foot-print pressure also contributed to the rut depth variations. Using Random Forest (RF) techniques considerably improved the fitting of the field-determined variations in soil moisture, cone index and wood-forwarding rut depth to greater than 80 %. From MR to RF, the uncertainty range narrowed for best-fitted pore-filled soil moisture content from ± 15 to ± 4.5 %, for best-fitted soil cone penetrability from ± 0.7 to ± 0.4 MPa, and for best-fitted rut depth from ± 13 to ± 5 cm.

Dedication

I dedicate this thesis to God, who gave me the desire and ability to reach for my dreams, my husband, who is a constant source of inspiration, strength, and love, and my parents, who have supported and loved me throughout my entire graduate career.

Acknowledgements

I am sincerely grateful to those who have help make this project a success. My deepest gratitude to my supervisor, Dr. Paul Arp, without whom this project would not have been created. His support throughout this process has helped mold a superior product. I am also grateful to my other advisors, Dirk Jaeger and Jasen Golding, who have supported me throughout this process. I thank JD Irving for their financial support and desire to see this project succeed.

To all my coworkers at the Forest Watershed Research Centre, I am extremely grateful. I am indebted to Jae Ogilvie for his wealth of GIS knowledge and helpful advice. Mark Castonguay's efforts on this project started prior to my participation. His creativity and knowledge helped set up the machine sensors and his field experience served as a great support during the summer field work. To Shane Furze and Doug Hiltz, I have deep appreciation, as they have withstood years of long discussions and problem solving with me.

This project was a success through the efforts of many contributed to the worthy cause of mitigating the human footprint on the forest and improving environmental stewardship.

Table of Contents

Αŀ	ostra	ct		ii
De	edico	ation		iv
A	ckno	wledgr	nents	V
Ta	ble c	of Cont	ents	X
Lis	of T	ables		xiii
Lis	st of F	igures		xix
Αl	obrev	/iations	5	хх
1	Intro	oductio	on	1
	1.1	Mode	elling forest soil trafficability	1
		1.1.1	Machine variability	2
		1.1.2	Soil physical and hydraulic properties	4
		1.1.3	Trafficability models	5
	1.2	Resec	arch question (Basic Hypotheses)	6
	1.3	Thesis	Outline	8
2	Relo	ating th	e cone penetration and rutting resistance to variations in forest	
	soil	prope	rties and daily moisture fluctuations	10
	2.1	Introc	luction	12
	2.2	Mate	rials and Methods	13
		2.2.1	Location Description	1.3

		2.2.2	Field Experiment	16
		2.2.3	Hydrological Modelling	17
		2.2.4	Data Analysis and Model Projections (MC $_{\!$	17
	2.3	Result	8	20
		2.3.1	Soil Moisture and CI Measurements	20
		2.3.2	Estimating Soil Moisture and CI through Hydrological Modelling	22
		2.3.3	Predicting potential ATV-caused soil rutting depth	32
	2.4	Discus	ssion	33
	2.5	Conc	luding Remark	40
	2.6	Ackno	owledgments	40
3	Trac	k-mon	itoring and analyzing machine clearances during wood	
	forw	arding		41
	3.1	Introd	uction	43
	3.2	Metho	ods	44
		3.2.1	Site Description	44
		3.2.2	Machinery and Sensory Installations	46
		3.2.3	Data Production	51
		3.2.4	DTW Delineation	53
		3.2.5	Hydrological Modelling	54
		3.2.6	Data Processing	55
		3.2.7	Histogram and Frequency Distribution Assessment	55
		3.2.8	Multiple Regression Analysis	56
	3.3	Result	s and Discussion	56
		3.3.1	Wood-Forwarding Track Patterns	56
		3.3.2	Normalized Clearance Distribution Patterns	61
		3.3.3	Box Plots	65
		3.3.4	Normalized Clearance	65
		3.3.5	Block-Specific Examples	68
	3.4	Furthe	er Observations	72

		3.4.1	Clearances by Machine Type and Number of Passes	72
		3.4.2	Machine Speed	72
		3.4.3	Bare-Ground Operations	73
		3.4.4	Season and Weather Details	73
	3.5	Conc	lusion and Concluding Remarks	74
	3.6	Ackno	owledgments	77
4	Soil	moistu	re and cone penetrability conditions in forest soils	78
	4.1	Introd	luction	80
	4.2	Metho	ods	82
		4.2.1	Block Descriptions	82
		4.2.2	Data sources and processing	86
		4.2.3	Field Measurements	87
		4.2.4	Temporal MC Variations	89
		4.2.5	MC and CI Variations, plot-by-plot	93
		4.2.6	Statistical analyses, followed by generalized block-generated	
			MC _{PS} and CI projections	95
	4.3	Result	s & Discussions	97
		4.3.1	General observations and trends	97
		4.3.2	Temporal Soil Moisture Derivations	104
		4.3.3	CI Derivation	112
		4.3.4	Forecasting Block-specific Soil Moisture and Penetrability	
			Conditions	117
		4.3.5	Additional comments	118
	4.4	Conc	lusion	121
	4.5	Ackno	owledgments	121

5	Soil	Traffic	ability Forecasting	122
	5.1	Introd	luction	124
	5.2	Mate	rials and Methods	126
		5.2.1	Block Descriptions	126
		5.2.2	Wood Forwarding	130
		5.2.3	Data Sources	131
		5.2.4	Field Measurements	132
		5.2.5	Soil Moisture Modelling	132
		5.2.6	Cone Index and Rut Depth Modelling	134
		5.2.7	Statistical Analyses	135
		5.2.8	Soil Trafficability Model (STRAM)	136
	5.3	Result	ts	137
		5.3.1	MC _{PS} , CI, and rut-depth projections	144
	5.4	Discu	ssion	150
	5.5	Conc	luding Remarks	154
	5.6	Ackno	owledgment	154
6	Con	clusio	n	155
	6.1	Thesis	Summary	155
	6.2	Origin	nal Contribution	157
		6.2.1	Temporal Cone Index	157
		6.2.2	Sensor Analysis	157
		6.2.3	STRAM Model	158
	6.3	Sugge	estions for Future Work	158
		6.3.1	Machine Compressed Snowpack Module	158
		6.3.2	Machine Mounted Sensors 2.0	158
		6.3.3	Integrating Real-Time Weather Forecasts	159
		6.3.4	Model Adaptability: External Validation	159
		6.3.5	Model Adaptability: Agriculture	159
Do	ferer	nces		180

A	A Chapter 2 Appendice				
	A.1	Publication Copyright Permission: Chapter 2	181		
В	Cho	pter 3 Appendices	182		
	B.1	Publication Copyright Permission: Chapter 3	182		
	B.2	Percent Frequency of Normalized Clearance	183		
	B.3	Normalized Clearance by Block	186		
	B.4	ForHyM Site Results	189		
С	Cho	pter 4 Appendices	191		
	C.1	Publication Copyright Permission: Chapter 4	191		
	C.2	Soil physical properties by block	192		
	C.3	ForHyM Calibration Site Results	194		
D	Cho	pter 5 Appendices	195		
	D.1	Publication Copyright Permission: Chapter 5	195		
	D.2	Rut Depth Severity Classes	196		
	D.3	Temporal Soil Moisture Modelling	197		

Vita

List of Tables

2.1	Location descriptions used for initializing ForHyM	15
2.2	ForHyM initialization requirements by soil layer per plot and location	18
2.3	ForHyM calibration for the Fredericton area: default multipliers	23
2.4	Best-fitted regression model for measured (actual) versus modelled	
	top 15-cm soil MC $_{\!$	25
2.5	Correlation matrix for plot- and layer-determined CI, OM, Sand, CF	
	and ForHyM-estimated D_b , MC_V , MC_{PS}	29
2.6	Factor analysis of Table 2.5	29
2.7	Linear regression results for measured vs. modelled CI by depth and	
	location	31
2.8	Review of functional relationship between CI and soil properties	32
3.1	Machine specifications	50
3.2	Block description by machine, forest, operation and soil type,	
	operation date, and ocular DTW % area coverage	51
3.3	Variability in normalized clearance, number of passes, and speed by	
	machine and operation type	61
3.4	Best-fitted Eq. 3.1 and Eq. 3.5 regression results for the clearance	
	frequency distributions and the normalized clearances ≤ 1 , by	
	machine and block; speed, passes, and DTW coefficients $x10-2$; $f =$	
	0.122±0.002	63
3.5	Correlation matrix for the Eq. 3.6 variables and associated per block	
	entries in Table 3.4	69

4.1	Block description by forest type, stand properties (elevation, slope,	
	aspect), and soil association type, as further described in Table C.1	
	(Appendix C.)	84
4.2	ForHyM calibration variables for snowpack and saturated soil	
	permeability by block, including weather and hydrometric station	
	locations for primary ForHyM input data	91
4.3	ForHyM soil profile information used to initialize each blocks	92
4.4	Pearsons correlation matrix (non-shaded) with significance levels	
	(shaded grey) for each variable pair. Also shown: factor analysis	
	results following oblique factor rotation (factor loadings considered	
	salient in bold).	101
4.5	Mean block-specific soil property values including soil moisture	
	content at ridge top (MC $_{\mbox{\footnotesize{PS0}}}$) and minimum upslope open-channel	
	flow initiation area FIA	105
4.6	Best-fitted MC_{PS} % and MC_{V} % models based on using	
	plot-generated versus plot-projected	107
4.7	Best-fitted CI models based on using plot-generated versus	
	plot-projected and log ₁₀ plot-generated Cl	113
5.1	Historical rut depth model	125
5.2	Block description by geographical location, species specific forest	
	type, block properties (elevation, slope, aspect), and soil association	
	type, as well as plot counts for MC/CI, and rut field plots (highlighted	
	in grey)	129
5.3	Machine specifications (Jones <i>et al.</i> , 2018)	131
5.4	Model parameters for stands 1, 2, 3, and 9. MC_{PS} (%) refers to the	
	ForHyM-modelled soil moisture content at highest elevation within	
	each block at the time of wood forwarding	134
5.5	Soil physical properties and rut measurements	1.30

5.6	Pearson's correlation matrix (non-shaded) with significance levels	
	(shaded grey) for each variable pair, and Factor analysis showing	
	plot results with oblique rotation	140
5.7	Regression results for MC_{PS} and CI from Jones and Arp (2019),	
	regression results for rut depth and variable importance for Random	
	Forest Model for MC _{PS} , CI and rut depth	142
5.8	Monthly region-specific $\mathrm{DTW}_{\mathrm{FIA}}$ choices useful for forecasting soil	
	trafficability across Blocks 1, 2, 3, and 9 and northwestern New	
	Brunswick in general	153
C.1	Soil association, landform and lithology for blocks 1-11	192
C.2	Soil physical and moisture properties by block	193
D.1	Rut depth severity classes	196
D.2	ForHyM soil profile information used to initialize each stands	197
D.3	ForHyM calibration variables for snowpack and saturated soil	
	permeability	199

List of Figures

1.1	Simple flowcharf of model connections between ForHyM and spatial	
	trafficability maps	8
2.1	Overview depicting of the three Fredericton locations and	
	site-specific plot locations.	14
2.2	Measured MC_V and Cl at various depths for each plot	21
2.3	Scatterplots of measured $log_{10}CI$ versus measured $log_{10}MC_V$ and	
	weekly CI / CI _{max}	22
2.4	ForHyM time-series plots for weather outputs and modelled	
	hydrological outputs	24
2.5	Actual versus ForHyM best-fitted scatterplots for MC_V , stream	
	discharge, and snowpack depth	25
2.6	ForHyM-generated MC $_{\rm V}$ and MC $_{\rm PS}\%$ projection for the 0-15, 25-30,	
	30-45 and 45-60 cm soil layers by location and plot	27
2.7	Plotting plot-by-plot measured CI vs. OM, Sand, PS, MC _{PS} , and CF	28
2.8	Modelled CI (Eq. 2.10) in relation (a) to MC _{PS} and PS at CF = 20%,	
	and (b) to CF and MC _{PS} at SP = 20%	30
2.9	For HyM-generated unfrozen MC $_{\mbox{\scriptsize PS}}$, CI, and rutting from April 2013 to	
	April 2017	34
2.10	Cartographic depth-to-water index, overlain on the hill-shaded	
	LiDAR-derived bare-earth DEM by site and season	35
2.11	Soil MC _{PS} and rut depth interpretations of the season representative	
	DTW patterns in Figure 2.10	36

3.1	Map of New Brunswick showing elevations, ecoregions (GeoNB,	
	2018) and harvestblock locations with GPS-tracked clearances by	
	wood-forwarding machine type (JD11, JD15, TC)	45
3.2	Sensors installed on the John Deere 1110E, John Deere 1510E, and	
	Tigercat 635D	48
3.3	Ultrasonic distance sensor (left), datalogger box and inclinometer	
	(right) installed in the Tigercat 635D	49
3.4	Various sensor distance measurements and error potential from the	
	ultrasonic distance sensor.	49
3.5	Cartographic depth-to-water index (DTW) diagram (Ogilvie, 2017)	54
3.6	Composite of JD 1110E stands, including the point locations of the	
	machines underlain by the 4 ha DTW map	57
3.7	Composite of JD 1510E stands, including the point locations of the	
	machines underlain by the 4 ha DTW map	58
3.8	Composite of TC 635D stands, including the point locations of the	
	machines underlain by the 4 ha DTW map	59
3.9	Mean machine specific normalized clearance versus number of	
	passes (first 10 and all passes), empty vs. full loads, and machine	
	speed versus empty or full loads	60
3.10	Weekly cumulative rainfall, overall cumulative rainfall, and	
	normalized sensor clearance trends for the TC 635D during	
	2012-2014	66
3.11	TC block #41 showing weather-affected DEM-derived DTW patterns	
	based on assuming 4 ha, 1 ha and 0.25 ha of upslope flow	
	accumulation area for flow initiation	70
3.12	Visual correlation between DTW and normalized clearance, number	
	of passes per track, and machine speed, for blocks 47, 32, 34, and 10.	71
3.13	Normalized clearances across block 2, showing low TC clearances	
	on DTW >4 m ground following a 110 mm per day storm event in July	
	2014, with two close-ups, with DTW background	75

4.1	Digital elevation model for New Brunswick (10 m resolution) with	
	regional upland and lowland delineations, block locations, and	
	weather station locations	83
4.2	Penetrometer being used inside and outside forwarder tracks without	
	brushmats	88
4.3	Cartographic depth-to-water index (DTW) diagram (Murphy et al.,	
	2009b)	94
4.4	Cartographic DTW <1m pattern by minimum upslope	
	open-channel flow initiation area (FIA), i.e., $\mathrm{DTW}_{\mathrm{FIA}},$ to emulate	
	changes in soil moisture content by weather and season	94
4.5	Spatial raster examples for DTW (1), DEM (2), $D_{\rm b}$ (3), CF (4) for block-	
	specific MC_{PS} projections (Block 3)	96
4.6	Digital soil mapping process combining topographic and soil	
	features (A) with temporal features (B) to generate best-fitted	
	weather-affected $\mbox{MC}_{\mbox{\scriptsize PS}}$ (B) and CI (C) projections for each block.	97
4.7	Boxplots of MC _{PS} , CI, CF, sand and $D_{\rm b}$ within the top 15 cm soil layer	
	inside and outside the wood-forwarding tracks	99
4.8	Scatterplots pertaining to CI, $D_{b}\text{,}$ and MC_{PS} inside and outside	
	brushmatted and non-brushmatted tracks	99
4.9	Scatterplots for top 15 cm MC_{PS} and CI versus top 15 cm CF, sand,	
	OM and $D_b.\ \dots\dots\dots\dots$	102
4.10	Boxplots of field-determined CI versus soil depth for Blocks 1 to 9,	
	including significance value of implied trend	103
4.11	Daily variations in Block 1 and Block 9 for air temperature and	
	precipitation (ForHyM input) and stream discharge, MC_{PS} for top 15	
	cm of mineral soil, estimated field capacity, snowpack depth, and	
	frost depth (ForHyM output; (Jones <i>et al.</i> , 2018))	105
4.12	Scatterplots of actual versus best-fitted MC $_{PS}$ scatterplots. Eq. 4.12	
	demonstrates the influence of block-generated DTW mapping on	
	MC_{PS} alone	109

4.13	Confusion matrix for actual versus Eq. 4.14 projected MC _{PS} (left) and	
	cumulative conformance probability for Eqs. 4.12, 4.13, 4.14, and	
	4.16 (right). Blue squares align 1 on 1 for the actual versus projected	
	MC% classes, while the shades from dark to light red represent	
	increasing projection differences	110
4.14	Overlay of field- and track- determined MC_{PS} on the Equation 4.16	
	generated MC _{PS} projections for Blocks 1 to 11 (blocks 9-11 have only	
	field measured MC _{PS})	111
4.15	Scatterplots of actual versus best-fitted CI scatterplots	115
4.16	Confusion matrix for modelled vs Eq. 4.18 projected CI and	
	cumulative conformance probability for Eqs. 4.18 and 4.19	115
4.17	Eq. 4.18 generated CI projections at 15 cm depth for Blocks 1-9	
	outside wood-forwarding, and for 15, 30, 45 and 60 cm soil depths	
	outside and inside the wood forwarding tracks for Block 3	116
4.18	ForHyM modelled $\ensuremath{MC_{PS}}$ for ice and water combined, in relation to	
	soil moisture retention at field capacity with spatially projected $\mbox{MC}_{\mbox{\scriptsize PS}}$	
	and Cl	119
5.1	Map showing block locations (Blocks 1 to 11), with Blocks 1, 2, 3, and	
	9 selected for rut depth determinations following wood forwarding	
	and a grapple skidder	128
5.2	Plot specific location including machine tracks, field plot locations,	
	and photos from within the blocks	130
5.3	Flowchart for the soil trafficability model (STRAM): generating the rut	
	depth raster for Block 3	137
5.4	Comparison between modelled multiple linear regression and	
	Random Forest for MC_{PS} , CI and rut depth	141
5.5	Best-fitted RF- and MR- \ensuremath{R}^2 and RSME value achieved using predictor	
	variables in the order of decreasing numerical significance or	
	influence	143

5.6	Cumulative conformance probability for differences in MC _{PS} , CI, and	
	rut depth for RF and MR	144
5.7	Field-measured rut-depth locations with number of passes along rut	
	tracks and rut depth across Blocks 1, 2, 3 and 9, also showing the	
	block-specific weather-affected DTW $_{\mbox{\scriptsize FIA}}$ assignments	145
5.8	Close-ups A and B from Figure 5.7 showing rut-depth measurement	
	locations in Block 9 overlaid on a 10 cm resolution hill-shaded DEM	
	and a high-resolution surface image one year after field operations.	
	Also shown is the DEM-generated DTW 1 m extent (top;	
	blue-shaded, 50% transparent) and its corresponding DTW = 0.5 m	
	contour (bottom; red). The 10 cm DEM (top) was generated from	
	scanned optical AUV surface images (bottom; Phantom 4) $\dots \dots$	146
5.9	Measured $\mbox{MC}_{\mbox{\scriptsize PS}}$ and CI values at 15 cm soil depth overlaid on the	
	corresponding Eq. 5.2 and Eq. 5.3 map projections for Blocks 1, 2, 3	
	and 9, using FIA = 1, 16, 1, 0.25, respectively	148
5.10	Random Forest modelled 2- and 10-pass rut depths for Blocks 1, 2, 3,	
	9 with machines carrying full loads, with the field plot results overlaid,	
	using FIA = 1, 16, 1, 0.25, respectively	149
5.11	Historical weather for Block 1 from 2000 to 2015 showing cumulative	
	precipitation, historical snowpack and modelled frost depth, and	
	temperatures, as well as ForHyM-modelled weekly modelled	
	average A & B horizon MC $_{\mbox{\footnotesize{PS}}}.$	152
5.12	Year-round RF-generated soil trafficability projections by month for	
	Block 1, with focus on 2 passes and 2014 weather-affected $\mathrm{DTW}_{\text{FIA}}$	
	assignments	153
B.1	Percent frequency of normalized clearance for the JD 1110E by	
	block	183
B.2	Percent frequency of normalized clearance for the JD 1510E by	
	block	184

В.З	Percent frequency of normalized clearance for the TC 635D by block.	185
B.4	Normalized Clearance by block for pass number, speed class, and	
	DTW class for the JD 1110E	186
B.5	Normalized Clearance by block for pass number, speed class, and	
	DTW class for the JD 1510E	187
B.6	Normalized Clearance by block for pass number, speed class, and	
	DTW class for the TC 635D	188
B.7	Daily variations in air temperature and precipitation, with modelled	
	stream discharge, volumetric soil moisture content including field	
	capacities and snowpack depth, frost depth, and volumetric soil	
	moisture content for the wider NWU areas	189
B.8	Daily variations in air temperature and precipitation, with modelled	
	stream discharge, volumetric soil moisture content including field	
	capacities and snowpack depth, frost depth, and volumetric soil	
	moisture content for the wider MWU+LL areas	190
C.1	Modelled vs measured ForHyM generated calibration outputs for	
	snowpack and stream discharge for Northwestern Uplands,	
	Midwestern Uplands and Lowlands	194
D.1	Modelled vs measured ForHyM generated calibration outputs for	
	snowpack and stream discharge for stands 1-3, stand 9	198

Abbreviations & Acronyms

Units

cm Centimeter

°C Degree Centigrade

ha Hectare

MPa Megapascals

m Meter

kN kilonewtons

kPa kilopascals

% Percent

Soil Properties

D_b Bulk Density

CF Coarse Fragment

CI Cone Index

Fl Flow Initiation

MC Soil Moisture

MC_v Volumetric Soil Moisture

MC_g Gravimetric Soil Moisture

MC_{ps} Pore-space filled Soil Moisture

OM_g Gravimetric Organic Matter

PS Pore Space

RD Rut Depth

Statistics

Coeff. Coefficient

Eq. Equation

MAE Mean Average Error

RMSE Root Mean Square Error

Std. Dev., SD Standard Deviation

Std. Err., SE Standard Error

Geospatial Analysis

DEM Digital Elevation Model

DTW Depth to Water Index

LiDAR Light Detecting and Ranging

WAM Wet Area Mapping

Locations

BB Black Brook

DD Deersdale

DR Dorn Ridge

LL Lowlands

MWU Midwestern Uplands

NB New Brunswick

NWU Northwestern Uplands

OP Odell Park

SM Silver Maple

UNB University of New Brunswick

Machinery & Operations

CC Clearcut

CT Commercial Thinning

JD John Deere

SHW Shelterwood Cut

TC Tigercat

Vegetation

BF Balsam Fir (Abies Basalmea)

BE Beech (Fagus grandifolia)

Bl Birch (Betula sp.)

BS Black Spruce (*Picea nigra*)

HW Hardwood

MA Maple (Acer sp.)

MX Mixedwood

NS Norway Spruce (*Picea abies*)

PO Poplar (*Populus* sp.)

RS Red Spruce (*Picea rubens*)

SW Softwood

SM Sugar Maple (Acer saccharum)

Unk Unknown

WB White Birch (Betula papyrifera)

WS White Spruce (*Picea glauca*)

Chapter 1

Introduction

The increased use of heavy machinery in forest operations has led to serious environmental problems such as a decrease in plant development (Prose, 1985; Ayers, 1994; Grigal, 2000; Blouin *et al.*, 2004), changing soil hydraulic properties (Startsev and McNabb, 2000; Hamza and Anderson, 2005; Zhang *et al.*, 2006; Bryant *et al.*, 2007; Bonell *et al.*, 2010), and soil degradation, in the form of rutting (creating potentially deep tracks, displacing soil), compaction (compression of the soil), and erosion (structural loss) (Halvorson *et al.*, 2001; McNabb *et al.*, 2001; Akay *et al.*, 2007; Jamshidi *et al.*, 2008; Labelle, 2008; Labelle and Jaeger, 2011). Understanding and predicting soil trafficability, or the soils ability to support machine traffic, has become crucial to help limit the impact of heavy forest operations on soils. Knowing where to build roads and trails, and when to allow heavy operating machinery onto those trails can increase productivity and reduce costs associated with machine downtime, and trail maintenance due to excessive rutting and increased water pooling.

1.1 Modelling forest soil trafficability

The problem faced when trying to forecast soil trafficability is the ability to predict, not only where a machine will have issues, but also, what time of the year it will face them, i.e. seasonal planning and day to day operations. A

temporal knowledge of hydrothermal soil properties and atmospheric weather conditions helps to understand how moisture moves through specific soils over time. Spatially interpolating those soil and moisture properties as well as applying varying scenarios of forest operational machinery allows for more complex modelling of soil trafficability. In order to properly predict trafficability, a better understanding is needed on the variables at play.

1.1.1 Machine variability

The forest industry utilizes a wide variety of machines to maintain forest operations, from forwarders, grapple-skidders, and harvesters to chippers, loaders, and transport trucks, all of which have a different impact on the soil. Each machine has varying tire parameters, load weight and distribution, which contribute to how they interact with the soil beneath it. The weight and payload of the machine need to be considered when constructing management plans for certain soil types. Increased weight load on soil can cause compaction which can have lasting effects on soil and plant productivity (Nawaz et al., 2013; Taylor and Burt, 1987). Soil compaction increases the D_b (Rab et al., 2005; Brady and Weil, 2008; Berisso et al., 2012; Bagheri et al., 2012) and lowers porosity and aeration (Startsev and McNabb, 2001; Parkhurst et al., 2018). Utilizing lighter machines with smaller loads for forest operations can significantly minimize soil disturbance (Radford et al., 2000).

Specific tire parameters can be important when considering their effects on efficiency on various soils. Studies have shown that different machine tires can be used in different harvesting scenarios, for example, high flotation tires maximize the soil/tire contact point to lower the load pressure on the ground (Taylor and Burt, 1987; Jun *et al.*, 2004). Larger tire footprints allow for the axle load weight to be dispersed over a larger area, minimizing compaction. Similarly, varying levels

of tire pressure can be use to increase or decrease the overall tire footprint (Raper et al., 1995; Elwaleed et al., 2006). Elwaleed et al. (2006) found that by reducing the pressure in agricultural tires from 221 kPa to 193 kPa, the ease of motion of the tires increased, allowing more fluid movement over the soil. On the other hand, a study by Eliasson (2005), found that tire pressure had insignificant effects on soil disturbance when compared to the number of passes. A vehicle that goes over the same area of land multiple times will do more damage to the soil, even with a lower tire pressure. Although the biggest changes in soil mechanical properties happen during the first pass.

Vehicle mobility parameters are forces that affect the tire/soil interaction point, which include wheel traction and rolling resistance. Wheel slippage, dependent on traction, can lead to soil disturbance through compression and loss of shear strength. Multiple studies have tested the mobility of vehicles and their effects on soil disturbances (Shoop, 1989; Raghavan et al., 1977; Davies et al., 1973; Suvinen, 2006; Fervers, 2004; Prakash, 2014). Shoop (1989) examined the differential interface velocity (DIV), the speed of the wheel minus the true speed of the vehicle and observed that traction between the vehicle tires and the soil, was strongly influenced by soil moisture content (MC), bulk density (D_b) and potential frost depth of the soil. They summarized low soil MC tends to have high cohesion, caused by the empty pores, but with increasing MC the traction and strength of the soil decreases and the vehicle has greater wheel slippage. Raghavan et al. (1977) ascertained that vehicle slippage compacts the soil the most when slippage of the tires reaches between 15-20 % of the tire rotation velocity. Increased slippage cause excess soil displacement. Understanding the variables at play under the tire/soil contact point can improved modelling of any soil disturbances associated with it.

The evaluation of wheel numerics involves simple models of the tire/soil contact point. Generally these models utilize tire parameters (tire diameter, width, section

height, and deflection) to predict the torque, force, and sinkage of the tire on the soil. A commonly used wheel numeric is represented as nominal cone index (NCI), a dimensionless factor which looks at non-tracked off road vehicles with multiple wheels (Turnage, 1984; Saarilahti, 2002c; Vega-Nieva *et al.*, 2009). NCI utilizes the soils cone index (CI), or its strength of resistance, as well as tire and machine parameters to predict a numeric representation of the effects of machine on soil.

1.1.2 Soil physical and hydraulic properties

The strength of a soil, or its ability to withstand shear stress under pressure, is an increasingly important topic of research, especially as mechanized forest operations increases in scale, testing the operational limits of the soil. Extensive study has been done to better understand, measure, and predict soil strength and how external properties affect it. Advancements in the topic began during World War II to assess vehicle mobility by the U.S. Army Waterways Experiment Station (WES). They pioneered the efficient method of testing soil strength with the use of a cone penetrometer, which measures the cone index (CI), or the soil resistance to penetration of a right-circular cone (Rohani and Baladi, 1981). The cone penetrometer uses calibrated size- and angle- specific cones to determine the pressure to push the probe into the soil.

Soil strength is dependent on many factors including soil texture, moisture content (MC), and bulk density (D_b) (Towner, 1974; Muller and Schindler, 1998; McNabb *et al.*, 2001). A soil's moisture level can have a drastic effect on its capacity to withstand displacement. Studies have shown that increasing soil moisture content (MC) reduces particle cohesion and allows for easier displacement (Vaz *et al.*, 2011; Lin *et al.*, 2014). Likewise, soils rich in organic matter tend to hold onto moisture and therefore reduce soil strength but frozen soils increase strength by increasing particle tension (Andersland and Ladanyi,

1994; Shoop, 1995; Bronick and LaI, 2005; Huntington, 2007). Many studies have examined the relationship between strength and texture: sandier soils tend to have lower moisture holding capabilities but have less particle cohesion from low D_b and OM levels (Brady and Weil, 2008; Balland *et al.*, 2008; Kumar *et al.*, 2012). Similarly, clay rich soils can absorb more water and have a range of optimal strength prior to distortion from heavy machinery (i.e. strong when dry, but very weak when wet) (Arnup, 1999).

1.1.3 Trafficability models

Three modelling approaches are available for simulating wheel/soil interactions to better understand the effects of heavy machinery on soil strength: (i) theoretical/mathematical, (ii) empirical, and (iii) semi-empirical.

The theoretical models are based around terrain-model equations which utilize ideal terrain and require known stress limits to model vehicle performance. The finite element method (FEM) is an example of a theoretical/mathematical model structure. Fervers (2004) utilized FEM to investigate the interaction of tires on soil, focused on modelling the influence of different tire inflation on different soils in a 2-D mathematically derived tire model.

Empirical trafficability models use a given dataset to generate empirical equations to predict vehicle performance. The WES method was developed by the US Army Corps Engineer in conjunction with the cone penetrometer and the nominal cone penetration index (NCI). The WES method calculates the mobility index (MI) for a given machine with a given number of passes over the soil (Saarilahti, 2002a; Eichrodt, 2003).

Semi-empirical models combine theoretical soil mechanics with empirical formulations to predict soil trafficability across the land by way of global

information system (GIS) technology. By spatially analyzing soil properties, models and maps can be created to visually represent areas of high trafficability risk. Generally these models utilize shapefiles, point or polygon shapes which represent a given dataset (i.e. water bodies, soil polygons, etc), rasters, scalable graphics made up of individual pixel cells which store single data values (i.e. digital elevation model (DEM), terrain slope, etc), and GIS integrated tools to create trafficability maps or cost-efficient trail models. A study by Suvinen (2006) created a terrain tractability model and optimal off-road routing which produced a cost surface based on vehicle parameters, terrain, vegetation, and It generates different route alternatives based on different weather inputs. conditions, for example getting from point A to point B using different routes, based on the time of the year, the machine traveling, and the under laying substrate. A similar study by Campbell et al. (2013) used empirically derived rut relationships to create trafficability maps for trail damage severity. They used depth-to-water (DTW), a predicted depth to measurable water raster input, combined with field derived soil properties (soil texture, D_b, and MC) to create a rut depth calculation which classified trail damage.

1.2 Research question (Basic Hypotheses)

The research in this thesis is based on these questions:

- 1. Can field measured cone index and soil moisture content be used to predict soil trafficability?
 - H₁ Field measured cone index and moisture content correlate to published modelled equations via spatial wet-areas-mapping and temporal rut modelling, predict and validate soil trafficability.
 - $\rm H_0$ There is no significant correlation between field measured cone index and moisture content to modelled indices, which then produces poor soil trafficability predictions.

- 2. Can soil trafficability be predicted spatially and temporally?
 - H₁ Soil trafficability can be predicted temporally via the Forest Hydrology Model, and spatially using digital soil maps (DSL), and other digital elevation map (DEM) derivatives.
 - H_0 Trafficability can not be predicted both temporally and spatially.

The purpose of this thesis is to report and to examine the effects of heavy forestry machinery on soil rutting by building upon previous research (Vega-Nieva *et al.*, 2009; Campbell, 2012; Campbell *et al.*, 2013) through comparing model outputs to field measurements (results from machine mounted rut sensors and cone penetrometers vs. spatial trafficability maps) and creating a tool which will help increase forecast areas of potential high-risk rutting, specifically integrating forecasting by season. This will be accomplished by:

- (i) understanding the temporal relationship between soil moisture and soil strength using weekly field measurements of both,
- (ii) analyzing the effects of heavy equipment using clearance and GPS tracked sensors,
- (iii) creating pedotransfer functions of temporal and spatially modelled soil moisture and soil strength,
- (iv) verifying trafficability model outputs with field measured rut data using Random Forest statistical analysis,
- (v) creating a user-friendly trafficability ArcGIS model to generate spatial trafficability predictions, connecting STELLA-based ForHyM and ArcGIS-based model,
- (vi) generating trafficability maps generated for site specific cut-blocks in Black Brook, Deersdale, and Dorn Ridge.

The previous studies specific to this research focused on (i) spatial assessment of trail-soil rutting based on wet-areas mapping (Vega-Nieva et al., 2009; Campbell, 2012; Campbell et al., 2013). This project builds on this research to produce a usable tool in reference to when (via temporal ForHyM) and where (via spatial modelling) to minimize off-road soil trafficability impacts. The formulation and subsequent application of the tool is primarily intended for forest operations planning, but generalizations should also be possible to assess, e.g., weather-affected soil disturbances due to snowmobiles, all-terrain vehicles, mountain-bikes, and hiking trails.

A flowchart in **Figure 1.1** shows the soil trafficability modelling (STRAM) development, essentially involving the field validation of hydrological modelling at the daily level, and spatial interpretation of the same involving digital elevation modelling at 1 to 10 m resolution.

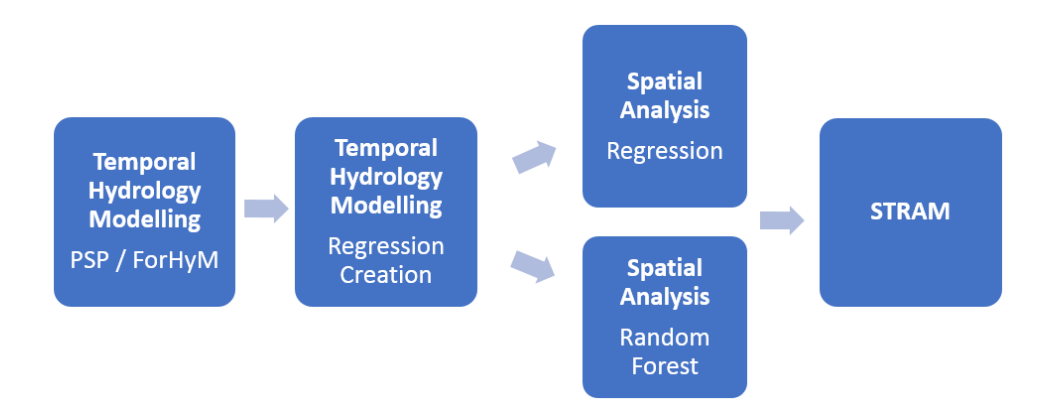


Figure 1.1: Simple flowchart of model connections between ForHyM and spatial trafficability maps.

1.3 Thesis Outline

The Chapters in the main body of this Thesis (Chapters 2, 3, 4, and 5) refer to individual publications. This Chapter serves the general introduction purpose.

Chapter 2 (Jones and Arp, 2017) titled "Relating the cone penetration and rutting resistance to variations in forest soil properties and daily moisture fluctuations" focuses on presenting the relationship between soil strength (i.e. cone penetration) with soil properties and measured soil moisture, as these vary on 3 sites in Fredericton, NB over a 32 week spring-to-fall period.

Chapter 3 Jones *et al.* (2018) titles "Track-monitoring and analyzing machine clearances during wood forwarding" examines machine-specific wood-forwarding clearance data across 11 harvest blocks in northwestern New Brunswick. This examination was done using soil moisture, machine speed, and number of passes as machine clearance predictor variables.

Chapter 4 Jones and Arp (2019a) titled "Soil moisture and cone penetrability conditions in forest soils" focuses on forecasting soil moisture (MC) and soil strength (CI) variations across the harvest blocks in Chapter 3, with validations.

Chapter 5 (Jones and Arp (2019b); submitted for publication) titled "Soil Trafficability Forecasting" uses the results from Chapters 2, 3 and 4 to evaluate the Soil Trafficability Model (STRAM) by way of multivariate and Random Forest regression techniques.

Chapter 6 concludes with a summary of main research developments and findings, a list of original contributions, and recommendations for future work.

Chapter 2

Relating the cone penetration and rutting resistance to variations in forest soil properties and daily moisture fluctuations

Marie-France Jones and Paul Arp
Faculty of Forestry and Environmental Management,
University of New Brunswick, Fredericton NB, Canada E3B 6C2

Foreword:

The following chapter is a published article within the Open Journal of Soil Science. It was submitted on May 19, 2017 and accepted for publication on July 17, 2017. Publication permission can be found in **Appendix A.1**.

Citation:

Jones, M.-F., Arp, P.A. (2017) Relating the cone penetration and rutting resistance to variations in soil properties and daily moisture fluctuations. *Open Journal of Soil Science*, 7, 149-171. doi.org/10.4236/ojss.2017.77012

Abstract

Soil resistance to penetration and rutting depends on variations in soil texture, density, and weather-affected changes in moisture content. It is therefore difficult to know when and where off-road traffic could lead to rutting-induced soil disturbances. To establish some of the empirical means to enable the "when" and "where" determinations, an effort was made to model the soil resistance to penetration over time for three contrasting forest locations in Fredericton, New Brunswick: a loam and a clay loam on ablation / basal till, and a sandy loam on alluvium. Measurements were taken manually with a soil moisture probe and a cone penetrometer from spring to fall at weekly intervals. Soil moisture was measured at 7.5 cm soil depth, and modelled at 15, 30, 45 and 60 cm depth using the Forest Hydrology Model (ForHyM). Cone penetration in the form of the cone index (CI) was determined at the same depths. These determinations were not only correlated with measured soil moisture but were also affected by the variations in soil density (or pore space), texture, and coarse fragment and organic matter content ($R^2 = 0.54$; all locations and soil depths). The resulting regression-derived CI model was used to emulate how CI would generally change at each of the three locations based on daily weather records for rain, snow, and air temperature. This was done through location-initialized and calibrated hydrological and geospatial modelling. For practical interpretation purposes, the resulting CI projections were transformed into rut depth estimates regarding multi-pass off-road all-terrain vehicle traffic.

Keywords

Soil resistance to penetration, cone index, soil moisture, texture, coarse fragments, organic matter, weather records, hydrological modelling, soil trafficability, rutting depth, recreational vehicles

2.1 Introduction

The soil cone index (CI), a measure of a soils resistance to penetration (MPa), is a commonly used soil mechanical property to determine soil strength (Lowery and Morrison, 2002; Eid and Stark, 1998). This strength generally increases with increasing clay, coarse fragment (CF, %) and soil density (D_b, g/cm²), or reduced pore space (PS), but decreases with increasing soil moisture (MC, %) and organic matter content (OM, %) (Balland *et al.*, 2008; Vega-Nieva *et al.*, 2009; Vaz *et al.*, 2011; Lin *et al.*, 2014). Hence, non-cohesive soils such as sands and sandy loams are more easily penetrated than clay soils (Balland *et al.*, 2008; Brady and Weil, 2008; Kumar *et al.*, 2012), wet soils have low penetration resistances and the resistance to penetration is low for organically enriched soils but high for stony and frozen soils (Andersland and Ladanyi, 1994; Bronick and Lal, 2005; Huntington, 2007).

In practice, off-road traffic may increase soil compaction and CI, which negatively affects crop growth by way of reduced root development (Culley et al., 1981; Soane and van Ouwerkerk, 1994; Chen and Weil, 2010, 2011; Kumar et al., 2012). In urban developments, increased CI due to soil compaction decreases soil infiltration of water and tree root growth (Gregory et al., 2006; Kozlowski, 2008). However, sufficient CI-index soil strength is needed to allow on-and off-road traffic in agriculture and forestry operations (Moehring and Rawls, 1970; Carter et al., 2007), while off-road recreational traffic needs to be controlled to avoid soil rutting. In this, the resistance of soils to rutting is directly proportional to the ratio between tire footprint pressure and CI (Saarilahti, 2002c; Affleck, 2005). The former increases with increasing loading and decreasing footprint area, which in turn, decreases with increasing tire width, wheel diameter, and with decreasing tire pressure. In the field, rut depths further increase from single to multiple passes, and with slope-induced tire spinning (Han et al., 2006).

Efforts to minimize soil rutting requires reliable forecasting of off-road soil trafficability. Doing this, however, is challenging because soil and machine-use conditions may vary daily from location to location. By location, low CI conditions do not last as long for sandy soils than for loams and clays. In addition, soil trafficability varies by the extent of soil freezing and thawing, especially when traffic turns frozen soils into mud (Shoop, 1995).

The objective of this chapter is determining how manually derived soil CI determinations change in response to weekly spring-to-winter changes in MC and temperature for three contrasting soil conditions. The data so generated allowed for (i) quantifying the relationship between CI and soil MC, (ii) emulating and interpreting the changes in soil moisture, CI, and rutting depth, and (iii) daily year-round modelling of soil trafficability by soil texture and soil depth. While machine-based cone penetration testing methods (CPT: Robertson (2016)) would be more accurate and precise, manual CI determinations have the greater portability and affordability advantage for assessing how soil trafficability conditions vary from location to location across landscapes and seasons.

2.2 Materials and Methods

2.2.1 Location Description

Three forest sites in Fredericton, New Brunswick, were chosen for this study (**Figure 2.1**, **Table 2.1**):

- i. a mixed-wood stand on sandy clay loam in a wooded section on the University of New Brunswick campus (UNB);
- ii. a hemlock (*Tsuga canadensis*) stand on a rich loam in Odell Park (OP);

iii. a silver maple site (*Acer saccharinum*) on an alluvial sandy loam next to a fresh-water marsh within the floodplain of the Nashwaaksis stream (SM).

The two non-alluvial soils developed on grey sandstone ablation / basal till. Elevation for the three sites ranges from 6 to 70 m (Stobbe, 1940). The topography varies from undulating to hilly. The upland forest vegetation is representative of the Acadian forest species, i.e., sugar maple (*Acer saccharum*), red maple (*Acre rubrum*), white birch (*Betula papyrifera*), balsam fir (*Abies balsamea*), black spruce (*Picea mariana*), and hemlock (*Tsuga canadensis*). The 1950-2017 Fredericton weather record has a mean annual temperature of 6.6 °C, with monthly means of -1.8 and 14.9 °C for January and July, respectively. Mean annual precipitation amounts to 1100 mm, including 250 mm of snow (Department of Environment and Climate Change Canada, 2016a).

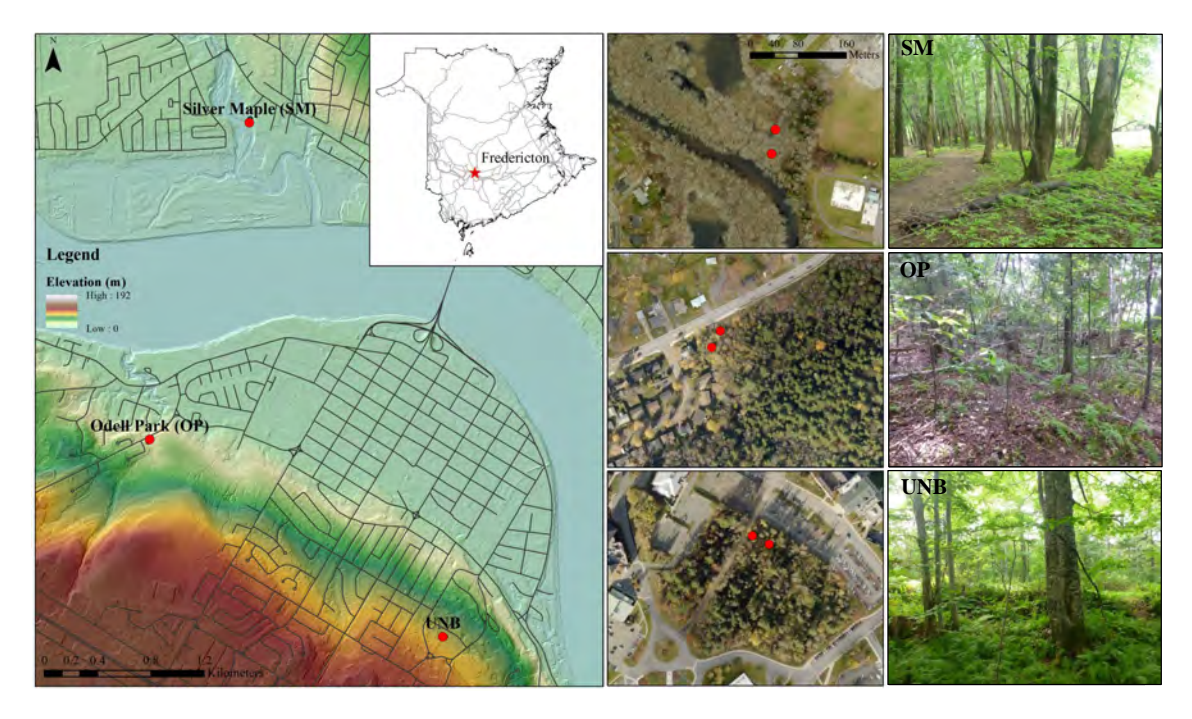


Figure 2.1: Overview depicting of the three Fredericton (New Brunswick) locations (left), and site-specific plot locations for SM (top), OP (middle), UNB (bottom) (Imagery Source: Esri, DigitalGlobe, GeoEye, Earthstar Geographics, CNES/Airbus DS, USDA, USGS, AEX, Getmapping, Aerogrid, IGN, IGP, swisstopo, and the GIS User Community).

Table 2.1: Location descriptions used for initializing ForHyM.

Site Parameters	UNB	Silver Maple	Odell Park	
Latitude (N)	45°56′40	45°57′28	45°58′46	
Longitude (W)	66°38′34	66°40′17	66°39′44	
Elevation (m)	70	8	29	
Slope (%)	4.5	2.5	2.7	
Aspect (°)	30	132	24	
Canopy Coverage Deciduous: Coniferous	20:40	70:0	30:30	
Rooting habit	Shallow	Deep	Shallow	
Forest floor depth (cm)	8	2	5	
Soil Series	Sunbury / Till	Riverbank / Glaciofluvial Deposits	Sunbury / Till	
Soil Classification	Gleyed Sombric Brunisol	Gleyed Humic Regosol	Orthic Humo-Ferric Podzol	
Mineral soil texture	Sandy Ioam	Loamy sand - Sandy loam	Silty loam - Sandy loam	
Subsoil texture	Sandy loam	Loamy sand	Silty loam	

2.2.2 Field Experiment

Soil layers were described and samples were taken from freshly dug soil pits at each of the three locations. Five soil volumetric moisture content (MC_V) and CI readings were taken manually each week from May 29, 2015 to November 2, 2015 within two circular plots (1.5 m radius) near the soil pits at each location. This was done using a Delta T HH2 moisture meter and a Humboldt digital cone penetrometer (cone area at base = $1.5 \, \mathrm{cm}^2$; cone angle 60°). The MC_V reading were taken at 7.5 cm mineral soil depth. The CI readings were obtained at 15, 30, 45, and 60 cm depths, but were not recorded where obstructed by logs, coarse roots, and surface-accumulated rocks.

The soil samples were placed into labeled freezer bags for storage. Prior to analysis, the samples were dried in a forced-air oven 75°C for 24 hours, crushed with a mortar and pestle and passed through a 2 mm sieve to remove and determine the CF. The fine-earth fraction was used to determine its sand, silt, and clay content using the hydrometer method (Shelrick and Wang, 1993). The soil carbon content (C, %) of this fraction was determined using the LECO CNS-2000 analyzer. Soil OM content by weight (OMg) was determined by setting OMg = $1.72 \times C$ %. The pore-space filled moisture content (MCps) was inferred by assuming that the soil gravimetric moisture content (MCg), Db and the PS would be affected by depth and OM content as follows (Balland *et al.*, 2008):

$$D_b = \frac{(1.23 + (D_p - 1.23) \times (1 - exp(0.0106 \times Depth)))}{1 + 6.83 \times OM_w}$$
 (2.1)

$$MC_g = MC_V \times D_b \tag{2.2}$$

$$MC_{PS} = \frac{MC_V}{PS} \tag{2.3}$$

where D_P is particle density (2.65 g/cm³), and PS is cm³ of pore space.

2.2.3 Hydrological Modelling

The forest hydrology model (ForHyM) (Arp and Yin, 1992; Yin and Arp, 1994; Jutras, 2012) was used to emulate the changes in daily soil moisture, soil temperature and snowpack conditions for each of the three locations from 2006 to 2017. Doing this involved compiling the daily Fredericton weather records for air temperature, precipitation (rain, snow), stream discharge and snow depth on open ground (Department of Environment and Climate Change Canada, 2016a,b). Also specified were elevation, slope, aspect, and extent of forest cover (Table 2.1). The model-internal water and head flow parameters pertaining to soil permeability, thermal conductivity, and heat capacity were plot-adjusted by texture, OM, and CF content (**Table 2.2**), and by comparing actual with modeled soil moisture content. This was done through manually resetting the default values for: (i) the air-to-snow-pack heat-transfer coefficient; (ii) the initial snowpack density of freshly fallen snow to reflect the open-ground conditions at the weather station (Balland et al., 2006), and (iii) the lateral soil permeability to account for lateral flow tortuosity (Jutras and Arp, 2010, 2013). These adjustment ensured that the model output conformed to actual snowpack depth and stream discharge records.

2.2.4 Data Analysis and Model Projections (MC_V, CI, rut depth)

The data and ForHyM estimates for MC_V , CI, texture, CF, OM, D_b , and PS were entered into a spreadsheet by location, date, and soil depth. This compilation served (i) to generate basic statistical summaries, (ii) to analyze the measured and modelled time-series plots for MC_V and CI, and (iii) to determinate the best fitted linear and multiple regression models with CI as dependent variable, and with MC_V (measured, modelled), soil texture, OM, CF, PS, and soil depth as independent variables. A linear regression model served to relate CI at 15, 30, 45 and 60 cm soil depth to measured and ForHyM modelled MC_V . A multiple

Table 2.2: ForHyM initialization requirements by soil layer per plot and location.

Site	Plot	Layers	Depth (cm)	Sand (%)	Clay (%)	Silt (%)	OM (%)	CF (%)	Rooting		
UNB	1	LF	-8	(Organic		Organic		100	0	Plentiful fine
		Ah	0-15	43 14 43		25	1	Plentiful fine			
		Bmg	15-40	66	10	24	5	10	Abundant fine-med		
		Cxg1	40-70	66	10	24	1	20	Few coarse		
		Cxg2	70+	66	10	24	0	70			
	2	LF	-8	(Organic	•	1	0	Plentiful fine		
		Ah	0-15	43	17	40	7	1	Plentiful fine		
		Bmg	15-40	66	10	24	2	10	Abundant fine-med		
		Cxg1	40-70	66	10	24	1	20	Few coarse		
		Cxg2	70+	66	10	24	0	50			
SM	1	L	-2	(Organic	;	100	0			
		Ah	0-15	48	17	35	10	0	Abundant fine		
		Cg1	15-65	44	17	39	5	10	Few coarse		
		Cg2	65-105	35	18	47	0	15	Few coarse		
		Cg3	105+	35	18	47	0	15			
	2	L	-2	(Organic	:	100	0			
		Ah	0-15	48	17	35	20	0	Abundant fine		
		Cg1	15-45	44	17	39	10	5	Few coarse		
		Cg2	45-95	35	18	47	0	10	Few coarse		
		Cg3	95+	35	18	47	0	15			
ОР	1	LFH	-5	(Organic	;	1	0	Plentiful fine		
		Ahe	0-15	58	18	24	10	1	Plentiful fine-med		
		Bf	15-40	54	20	26	5	5	Abundant med		
		ВС	40-90	54	20	26	1	10	Few coarse		
		С	90+	56	12	32	0	10			
	2	LFH	-5	(Organic		1	0	Plentiful fine		
		Ahe	0-15	58	18	24	10	1	Plentiful fine-med		
		Bf	15-35	54	20	26	5	15	Abundant med		
		ВС	35-70	54	20	26	1	15	Few coarse		
		С	70+	56	12	32	0	15			

regression model served to relate CI to MC_V (%), PS (%), and CF (%) as follows:

$$log_{10}CI = a + b \times PS + c \times MC + d \times CF$$
 (2.4)

where MC_{PS} is the water-filled portion of the pore space, in percent. The best-fitted model so generated was incorporated into the ForHyM model to determine how MC_V , CI, and rutting depths pertaining to all-terrain vehicles (ATV) traffic would vary over time at each of the three locations. The equations adopted for rut modelling were as follows (Saarilahti, 2002d; Vega-Nieva *et al.*, 2009):

Potential rut depths for n passes:

$$Z_n = \frac{1627}{NCI} \times n^{\frac{1}{2}} \tag{2.5}$$

with nominal cone index (NCI) given by:

$$NCI = \frac{(1000 \times CI \times b \times d)}{W} \times \sqrt{(\delta/h) \times \frac{1}{(1+2d)}}$$
 (2.6)

where b is tire width (m), d is tire diameter (m), h is section height (m), δ is tire deflection (m) given by 0.008 + 0.001 (0.365 + 170/p), p is tire inflation pressure (kPa), W is vehicle weight + load (kN) per number of wheels, and n is number of vehicle passes along the same track. Potential rutting depths for an all-terrain recreational vehicle (ATVs) were determined, using the following specifications: W = 3.1 kN; b = 0.254 m; d = 0.62 m; h = 0.3 m; p = 34.4 kPa; n = 10 passes.

To visually represent the temporal changes in MC topographically and over seasons, the MC_{PS} was spatially related to the depth-to-water index (DTW). This index was generated from a 1-m resolution bare-earth digital elevation model (DEM, vertical and horizontal error \pm 15 cm) for the Fredericton area (GeoNB, 2015a). This index determines the elevational rise along the least slope-path from each cell across the landscape to its nearest open-water cells corresponding to streams, lakes, rivers and open shores (Murphy *et al.*, 2009b; White *et al.*, 2012).

Changing the upslope flow accumulation area by channel flow initiation (FI), i.e., changing the amount of upstream area needed to initiate streamflow, allows for indexing DTW by season. For example, FI = 4 ha generally represents permanent streamflow at the end of summer, FI = 0.25 ha represents the extent of ephemeral stream segments that flow during and after snowmelt, and FI = 1 ha represents channel flow during transitional periods from fall to winter. The resulting DTW rasters with FI = 4, 1, and 0.25 ha were used to determine how the soil moisture conditions and rutting depths would vary across the terrain associated for the three sampling locations by season. FI was determined through prior field validation and studies Murphy *et al.* (2007). This was done by applying Eq. 2.7 and Eq. 2.8, i.e. (Murphy *et al.*, 2009b; Balland *et al.*, 2008):

$$MC_{PS} = 1 - [1 - MC_{PS}(DTW_{ridge})] \times \left[\frac{(1 - exp(-k \times DTW))}{(1 - exp(-k \times DTW_{ridge}))} \right]^{P}$$
(2.7)

$$RD_{n} = RD_{n,ridge} - [RD_{n,ridge} - RD_{n,DTW=0}] \times$$

$$\left[\frac{(1 - exp(-k \times DTW)}{(1 - exp(-k \times DTW_{ridge})}) \right]^{P}$$
(2.8)

with p=2, p and k as soil-specific parameters ranging from 0.2-2, and DTW_{ridge} (m), $RD_{n,ridge}$ and $RD_{n,DTW=0}$ (mm) as rut depth determined from the driest and wettest parts of each.

2.3 Results

2.3.1 Soil Moisture and CI Measurements

Each of the three sites showed distinct variations in soil properties, strength, and moisture readings over the course of 23 weeks. Given the plot-by-plot soil property differences, and tracking the changes in soil moisture over time,

revealed that the OP plots drained quickly. In contrast, the UNB plots varied the most from wet to dry and back again to wet from spring to fall (**Figure 2.2**). In direct correspondence, resistance to cone penetration varied the least for the two SM plots, and the most for the UNB plots. These differences arose from the compacted and poorly drained sandy loam for the UNB plots, the well-drained loamy sand with low CF content for the OP plots, and the seasonally recurring flooding of the SM plots (**Tables 2.1** & **2.2**). The high springtime levels for MC_V within the top 15 cm of the soil at the UNB and SM are due to the high Ah-layer OM contents, which according to Eq. 2.1 - lowers the D_D and enhances the soil-filled PS between the CF.

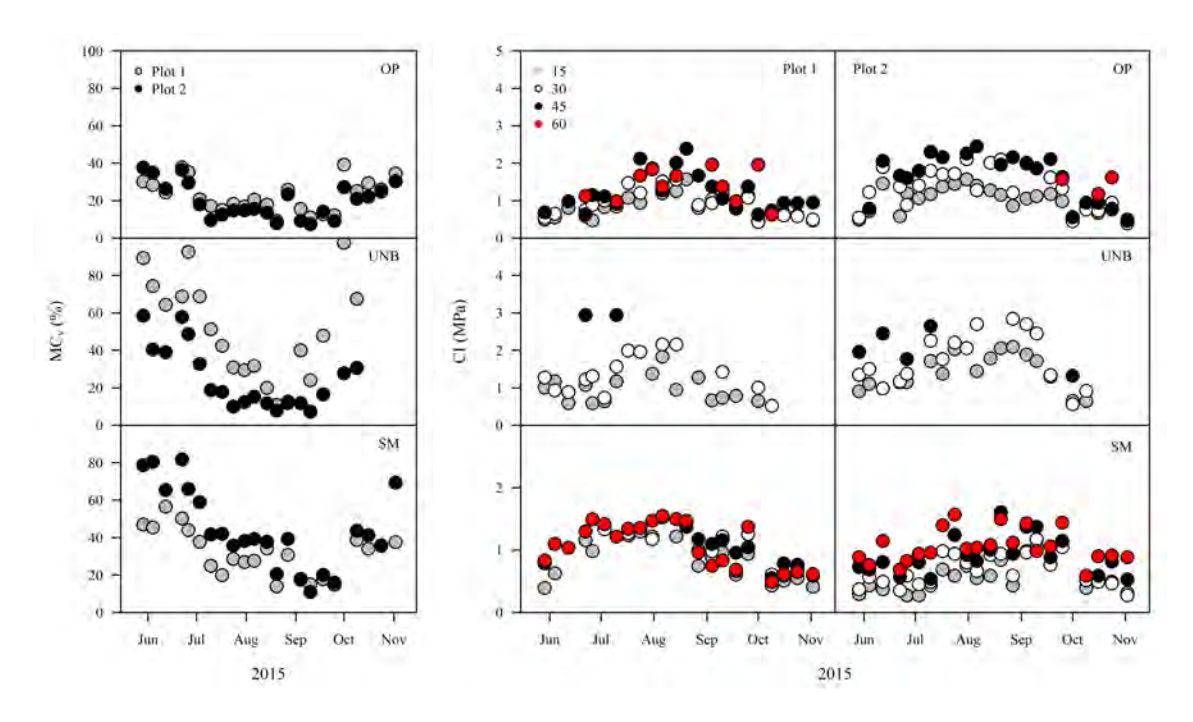


Figure 2.2: Left: Measured MC_V for the top 15 cm of soil. Right: Measured CI at 15, 30, 45, and 60 cm depth (right) for Plots 1 and 2 at the OP, UNB, and SM locations.

Plotting the CI measurements at 15 cm depth to the MC_V measurements revealed that the log-transformed CI and MC_V values are linearly related to one another as

shown in Figure 2.3 (left), as follows:

$$log_{10}CI_{15cm} = .62 - 0.52 \times log_{10}MC_V + 0.20 \times UNB$$

 $R^2 = 0.60, RSME = 0.13, MAE = 0.10$ (2.9)

with the UNB location coded 1 when applicable and 0 otherwise. Similarly strong correlations between MC and CI have been reported elsewhere (Young and Berlyn, 1968; Busscher *et al.*, 1997; Vaz *et al.*, 2011). With respect to increasing soil depth, CI tends to increase, as shown in Figure 2.3 (right) - CI increases, by plotting the ratio of the weekly averages of CI over CI_{max} per plot by location. A similar trend has been reported (Carter *et al.*, 2000; Campbell *et al.*, 2013; Porsinsky *et al.*, 2006).

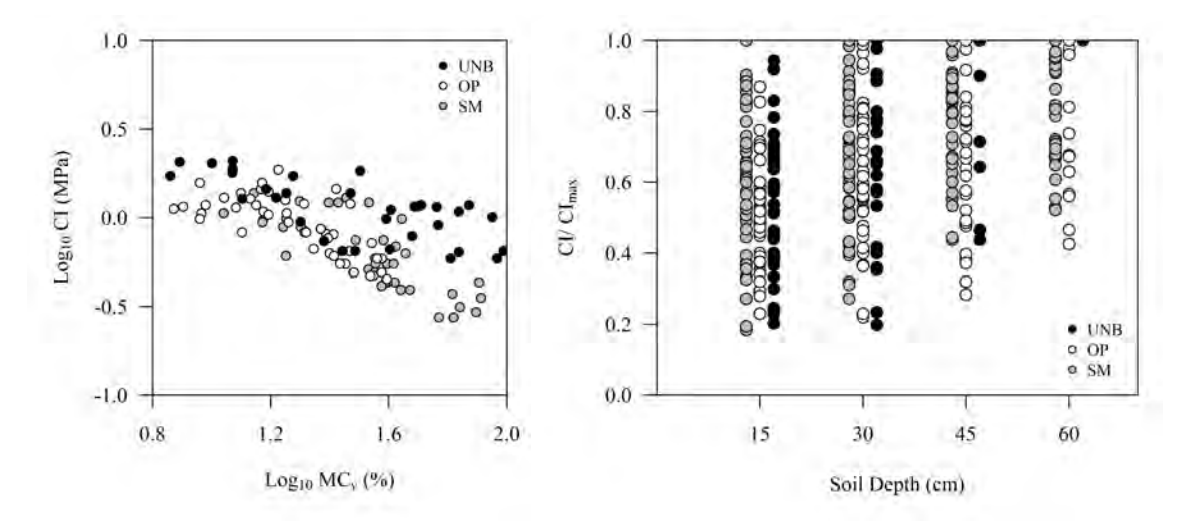


Figure 2.3: Scatterplots of measured $log_{10}Cl$ versus measured $log_{10}MC_V$ (left) and of the weekly averages of Cl / Cl_{max} for the OP, UNB, and SM locations (right).

2.3.2 Estimating Soil Moisture and CI through Hydrological Modelling

The modelling of the year-round MC conditions required Fredericton-specific ForHyM initialization and calibrations. These included Fredericton-specific calibrations for snowpack depth and stream discharge required using daily Fredericton Airport weather records for rain, snow and air temperature, and

adjusting the ForHyM-default settings for lateral and downward water flow, as listed in **Table 2.3**. The plot-specific ForHyM initializations for are listed in **Table 2.1** and **Table 2.2** refer to entering the plot- and/or layer-specific values for slope, aspect, vegetation type and cover, forest floor depth, percentages for sand, silt, clay, CF, OM, and layer depth. Shown in **Figure 2.4** are resulting time-series plots for air temperature and precipitation (input), snow pack depth, stream discharge, MC_V (top 15 cm, actual and modelled), and frost depth (modelled). The resulting scatter plots in **Figure 2.5** for actual and best-fitted ForHyM snowpack depth and top 15 cm MC_V demonstrate a reasonable good fit, with $R^2 = 0.81$ for the snowpack, 0.62 for stream discharge, and 0.76 for the MC_V (**Table 2.4**).

Table 2.3: For HyM calibration for the Fredericton area: default multipliers.

Parameters		Multipliers
Snowpack Multipliers	Snow-to-air temperature gradient multiplier	0.16
	Density of fresh snow	0.2
K _{sat} Multipliers	Surface runoff	1
	Forest floor infiltration	1
	Forest floor interflow	0.01
	A&B horizon infiltration	1
	A&B horizon interflow	0.02
	C horizon infiltration	1
	C horizon interflow	0.01
	Deep water percolation	1

For the purpose of predicting how CI would vary across time by soil texture, D_b and CF content (**Table 2.2**), it was necessary to use the ForHyM-generated depth- and time-dependent MC_V output for the 0 - 15, 15 - 30, 30 - 45 and 45 - 60 cm soil layers as predictor variables. Doing this involved estimating how much of the infiltrating

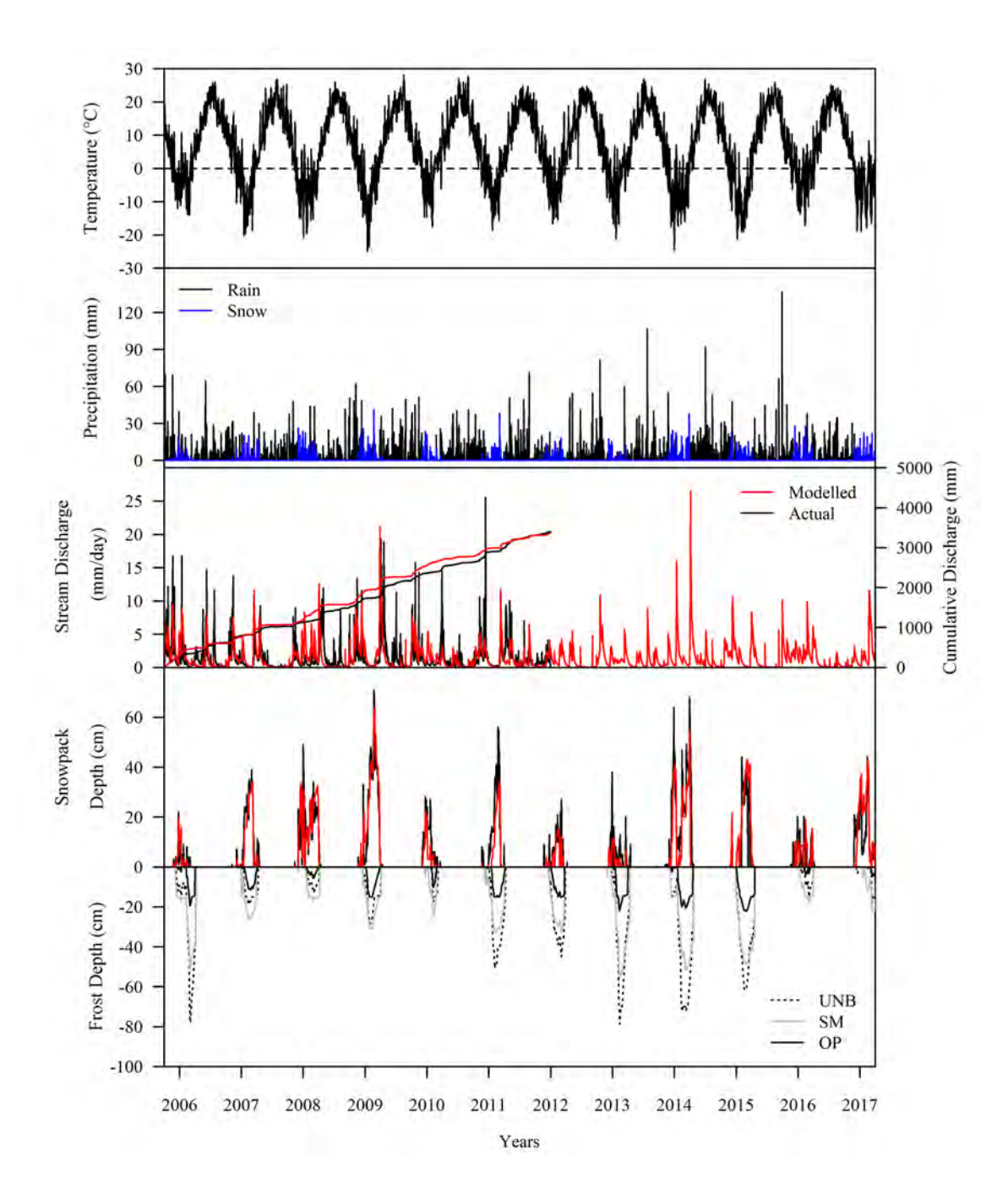


Figure 2.4: ForHyM time-series plots for daily air temperature and precipitation (ForHyM input), actual as well as modelled output for stream discharge and snowpack depth for Fredericton, NB, as well as location-specific modelled frost depth.

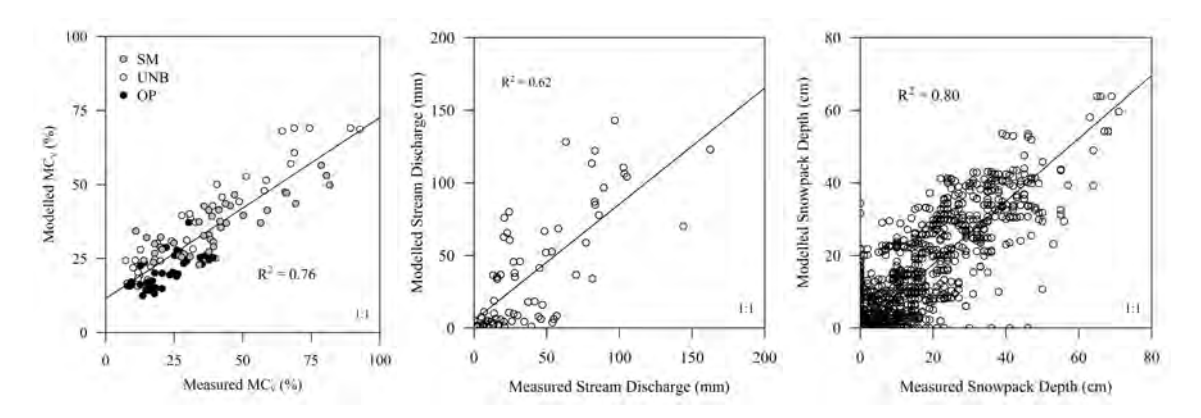


Figure 2.5: Actual versus ForHyM best-fitted scatterplots for MC_V (top 15 cm) (left), monthly stream discharge (middle), and snowpack depth (right).

Table 2.4: Best-fitted regression model for measured (actual) versus modelled top 15-cm soil MC_V by location (UNB, SM, OP) and overall.

Parameter	n	Intercept (SE)	Coefficient (SE)	t- value	p- value	Adj.R ²	RSME	MAE
UNB	37	13.88 (1.69)	0.68 (0.04)	17.31	< 0.001	0.90	5.47	4.50
SM	41	20.54 (1.82)	0.38 (0.04)	9.17	< 0.001	0.67	4.77	3.91
Odell Park	41	11.69 (1.75)	0.41 (0.07)	5.72	< 0.001	0.44	4.01	3.06
All Sites	118	11.53 (1.19)	0.61 (0.03)	19.36	< 0.001	0.76	6.57	5.48

and percolating water would be retained at any time within the fine-earth fraction of each layer. For example, the available for water retention would decrease with increasing CF content. Consequently, there would be less PS to fill between the CF during wet weather conditions, and there is also less water available for root uptake during warm summer weather (Baetens *et al.*, 2009). This being so, the ForHyM-generated projections in 2.6 by location and soil layer show greater MC_V and MC_{PS} variations for the stony UNB location, followed by the less stony SM and the more sandy OP locations. In combination, the ForHyM projections in **Figure 2.6** capture the plot-by-plot MC_{PS} variations such that $OP_{MC} > SM_{MC} > UNB_{MC}$.

Figure 2.7 and the correlation coefficients in Table 2.5 show how CI varies with varying soil texture (sand), CF, OM, PS, and MC_{PS}. In general, CI decreases with increasing PS and sand content due to decreasing particle-to-particle contacts. Increasing OM content decreases CI by way of soil aggregation, i.e. by further loosening the point of contact among the aggregated soil particles. The CF-induced increase in CI refers to the increasing strength needed to displace the coarser particles away from cone penetration path (Rücknagel *et al.*, 2013). Together, sand, OM CF and PS affect the daily variations in CI and MC retention through their combined effect on soil pore space, texture, and drainage (Alexander and Skaggs, 1987; Balland *et al.*, 2006; Wesseling *et al.*, 2009).

Subjecting the correlation matrix in **Table 2.6** to factor analysis reveals that the CI variations can be grouped into three CI determining factors. Factor 1 is a Location Factor, which relates a component of the CI variations to location- and layer-specific CF and PS determinations. Factor 2 is a MC Factor, which relates some of the CI variations to MC_{PS}. Factor 3 is strongly related to Sand, but has a non-salient effects on CI.

Using PS, MC_{PS}, and CF as independent variables produced the following best-

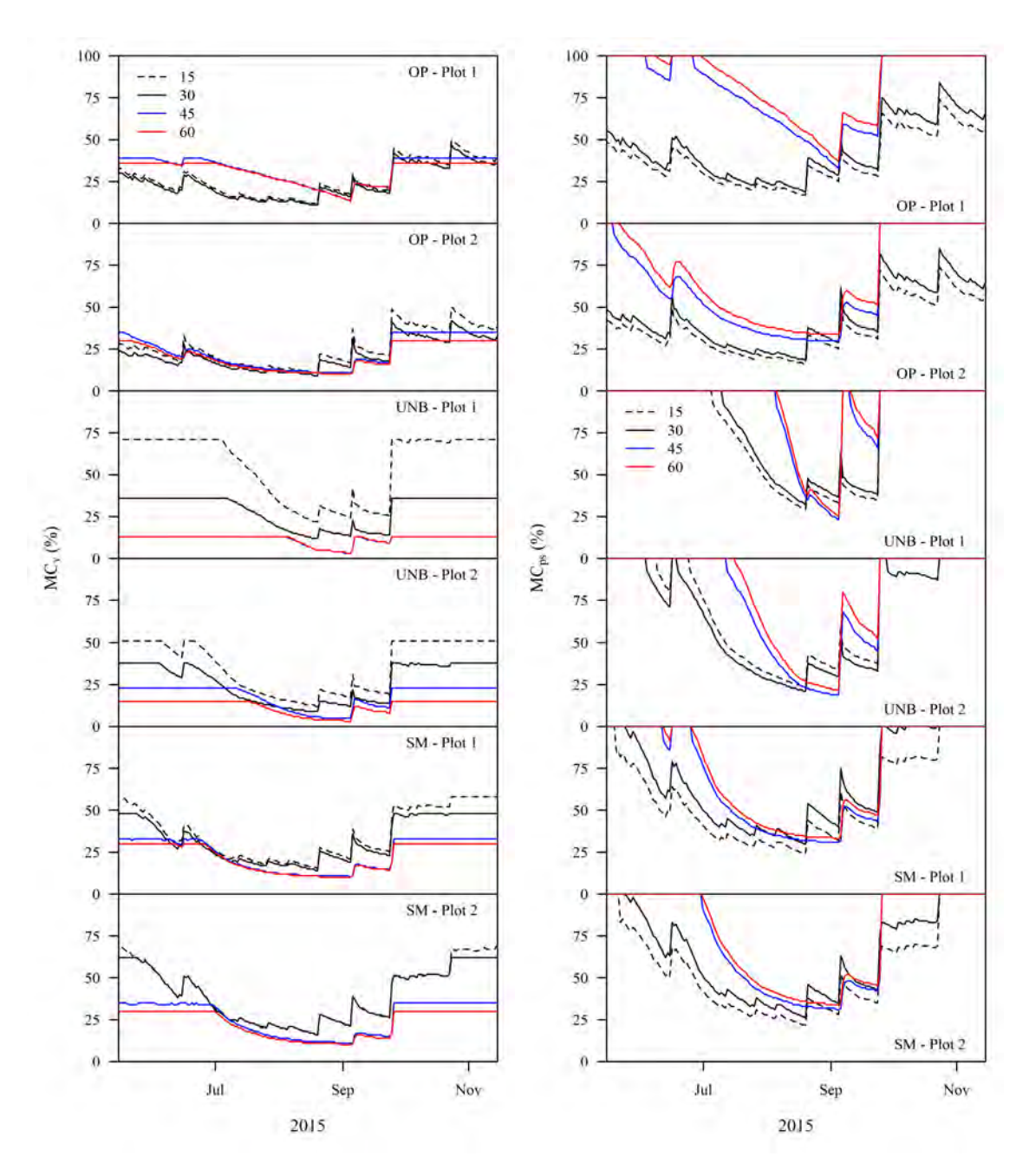


Figure 2.6: ForHyM-generated MC $_{\rm V}$ and MC $_{\rm PS}$ % projection for the 0-15, 25-30, 30-45 and 45-60 cm soil layers by location and plot.

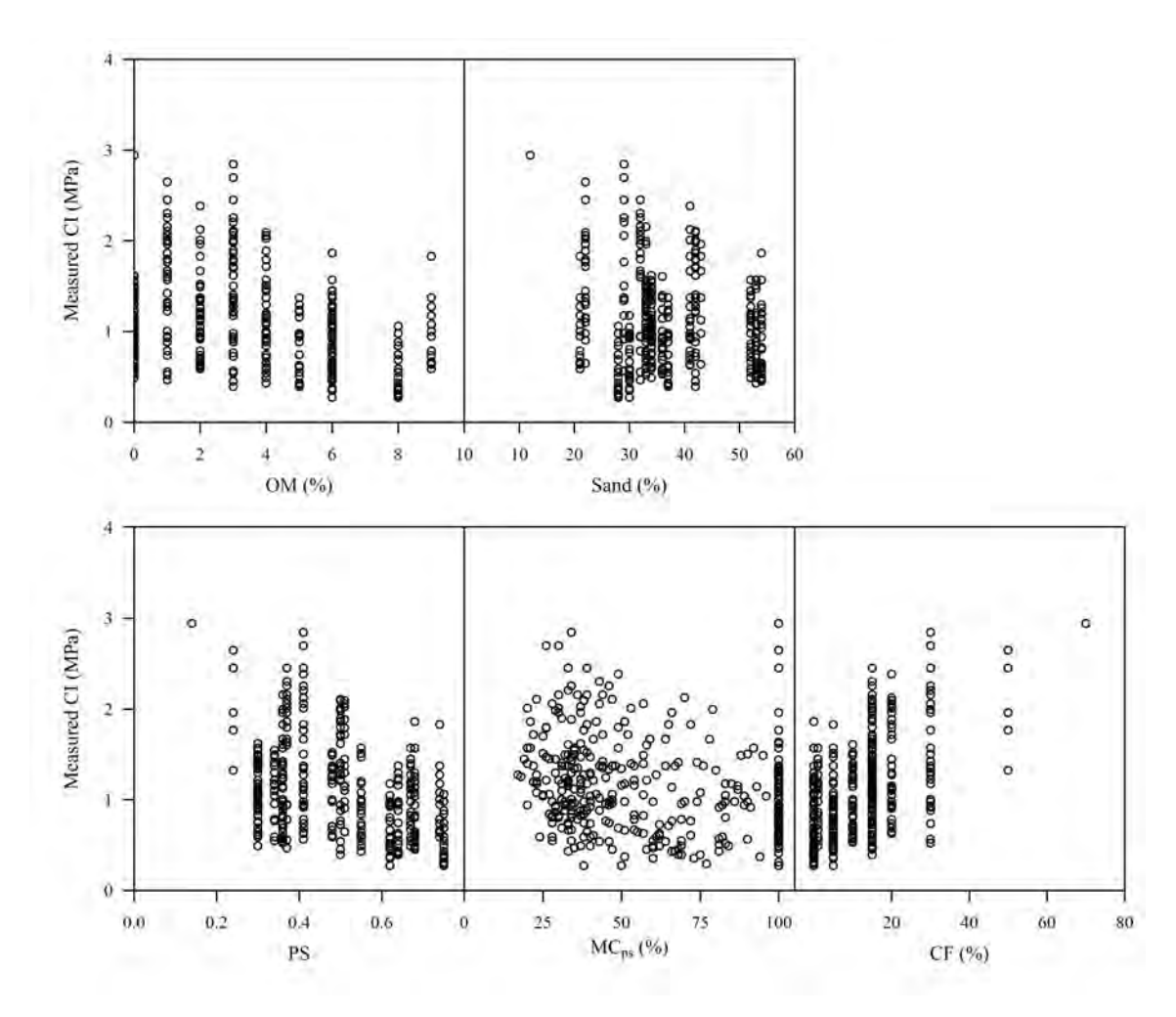


Figure 2.7: Plotting plot-by-plot measured CI vs. OM, Sand, PS, MC_{PS}, and CF, showing PS, MC_{PS}, and CF as stronger CI predictor variables than OM and Sand.

Table 2.5: Correlation matrix for plot- and layer-determined CI, OM, Sand, CF and ForHyM-estimated D_b , MC_V , MC_{PS} .

Variables	CI	MC _{PS}	MC _V	SP	CF	Sand	D _b	ОМ
CI	1							
MC _{PS}	-0.26	1						
MC_V	-0.52	0.72	1					
SP	-0.39	-0.37	0.32	1				
CF	0.55	0.35	-0.18	-0.74	1			
Sand	-0.16	-0.30	-0.20	0.21	-0.42	1		
D_b	0.39	0.36	-0.32	-1	0.73	-0.20	1	
ОМ	-0.31	-0.31	0.35	0.96	-0.59	0.07	-0.97	1

Table 2.6: Factor analysis of Table 2.5

Parameters	Factor 1	Factor 2	Factor 3
CI	0.72	0.75	-0.02
MC_{PS}	0.18	-0.88	-0.26
SP	-0.92	0.11	-0.09
CF	0.86	0.03	-0.23
Sand	0	0.15	1.00

fitted multiple regression result for all soil layers and locations combined:

$$log_{10}CI = 0.26 - 0.29 \times PS - 0.41 \times MC_{PS} + 1.04 \times CF$$

$$R^{2} = 0.54, RMSE = 0.36, MAE = 0.29$$
(2.10)

This result is illustrated in **Figure 2.8** by way of the 3D plots, which reveal moderate CI increase with decreasing MC_{PS} and a rapid CI increase with increasing CF. In reality, CI and soil strength should decrease again as MC_{PS} drop towards zero as the soil becomes more brittle due to reduce particle-to-particle hydrogen-bonding at low MC (Manuwa, 2012).

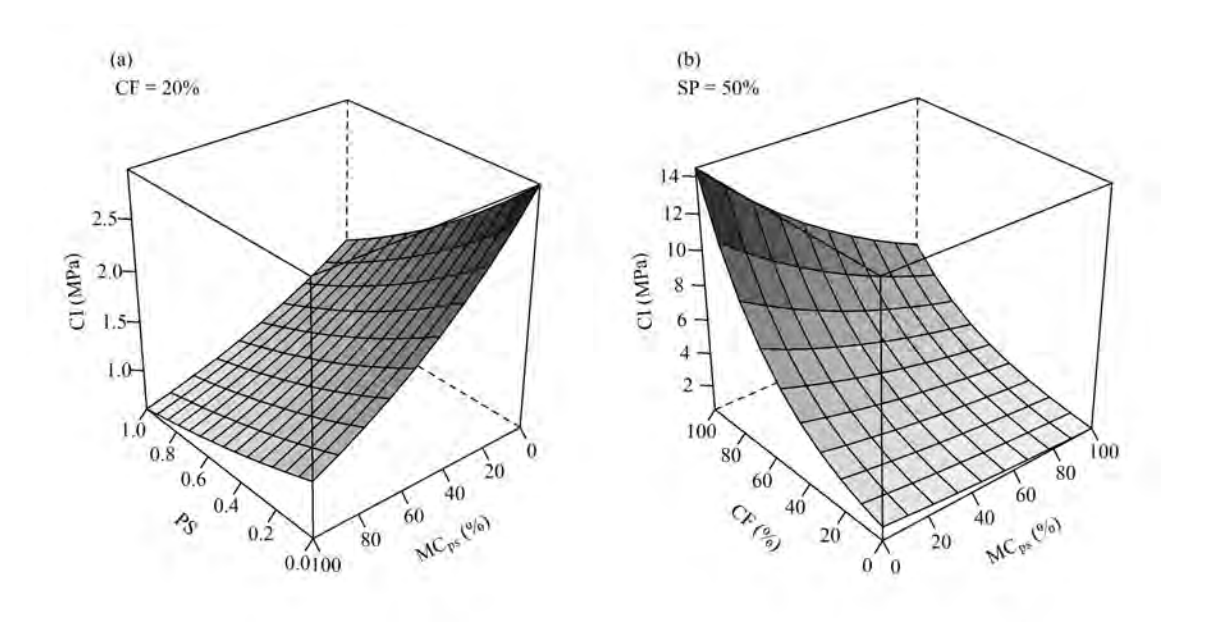


Figure 2.8: Modelled CI (Eq. 2.10) in relation (a) to MC_{PS} and PS at CF = 20%, and (b) to CF and MC_{PS} at SP = 20%.

While Sand and OM are important water retention and porosity predictor variables (Hausenbuilder, 1978; Krzic *et al.*, 2004), including them as part of the multiple regression process did not significantly improve the best-fitted results, likely due to the significant correlations between OM and PS and between Sand and CF in **Table 2.5**. However, adding the sampling locations to the predictor variables (each location within the data set coded 1 and 0 where applicable,

else 0) improved the best-fitted result as follows:

$$log_{10}CI = 0.44 - 0.50 \times PS - 0.39 \times MC_{PS} + 0.69 \times CF - 0.09 \times SM$$

 $R^2 = 0.60; RMSE = 0.33, MAE = 0.27$ (2.11)

This means that the CI values at the SM plots are, on average, slightly lower than at the other locations. This difference may be related to unaccounted difference pertaining to, e.g., CF size (generally smaller than at the other two locations), and differences in rooting pattern.

Repeating this analysis by location and by soil depth produced the best-fitted results listed in **Table 2.7**. From this, it can be noted that R^2 remained about the same by location, varying only from 0.41 (SM) to 0.66 (UNB), but decreased with increasing soil depth from 0.6 at the top to 0.1 at 60 cm soil depth. This decrease would mostly be due to the location-by-location D_b , MC and CF differences. This is because (i) the ForHyM-generated MC estimates already take the effect of CF on MC_{PS} into account, and (ii) the CI readings become increasingly erratic when pushed through soils with increasing CF content.

Table 2.7: Linear regression results for measured vs. modelled CI by depth and location.

Parameter	n	Intercept (SE)	Coefficient (SE)	t- value	p- value	Adj. R ²	RMSE	MAE
All depths	380	0.01 (±0.05)	1.04 (±0.04)	23.13	< 0.001	0.58	0.34	0.27
15 cm	119	0.04 (±0.08)	1.05 (±0.09)	11.36	< 0.001	0.52	0.29	0.24
30 cm	114	-0.06 (±0.09)	1.05 (±0.08)	13.92	< 0.001	0.63	0.34	0.28
45 cm	90	-0.21 (±0.12)	$1.25~(\pm 0.10)$	12.75	< 0.001	0.64	0.35	0.28
60 cm	58	0.53 (±0.19)	0.56 (±0.16)	3.45	0.001	0.16	0.32	0.27
SM	167	0.23 (±0.07)	0.77 (±0.07)	10.72	< 0.001	0.41	0.27	0.23
Odell Park	145	-0.47 (±0.13)	1.51 (±0.12)	12.76	< 0.001	0.53	0.35	0.27
UNB	69	0.01 (±0.01)	1.02 (±0.09)	11.59	<0.001	0.66	0.38	0.31

The dependency of CI data on soil PS, MC, and CF content was further evaluated through multiple regression analysis based on literature-generated CI formulations (**Table 2.8**). The results of so doing indicated that (i) Eq. 2.10 provides the best data representation overall, (ii) the linear formulations for CI are somewhat weaker than the logarithmic formulations. Also, (iii) soil porosity (or density) and MC are the more persistent and significant CI predictor variables than either sand or CF content alone.

Table 2.8: Review of functional relationship between CI and soil properties.

#	Ea	Coefficient Parameters					Adj.	RMSE	MAE	
π 	Eq.	а	b	С	d	е	f	R ²	KIVIJL	IVIAL
1	$log_{10}CI = a + bPS$ + cMC _{PS} + cCF	0.26 (±0.05)	-0.29 (±0.07)	-0.40 (±0.03)	1.04 (±0.10)			0.52	0.36	0.29
2	$log_{10}Cl = a + bPS$ + cMC _{PS} + dS	0.74 (±0.05)	-0.78 (±0.06)	-0.40 (±0.03)	-0.31 (±0.09)			0.36	0.42	0.34
3	$log_{10}CI = a + bPS$ + cMC _{PS}	0.62 (±0.04)	-0.80 (±0.06)	-0.37 (±0.03)				0.33	0.43	0.34
4	$CI = a+b MC_V + cS + dD_b$	2.26 (±0.13)	-2.21 (±0.17)	-1.50 (±0.24)	-0.001 (±0.01)			0.33	0.42	0.34
5	$log_{10}Cl = a + bMC_V + cD_b$	0.04 (±0.04)	-0.73 (±0.07)	0.12 (±0.02)				0.35	0.21	0.16
6	$CI = a + bMC +$ $cD_b + dMC_G^2 +$ $eD_b^2 + fMC_gD_b$	0.92 (±0.43)	-3.44 (±1.62)	1.20 (±0.46)	3.89 (±1.47)	-0.26 (±0.14)	-0.85 (±0.64)	0.39	0.42	0.33

^{1:} this study; 2: (Vega-Nieva et al., 2009); 3: (Campbell et al., 2013); 4: (Kumar et al., 2012)

2.3.3 Predicting potential ATV-caused soil rutting depth

ForHyM was used to transform the MC_{PS} and CI projections over time into likely ATV-generated rut depths April 2013 to April 2017, using the average top 15 cm PS and CF values and Eqs. 2.5, 2.6, and 2.10, for the two plots at the three sampling locations. The results are represented by the time-series plot in **Figure**

^{5: (}Meek, 1996) 6: (Busscher and Sojka, 1987)

2.9. As to be expected, deepest ruts would be incurred during the spring and fall, with minor blips during summer. Ruts could also be incurred during winter when some of the frozen soils would thaw due to interim warm weather and upward geothermal heat flow underneath the heat-insulating snow accumulation (Šušnjar *et al.*, 2006). While trafficability advisories due to wet soil conditions exist from fall to spring, such advisories are generally aimed at climate regional levels and therefore fall short in terms of being precise regarding the when and where.

The extent to which soil rutting would be seasonally affected across the general neighbourhood of each of the three location was ascertained through digitally generating the elevation-derived cartographic depth-to-water index (DTW) associated with 4, 1 and 0.25 ha upslope areas for streamflow initiation (Murphy et al., 2009b) (Figure 2.10). Using these patterns in combination with Eqs. 2.5 and 2.6 produced the spatial MC_{PS} and potential ATV-related rut depth maps in Figure 2.11, intended to be representative of the off-road soil trafficability conditions during spring, end of summer and the fall to winter transition. As shown, the UNB location has the potential to be the most trafficable among the three locations in the summer, but would be least during spring and fall. In contrast, the OP location would have the least traffic impact across the area and seasons based on texture-facilitated soil drainage. However, moderate soil rutting would occur within the 4-ha DTW<1 m zone at OP. Overall, the soil rutting conditions follow the sequences: dry weather: UNB <OP <SM; wet weather: OP <SM <UNB (Figure 2.9).

2.4 Discussion

This chapter describes ways and means by which the resistance of soils to cone penetration can be analyzed and modeled at the daily level year-round, over many years, and for the varying soil conditions by select locations. The results so obtained are - apart from study specific biases - generally consistent with what

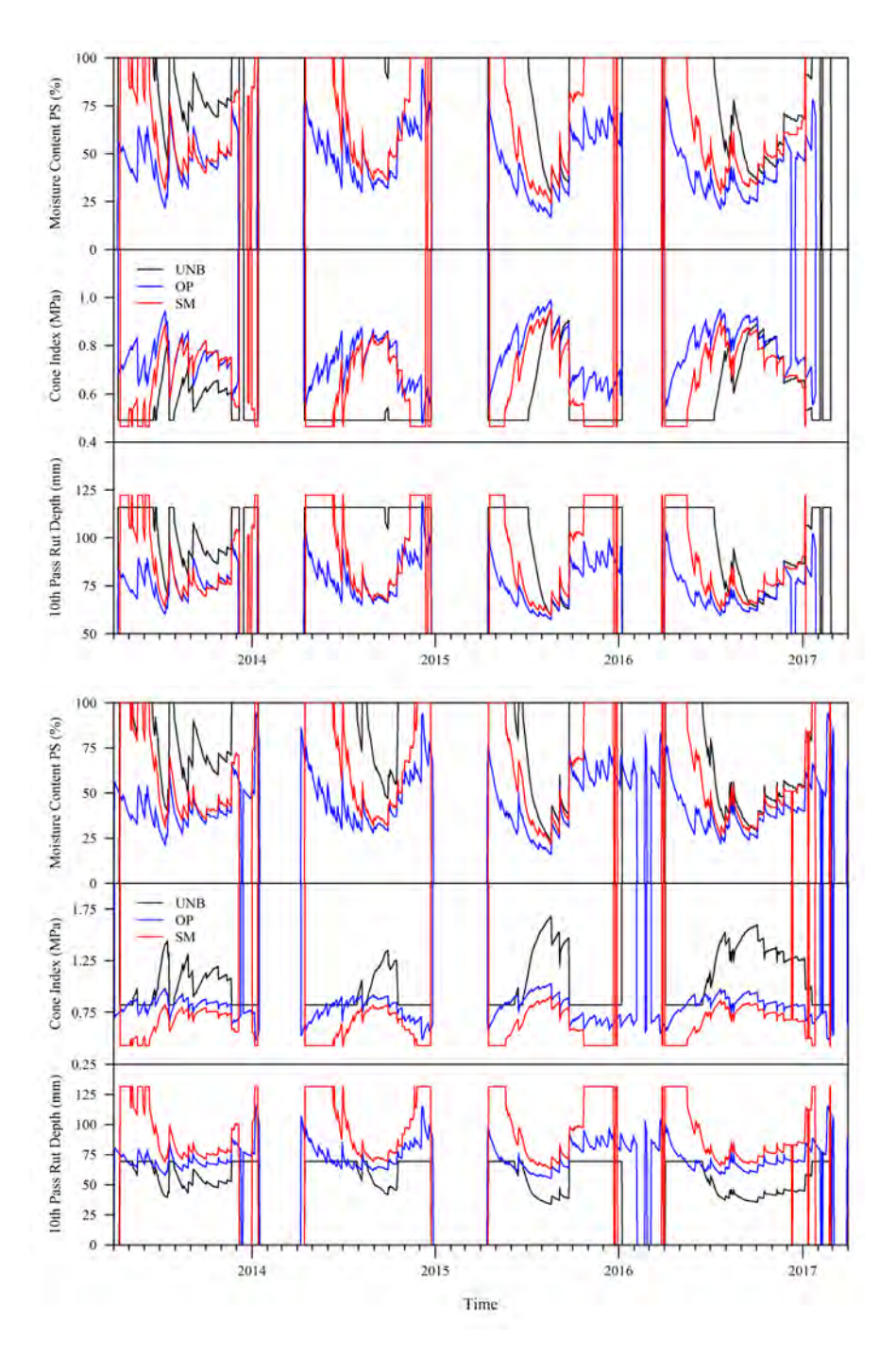


Figure 2.9: ForHyM-generated unfrozen MC_{PS}, CI, and rutting from April 2013 to April 2017 for the topsoil (top 15 cm of soil) for plot 1 (top) and plot 2 (bottom) at UNB, OP, and SM.

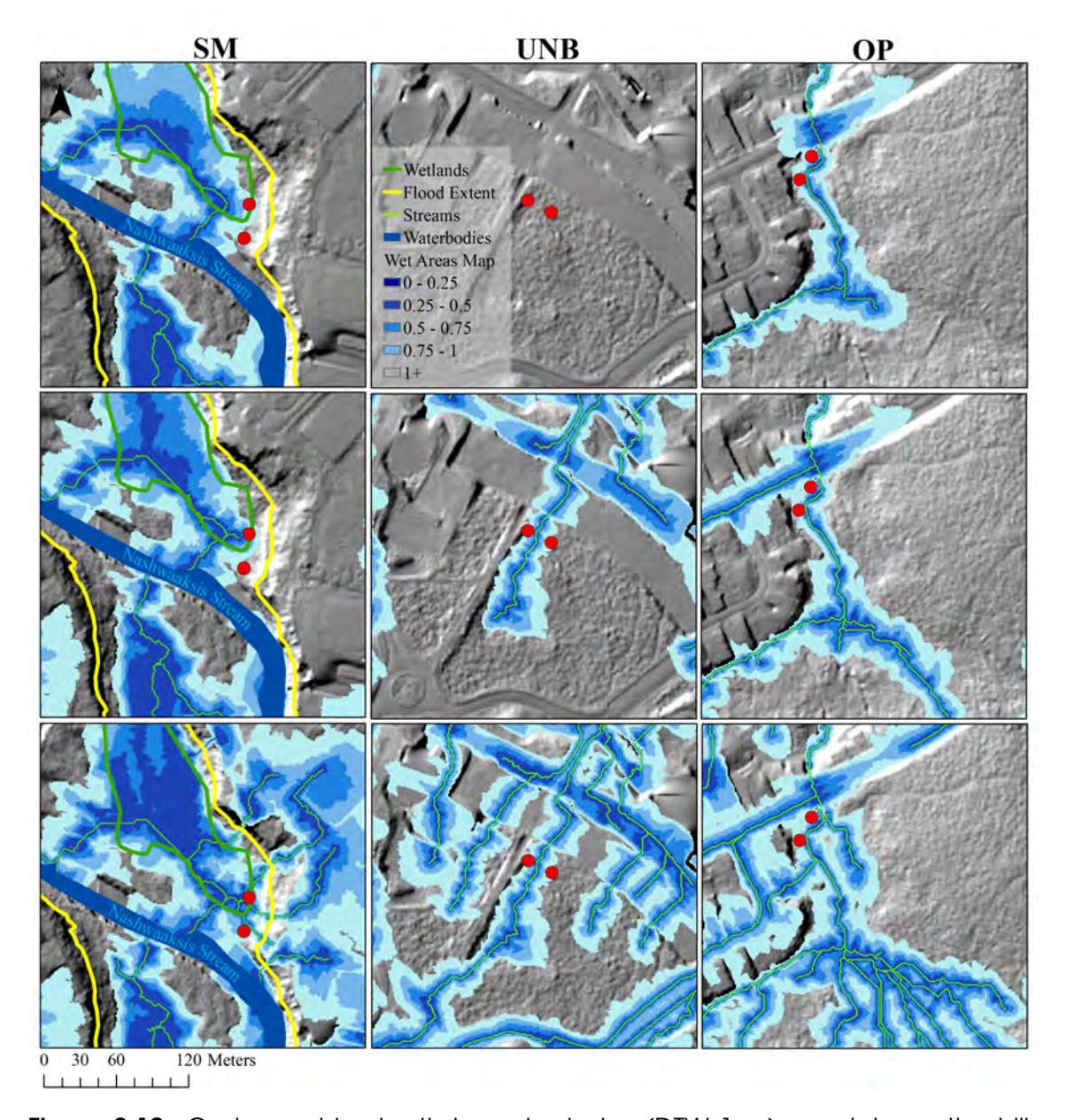


Figure 2.10: Cartographic depth-to-water index (DTW 1 m), overlain on the hill-shaded LiDAR-derived bare-earth digital elevation model for the UNB, OP, and SM locations for the end-of-summer (top), the spring-to-summer as well as fall-to-winter transitions (middle), and early-spring conditions, as emulated using upslope stream-flow initiation areas amounting to 4, 1 and 0.25 ha, respectively.

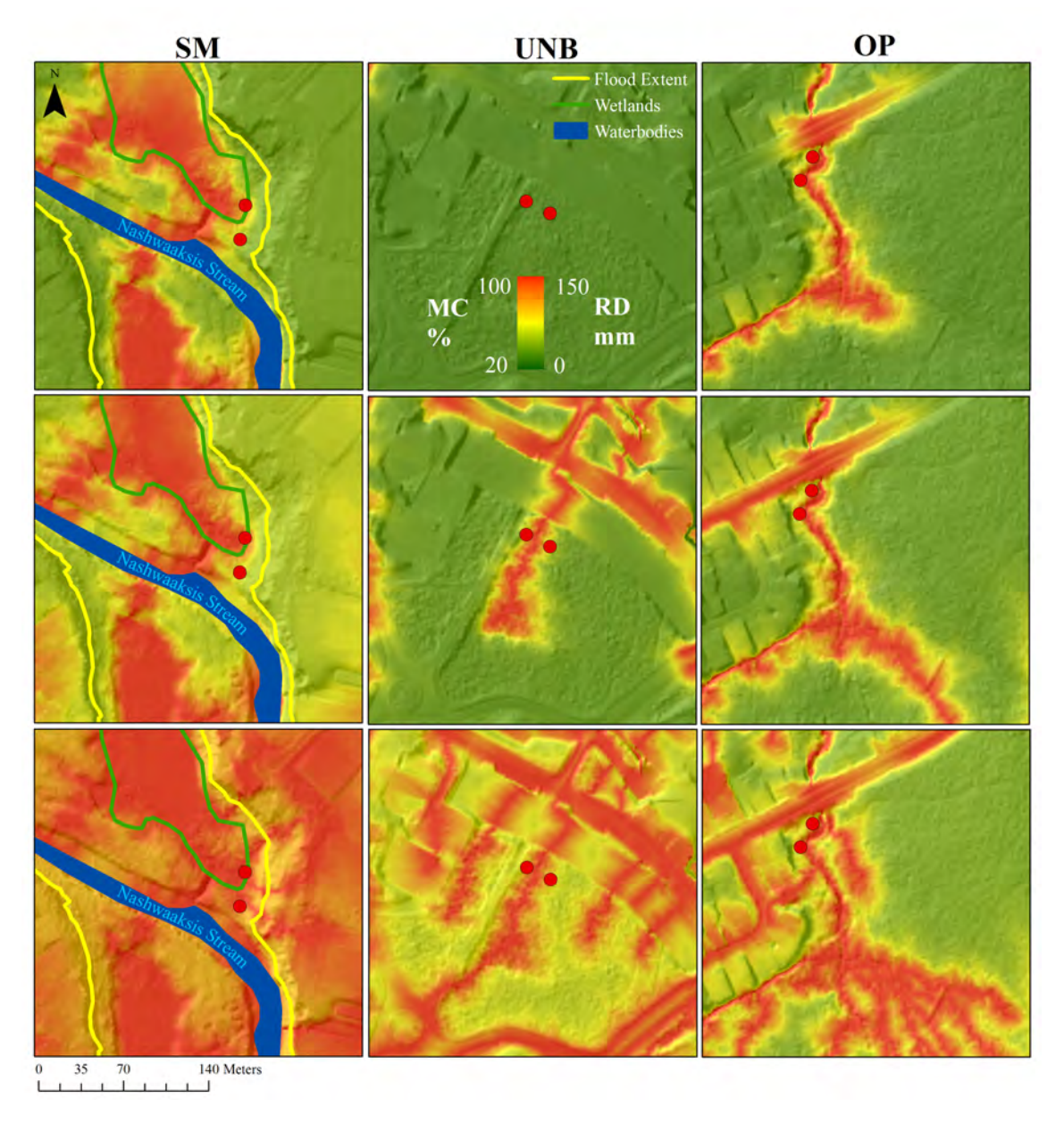


Figure 2.11: Soil MC_{PS} and rut depth interpretations of the season representative DTW patterns in **Figure 2.10**. Top: end-of summer. Middle: spring-to-summer and fall-to-winter transitions. Bottom: after the snowmelt season.

has been reported in the literature. These biases would inter alia refer to differences in CI methodology by, i.e., cone dimensions, speed of cone penetration, and field versus laboratory testing (Vega-Nieva *et al.*, 2009).

While the plot-by-plot determinations of this study are limited to three contrasting forest locations, they are at least representative of how MC, CI, and rutting depth can vary by soil properties, season and topographic position for the Fredericton region, as demonstrated through daily and spatial modeling. The extent to which this approach can be generalized requires additional research. For example, the spatial and DTW-dependent soil trafficability formulation for CI and rut depth should be tested across a wider range of glaciated landforms. Similarly, the meteorological data used in ForHyM is limited to the Fredericton airport weather station which is applied across all sites. For a better general understanding of weather impacts different meteorological parameters would be needed. For this study the data was limited to the single airport dataset which limits the extend of meteorological data on the model. Doing so would involve extending the above regression analyses across a wider range of independently varying soil types and properties. For example, where soils are cemented because of pedogenic Fe and Ca accumulations, the approach would need a cementation predictor variable. In some cases, the mix of the best-fitting regression variable and regression coefficients may also differ, as demonstrated above in, e.g., **Table 2.8**.

Key to applying the approach across time and landscapes is the ability to estimate how soil trafficability changes in direct response to spatially and temporally varying topo-pedo-hydrological conditions, meter-by-meter. Traditional soil survey maps can be helpful in this regard by only if the individual map units and borders conform to actual soil drainage contours. To this extent, further progress can be made by:

i. refining and adjusting each map unit to its landform- and DEM- defining

drainage position;

- ii. exploring how the trafficability affecting soil properties (MC, texture, CF, OM, $D_{\rm b}$, depth) vary across the landscape of interest from the highest to the lowest elevation points, and
- iii. determining the point of streamflow initiation inside each flow channel either through field observations or through DEM-based flow-initiation algorithms.

Together, these refinements would add further precision to the MC and rut depth maps in **Figure 2.11**. For example, there would be a noticeable difference between DTW, MC_{PS} and ATV rut depth projections within and outside the floodplain associated with the SM location.

Some progress towards these refinements has already been made in terms of checking existing trail conditions in terms of ATV-induced rutting extent, and by correlating this extent to the ridge-to-valley of the cartographic depth-to-water index (DTW; Murphy et al. (2009b)). The multi-pass implications on wood-forwarding rutting depth have been reported by Meek (1996) and were further evaluated by Vega-Nieva et al. (2009) by way of Eqs. 2.5 & 2.6. However, much more work needs to be done by not only addressing the DTW-emulated variations in soil wetness but also by addressing the changes in D_b, texture, CF and OM content as these would vary from ridge tops to valleys in a systematic manner. For example, upslope soils would generally be thinner and coarser with less OM than downslope soils. The reverse could occur in severely eroded medium-textured soils, with the more cohesive soil remains upslope and the more easily eroding sand and silt fractions accumulating downslope.

Since the above analysis is restricted to bare ground conditions and mineral soil layers, rut-reducing surface accumulations of snow, ice, forest litter, peat, and roots are not addressed. Bare-ground conditions, however, exist forested landscapes along non-paved roads, after ground-exposing operations such as root extractions, mounding and plowing, and underneath forest cover where litter accumulations are low or absent due to fast litter decomposition rates. The latter condition is more prevalent under hardwood and pine forests than under fir and spruce forests. Repeated recreational traffic in such areas under moist to wet weather conditions would induce significant rut-induced damage through trail braiding, soil erosion, gulley formation, and stream and lake sedimentation (Campbell *et al.*, 2013).

Also not addressed are the effects of snow and ice build-up on top of the soil during winter, which would increase the resistance to soil penetration, compaction, and rutting by increasing the soil bearing capacities. Since not all the water is frozen in sub-zero clay and OM-enriches soils, there could be problems associated winter-based soil rutting followed by instantaneous flash freezing. In summary, the above soil rutting assessment is only applicable for bare ground conditions. Soils covered by forest litter, slash, snow, and ice would obviously reduce rutting.

2.5 Concluding Remark

In summary, the above soil rutting assessment via manual testing of the temporal changes in the soil resistance to penetration is limited to the immediate area at and around the three sampling locations of this study. More research is needed to extend and test this research regarding general applicability. As shown, the approach taken would allow this by way of hydrological and digital elevation modeling, and further procurement of CI-relevant soil information.

2.6 Acknowledgments

This research was supported by a Collaborative Research Developement Project sponsored by J.D. Irving Limited, and the Natural Science and Engineering Council of Canada. Special thanks go to Doug Hiltz, Friedrich Wthrich, and Brittany Hartery for weekly field sampling.

Chapter 3

Track-monitoring and analyzing machine clearances during wood forwarding

Marie-France Jones, Mark Castonguay, Dirk Jaeger, and Paul Arp Faculty of Forestry and Environmental Management,
University of New Brunswick, Fredericton NB, Canada E3B 6C2

Email: arp2@unb.ca

Foreword:

The following chapter is a published article within the Open Journal of Forestry. It was submitted on April 1, 2018 and accepted for publication on June 29, 2018. Publication permission can be found in **Appendix B.1**.

Citation:

Jones, M.-F., Castonguay, M., Jaeger, D., Arp, P.A. (2018) Track-monitoring and analyzing machine clearances during wood forwarding. *Open Journal of Forestry*. 8, 1-28. doi.org/10.4236/ojf.2018.83020

Abstract

This chapter reports on track-monitoring and analyzing machine clearances during wood forwarding across seasons and weather, using ultrasonic distance sensors in combination with time-stamped GPS xy locations, at 10 sec intervals. The resulting data, obtained from 54 harvesting blocks, were analyzed by machine type (two wood forwarders and one grapple skidder), stand type (softwood plantation versus natural hardwood stands), month, slope, cartographic depth-to-water (DTW) classes, number of passes along track, and machine speed. For the most part, clearances were highly variable, due to passing over stumps, rocks, harvest slash, brush mats, ruts, and snow cover when This variability was on average greater for the lighter-weight wood forwarders than for the heavier-weight skidder, with the former mostly moving along equally spaced lines on brush mats, while the paths of the latter spread away from central wood-landing sites. In terms of trends, machines moved (i) more slowly on wet ground, (ii) faster during returning than forwarding, and (iii) fastest along wood-landing roads, as to be expected. Low clearances were most notable during winter on snow-covered ground, and on non-frozen shallow DTW and wet multiple-pass ground. During dry weather conditions, clearances also increased from low-pass tracks to multi-pass tracks due to repeat soil compaction of broadened tracks. These results are presented block-by-block and by machine type. Each block-based clearance frequency pattern was quantified through regression analysis and using a gamma probability distribution function.

Keywords

Wood forwarding, GPS tracks, clearance frequencies, number of passes, speed, ground conditions, depth-to-water (DTW)

3.1 Introduction

Modern wood forwarding operations require heavy machines to move across sensitive terrain and soil conditions. In this regard, improper timing by season and weather can lead to substantive soil compression and rutting across and along flow channels, across ridge tops, through depressions, and moist to wet soils. As soils become compacted and/or displaced, studies have shown that:

- i. soil porosity is reduced affecting the oxygen levels and gas distributions within the soil (Czyz, 2004; Berisso *et al.*, 2012);
- ii. increasing soil bulk density affects plant root distribution and decrease hydraulic conductivity thereby reducing plant available water while enhancing runoff and soil erosion (Horn *et al.*, 1995; Startsev and McNabb, 2000; Jamshidi *et al.*, 2008);
- iii. roots are damaged, facilitating root rot (Grigal, 2000; Kozlowski, 2008);
- iv. soil compaction has lasting effects on soil, with natural soil-structure recovery varying from a few years to decades (Prose, 1985; Brady and Weil, 2008; Ezzati *et al.*, 2012).

This chapter focuses on monitoring and examining machine-to-ground clearances in relation to number of passes, wood forwarding machine speed, and dry to wet ground conditions involving 54 harvest blocks in New Brunswick, Canada. For this purpose, two forwarders (JD 1110E and 1510E) and one grapple skidder (TC 635D) were equipped with ultrasonic distance sensors, and GPS data loggers. The wood-forwarding operations involved retrieving logs from clear cuts, shelter-wood cuts, and commercially thinned forest plantations. The thinning operations involved laying out brush mats used to reduce soil compression impacts (Labelle and Jaeger, 2012). The dry to wet variations in ground conditions were related to changing seasons and weather in time, and to topography across each harvest block by way of the cartographic

depth-to-water index (Murphy et al., 2011; White et al., 2012).

3.2 Methods

3.2.1 Site Description

This harvest-block study was spread across four ecoregions in New Brunswick, focusing on a North-western area near Saint-Quentin, and a mid-western area centralized near Juniper and Dorn Ridge, as described below (**Figure 3.1**). For this study, the areas were split into three groups - Northwestern uplands (NWU), Midwestern uplands (MWU), and lowlands (LL).

The NWU study area (elevation range 230 to 450 m) is located on the Chaleur uplands in northwest New Brunswick, north of Grand Falls and encompasses both the highlands and the northern part of the Southern Uplands ecoregion. The forest cover includes tolerant hardwoods, mixed woods and forest plantations (spruce species). Dominant tree species refer to sugar maple (Acer saccharum Marsh.), balsam fir (Abies balsamea L.), yellow birch (Betula alleghaniensis Britt.), red spruce (Picea rubens Sarg.), black spruce (Picea mariana Mill.) and white spruce (Picea glauca (Moench) Voss). Mean annual air temperature from 1990-2016 amounted to 3.6°C, with mean annual January and July air temperatures at -5.3°C and 12.5°C. Mean annual precipitation was 1140 mm, with 310 mm as snow Department of Environment and Climate Change Canada Black Brook is underlain by Ordovician-Silurian carbonates and (2016a).Ordovician-Silurian-Devonian deep-water clastics. The terrain varies from rolling to hummocky, interspersed by steeply incised valleys. Surficial deposits vary from residuals to stony ablation and loamy lodgement tills, glaciofluvial deposits (moraines, kames, eskers), and alluvium.

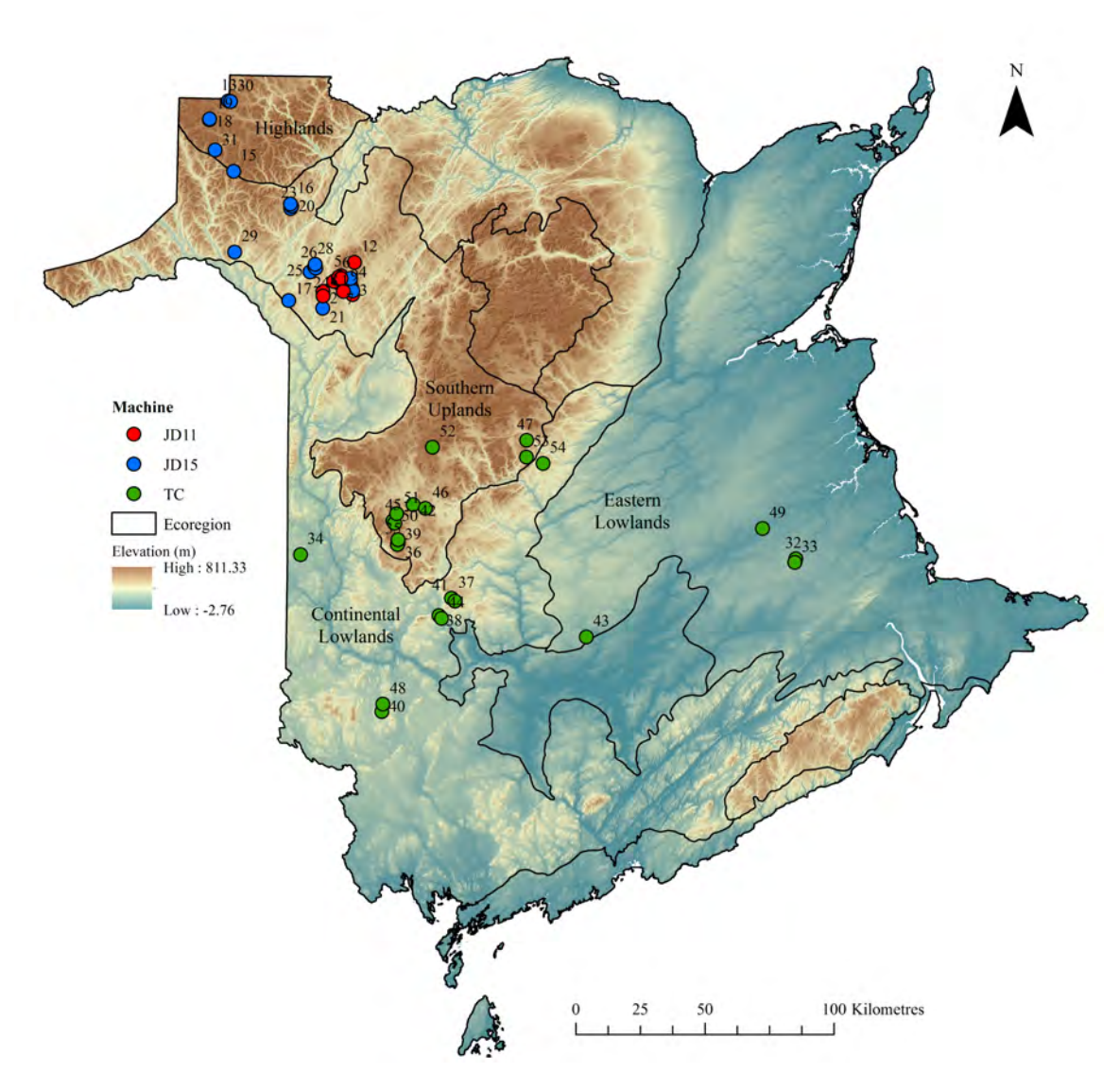


Figure 3.1: Map of New Brunswick showing elevations, ecoregions (GeoNB, 2018) and harvestblock locations with GPS-tracked clearances by wood-forwarding machine type (JD11, JD15, TC).

The MWU study range (elevations 250 to 580 m) is located in mid-western New Brunswick, near Juniper and encompasses the lower part of the Southern Uplands ecoregion. The forest cover consists of tolerant hardwoods with sugar maple and white birch (*Betula papyrifera* Marsh), mixed with balsam fir and black spruce, and interspersed by black and white spruce forest plantations. Mean annual air temperature from 1990-2016 amounted to 5.2°C, with mean annual January and July air temperatures at -3.5°C and 13.9°C. Mean annual precipitation was 1180 mm, with 280 mm as snow Department of Environment and Climate Change Canada (2016a).

The LL study range (elevations 120 to 290 m) is located around 50 km northwest of Fredericton and covers both the Continental Lowlands and Eastern Lowlands ecoregions. This area is predominantly covered by tolerant hardwoods consisting of yellow birch, beech (Fagus grandifolia Ehrh.), and sugar maple, mixed with balsam fir, Eastern white cedar (Thuja occidentalis L.) and black spruce. The mean annual air temperature from 1990-2016 amounted to 5.5°C, with mean annual January and July air temperatures at -2.8 and 13.8°C. Mean annual precipitation amounted to 1100 mm, with 250 mm as snow Department of Environment and Climate Change Canada (2016a). Both MWU and LL are located on the Miramichi Caledonia highlands at the northeast stretch of the Appalachian Mountain range. Surficial deposits on rolling to moderate terrain vary from bouldery loamy lodgement till to moraines, eskers, kames and sandy glaciofluvial outwash plains. Bedrock formations on LL mainly refer to Cambrian-Ordovician-Silurian deep-water clastics, and on MWU mainly Carboniferous to Silurian felsic to mafic extrusions.

3.2.2 Machinery and Sensory Installations

In NWU, two John Deere (JD) forwarders, i.e., model JD 1110E equipped with tire chains (referred to as JD11 below), and model JD 1510E with front and back tire

tracks (referred to as JD15 below) were used for tracking wood-forwarding machine clearances (Table 3.1, Figure 3.2). In MWU and LL, Tigercat model TC 635D grapple skidder (referred to as TC below) was used, with chained tires in front and tracked tires in the rear. Machine clearances were tracked using custom-built data loggers (c/o FPInnovations Ltd., Montreal, Canada, Figure 3.3) to record time-stamped GPS locations and machine-to-ground clearances during back and forth machine travel within up to 54 harvesting blocks from February 2012 through November 2014, all at time-stamped 10-second intervals. The dataloggers were installed within the operator cabs, with polycarbonate GPS antennas firmly attached to the cab roofs. Clearance tracking involved two ultrasonic sensors, each vertically placed in an open steel pipe welded or bolted to the least vulnerable position on the outside chassis of each machine, with sensor wires safely guided to the dataloggers. On the two forwarders, the ultrasonic sensors were mounted on the right and left of the chassis (145 cm for JD11 and 140 cm for JD15 from the ground up to sensor). On the TC, the sensors were mounted on the front and back of the chassis (170 cm and 152 cm from the ground to sensor, respectively). The sensors signalled machine clearances to ground, stumps, protruding rocks and brush piles directly below the sensors, adjacent to the tracks (Figure 3.4). Each sensor was calibrated to ensure sensor accuracy by testing distance to ground. No recalibration was done under the different seasons to account for variations in temperature which may introduce potential error to the sensor data.

Operations involved JD11 and JD15 wood forwarding from commercially thinned forest plantations in northwest NB, mostly centred on NWU, and TC wood forwarding from shelter-wood and clear-cutting operations in central west NB, mostly centered on MWU and LL. The commercial thinning operations involved laying out brush mats (Labelle, 2012). The shelter-wood and clearcutting operations proceeded on bare ground covered by organic forest floor accumulations about 5 to 10 cm thick. JD15 operations were clearance

monitored year-round, including operations on snow accumulations. The JD11 and TC operations were monitored spring to fall.



Figure 3.2: Sensors installed on the John Deere 1110E (top), John Deere 1510E (middle), and Tigercat 635D (bottom).





Figure 3.3: Ultrasonic distance sensor (left), datalogger box and inclinometer (right) installed in the Tigercat 635D.

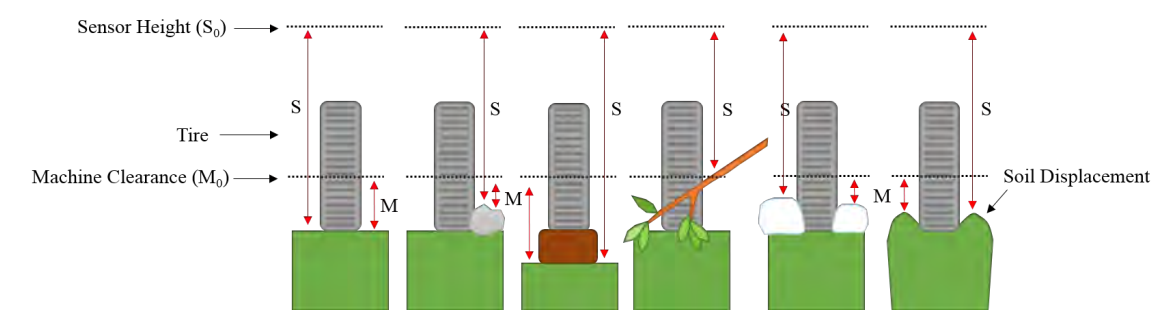


Figure 3.4: Various sensor distance measurements and error potential from the ultrasonic distance sensor. Left to right: rutting due to soil compaction, protruding rock, stump, branches and slash, soil displacement.

Table 3.1: Machine specifications.

Machine Specs	JD		JD	JD15		TC		
	Front	Rear	Front	Rear	Front	Rear		
Vehicle Weight (ton)	16	o.5	17	7.3	21.4			
Full Load Weight (ton)	11	.0	12	2.0	1	5		
Chassis Clearance, M ₀ (cm)	6	0	60	0.5	63	3.5		
Sensor-to solid-ground clearance, S ₀ (cm)	14	1 5	13	9.7	170.2	152.4		
Wheel Rim (cm)	67	' .3	67	7.3	81	.3		
Number of Wheels	4	4	4	4	2	4		
Tire Type	710/4	5-26.5	710/4	5-26.5	35.5Lx32	30.5Lx32		
Accessories	Chains	Tracks	Tracks	Tracks	Chains	Tracks		
Diameter (cm)	13	4.1	13	134.1		184.4		
Section Height (cm)	33.4		33.4		59.9	51.6		
Width (cm)	71	.1	7	71.1		77.5		
Pressure (max, psi)	32		32		32			
Foot print area (m²)	2.1	4.2	8	8.3		6.1		
Foot print pressure (atm) ^a	0.63	0.32	0.	0.34		0.24		
Soil compression (cm) ^a capacity (≈ plastic limit to remain the same with 1 pass); not fro	zen; bulk	density		· _			
10 passes	4-7 8-19	2-5 5-11		-16	10-22	2- 4 4-7		
100 passes	20-50	8-20		-45	20-62	4-7 7-16		
<u>.</u>								
Sensor Installation	26-0	ct-12	25-0	ct-12	14-M	ay-12		
Number of Data Points								
2012		,578		232,974		382,652		
2013	589	,146		,631	789,204			
2014		-	72,	72,065		778,562		

^a Derived from the above machine specifications, and using the methods described in Balland *et al.* (2008); Vega-Nieva *et al.* (2009); Jones and Arp (2017). ^b Fully loaded.

3.2.3 Data Production

The logged data generated over 4.1 million data points across 54 harvesting blocks (Table 3.2). Data due to sensor malfunction, fixed distance-to-ground obstructions, machine idling, or traveling on paved and unpaved roads were removed. The remaining data were entered to determine point-for-point machine elevation (M), direction, slope (m/m), and speed (m/sec) along each Data were catalogued for each forwarding (loaded) and returning track. (unloaded) pass towards the loading zones. The number of passes per same forwarding and returning track was also determined. All data were processed through ArcGIS, which also included determining track densities and number of passes per same track using point buffering (2.5 to equal 5 m width of machine) and overlapping tools (Buja, 2012). The data was averaged to the 90th percentile which helped to reduce the observations and increase processing time for the data analysis. The sensor-to-ground distance data (S) were normalized relative to the sensor-to-ground distance on solid ground measured at installation (S_0), referred to below as normalized sensor clearances (S/S_0), or normalized clearances for short. These numbers can be converted into actual machine clearances (M) by setting $M = S (S_0 - M_0)$, where M_0 is the machine-to-solid-ground (chassis) clearance (Table 3.1, Figure 3.4). Hence, at zero machine clearance (M = 0), S/S $_0$ = 1- M_0/S_0 . For tracks with S < S $_0$ - M_0 , machines bottoms would have sunk below the signal reflecting surface, as would be the case when the machines grind into wet soil or move across deep snow accumulations.

Table 3.2: Block description by machine, forest, operation and soil type, operation date, and ocular DTW % area coverage.

Machine	Block ID	Forest Type	Operation	Operation Date	DTW %
JD 1110E	1	SW-BS	CT	Jan-14	0.95
	2	SW-WS	CT	Apr-May/14	0.5

Continued on next page

Table 3.2 – Continued from previous page

Machine	Block ID	Forest Type	Operation	Operation Date	DTW %
	3	SW-WS	СТ	Aug-14	0.4
	4	SW-WS	CT	Aug-14	0.3
	5	SW-WS	CT	Nov-12	0.25
	6	SW-WS	CT	Mar-May/14	0.2
	7	SW-WS	CT	Aug-Sep/12	0.15
	8	SW-WS	CT	May-Jun/14	0.1
	9	SW-BS	CT	Jun-14	0.05
	10	SW-WS	CT	Jul-Aug/14	0.05
	11	SW-WS	CT	Jul-14	0.05
	12	SW-WS	CT	Dec-12	0.01
JD 1510E	13	SW-BF	CC	Nov-Dec/12	0.95
	14	SW-BS	CT	Jan-Feb/13	0.7
	15	MW-BF	SHW	Dec-12	0.6
	16	SW-SPBF	CC	May-14	0.5
	17	Unk	CT	Jan-Feb/13	0.4
	18	SW-BF	CC	Nov-Dec/12	0.4
	19	SW-BF	CC	Dec-12	0.4
	20	HW-WB	CC	Jun-14	0.25
	21	MX	CC	Jan-13	0.2
	22	SW-RP	CT	Oct-Nov/12	0.1
	23	HW-WB	SHW	Jun-14	0.1
	24	SW-BF	CT	May-June/14	0.1
	25	SW-BF	CT	May-June/14	0.1
	26	SW-BF	CT	Jun-14	0.1
	27	Unk	CT	Nov-12	0.05
	28	HW-SM	SHW	Jan-13	0.05
	29	HW-BI	SHW	Dec/12- Jan/13	0.05
	30	SW-BF	CC	Nov-Dec/13	0.05
	31	HW-BI	SHW	Nov-12	0.05
TC 635D	32	MX-PO	CC	Sep-14	0.75
	33	MX-PO	CC	Sep-14	0.75
	34	Unk	CC	Jul-Aug/13	0.7
	35	HW-MA	SHW	Jul-12	0.35
	36	HW-MA	SHW	Jul-12	0.35

Continued on next page

Table 3.2 - Continued from previous page

Machine	Block ID	Forest Type	Operation	Operation Date	DTW %
	37	HW-SM	SHW	Oct-14	0.25
	38	SW-NS	CC	Jul-13	0.2
	39	HW-MA	SHW	Jul-12	0.2
	40	Unk	CC	Jul-14	0.15
	41	HW-SM	SHW	Sep-Oct/14	0.15
	42	Unk	CC	Aug-13	0.15
	43	HW-BI	CC	Sep-14	0.1
	44	SW-NS	CC	Jun-13	0.1
	45	HW-MA	SHW	Aug-Sept/12	0.1
	46	HW-MA	SHW	Oct-Nov/13	0.1
	47	SW-RS	CT	Aug-13	0.1
	48	Unk	CC	Jun-Jul/14	0.05
	49	MX-PO	CC	Aug-Sep/14	0.05
	50	HW-MA	SHW	Sep-Oct/12	0.05
	51	SW-NS	CC	Aug-12	0.05
	52	Unk	SHW	Jun-14	0.05
	53	HW-BE	SHW	Jun-Aug/13	0.05
	54	HW-BE	SHW	Jun-13	0.05

3.2.4 DTW Delineation

Each data point was placed into its geospatial elevation context using digital elevation models (DEMs) and associated depth-to-water maps (DTW, **Figure 3.5**; Murphy *et al.* (2009a)). The DTW map delineates the extent of the least elevation rise next the nearest water bodies such as streams, rivers, and lakes (Murphy *et al.*, 2009a; White *et al.*, 2012). The DTW map, when derived for the end-of-summer water level for water bodies emulates soil drainage across the mapped areas from very poor (DTW < 10 cm), to poor (10 < DTW < 25 cm), imperfect (25 < DTW < 50 cm), moderate (50 < DTW < 100 cm), well (1 < DTW < 20 m) and excessive (DTW > 20m) (Murphy *et al.*, 2009a). The end-of-summer

DTW condition was emulated using 4 ha of upslope flow accumulation area for permanent stream flow initiation. For visualizing the varying DTW extent away from local flow channels by weather and season, ephemeral stream flow was initiated using 1 and 0.25 ha of upslope flow accumulation areas.

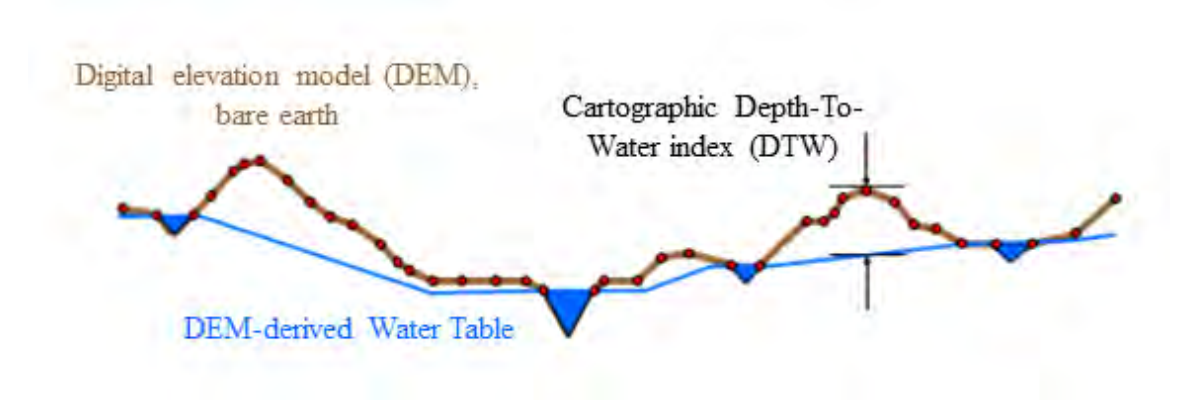


Figure 3.5: Cartographic depth-to-water index (DTW) diagram (Ogilvie, 2017).

3.2.5 Hydrological Modelling

For contextual evaluation purposes, daily temporal variations in upland soil moisture, snowpack depth and frost depth were simulated for the NWU and for the combined MWU and LL areas using weather records for daily precipitation (rain, snow) and air temperature (daily means) from September 2011 to end of 2014 from Edmundston and Fredericton weather stations (Department of Environment and Climate Change Canada, 2016a) (Appendix B.7 and B.8). Soil properties were set as follows: NWU = soil depth 1.5 m, loam to sandy loam, organic matter content 5-1%, coarse fragment content 20-30%; forest floor depth 10 cm; MWU = soil depth 1.20 m, sandy loam, organic matter content 1-10%, coarse fragment 25%, forest floor depth 5 cm. LL = soil depth 1.0 m, loamy sand, organic matter content 1-5%, coarse fragment 30%, forest floor depth 10 cm.

3.2.6 Data Processing

For geospatial visualization purposes, the individual data points per harvest block were mapped on top of the hill-shaded bare-earth DEM, with DTW drainage classes overlaid. The normalized clearance data were compiled into a single spreadsheet to enable the machine clearance analysis in relation to (i) month of harvesting, (ii) weather-induced soil wetness, (iii) machine speed, (iv) machine load, (v) back and forth track direction, (vi) number of passes, (vi) machine type, (vii) harvesting type (clearcutting, commercial thinning, shelter-wood cutting), (viii) slope, and (ix) DTW. This was done for each harvest block to allow for detailed per block analyses in terms of (i) histogram and frequency distribution assessment, and (ii) to determine how the clearance data were affected by pass number, machine speed, and by DTW classes.

3.2.7 Histogram and Frequency Distribution Assessment

The histograms for the normalized clearance data were clustered about 1, with values > 1 trailing off sharply, while values < 1 trailed off slowly towards 0, following a probability distribution function (pdf) given by (Devore, 1999):

$$pdf = \frac{1}{\Gamma(k)0^k} x^{k-1} e^{-x/0}$$
 (3.1)

where $x = (c_{max} - c)/f$, for which c_{max} is the maximum normalized clearance value (range of 0.2-0.6), $\Gamma(k)$ is the gamma function, k is its shape parameter, and and f are scale parameters for x and c, respectively. For the pdf non-linear least-squares fitting process, c_{max} , k, and f were used as adjustable parameters, with f kept in common across all blocks. Using Eq. 3.1 implies the following properties for $(c_{max} - c)/f$: mean = k, variance = k^2 , skewness = $2/k^{0.5}$, mode (for $k \ge 1$) = (k-1) (Devore, 1999). Hence, increasing k and implies widening the distribution function.

3.2.8 Multiple Regression Analysis

The normalized clearance data were summarized by way of a pivot table using the following class specifications:

- i. speed (m/sec);
- ii. number of passes (10, 20, 30, etc.);
- iii. DTW (1 = 0-0.5 m, 2 = 0.5-1 m, 3 = 1-2 m, 4 = 2-4 m, 5 = 4-8 m, 6 = 8-16 m, 7 = 16-32 m, 8 32 m);
- iv. forwarding (1) versus returning (0).

The data so assembled were examined using multivariate regression analysis, using the 1 normalized clearance data as dependent variables, and number of passes, speed, and DTW classes as independent variables, by harvest block. Other topographic derivatives were analyzed (elevation, slope, aspect), but were found to be insignificant in comparison to the machine parameters.

3.3 Results and Discussion

3.3.1 Wood-Forwarding Track Patterns

Figures 3.6-3.8 show the wood forwarding and end-of-summer drainage (DTW) patterns per harvest block, by machine type. As mapped, drainage varied in area by block from poor to imperfect (DTW $< 0.5 \, \text{m}$), and moderate (0.5 < DTW $< 1 \, \text{m}$) to well drained (DTW $> 1 \, \text{m}$). Within the DTW $< 0.5 \, \text{m}$ zone, soils were generally wet to moist. Within the 0.5 < DTW $< 2 \, \text{m}$ zone, soil wetness tends to be transitional from wet to dry depending on extent and weather-dependent upslope water seepage. Some of the main multiple-pass TC wood-forwarding

tracks straddled across these transitions, and were rutted extensively.

The average number of passes, as well as speed, and normalized clearance are listed in **Table 3.3**. Typically, machine clearance increased towards 1 with increasing pass numbers along the same track regardless of loading, however the lowest clearances are produced during the initial unloaded passes (**Figure 3.9**). Conversely, machine speeds were significantly faster when empty than when loaded. By machine type, wood forwarding speed was significantly lower for JD11 and JD15 than for TC while clearances increased with increasing machine speed, and especially so for JD11 (**Figure 3.9**).

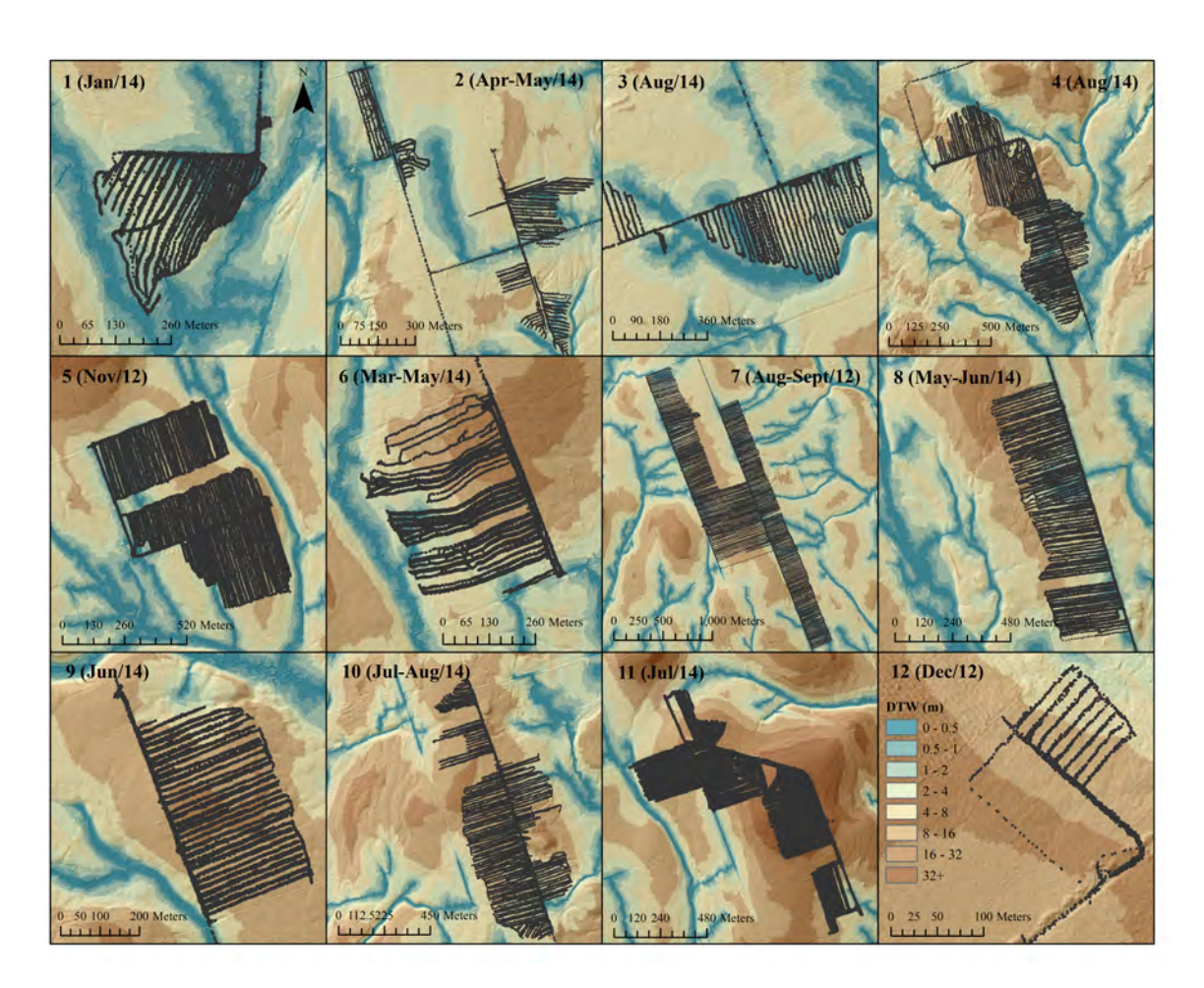


Figure 3.6: Composite of JD 1110E stands, including the point locations of the machines underlain by the 4 ha DTW map.

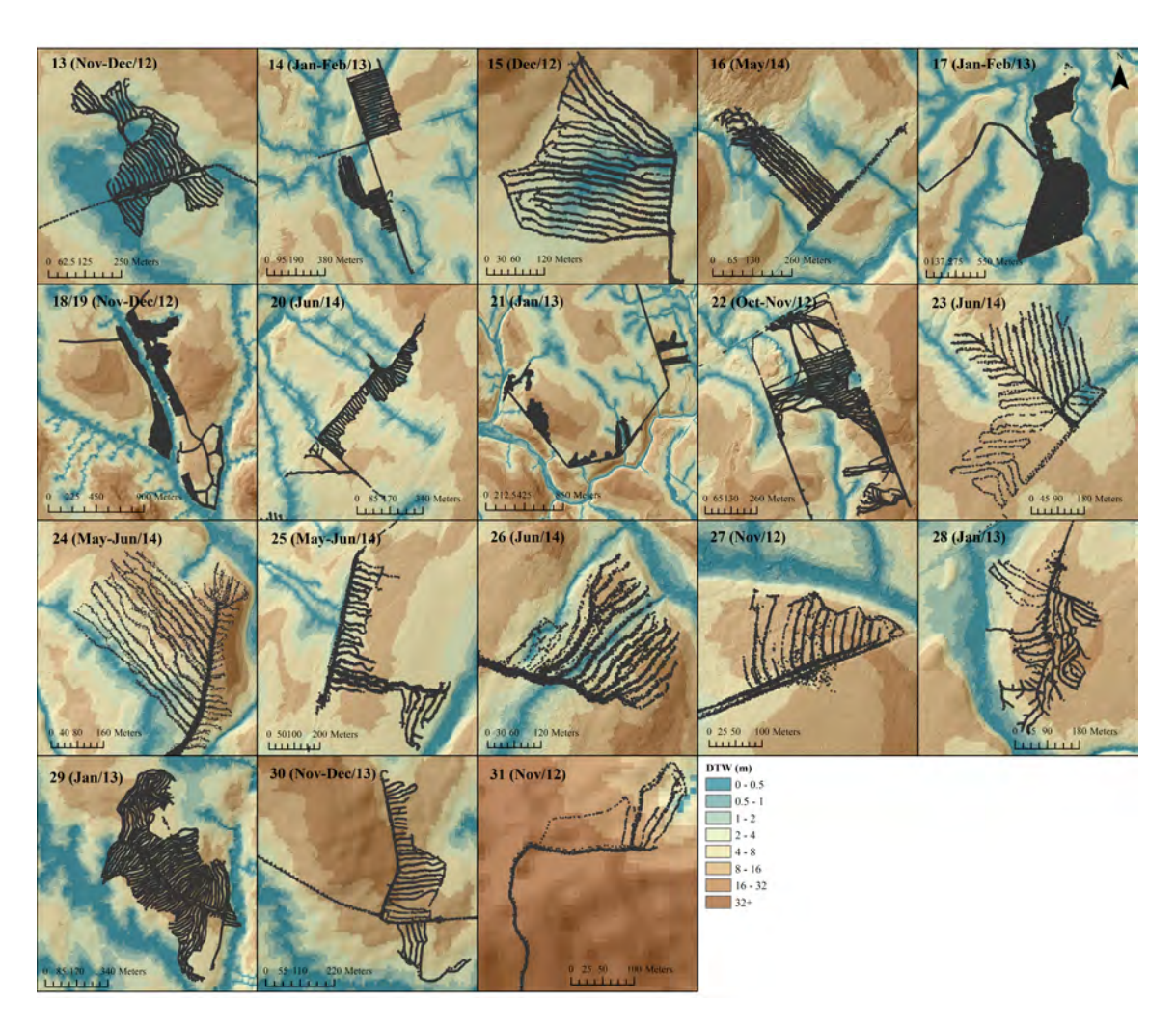


Figure 3.7: Composite of JD 1510E stands, including the point locations of the machines underlain by the 4 ha DTW map.

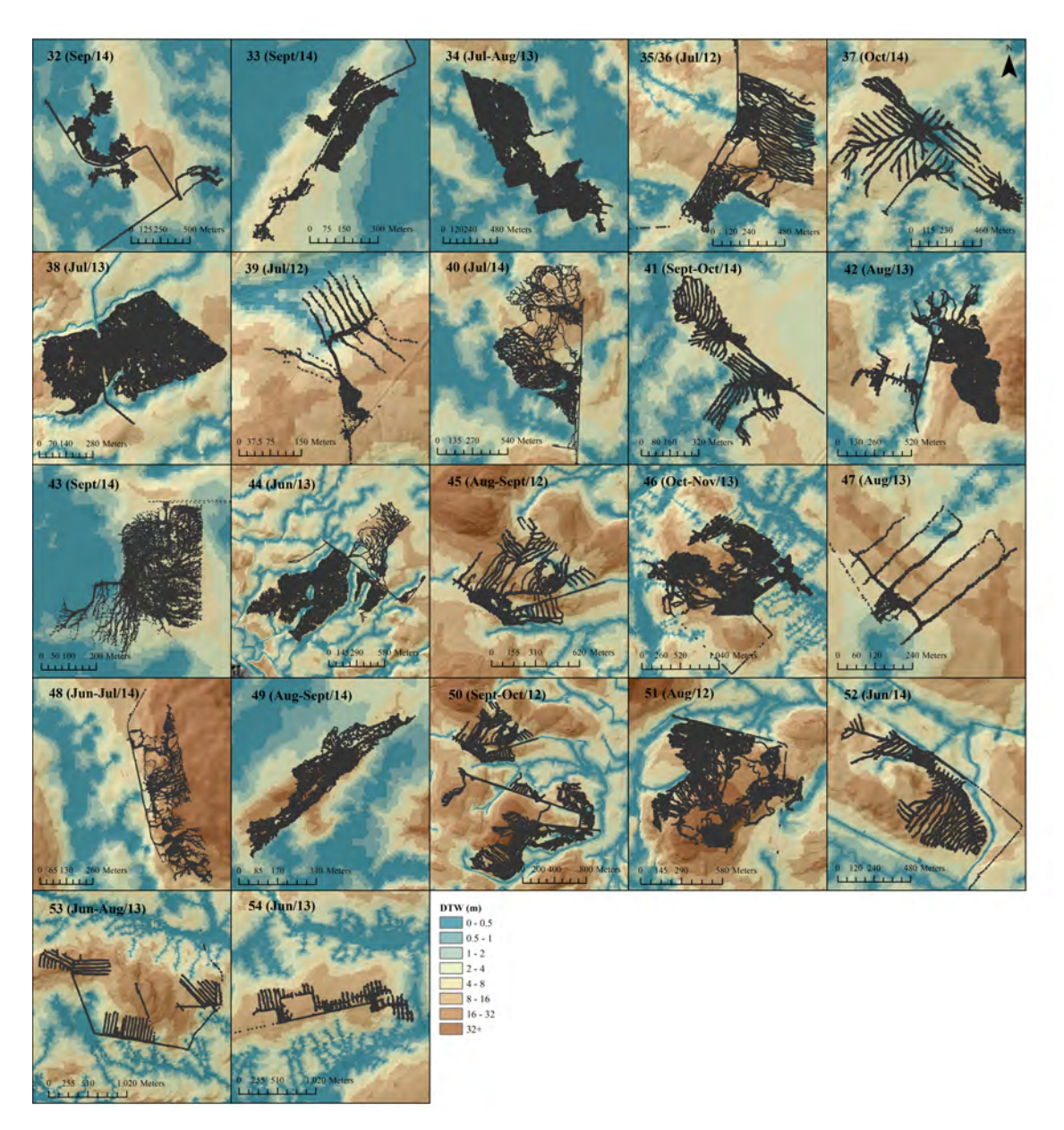


Figure 3.8: Composite of TC 635D stands, including the point locations of the machines underlain by the 4 ha DTW map.

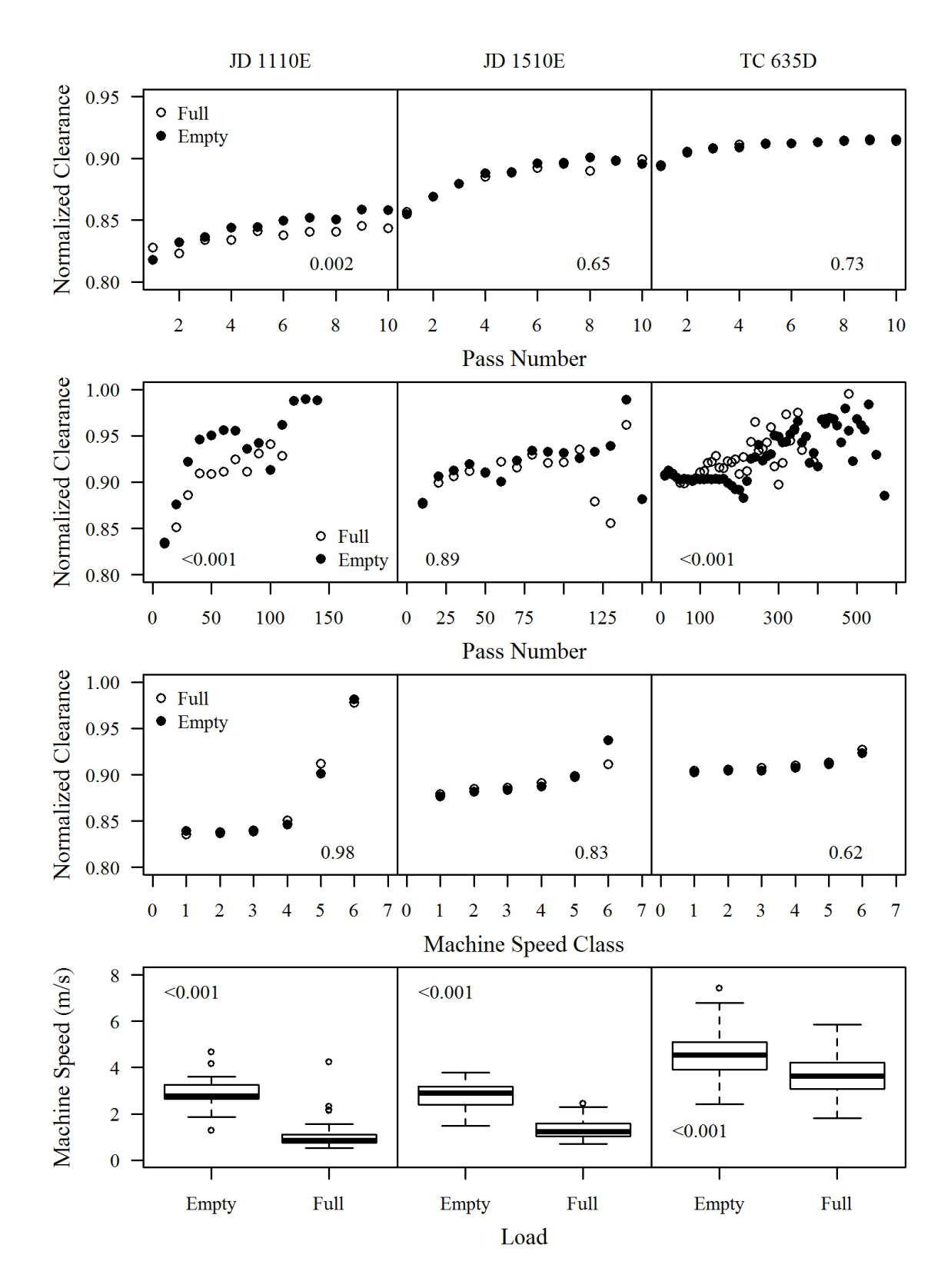


Figure 3.9: Mean machine specific normalized clearance versus number of passes (first 10 and all passes), empty vs. full loads, and machine speed versus empty or full loads.

Table 3.3: Variability in normalized clearance, number of passes, and speed by machine and operation type.

		JD11		JD15			TC	
		CT	CC	CT	SHW	CC	CT	SHW
	Mean	0.84	0.88	0.89	0.89	0.91	0.92	0.91
Normalized	SD	0.11	0.10	0.10	0.10	0.08	0.08	0.09
Clearance	Min	0.39	0.37	0.37	0.37	0.52	0.52	0.52
	Max	1.00	1.00	1.00	1.00	1.00	1.00	1.00
	Mean	7	11	12	8	28	10	29
Number of	SD	12	19	18	14	39	10	40
Passes (n)	Min	1	1	1	1	1	1	1
	Max	252	186	198	154	548	58	568
	Mean	1.7	2.14	2.17	1.92	3.96	4.03	4.7
Speed	SD	2.73	2.8	2.68	2.56	3.63	4.24	4.11
(m/s)	Min	0	0	0	0	0	0	0
	Max	24	24	23.17	23.17	24	23.65	23.98

CT: commercial thinning, CT: clearcut, SHW: shelterwood cut

3.3.2 Normalized Clearance Distribution Patterns

The histograms of the standardized clearances per block follow a left-skewed pattern, as shown in the Appendix (**Figures B.1**, **B.2**, and **B.3**). The corresponding Eq. 3.1 generated probability distributions are overlaid on these histograms, with corresponding best-fitted k, c_{max} and values listed in **Table 3.4**, by harvest block. Examining these values revealed that $log_{10}k$ correlates with such that

$$log_{10}k = (1.16 \pm 0.05) - (0.76 \pm 0.09) \times \theta$$

$$R^2 = 0.602$$
(3.2)

The combination of k and as in $log_{10}k$ correlates with c_{max} and machine type, i.e.:

$$log_{10}k\theta = -(1.7 \pm 0.2) - (1.7 \pm 0.2) \times c_{max} + (0.22 \pm 0.02) \times JD11$$

$$R^2 = 0.755$$
(3.3)

(JD11, JD15 and TC coded 1 when present, otherwise 0).

In general, increasing $k\theta$ values reflect a broadening of the clearance frequency distributions, and Eq. 3.3 implies that this broadening increases with increasing c_{max} , with further increases to be noted for the JD11 operations. This can be attributed to differences in machine operation, as follows:

- i. JD11 was mainly used for commercial thinning, which involved generating brush mats from tree delimbing and topping by single-grip harvesters along wood forwarding trails; the broadening of the clearance distributions would be due to the ultrasonic signals bouncing off machine-induced brush-mat sagging and lifting.
- ii. By machine type, the k product varied as flows: JD11 = 3.9 ± 0.4 , JD15 = 2.8 ± 0.1 ; TC = 2.5 ± 0.1 ; JD11 significantly higher than JD15 and TC, p-value < 0.001, and JD15 significantly higher than TC, p-value = 0.14.
- iii. Using the <10% tail of the standardized clearance marker produced the following sequence: JD11 = 0.67 \pm 0.02; JD15 = 0.80 \pm 0.02, TC = 0.84 \pm 0.01 (p-value <0.05). Hence, forwarding wood on brush mats produced longer standardized clearance trails towards zero-clearance than forwarding on bare ground. By Eq. 3.4, the 10th percentile clearances per block are directly relatable to the best-fitted Gamma distribution parameters as follows:

10th percentile clearances =
$$-(0.35\pm0.10)-(0.73\pm0.4)\times log_{10}k\theta$$
 + $(1.23\pm0.09)\times c_{\text{max}}$ (3.4)
$$R^2=0.892$$

iv. Trails for the shelterwood and clear-cut operations without brush mats had standardized clearance peaks at or near 1. Clearances greater than 1 are due to machine movements over stumps, rocks and uneven ground. The c_{max} ranges were similar by machine type, as follows: 1.04 < JD11 < 1.22;

Table 3.4: Best-fitted Eq. 3.1 and Eq. 3.5 regression results for the clearance frequency distributions and the normalized clearances ≤ 1 , by machine and block; speed, passes, and DTW coefficients x10-2; f = 0.122 ± 0.002 .

			Gamn	na Dist. Fur	nction (Eq.	3.1)	Nor	malized CI	earances <	≤1 (Eq. 3.5	5)
ID	n	10th Percen-		ameters (\pm	•	Adj.	Inter- cept		efficients (±		Adj.
		tile	γ (BS)	μ (Bx)	β (k)	R ²	(SE)	Speed	Passes	DTW	R ²
2	284	0.64	0.47 (0.08)	1.22 (0.05)	10.01 (2.94)	0.99	0.69 (0.02)	1.09 (0.21)	10.95 (1.72)	0.51 (0.22)	0.33
3	200	0.72	0.56 (0.08)	1.04 (0.02)	3.45 (0.75)	0.99	0.81 (0.07)	2.34 (0.15)		0.69 (0.15)	0.59
4	1750	0.66	0.53 (0.01)	1.13 (0.03)	6.58 (1.99)	0.99	0.72 (0.01)	1.68 (0.07)	10.35 (0.07)		0.40
7	1680	0.65	0.65 (0.05)	1.21 (0.03)	6.63 (0.91)	0.99	0.69 (0.01)	1.69 (0.11)	12.00 (0.81)	-0.53 (0.14)	0.21
8	1047	0.65	0.50 (0.13)	1.19 (0.60)	8.57 (3.54)	0.99	0.70 (0.01)	1.61 (0.12)	13.90 (0.66)	-0.91 (0.12)	0.40
9	366	0.63	0.50 (0.01)	1.19 (0.05)	9.06 (3.13)	0.99	0.71 (0.02)	1.04 (0.17)	19.77 (1.17)	-1.31 (0.32)	0.48
10	996	0.65	0.44 (0.14)	1.22 (0.05)	10.82 (5.09)	0.99	0.69 (0.01)	1.65 (0.09)	12.94 (0.58)	-0.20 (0.09)	0.52
11	1038	0.64	0.64 (0.12)	1.15 (0.03)	6.00 (1.46)	0.98	0.72 (0.01)	1.84 (0.10)	8.74 (0.45)		0.42
12	124	0.77	0.23 (0.01)	1.20 (0.01)	12.44 (0.79)	0.81	0.85 (0.02)			1.33 (0.51)	0.04
13	242	0.78	0.60 (0.04)	1.30 (0.02)	6.73 (0.68)	0.99	0.77 (0.02)		7.23 (1.04)	1.07 (0.27)	0.19
14	989	0.84	0.43 (0.01)	1.30 (0.01)	8.01 (0.01)	0.98	0.87 (0.01)		4.45 (0.62)		0.05
15	210	0.78	0.77 (0.12)	1.17 (0.02)	3.14 (0.62)	0.94	0.79 (0.02)	1.23 (0.20)	5.62 (0.96)		0.25
16	326	0.77	0.54 (0.04)	1.17 (0.01)	5.04 (0.60)	0.91	0.83 (0.02)	0.60 (0.19)	3.57 (1.32)		0.04
17	2550	0.81	0.57 (0.08)	1.25 (0.03)	5.36 (1.15)	0.99	0.83 (0.01)		5.61 (0.36)	0.18 (0.08)	0.09
18	96	0.78	0.71 (0.04)	1.25 (0.01)	4.44 (0.22)	0.94	0.94 (0.04)		-6.52 (2.96)		0.04
19	134	0.82	0.56 (0.02)	1.26 (0.01)	5.45 (0.21)	0.93	0.82 (0.01)	0.61 (0.21)	4.10 (1.22)	0.42 (0.19)	0.18
20	78	0.87	0.16 (0.01)	1.18 (0.01)	13.64 (0.41)	0.98	0.79 (0.03)	0.01 (0.01)		2.18 (0.49)	0.27
21	674	0.8	0.94 (0.09)	1.16 (0.01)	2.36 (0.25)	0.89	0.78 (0.01)	0.60 (0.12)	8.53 (0.75)		0.17
23	219	0.84	0.30 (0.05)	1.21 (0.02)	9.06 (2.08)	0.97	0.79 (0.02)		12.15 (1.65)		0.20
24	2146	0.77	0.49 (0.07)	1.14 (0.01)	4.81 (0.84)	0.98	0.92 (0.01)	0.30 (0.01)		-0.79 (0.11)	0.03
25	357	0.82	0.37 (0.06)	1.16 (0.02)	6.71 (1.41)	0.99	0.97 (0.02)	0.57 (0.17)	-2.87 (1.00)	-0.91 (0.34)	0.08
26	807	0.79	0.35 (0.04)	1.22 (0.01)	9.46 (0.38)	0.99	0.84 (0.01)	0.50 (0.13)	1.51 (0.61)	0.47 (0.12)	0.05
28	382	0.85	0.76 (0.04)	1.26 (0.01)	3.85 (0.33)	0.86	0.80 (0.01)		7.26 (0.86)		0.16

Continued on next page

Table 3.4 – Continued from previous page

			1			<u> </u>	orevious po				
			Gamn	na Dist. Fur	ction (Eq.	3.1)	Nor	malized Cl	earances <	≤1 (Eq. 3.5	5)
ID	n	10th Percen-		ameters (±		Adj.	Inter- cept		efficients (=		Adj. R ²
		tile	γ (BS)	μ (Bx)	β (k)	R ²	(SE)	Speed	Passes	DTW	
29	275	0.82	0.66 (0.11)	1.22 (0.01)	4.24 (0.45)	0.99	0.82 (0.01)		4.88 (0.70)	0.39 (0.18)	0.19
30	56	0.76	0.98 (0.01)	1.16 (0.01)	2.51 (0.29)	0.97	0.60 (0.04)	1.10 (0.38)	13.10 (3.40)	2.12 (0.48)	0.53
31	32	0.89	0.30 (0.01)	1.20 (0.01)	7.05 (0.27)	0.97	0.71 (0.03)		7.83 (3.20)	2.02 (0.36)	0.66
32	496	0.71	0.97 (0.05)	1.17 (0.01)	3.30 (0.01)	0.95	0.87 (0.01)	-0.36 (0.15)	-6.86 (0.71)	2.31 (0.19)	0.40
33	282	0.74	0.58 (0.04)	1.26 (0.01)	6.56 (0.43)	0.94	0.77 (0.02)	0.43 (0.21)	-3.70 (0.87)	3.64 (0.35)	0.30
34	306	0.87	0.40 (0.03)	1.19 (0.01)	5.25 (0.73)	0.98	0.96 (0.01)			-1.41 (0.21)	0.13
35	1300	0.7	0.51 (0.06)	1.16 (0.01)	4.33 (0.76)	0.94	0.80 (0.01)	0.60 (0.07)	6.78 (0.36)		0.25
36	1880	0.85	0.28 (0.04)	1.23 (0.02)	9.95 (2.08)	0.94	0.87 (0.01)	0.30 (0.07)	3.16 (0.27)		0.08
37	2264	0.79	0.47 (0.03)	1.20 (0.01)	6.05 (0.63)	0.99	0.94 (0.01)		-5.06 (0.34)	0.40 (0.11)	0.09
38	2881	0.85	0.38 (0.05)	1.27 (0.02)	8.18 (1.65)	0.98	0.83 (0.01)	0.17 (0.06)	1.51 (0.24)	1.21 (0.05)	0.17
39	586	0.92	0.21 (0.03)	1.21 (0.01)	10.64 (2.16)	0.99	0.88 (0.02)	0.23 (0.15)		0.81 (0.30)	0.01
40	734	0.88	0.31 (0.05)	1.24 (0.02)	8.76 (2.15)	0.99	0.91 (0.01)	0.24 (0.08)		0.30 (0.07)	0.04
41	2619	0.85	0.42 (0.12)	1.15 (0.03)	4.52 (1.90)	0.99	0.88 (0.01)	0.01 (0.01)	2.13 (0.23)		0.04
42	1362	0.87	0.40 (0.03)	1.20 (0.01)	5.83 (0.62)	0.98	0.86 (0.01)	0.13 (0.07)	2.24 (0.28)	0.42 (0.05)	0.08
43	246	0.78	0.35 (0.01)	1.28 (0.02)	10.83 (4.25)	0.98	0.83 (0.02)		-6.64 (1.13)	3.65 (0.23)	0.57
44	5867	0.84	0.44 (0.04)	1.19 (0.01)	5.45 (0.74)	0.99	0.85 (0.01)	0.08 (0.04)	2.90 (0.14)	0.55 (0.03)	0.11
45	4081	0.91	0.26 (0.01)	1.20 (0.01)	8.22 (0.58)	0.98	0.89 (0.01)	0.28 (0.04)	2.10 (0.17)	0.10 (0.04)	0.05
46	1205	0.85	0.27 (0.04)	1.29 (0.02)	12.42 (2.53)	0.97	0.87 (0.01)		2.47 (0.26)	0.19 (0.06)	0.07
47	87	0.91	0.36 (0.04)	1.20 (0.01)	5.59 (0.77)	0.97	0.88 (0.01)		4.41 (1.31)		0.11
48	274	0.82	0.40 (0.02)	1.24 (0.01)	7.64 (0.81)	0.98	1.00 (0.01)	0.72 (0.11)	1.65 (0.55)	-1.91 (0.14)	0.49
49	95	0.86	0.36 (0.01)	1.16 (0.01)	5.65 (0.42)	0.99	0.82 (0.02)		6.20 (1.47)	0.90 (0.40)	0.19
50	4028	0.89	0.31 (0.01)	1.17 (0.01)	6.18 (0.43)	0.99	0.90 (0.03)	0.42 (0.03)	1.22 (0.18)		0.04
51	3685	0.89	0.39 (0.05)	1.15 (0.01)	4.43 (0.65)	0.98	0.88 (0.01)	0.31 (0.03)	2.91 (0.17)	0.07 (0.03)	0.09
52	772	0.83	0.54 (0.09)	1.13 (0.01)	2.84 (0.61)	0.99	0.82 (0.01)		1.89 (0.43)	1.06 (0.10)	0.18
53	293	0.88	0.30 (0.05)	1.23 (0.02)	7.97 (1.76)	0.99	0.87 (0.01)		5.61 (0.78)	-0.36 (0.13)	0.15
54	597	0.79	0.47 (0.06)	1.20 (0.01)	5.68 (0.92)	0.99	0.89 (0.01)	0.29 (0.13)	-4.07 (0.58)	1.32 (0.14)	0.24

Continued on next page

Table 3.4 – Continued from previous page

			Gamm	na Dist. Fun	ction (Eq.	3.1)	No	rmalized Cl	earances <	1 (Eq. 3.5	5)
ID	n	10th Percen-	Par	ameters (\pm	SE)	Adj.	Inter- cept	Coe	efficients (\pm	SE)	Adj.
		tile	γ (BS)	μ (Bx)	β (k)	R ²	(SE)	Speed	Passes	DTW	R ²

3.3.3 Box Plots

The normalized data with clearances <1 are presented in Appendix B by way of box plots showing 10th, 25th, 50th, 75th and 90th normalized clearance percentiles and associated outliers per block and machine type by number of passes, speed and DTW classes (Figures B.4, B.5, and B.6 (Appendix B)). These plots show that machine clearances varied from block to block in relation by machine operations. For TC, these variations were in part attributable to the biweekly and June to November cumulative precipitation pattern from 2012 to 2014 (Figure 3.10), with lower clearances less prominent in the fall of 2012 following dry summer conditions, but more prominent in summer blocks where DTW < 1 m (Blocks 32, 35, 36; Figure B.6 (Appendix B)).

3.3.4 Normalized Clearance

Regressing the normalized clearances ≤ 1 values against number of passes, speed and DTW classes by way of

normalized clearance
$$\leq 1 = intercept + k_{pass} \times passes + \\ k_{speed} \times speed + k_{DTW} \times DTW$$
 (3.5)

produced the best-fitted interception and regression coefficient results also listed in **Table 3.4**, with R^2 values ranging from near 0 to 0.67. These results are summarized as follows:

i. Normalized clearances increased with increasing machine speed, with only

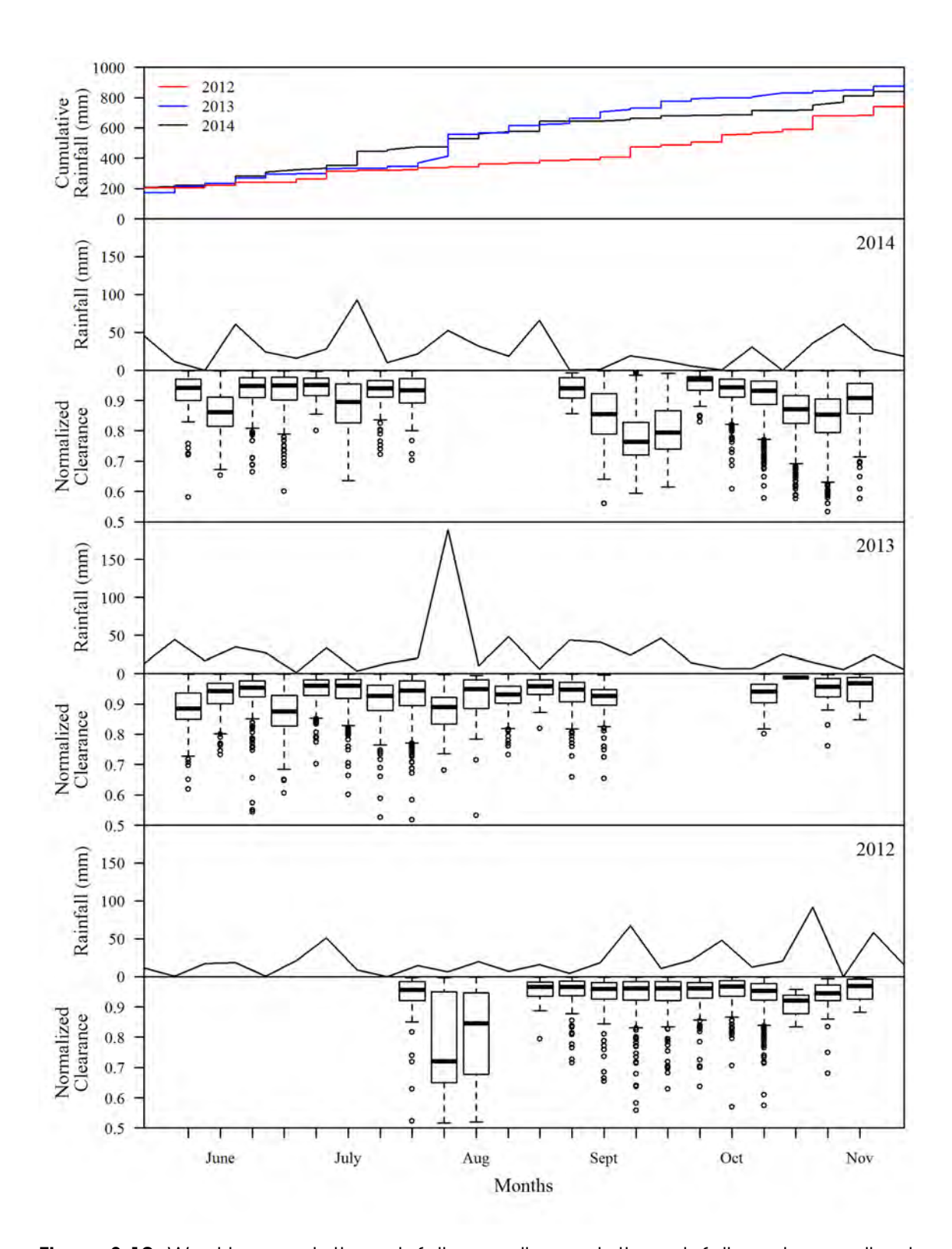


Figure 3.10: Weekly cumulative rainfall, overall cumulative rainfall, and normalized sensor clearance trends for the TC 635D during 2012-2014.

one reduction registered on a wet TC trail (block #32).

- ii. Increasing the number of wood-forwarding passes per track had mostly positive to no clearance effects, with two exceptions: on blocks #18 and #25. For the TC wood-skidding operations, increasing the pass numbers per track varied from mainly positive during dry conditions to negative during wet conditions, respectively.
- iii. The influence of DTW on TC clearances also varied from positive to negative. The positive trend occurred when the ground was dry due to increased soil resistance to compaction. The negative trend occurred when operating on wet ground during and after soil-saturating rain events, due to decreased soil resistance to compaction and tire slippage.

Analyzing the normalized clearance intercepts in **Table 3.4** in terms of their associated speed, number of passes and DTW regression coefficients generated the following multiple regression result:

clearance intercept =
$$(0.910\pm0.04)-(1.23\pm0.06)\times k_{pass}$$

$$-(0.041\pm0.005)\times k_{speed}-(0.052\pm0.003)\times k_{DTW} \tag{3.6}$$

$$R^2=0.946; RMSE=0.020$$

This equation implies that the normalized clearance intercept:

- i. is equal to 0.910 ± 0.04 , or 75 to 78% actual machine-to-ground clearances on average, when machine speed, number of passes and DTW have no clearance influence; in terms of actual depth, this number amounts to about 12 cm; a considerable part of this would be due to the compression of the organic forest floor accumulations;
- ii. decreases below 0.910 on dry to moist and wet soils with increasing number of passes and/or machine speed, this would be due to repeating soil compaction along the same track and increased shearing stress with increased tire rotation;

iii. decreases below 0.910 as the DTW-projected influence on soil resistance to compaction becomes stronger from very poor (where DTW is near 0) to well and excessive (where DTW is >1 m); i.e., a positive DTW influence causes the regression intercept to be lowest at DTW = 0; a negative DTW influence would do the opposite and may occur where DTW > 0 due to increased slope-induced wheel slippage.

Eq. 3.6 suggests that the lowest normalized intercept for class-averaged normal clearances ≤ 1 would amount to 0.910 -1.23 x ($k_{pass} = 0.19$) - 0.041 x ($k_{speed} = 2.34$) 0.052 x ($k_{DTW} = 3.65$) = 0.39. The lowest average normalized clearance intercept per number of pass, speed and DTW classes registered in **Table 3.4** was 0.60, for block #30 (JD15, Nov. 2012), i.e., approximately equal to chassis clearance, and this occurred on a well-drained soil (DTW > 2 m) following a rain event. The lowest non-averaged normalized signal-to-ground surface distance was 0.43, i.e., equivalent 60.1 cm, thereby amounting to 19.5 cm below the reflecting ground surface. This occurred on block #15 in January 2013 when the ground was covered with snow.

The correlation matrix in **Table 3.5** pertaining to the four Eq. 3.6 variables indicates that the influence of number of passes and machine speed on the clearance intercepts are positively correlated with one another, while both are negatively correlated to DTW clearance influence. Hence, DTW-influenced softening of the ground tends to decrease machine speed and reduces repeat traffic along the same track.

3.3.5 Block-Specific Examples

An example of low to extensive rutting is shown in **Figure 3.11** for TC block # 41 (Sept.-Oct. 2014), where soil conditions varied from dry to moist to wet due to season- and weather-induced variations in the local DTW pattern. Moderate soil

Table 3.5: Correlation matrix for the Eq. 3.6 variables and associated per block entries in **Table 3.4**

	Speed	Number of passes	DTW	Intercept
Speed	1			
Number of passes	0.495	1		
DTW	-0.262	-0.369	1	
Intercept	-0.547	-0.744	-0.26	1

n = 49

compression occurred along trails where soils remained dry at DTW > 1 m, with compression decreasing towards zero with increasing number of passes. On the landing site where DTW was < 0.5 m, soil ruts were deeper and number of passes per track increased up to 270. For the trail through transitional and somewhat sloped DTW zones, normalized clearances decreased with increasing number of passes per track. In general, the extent of soil compaction is highest at or near the plastic soil moisture limits, while soil displacement is highest at and above the liquid soil moisture limits.

The data for machine clearance, number of passes per track and speed are illustrated in **Figure 3.12** for harvest blocks 10, 32, 33, 43. The mapped dots so shown demonstrate the following effects:

- Normalised clearances along the central wood forwarding road in block 10 approach 1 at high track numbers and speed.
- ii. Rutting as indicated by persistently low clearances occur along the most frequently used TC skidding passes as shown for blocks 43, 32, and 33; elsewhere, TC clearances tend to be near 1. In contrast, the JD11 clearances along brush-matted wood forwarding tracks are lower due to brush-mat flexing.
- iii. TC machine track speeds vary more than JD11 track speeds, with TC being faster on higher DTW ground. JD11 speeds are consistently slower along the

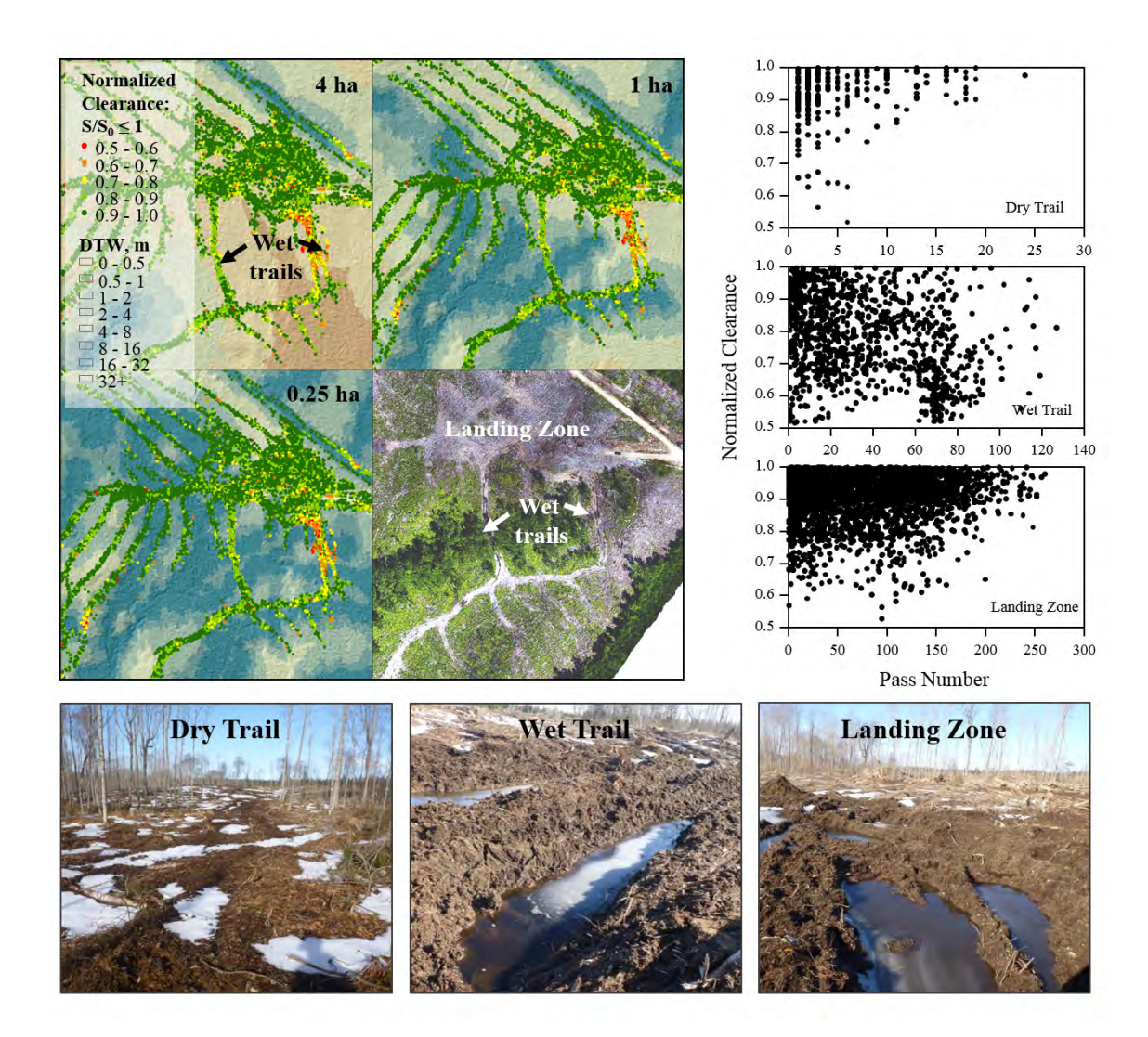


Figure 3.11: Top left panel: TC block #41 showing weather-affected DEM-derived DTW patterns based on assuming 4 ha (top-left), 1 ha (top-right) and 0.25 ha (bottom-left) of upslope flow accumulation area for flow initiation. The high-resolution surface image (bottom-right) shows ruts with low machine clearances along high multiple-pass connector trails. **Top right panel**: block 41 normalized clearance versus increasing number of passes along dry and wet forwarding trails and on landing site. **Bottom**: dry trail (no rutting), wet trail (deep rutting), and landing site (braided rutting) images. Normalized clearance in terms of chassis- to sensor-to solid-ground distances (front): $M_0/S_0 = 0.63$.

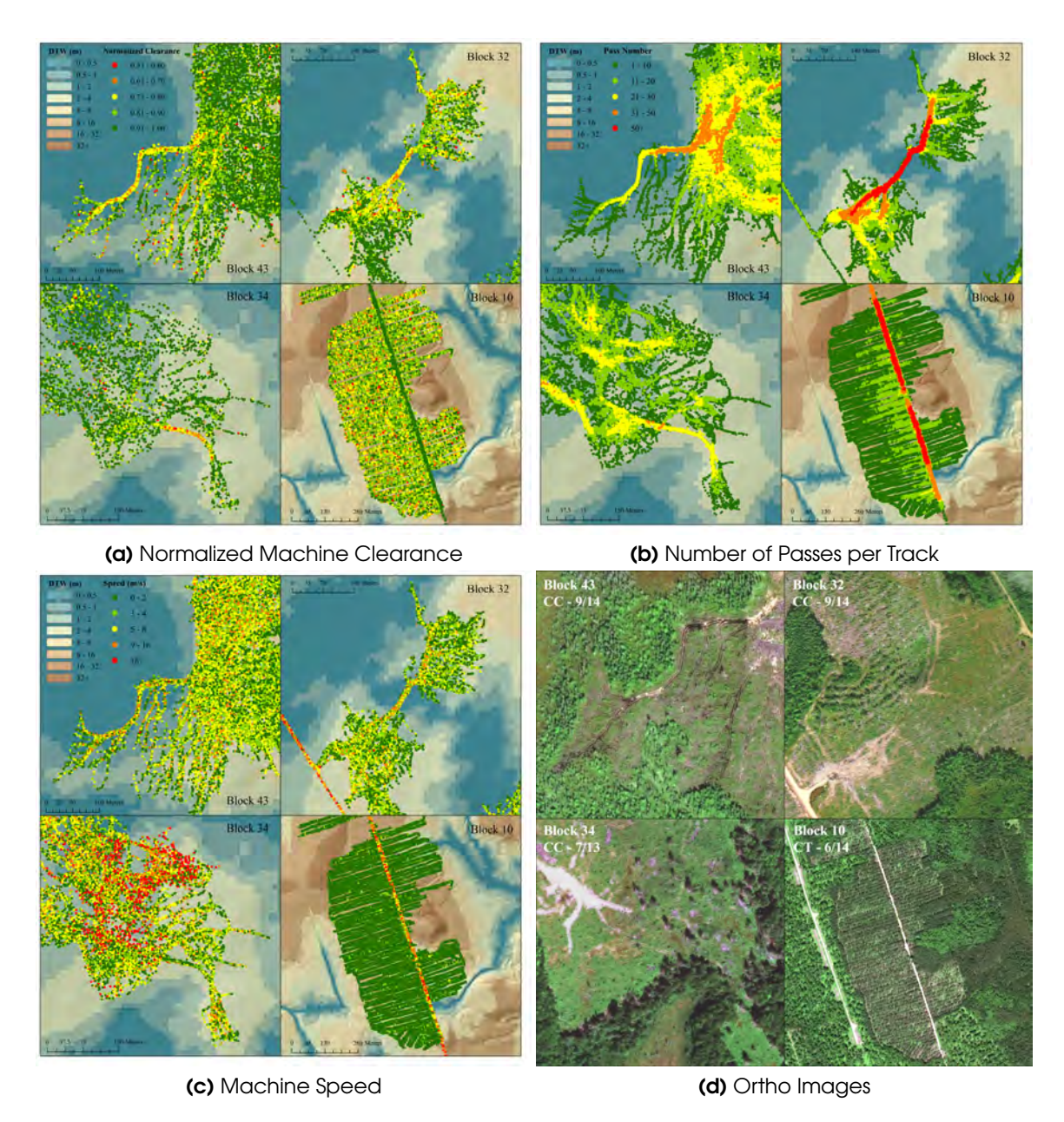


Figure 3.12: Visual correlation between DTW and normalized clearance (top left), number of passes per track (top right), and machine speed (bottom left), for blocks 47, 32, 34, and 10. Ortho imagery of blocks (bottom right) showcasing harvest type and soil disturbance (Imagery Source: Esri, DigitalGlobe, GeoEye, Earthstar Geographics, CNES/Airbus DS, USDA, USGS, AEX, Getmapping, Aerogrid, IGN, IGP, swisstopo, and the GIS User Community).

3.4 Further Observations

3.4.1 Clearances by Machine Type and Number of Passes

Some of the normalized clearance differences would be caused by differences in machine weight, loads, tire pressure, number of tires, and whether the tires are chained or tracked (Table 3.1). For example, TC has higher front footprint pressure about 2 to 3 times higher than the JD11 and JD15 forwarders, hence according to the Table 3.1 entries - soil compression should be deeper with TC than with JD11 and JD15 operations. This was indeed the case along repeated TC forwarding tracks on moist to wet ground (Figure 3.12). Under dry conditions, however, normalized clearance patterns peaked around one, except for the lower JD11 brush-mat clearances. Compared to JD15, JD11-exerted footprint pressure is about double (Table 3.1). Consequently, and consistent with the experimental machineload and brush-mat observations by Labelle and Jaeger (2012), JD11 brush-mat clearances were not only lower than for JD15 brush-mat clearances, but JD11 clearance were also significantly lower during forwarding than returning (Figure 3.9). In terms of increasing number of passes, brush-mat clearances flattened through repeated crushing and consolidating.

3.4.2 Machine Speed

Machine speeds are affected by soil-tire interactions, including soil compaction and soil displacement (Shmulevich *et al.*, 1998). In this regard, Liu *et al.* (2009) reported increasing soil displacement with increased tire rotation on dry ground. On soft ground, however, slow traffic increased soil compression and soil displacement (Grahn, 1991; Taghavifar and Mardani, 2014). For the JD11, JD15, and TC operations, machine speed was definitely affected by machine load, being lower when fully loaded than when empty, with TC speeds significantly greater than JD11 and JD15 speeds (**Figure 3.9**). This effect was likely due to operating under more open than dense stand conditions, i.e., forwarding logs

following clear-cutting and shelter-wood cutting versus logs following forest plantation thinning.

3.4.3 Bare-Ground Operations

When operating on bare ground during clear-cutting and shelter-wood harvesting, off-road clearances can also be expected to decrease with increasing footprint pressure and increasing number of passes due to increasing soil compression (Jamshidi *et al.*, 2008; Vega-Nieva *et al.*, 2009; Taghavifar and Mardani, 2014) (**Table 3.1**). This, however, did not happen because of the lateral sensor restrictions, and track broadening as the soil continue to be compressed with increasing number of passes (**Figures 3.2**, **3.9**). In contrast, clearances were low on wet ground and repeatedly so with increasing number of passes due to deep and recurring soil displacements as exemplified in **Figure 3.11**. In addition, soil rutting would become even deeper on wet slopes through load- and slope-induced tire and track slippage.

3.4.4 Season and Weather Details

With varying soil wetness by weather and across seasons, there is a general correspondence between TC clearances and ground conditions (**Figure 3.13**). For TC, lower clearances and deeper soil rutting were incurred within or across the harvest blocks on account of: (i) low DTW locations, (ii) snow accumulations, (iii) snow melt and prolonged rain events, and (iv) low evapotranspiration (Raven *et al.*, 1999; Ács *et al.*, 2011; Jones and Arp, 2017) before leaf-out (May - June) and after leaf-fall (October - November). In contrast, JD11 and JD15 clearances were less relatable to the varying ground conditions due to low footprint pressure (**Table 3.1**) and brush-mat operations.

An example of weather-induced soil rutting on dry ground (4 < DTW < 32 m) is shown in the form of normalized clearances < 0.8 in **Figure 3.13**. This occurred

during TC operations in block #48 two days after a 110 mm rain event in July 2014 (Hurricane Arthur). Similarly, Block #41 operations immediately after a 30 mm rain event on wet October soils led to extensive soil rutting (Figure 3.11). To avoid such occurrences, wood forwarding operations were generally deferred to occur on dry ground spring, summer and fall, and on frozen ground during winter. During the JD11 and JD15 winter operations (block #1, 12-15, 17-19, and 28-30), the normalized clearances were mostly affected by ultrasonic reflections from snow surfaces. Hence, clearances on snow-covered ground also decreased with increasing number of passes due to snow compaction and track widening. This would be of greater concern for NWU due to the snowpack present on site for the winter blocks of the JD11 and JD15 being almost twice as large as in the more southern blocks (Appendix B.7 and B.8). While this compaction has no effect on frozen soil rutting, it has been shown to cause soils along the tracks to freeze deeper and longer, thereby delaying soil thawing along the established tracks (Grady, 1982; Garcia et al., 2015).

3.5 Conclusion and Concluding Remarks

The assessment of the machine clearance data provided the following insights:

- i. The normalized clearances were affected by brush mat versus bare ground operations, with the former producing lower but still broader clearance distributions than the latter.
- ii. All of the block-based clearance histograms followed asymmetric Gamma frequency distributions.
- iii. Clearances increased systematically with increasing passes towards 1 on dry ground due to successive soil compression and track widening. On wet ground, clearances would decrease because of successive soil re-displacements.

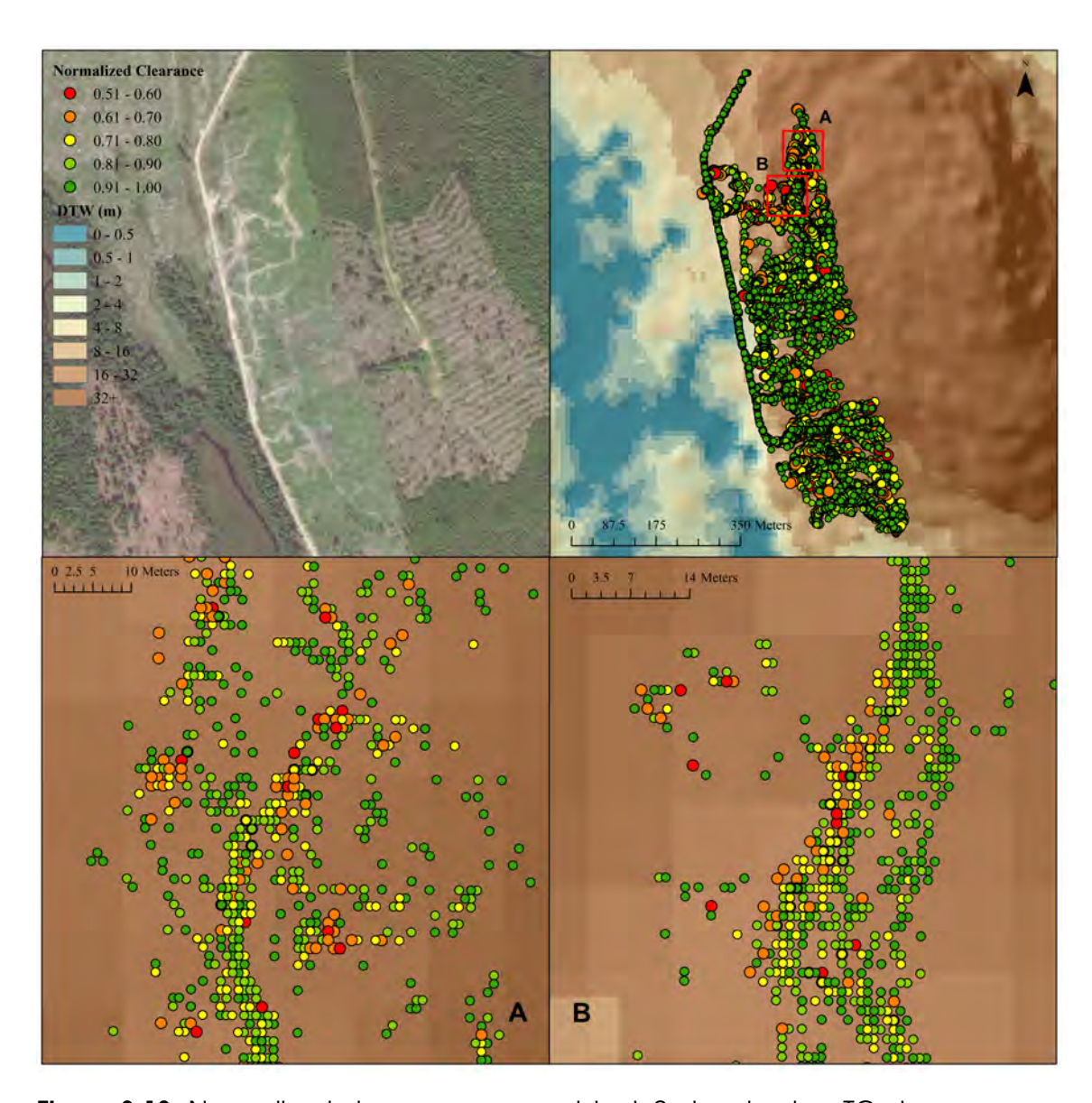


Figure 3.13: Normalized clearances across block 2, showing low TC clearances on DTW >4 m ground following a 110 mm per day storm event in July 2014, with two close-ups (bottom panels; A, B red boxes in top panel), with DTW background.

- iv. The TC centralizing wood-forwarding pattern following clear-cutting and shelter-wood operations included long tracks with number of passes exceeding 100 per track, which would lead to rutting along wet and along wet-to-dry transitional ground conditions.
- v. Number of passes, machine speed and low to high DTW classes all affected the normalized clearance results in terms of block and weather-specific conditions, with least effects registered along brush mat and dry-ground tracks, all based on fairly low machine footprint pressures in the order JD15 < JD11 < TC.</p>
- vi. Clearances along the same bare-ground tracks do not necessarily reflect rut depths due to track broadening and using machine-fixed positions for machine-to-ground distance monitoring. On brush mats, the clearance data reflect brush mat re-conditioning due to repeated track traffic.
- vii. Actual machine clearance can be obstructed due to ultrasonic sensor blockage by way of debris, and by the presence of snowpack accumulations.
- viii. The extent of soil rutting versus machine clearance needs to be evaluated separately by way of ,e.g., high-resolution block surveys following completion of block operations (Salmivaara *et al.*, 2018), or through machine-mounted LiDAR-based ground scanning (Giannetti *et al.*, 2017).
- ix. GPS tracking of tire rotation in connection with machine speed would assist in determining actual to potential soil displacement in terms of tire slippage and tread design.

3.6 Acknowledgments

This research was supported by J.D. Irving Limited (JDI) as a part of the NSERC-sponsored Cooperative Research Development (CRD) Project on Forest Soil Trafficability. Special thanks go Greg Adams at JDI for facilitating this project, and to FP Innovations personnel for the development and installations of the ultrasonic sensor dataloggers. Also many thanks to the Shane Furze, Doug Hiltz, and John Paul Arp for help with data retrieval and GIS processing.

Chapter 4

Soil moisture and cone penetrability conditions in forest soils

Marie-France Jones, and Paul Arp

Faculty of Forestry and Environmental Management,

University of New Brunswick, Fredericton NB, Canada E3B 6C2

Email: arp2@unb.ca

Foreword:

The following chapter is a published article within the Open Journal of Forestry. It was submitted on January 22, 2019 and accepted for publication on March 21, 2019. Publication permission can be found in **Appendix C.1**.

Citation:

Jones, M.-F., Arp, P.A. (2019) Soil moisture and cone penetrability conditions in forest soils. *Open Journal of Forestry*, 9, 109-142.

Abstract

This chapter details how forest soil moisture content (MC) and subsequent resistances to cone penetration (referred below as Cone Index, CI) vary by daily weather, season, topography, site and soil properties across eleven harvest blocks in northwestern New Brunswick. The MC and CI affecting soil variables refer to density, texture, organic matter content, coarse fragment content, and topographic position (i.e., elevation, and the seasonally affected cartographic depth-to-water (DTW) pattern). The harvest blocks were transect-sampled inside and outside their wood-forwarding tracks at varying times throughout the year. In detail, 61 % of the pore-filled moisture content (MC_{PS}) determinations inside and outside the tracks could be related to topographic position, coarse fragments, bulk density, and forest cover type specifications. In detail, 40 % of the CI variations could be related to soil depth, MC_{PS}, and block-specific cover type. Actual versus model-projected uncertainties amounted to $\Delta MC_{PS}~\pm~15\%$ and Δ CI \pm 0.5 MPa, 8 times out of 10. Block-specific MC and CI projections were obtained through (i) daily hydrological modelling using daily precipitation and air temperature weather-station records nearest each block, and (ii) digitally modifying these results based on the upslope to downslope variations in soil property, elevation, and DTW variations in each block, at 10 m resolution.

Keywords

Forest Soils, Soil Moisture, Cone Penetration, Digital Elevation Modelling, Cartographic Depth-to-Water, Multilinear Regression, Confusion Matrix

4.1 Introduction

Estimating soil moisture and subsequent resistance to cone penetration is at the base of forecasting potential soil disturbance effects due to off-road machine traffic. For example, modern forest harvesting operations including wood forwarding can lead to substantial soil compaction, rutting and displacements, rut-induced water logging and re-direction of flow patterns leading to soil erosion, operation inefficiencies, and increased wear of machinery component, especially when these operations are not properly timed. Machine-induced soil compaction and associated rut-induced soil displacements commonly occur on moist to wet ground, are long-lasting, and affect the growth of remaining or planted vegetation (Cambi et al., 2015; Solgi et al., 2018). The impacts are strongest along trails with multiple wood-forwarding passes, and on wood landing sites (Jones et al., 2018). To remain productive, post-harvest soils need to remain well drained with soil bulk densities at < 1.5 g cm⁻³ (Soane and van Ouwerkerk, 1994; Sutherland, 2003; Bassett et al., 2005; Brady and Weil, 2008; Chen and Weil, 2011).

Forecasting soil compaction and penetrability across time and terrain is, however, difficult due to changing weather-affected soil moisture conditions, and meter-by-meter changes in soil substrates and properties (Elbanna and Witney, 1987; Smith et al., 1997; Vaz et al., 2001). Soil penetrability is further modified by soil texture, coarse fragment content, and organic matter content. The presence of soil organic matter modifies this effect due to organically-supported soil aggregation and related pore-space stabilization. The presence of coarse fragments generally reduces soil compaction and penetrability by increasing the force needed to displace these fragments downward and laterally (Baetens et al., 2009; Rücknagel et al., 2013). Soil penetrability leads to deep rutting on wet soils mainly due to soil displacement and on moist soils mainly due to soil compaction. Dry and dense soils are mostly resistant to penetration, compaction

and rutting. Across terrains, soil penetrability changes due to:

- i. changes in soil moisture content, which generally varies from well to excessively well drained on ridge tops to moist to water saturated soils along streams, shorelines, wetlands, in low-lying depressions, and in toe-slope seepage zones;
- ii. changes in soil type, depth, texture, coarse fragment and organic matter content, and bedrock exposure;
- iii. changes in tracked versus non-tracked ground, which in turn depends on extent of machine foot print, load, number of passes, and surface conditions as affected by the presence of stumps, roots, logging slash, rocks, depth of forest litter, and brushmats.

This chapter focuses on presenting a framework to model temporal and spatial weather-, forest-, terrain-, and machine-induced plot-by-plot changes in volumetric soil moisture (MC_V) and soil penetrability cone index (CI) for a case study in northwestern New Brunswick, Canada. This study involved transect-sampling eleven forest blocks that were subject to clear cuts, selection cuts, shelterwood cuts, and pre-commercial thinning at different times of the year. The plot-generated MC_V data were expressed in terms of pore-space filled (MC_{PS}) soil moisture content to serve as a useful CI predictor (Vega-Nieva *et al.*, 2009). The data so obtained were used to model MC_V, MC_{PS} and CI in spatially and temporally. The spatial modelling component addressed emulating the data variations across the terrain from ridge tops to valleys as proposed by Vega-Nieva *et al.* (2009). The temporal component addressed emulating the data variations by weather and season using the Forest Hydrology Model (ForHyM) Jones and Arp (2017).

The goodness-of-fit of the resulting best-fitted MC and CI models were evaluated in terms of, level of uncertainty, and non-randomness indicators. This was done

in two ways: (i) focusing on the field-determined data only, and (ii) determining the extent to which province-wide elevation, cartographic depth to water (DTW), and soil property data layers (Furze, 2018) could also be used for local MC and CI projections, and hence soil trafficability prediction purposes. Knowing where and when locations are subject to rutting has become a vital component of planning best forest management practices. To that effect, rut-avoidance regulations are already in place across many federal and provincial jurisdictions. For example, ruts >15 cm deep are deemed to represent hazardous soil disturbances (Alberta Forest Products Association, 1994; Page-Dumroese *et al.*, 2000; Van Rees, 2002).

4.2 Methods

4.2.1 Block Descriptions

The harvest blocks for this study were selected across the mid-western to northwestern sections of New Brunswick (Figure 4.1). Table 4.1 informs about block-specific attributes pertaining to species composition, harvesting type with and without brushmats laid down along tracks, soil type, elevation, slope and aspect. Information about soil association, landform, and lithology for each block can be found in Table C.1 (Appendix C).

Northwestern Uplands (NWU)

Blocks 1-5 are located within the Southern Uplands Ecoregion of New Brunswick. Mean annual air temperature is 3.6°C. Mean monthly temperatures vary from -5.3°C (January) to 12.5°C (July). The area has a mean precipitation of 1140 mm with 310 mm of snow, inclusively (Department of Environment and Climate Change Canada, 2016a). The forested vegetation mainly consists of sugar maple (*Acer Saccharum Marsh.*), balsam fir (*Abies balsamea L.*), yellow birch (*Betula alleghaniensis* Britt.), and black spruce (*Picea mariana Mill.*). Blocks 1, 2,

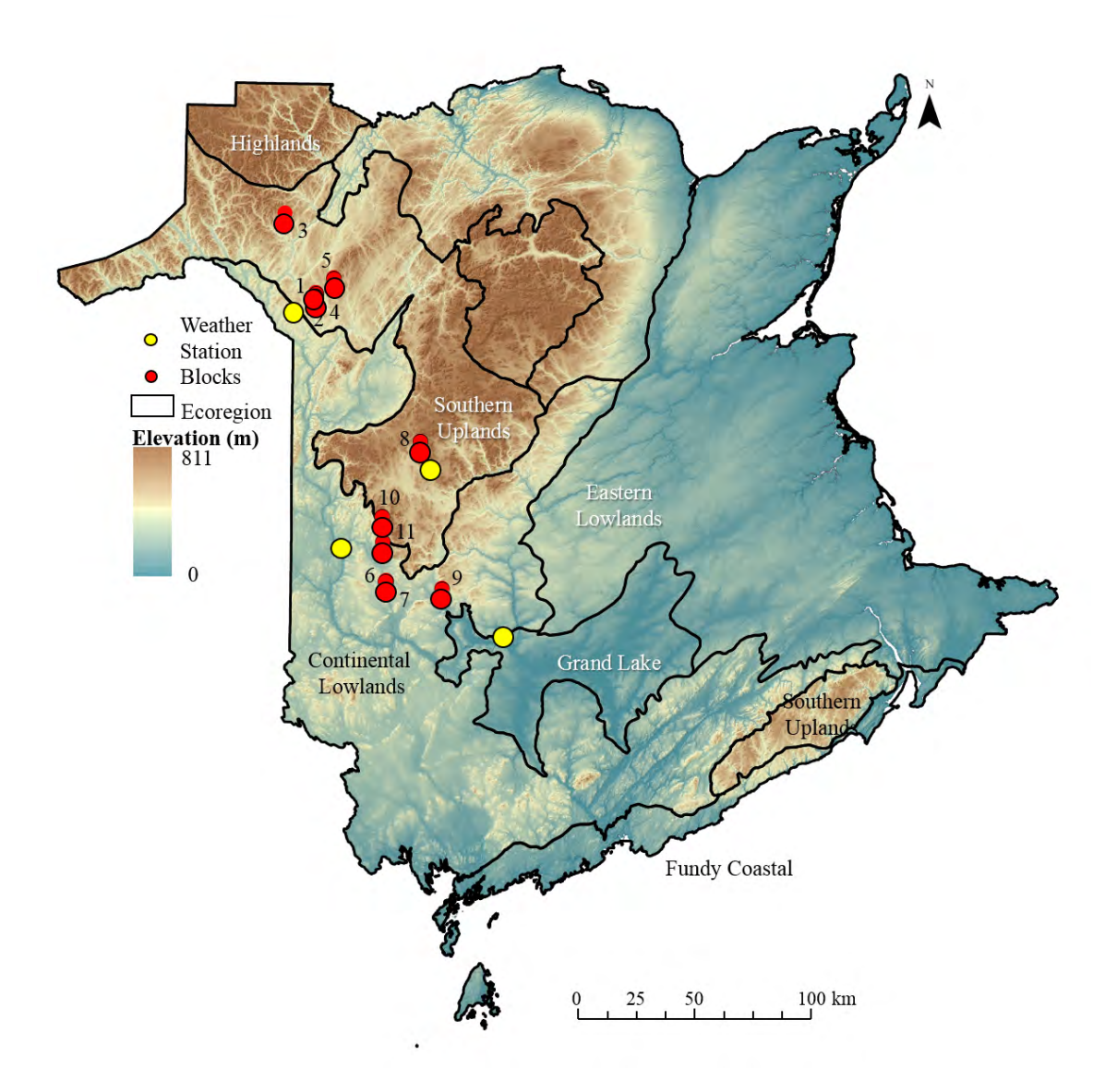


Figure 4.1: Digital elevation model for New Brunswick (10 m resolution) with regional upland and lowland delineations, block locations, and weather station locations.

Table 4.1: Block description by forest type, stand properties (elevation, slope, aspect), and soil association type, as further described in Table C.1 (Appendix C.)

Block	# of Plots	Lat / Long Coord.	Forest Type ¹	Tree Species ²	Oper- ation ³	Sample Date	Soil Association	Elevation (m)	Slope	Aspect (°)
14	29	47°15′4.07″ N 67°37′27.10″ W	J.	S/M	ت ا	27/5/2014	Victoria	267	2.5	158
24	28	47°14′21.82″ N 67°37′26.91″ W	Ы	S/M	ت ا	21/11/2014	Victoria	265	3.4	112
က	80	4732′23.62″ N 67°47′46.29″ W	IntHW	BI/RM	SHW	11/6/2014	Glassville	351	4.6	189
44	46	47°14′59.25″ N 67°37′18.82″ W	占	BS	O	12/6/2014	McGee	280	3.	127
54	33	47°18′20.72″ N 67°31′42.63″ W	Ы	MS	ت ا	15/7/2014	Glassville	388	9.1	149
9	56	47°12′15.03″ N 67°14′17.55″ W	MM M	EH/YB/M	SC	04/6/2014	Jacquet River	210	4.6	148
7		46°12′24.98″ N 67°15′55.073″ W	≫ M	EH/YB/M	S	04/6/2014	Jacquet River	203	5.5	158
∞	54	46°42′51.41″ N 67°3′38.87″ W	ToIHW	SM/YB	SHW	19/6/2014	Juniper	418	4.5	140
6	24	46°10′42.56″ N 66°56′30.53″ W	ToIHW	SM/YB	O	20/8/2014	Long Lake	277	2.0	182
10	147	46°26′23.96″ N 67°15′24.66″ W	ToIHW	SM/YB	SHW	19/6/2013	Popple Depot	422	8.9	185
=	11 159	46°20′44.44″ N 67°15′1.28″ W	ToIHW	SM/YB	SHW	25/6/2013	Mafic Volcanic	319	9.6	214

¹ SWPL: softwood plantation, IntHW: intolerant hardwood, MW: mixedwood, TolHW: tolerant hardwood. ² BS: black spruce; WS: white spruce, BI: birch, YB: yellow birch; RM: red maple; SM: sugar maple; EH: eastern hemlock. ³ CT: commercial thinning, CC: clear cut, SHW: Shelterwood, SC: select cut. ⁴ Tracks brushmatted.

4, 5 involved white and black spruce plantations, whereas Block 3 involved naturally grown birch and maple trees. The bedrock formations of the area consist of late Ordovician deep water marine clastics. The topography comprises gently rolling till-covered plateaus with steeply incised valleys.

Midwestern Uplands (MWU)

Blocks 8, 10, and 11 are located on the Miramichi Caledonia Highlands, which are also part of the Southern Uplands Ecoregion of New Brunswick. Mean annual air temperature is 5.2C. Mean monthly temperatures vary from -3.5°C (January) to 13.9°C (July). The area has mean precipitation of 1180 mm with 280 mm of snow (Department of Environment and Climate Change Canada, 2016a). Block 8 consisted of a naturally regenerated tolerant hardwood stand, with mostly sugar maples and yellow birch trees. The bedrock formations of the area consist of early Devonian felsic plutons, generally overlain by loamy lodgment tills and sandy glaciofluvial outwash sediments.

Lowlands (LL)

Blocks 6, 7, and 9 are located in the midwestern portion of the Continent Lowlands Ecoregion of New Brunswick. Mean annual air temperature is 5.5°C. Mean monthly temperatures vary from -2.8°C (January) to 13.8°C (July). Annual precipitation amounts to 1100 mm, of which 250 mm is snow (Department of Environment and Climate Change Canada, 2016a). Blocks 6, 7, and 9 supported natural mixedwood and tolerant hardwood stands, comprised of Eastern hemlock (*Tsuga canadensis* L. Carrire), yellow birch, sugar maples, beech (*Fagus grandifolia* Ehrh), and some balsam fir, Eastern white cedar (*Thuja occidentalis* L.), and black spruce. The bedrock formations of the area consist of early Devonian mafic volcanic and late Ordovician deep-water marine-clastics, generally overlain by ablation and boulder tills), glaciofluvial sediments and

eskers.

4.2.2 Data sources and processing

Data layers needed for the spatial and temporal evaluation and modelling the plot-by-plot data involved:

- i. Producing region-wide digital elevation models (DEMs, 1 m resolution) from GeoNBs LiDAR elevation point cloud data using LAS tools.
- ii. Producing the cartographic depth-to-water layer (DTW), for the purpose of emulating plot-by-plot changes on soil moisture content as affected by weather conditions at the time of field sampling (see below).
- iii. Using the province-wide 10 m resolution soil property data layers for soil bulk density (D_b), coarse fragments (CF), organic matter (OM), and texture developed by (Furze, 2018). This development used topographic, climatic and geological data layers to emulate soil drainage, horizon depth, depth, texture, coarse fragment content, organic matter content, and bulk density data as specified for 12,058 geo-referenced soil pedon locations.
- iv. Obtaining daily weather records for daily rain and snow amounts and snowpack depth from weather station, within or near the NWU, MWU and LL regions (Department of Environment and Climate Change Canada, 2016a) for block specific soil moisture emulations.
- v. Obtaining daily stream discharge records from hydrometric monitoring stations representative of stream water flow within or near the NWU, MWU and LL regions for hydrological model calibration (Department of Environment and Climate Change Canada, 2016b) to ensure that the soil moisture emulations were consistent with regional weather and stream discharge events.

vi. Acquiring forest inventory and road layers, to navigate to and access harvest blocks.

All raster and shapefile data layers were assembled with ArcMap software, using the same projection system (NAD 1983 CSRS New Brunswick Stereographic). Transect plots within blocks were georeferenced to align with data layers. The resulting coordinates were used to extract plot-specific data values from the elevation, DTW, D_b, CF, OM, and soil texture data layers. The DEM layer was also used to determine mean elevation, slope, and aspect for each block (**Table 4.1**), needed as additional input for the block-specific soil moisture modelling purpose.

4.2.3 Field Measurements

Soil property evaluations were done along 696 geo-referenced transect plots inside and outside wood-forwarding tracks (i) for Blocks 1 to 9 intermittently from May 27, 2014 through November 21, 2014, and (ii) for Blocks 10 and 11 in June 2013 (**Table 4.1**). The plots within blocks were established pairwise, each pair 100 m apart containing one plot within and one plot adjacent to the track on undisturbed soil, 10 m apart (**Figure 4.2**).

Soil samples were retrieved from the top 15 cm of mineral soil. Each sample was placed into labeled freezer bags for storage. Samples were dried in a forced-air oven at 75 °C for 24 hours, then crushed and passed through a 2 mm sieve to separate the fine earth from the CF. The latter was used to determine CF %. The former was used to determine (i) sand, silt, and clay % for each sample (sand % + silt % + clay % = 100 %), using the hydrometer method (Shelrick and Wang, 1993), and (ii) soil carbon % by oven-dry weight using a LECO CNS-2000 analyzer. The resulting soil carbon numbers were converted into soil OM via Eq. 4.1.

$$OM_a\% = 1.72 \times C\%$$
 (4.1)



Figure 4.2: Penetrometer being used inside and outside forwarder tracks without brushmats.

Soil density samples were also collected from each plot by tapping and extracting a metal ring of known volume (85 cm 3) into the mineral soil. Following frozen storage, these samples were weighed and dried in a forced-air oven at 75 $^{\circ}$ C for 24 hours. From this, soil bulk density (D_b) was determined as per Eq. 4.2.

$$D_{b} = \frac{Weight\ of\ dried\ soil\ (g) + Weight\ of\ coarse\ fragments\ (g)}{Volume\ of\ soil\ (cm^{3})} \tag{4.2}$$

The fine-earth bulk density of the soil between rocks and roots was estimated using the oven-dry weight fractions of sand ($Sand_W$), OM_W and mineral soil depth (cm) as predictor variables as per Eq. 4.3 (Balland *et al.*, 2008).

$$D_b = \frac{(1.23 + (D_b - 1.23 - (0.75 \times Sand_{wt}) \times (1 - exp(-0.0106 \times Depth))))}{1 + 6.83 \times OM_{wt}}$$
(4.3)

A Humboldt digital cone penetrometer (cone base = $1.5~\rm cm^2$; cone angle 60°) was used to determine soil penetrability through recording CI in MPa at 15, 30, 45, and 60 cm depths within each sampling plot. Similarly, a Delta T HH2 moisture meter (TDR: a time-domain reflectometer) was used to determine volumetric soil moisture content of the fine-earth fraction between coarse fragments for each plot at 15 cm mineral soil depth. Five CI and MC $_{\rm V}$ readings were obtained for each plot: one at the center point (location of GPS coordinates), and four

arranged at each cardinal direction (north, south, east, and west), 1 m apart from centre. For blocks 10 and 11, the CI measurements were taken once per subplot to the deepest depth reached with the penetrometer. Measurements were not recorded if obstructed by surface rocks, roots or logs. The subplots were then averaged to provide single numbers per plot for further analysis.

Since CI tends to be related to pore-space soil moisture content (MC_{ps}, see Vega-Nieva *et al.*, 2009), it was important to derive PS and MC_{PS} from inferred soil (D_b) and particle (D_p), as follows:

$$\frac{1}{D_p} = \frac{D_b}{D_p} - \frac{1 - OM_g}{D_m in} \tag{4.4}$$

$$PS \% = 1 - \frac{D_b}{D_p}$$
 (4.5)

$$MC_{ps} \% = \frac{MC_v \%}{PS \%}$$
 (4.6)

where MC_V is the volumetric moisture content of the fine earth, and D_{om} and D_{min} were set to 1.3 and 2.6 g/cm³, respectively.

4.2.4 Temporal MC Variations

Soil moisture was modelled block-by-block over time using the temporal aspatial Forest Hydrology Model (ForHyM) (Arp and Yin, 1992; Yin and Arp, 1994; Jutras, 2012). This model uses (i) daily weather records for temperature, and precipitation for input (**Table 4.2**), (ii) block-specific specifications for topography (elevation, slope, and aspect), (iii) soil-surveyed properties (horizon depth, texture, depth, OM, CF) as per mapped soil type (**Table 4.3**), and (vi) vegetation type and % canopy closure. These specifications were needed to emulate daily soil moisture, temperature, snowpack conditions and stream discharge. In this model, soil permeability at saturation was empirically related to D_p, D_b, and soil

sand fraction by weight (Sand_W) by setting:

$$log_{10}K_{sat} = -0.98 + 7.94 \times log_{10}(D_p - D_b) + 1.96 \times Sand_W$$

$$R^2 = 0.80$$
(4.7)

In ForHyM, K_{sat} and snowpack are further calibration-adjusted to quantify the extent of inflow (lateral flow) along layers versus downward percolation (vertical flow) into layers (**Table 4.2**, **Figure C.1** (Appendix C)). In soils where soil density increases with depth, downward K_{sat} is general less than the Eq. 4.7 specifications. Also of note is the ForHyM formulation for water retention at field saturation (FC_w), given by:

$$FC_W = SP_W \left(1 - exp \left[\frac{-0.588(1 - Sand_W) - 1.73 \times OM}{SP_W} \right] \right)$$

$$R^2 = 0.96$$
(4.8)

where FC_W, SP_W, and Sand_W all refer to total weight fractions per dried and gently crushed fine soil that passes through a 2 mm sieve. In combination, any ForHyM generated block-by-block soil moisture output by soil layer is a function of soil bulk density sand, organic matter, and coarse fragment content. Specifically, Eq. 4.8 implies that soil moisture retention at field capacity increases with increasing organic matter content and decreasing bulk density, sand, and coarse fragment content (Balland *et al.*, 2008).

Table 4.2: ForHyM calibration variables for snowpack and saturated soil permeability by block, including weather and hydrometric station locations for primary ForHyM input data.

	Blocks	A - NWU 1-5	B - MWU 8, 10, 11	C - LL 6, 7, 9	
	Weather Station ¹	Leonard Station Airport & Edmundston	Woodstock & Juniper	Fredericton CDA	
	Hydrometric Station ¹	Black Brook Watershed Data ²	Narrows Mountain Brook	Nashwaaksis Stream	
	Model Run Years	1990-2016	1990-2016	1940-2016	
Snowpack parameter	Snow-to-air temperature gradient	0.16	0.2	0.2	
adjustments	Density of fresh snow	0.16	0.15	0.2	
	Surface runoff	1	1	1	
	Forest floor infiltration	1	1	1	
Saturated	Forest floor interflow	0.01	1	0.01	
Soil Permeability	A&B horizon infiltration	1	1	1	
parameter	A&B horizon interflow	0.05	0.1	0.01	
adjustments	C horizon infiltration	1	1	1	
-	C horizon interflow	0.1	0.8	0.1	
	Deep water percolation	1	1	1	

¹ (Department of Environment and Climate Change Canada, 2016a)

² (Black Brook Watershed Research site, 2014)

Table 4.3: For HyM soil profile information used to initialize each blocks.

Region	Block	Vegetation	Layer	Depth	Texture	OM _W %	CF %
NWU	1, 2, 4, 5	SW,	LFH	5	Organic	100	0
		shallow	Α	10	SL	1	20
		rooted	В	75	SL	8	24
			С	100	S	1	35
NWU	3	IntHW,	LFH	5	Organic	100	0
		deep	Α	10	SL	20	20
		rooted	В	75	SL	5	24
			С	100	S	1	35
MWU	8	MW,	LFH	7	Organic	100	0
		medium	Α	5	SL	1	20
		rooted	В	40	SCL	5	20
			С	100	L	2	30
MWU	10, 11	ToIHW,	LFH	7	Organic	100	0
		deep	Α	10	SL	5	20
		rooted	В	40	SCL	2	20
			С	100	L	1	30
LL	6, 7	ToIHW,	LFH	7	Organic	100	0
		deep	Α	5	SL	5	20
	rooted	В	40	L	5	20	
			С	150	L	1	30
LL	9	ToIHW,	LFH	7	Organic	100	0
		deep	Α	5	SL	5	20
		rooted	В	40	L	5	20
			С	150	L	1	30

4.2.5 MC and CI Variations, plot-by-plot

In general, soil moisture increases from ridges and steep slopes to water-saturated wetlands, depressions and hyporheic zones adjacent to streams, rivers, lakes and shores. To some extent, this tendency is quantitatively related to the cartographic depth-to-water index (DTW) which is a metric that represents the least elevation rise to any point on the land way from the nearest open water locations, where DTW = 0. Conceptually, soil moisture levels should therefore decrease at DTW increases. For the changes in volumetric and pore-filled soil moisture content over time, this can be expressed as follows (Vega-Nieva et al., 2009):

$$MC_{PS,DTW} = \frac{MC_{V,DTW}}{PS} = 100 - [100 - MC_{PS0}] \times$$

$$\left[\frac{1 - exp(-k_{mc} \times DTW)}{1 - exp(-k_{mc} \times DTW_{max})} \right]^{p_{mc}}$$
(4.9)

where $MC_{PS,DWT}$ $MC_{V,DWT}$ the pore-filled and volumetric soil moisture content at any point in the landscape in relation to DTW, with DTW = 0 referenced to local flow channel network and other connected open-water features when bankfull. The local flow-channel network was generated by applying the D8 flow-accumulation algorithm to the 1 m resolution LiDAR-generated digital elevation model for New Brunswick, as described in **Figure 4.3**, The seasonality extent of the resulting flow network was emulated by varying the minimum upslope flow-accumulation area for flow initiation (termed flow initiation area, or FIA for short) by season and weather, as illustrated in **Figure 4.4**.

In Eq. 4.9, parameters k_{MC} and p_{MC} (0.5 and 1.5, respectively) quantify how $MC_{PS,DTW}$ varies with DTW across areas of interest as MC_{PS0} varies from, for example, 20 % on ridges to 100 % at and near water-filled flow channels. When soils become uniformly saturated, $MC_{PS,DTW}$ = 100 % everywhere. At other times, $MC_{PS0} \leq MC_{PS,DTW} < 1$.

Wet-Areas and Floodplain Mapping Concept Cartographic depth-to-water (DTW) Floodplain Channel DTW-inferred water table surface

- Prepare bare-ground DEM surface from LiDAR point cloud data, using the D8 fill, flow direction and flow accumulation algorithms, pixel by pixel.
- 2. Re-classify the flow accumulation pattern, by setting the minimum flow accumulation area threshold for flow initiation at 0.25, 1, 4 and 8 ha.
- 3. Use the wet-areas delineation algorithms to determine the cartographic depth-to-water index (DTW) along flow-conducting channels, using all flow channels and bank-full shorelines for DTW = 0 reference. Formally, DTW = $\left[\sum \frac{\mathrm{d}z_1}{\mathrm{d}x_1}\mathbf{a}\right]x_c$, where: dz/dx is the slope of the DTM cells along the path to the object with the smallest height difference; "i" is a single cell; $\mathbf{a} = 1$ and $\mathbf{a} = \sqrt{2}$ when the least slope path runs along or diagonally across the grid cells, respectively; " \mathbf{x}_c " is the cell size [m].
- 4. Subtract DTW from DEM to get the cartographically referenced water table elevation.

Figure 4.3: Cartographic depth-to-water index (DTW) diagram (Murphy *et al.*, 2009b).

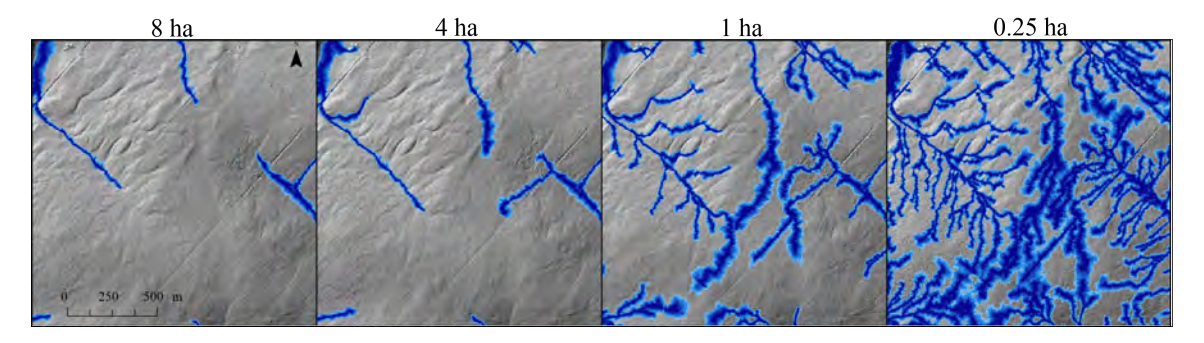


Figure 4.4: Cartographic DTW <1m pattern by minimum upslope open-channel flow initiation area (FIA), i.e., DTW_{FIA} , to emulate changes in soil moisture content by weather and season. For most of New Brunswick and the forested areas across Canada, the DTW 1m pattern for FIA = 4 ha reflects end of the summer soil moisture and drainage conditions from very poor to moderate.

Since soil moisture at any point in the landscape are also affected by block-by-block and plot-by-plot variations in soil properties and wood-forwarding tracks, MC_{PS} also needed to be evaluated as function forest cover and soil properties inside and outside wood-forwarding tracks. This was done by setting:

$$MC_{PS} = f(DTW, elevation, forest cover, soil properties, block, track, brushmat)$$
 (4.10)

with Forest Cover (SW, HW, MW), Block, Track and Brushmat coded 1 when applicable and 0 when not. The elevation variable accounted for additional topographic variations as they exist block-to-block across the NWU, MWU, and LL regions. The soil properties refer to plot-by plot variations in soil texture (sand, silt, clay content), soil density (D_b , inferred from sand and clay content), CF, OM, and layer depth. The block-by-block and plot-by-plot CI variations were evaluated similarly by setting:

$$CI = f(DTW, elevation, forest cover, soil properties, \\ block, track, brushmat)$$
 (4.11)

4.2.6 Statistical analyses, followed by generalized block-generated MC_{PS} and CI projections

The block- and plot-descriptive, field, laboratory, ForHyM-generated and raster-extracted data were compiled into a single datasheet, were summarized and were subjected to correlation, factor, multivariate regression analyses in R (R Core Team, 2015), using MC_V, MC_{PS} and CI as dependent variables. The resulting regression models for Eqs. 4.9, 4.10, and 4.11 were assessed in terms of scatterplots for the actual versus modelled values, the best-fitted regression coefficients for each independent variable of non-zero significance values (p-values <0.01), and R² and RMSE goodness-of-fit indicators. In addition, the conformance levels between actual and model projected 0-10, 10-20, 20-30,...% MC_{PS} classes and 0-0.5, 0.5-1, 1-1.5,... MPa CI classes were evaluated in terms of

confusion matrices, non-randomness, and cumulative conformance probabilities to determine the uncertainty range of best-fitted model projections. Subsequently, the MC_V , MC_{PS} and CI regression evaluations were repeated using variables amenable for area-wide projection purposes. These variables referred to (i) DTW, elevation, digitally-generated province-wide soil property rasters for Sand, CF, OM and D_b (**Figure 4.5**; Furze, 2008), (ii) block- and season- or month-specific assignments for FIA, (iii) soil depth, and (iv) forest cover type for non-tracked soil conditions. The process of doing so by soil depth and season (month) is illustrated in **Figure 4.6**.

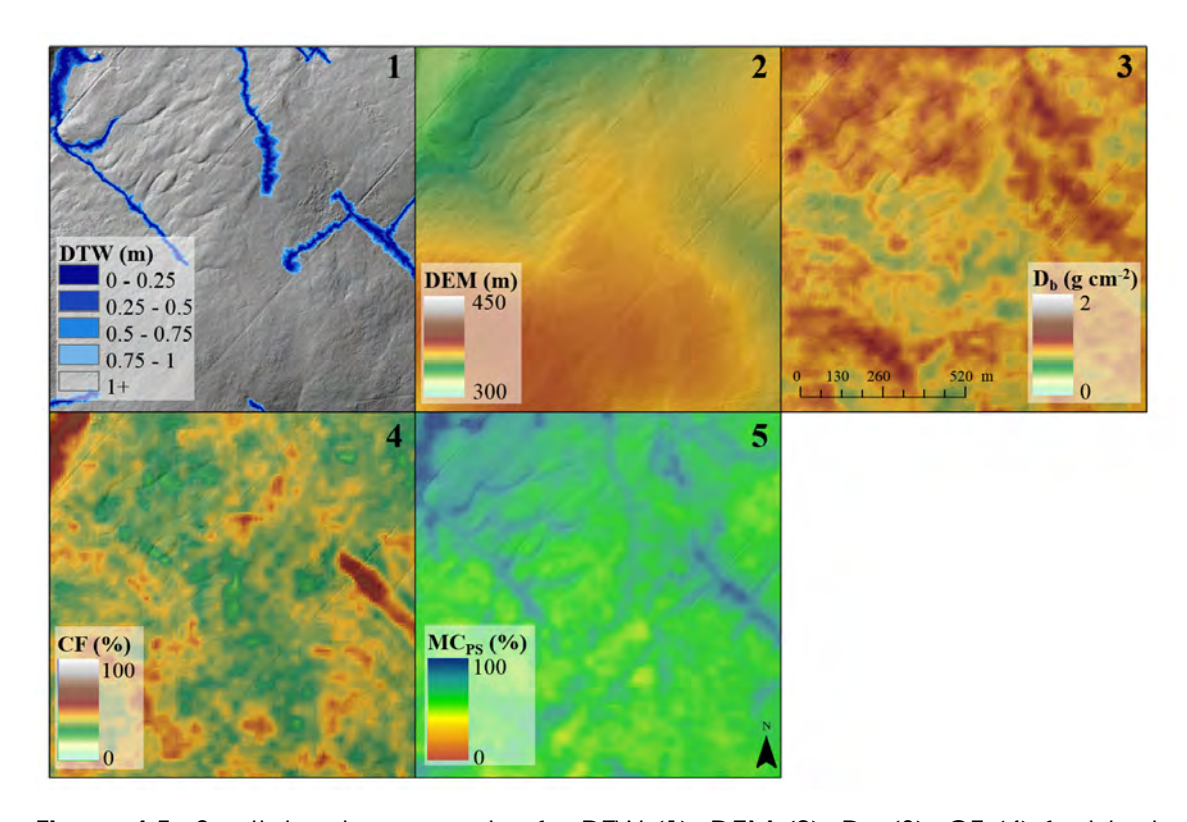


Figure 4.5: Spatial raster examples for DTW (1), DEM (2), D_b (3), CF (4) for block-specific MC_{PS} projections (Block 3).

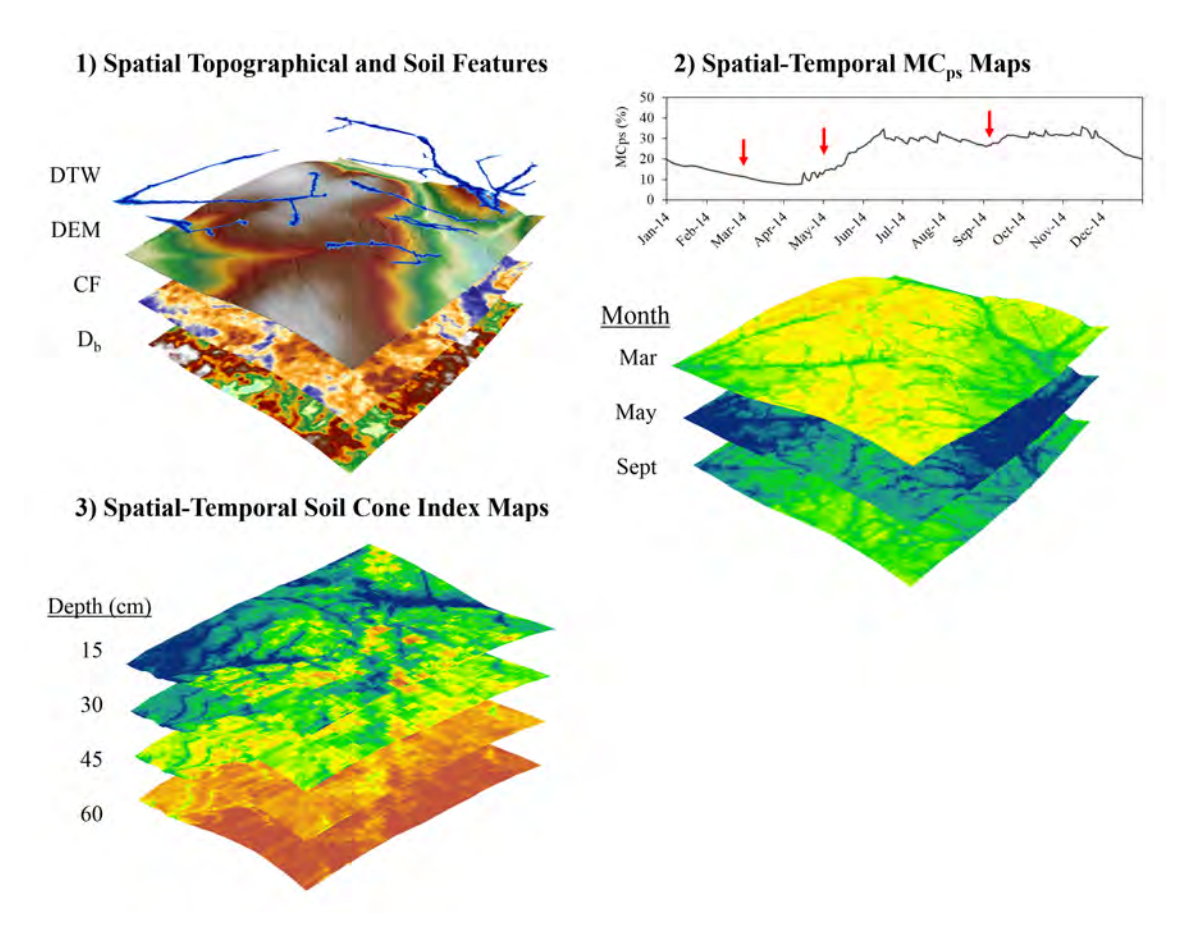


Figure 4.6: Digital soil mapping process combining topographic and soil features (A) with temporal features (B) to generate best-fitted weather-affected MC_{PS} (B) and CI (C) projections for each block (e.g., Block 3) by way of best-fitted Eqs. 4.9, 4.10, and 4.11 models.

4.3 Results & Discussions

4.3.1 General observations and trends

The plot-based determinations for sand, silt, and clay, OM, CF, MC_{PS}, and CI are summarized per block in **Figure 4.7** by box plot in in terms of number of plots, and minimum, maximum, average and standard deviation values in **Table C.2** (Appendix C). These plots reveal that the MC_{PS}, CI and D_b were not always higher inside than outside the wood-forwarding tracks, as one would expect (Allen, 1997; Han *et al.*, 2009; Labelle and Jaeger, 2011; Cambi *et al.*, 2015; Solgi *et al.*, 2018). Possible reasons for the lack of systematic MC_{PS}, D_b, and CI

increases refer to (i) the wide range of operational multi-track observations across ground conditions comprised of rocks, stumps, and variable forest litter depths including brushmats, and (ii) differences in MC_{PS} , D_b , and CI survey-ing methodologies, e.g., using D_b and MC sensors that required no soil displacement (Labelle and Jaeger, 2011) and hydraulic cone penetrators (Cambi *et al.*, 2015; Solgi *et al.*, 2018). The results reported below were obtained through manual soil extraction and probe insertions.

In terms of tracks with and without brushmats, it was found that measured values for D_b , CI, and MC_{PS} for the top mineral soil 15 cm were somewhat lower and less variable under matted than non-matted tracks (**Figure 4.8**). Systematic increases for D_b and CI from the matted and non-matted tracks as reported by Han *et al.* (2009) and Labelle *et al.* (2015) were therefore not found, likely due to the strongly varying substrate conditions along the tracks.

In terms of the higher trending MC levels on matted versus non-matted plots, Roberts *et al.* (2005) and Moroni *et al.* (2009) reported lower cumulative soil moisture losses under matted than non-matted tracks likely through mulch-related shading, insulation, and lowered evaporation benefits.

The overall trends between MC_{PS} and CI versus CF, sand, OM and D_b are presented in **Figure 4.9**. As shown, increasing CF generally lowered MC_{PS} presumably due to (i) increasing porosities between the fragments, (ii) subsequent increases in soil moisture loss due to increased soil permeability, and (ii) enhanced evaporation due to fact that CF conduct heat faster than soil (Poesen and Lavee, 1994; Chow *et al.*, 2007).

The increasing MC_{PS} trend with increasing D_b relates to decreasing pore space. Similarly, decreasing MC_{PS} with increasing OM % relates to increased pore space due to OM-facilitated soil granulation (Han *et al.*, 2006). There is also the

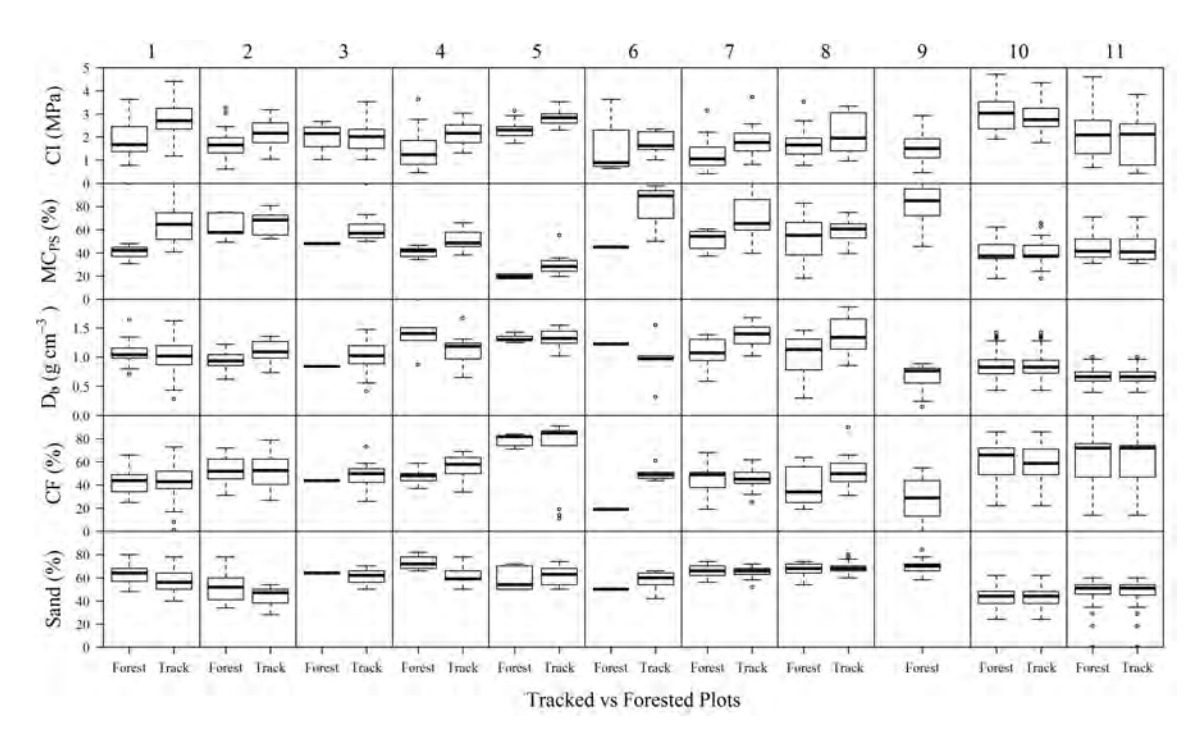


Figure 4.7: Boxplots of MC_{PS} , CI, CF, sand and D_b within the top 15 cm soil layer inside and outside the wood-forwarding tracks.

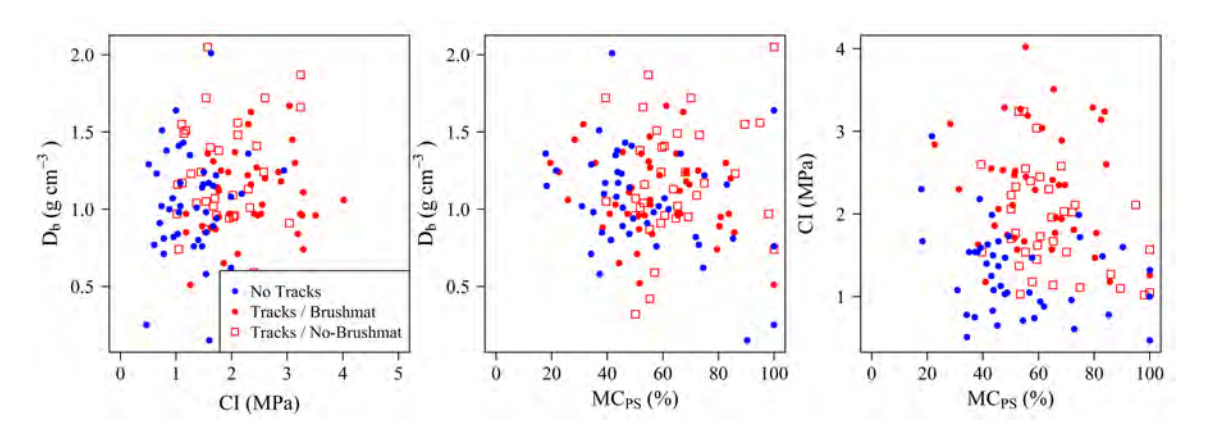


Figure 4.8: Scatterplots pertaining to CI, D_b , and MC_{PS} inside and outside brushmatted and non-brushmatted tracks.

possibility of decreasing MC_{PS} due to increasing hydrophobicity as OM-containing soils dry out (Vogelmann *et al.*, 2013). In contrast, the increasing MC_{PS} trend with increasing sand % may be due to preferential pore space saturation in sandier topsoil portions.

In terms of CI, increasing levels of CF contributes to increasing soil resistance to penetration because of skeletal soil stabilization (Manuwa, 2012) and the need to push some of the fragments to the side to gain greater penetration depths. Increasing sand % generally decreases the strength of the soil, due to lower particle-to-particle cohesion. The opposite occurs with increasing clay % (Raven *et al.*, 1999). The trend between increasing CI and increasing soil depth (**Figure 4.10**) because of depth-related increases in D_b (Carter *et al.*, 2007).

Analyzing the trends among the MC_{PS} and CI affecting variables more closely produced the correlation matrix and its factor analysis results in **Table 4.4**. The bolded Factor 1-3 loadings indicate that:

- i. Factor 1 is positively associated with increasing CI, CF, D_b, elevation and tracks, but negatively associated with increasing soil organic matter content.
- ii. Factor 2 is positively associated with higher elevations where tolerant hardwood forests dominate, where brushmats were rarely used, and where soils are somewhat sandier.
- iii. Factor 3 is positively associated with increasing MC_{PS} but negatively associated with increasing CF, sand, and decreasing DTW, as to be expected. Also, soil pores tend to be drier at higher elevations but fill more easily and remain wet or moist longer inside than outside the tracks.

Table 4.4: Pearsons correlation matrix (non-shaded) with significance levels (shaded grey) for each variable pair. Also shown: factor analysis results following oblique factor rotation (factor loadings considered salient in bold).

Variable CI MC _{PS}	ប	MC _{PS}	۵	ŗ.	Sand	MO	log ₁₀ DTW	Eleva- tion	Brush- mat	Tracks	HW Block	Factor 1	Factor 2	Factor 3
CI (MPa) 1.00	1.00	0.0327	0.0314 < 0 .	<0.0001	0.0861	0.9226	0.1490	0.0004	0.0001	<0.0001	0.1228	0.65	-0.01	0.35
MC _{PS} (%)	-0.156	1.00	0.0160	<0.0001	0.3518	0.6240	<0.0001	0.0020	<0.0001	0.0252	0.0036	-0.01	-0.01	-0.83
$D_{\rm b}$ (g cm ⁻³)	0.157		1.00	<0.0001	0.0444	<0.0001	0.6792	0.2314	0.4205	0.0045	0.0000	0.63	90.0	0.22
CF (%)	0.304	•	0.350	1.00	0.2348	0.1042	0.0008	0.0001	0.0002	0.0118	0.0040	0.50	-0.01	0.64
Sand (%)	-0.126	-0.069	0.147	-0.087	1.00	0.2299	0.3202	0.0186	<0.0001	0.0145	<0.0001	-0.09	0.58	0.22
(%) MO	0.007	-0.036	-0.441	-0.119	0.088	1.00	0.0957	0.3076	0.8362	0.1618	0.7021	-0.54	-0.04	-0.12
log ₁₀ DTW	0.178	-0.410	0.030	0.243	0.073	0.122	1.00	0.0003	0.3198	0.3947	0.5117	0.02	0.20	0.75
Elevation (m)	0.255	-0.224	0.088	0.274	0.172	-0.075	0.259	1.00	0.0870	0.5479	<0.0001	0.40	0.79	09.0
Brushmats	0.291	-0.283	0.059	0.265	-0.345	0.015	-0.073	-0.125	1.00	0.7640	<0.0001	0.04	-0.74	0.24
Tracks	0.539	0.163	0.206	0.184	-0.163	-0.103	-0.063	0.044	0.022	1.00	0.7454	0.75	0.01	-0.12
HW Blocks	-0.113	0.211	-0.190	-0.209	0.301	0.028	0.048	0.618	-0.697	-0.024	1.00	0.07	0.94	0.01

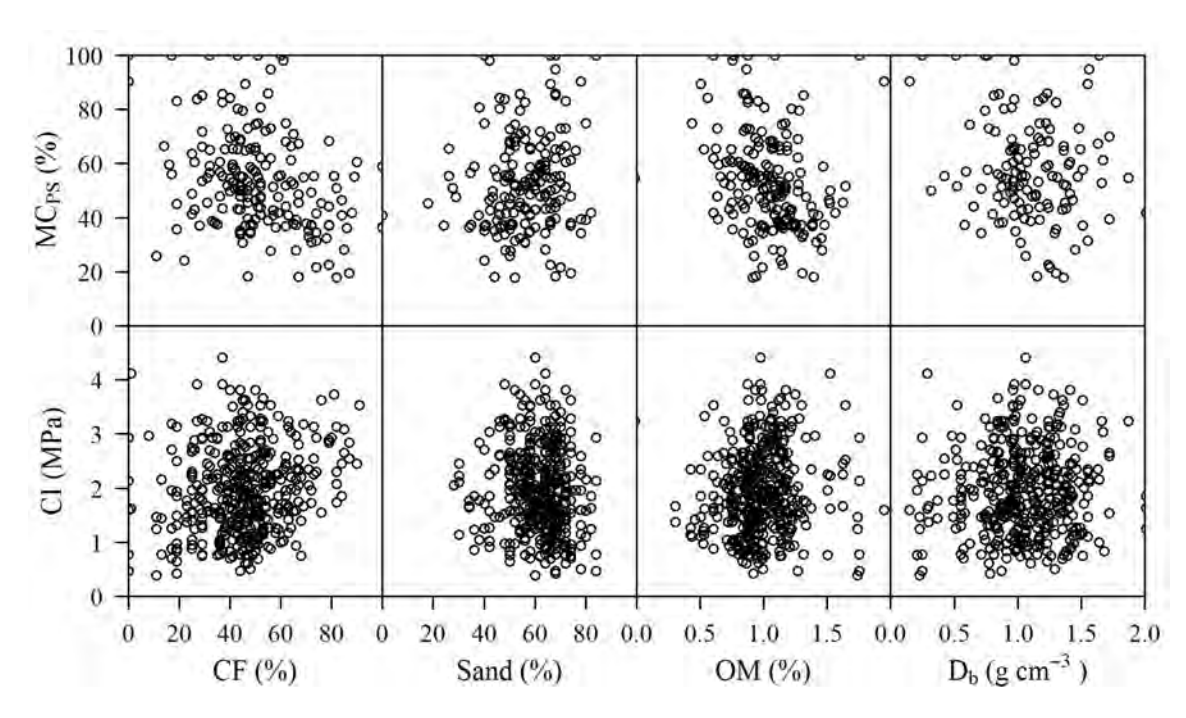


Figure 4.9: Scatterplots for top 15 cm MC_{PS} (top) and CI (bottom) versus top 15 cm CF, sand, OM and D $_{\rm b}$.

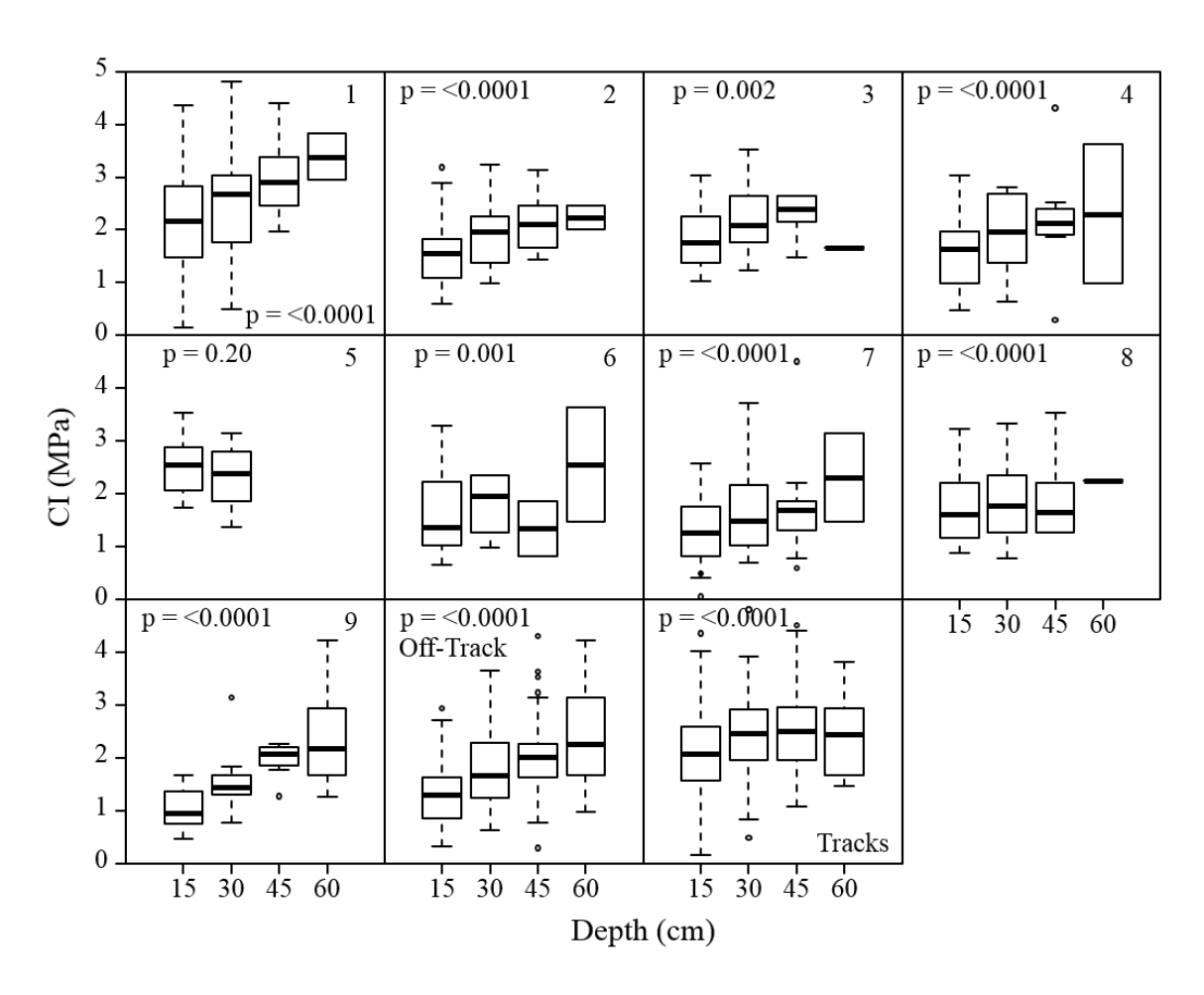


Figure 4.10: Boxplots of field-determined CI versus soil depth for Blocks 1 to 9, including significance value of implied trend. Also shown (bottom): summary boxplots of all CI determinations off-track and inside tracks.

4.3.2 Temporal Soil Moisture Derivations

The ForHyM-generated results for daily soil moisture, stream discharge, snowpack depth and depth of soil frost are illustrated in **Figure 4.11**, which also displays the reported weather station records for rain, snow snowpack depth, and air temperature for Blocks 1 and 9 from 2011 to end of 2014. The daily MC_{PSO} output so produced block-by-block (**Table 4.5**) was obtained through calibrating the ForHyM output with reported snowpack depth and cumulative stream discharge values for each of the three regions (**Figure C.1** (Appendix)). These calibrations involved adjusting the ForHyM parameters for snowpack depth and lateral versus vertical layer-by-layer soil permeability, as detailed in **Table 4.5**.

Fitting the actual plot-specific MC_{PS} determinations for the top 15 cm of mineral soil versus the corresponding log10DTW values with FIA = 1 ha across all the plots by way of Eq. 4.9 produced the following equation once FIA and MC_{PSO} was specified for each block:

$$MC_{PS,DTW} = 100 - [100 - MC_{PS0}] \times \left[\frac{1 - exp(-0.5 \times DTW)}{1 - exp(-0.5 \times DTW_{max})} \right]^{1.5}$$

$$R^2 = 0.29$$
(4.12)

This result improved considerably by using $log_{10}DTW_{1ha}$ as an additional MC_{PS} predictor variable:

$$MC_{PS} = 48.16 - 5.80 \times log_{10}DTW1ha + 0.19 \times MC_{PS,DTW}$$

$$R^{2} = 0.38$$
(4.13)

In detail, the inclusion of $log_{10}DTW_{1ha}$ spread the MC_{PS} prediction range from about 30 to 75 % (Eq. 4.12) to about 20 to 90 % (Eq. 4.13). Even further improvements were obtained by including the plot determinations for D_b, Elevation, HW and Track as independent variables. This led to the best-fitted

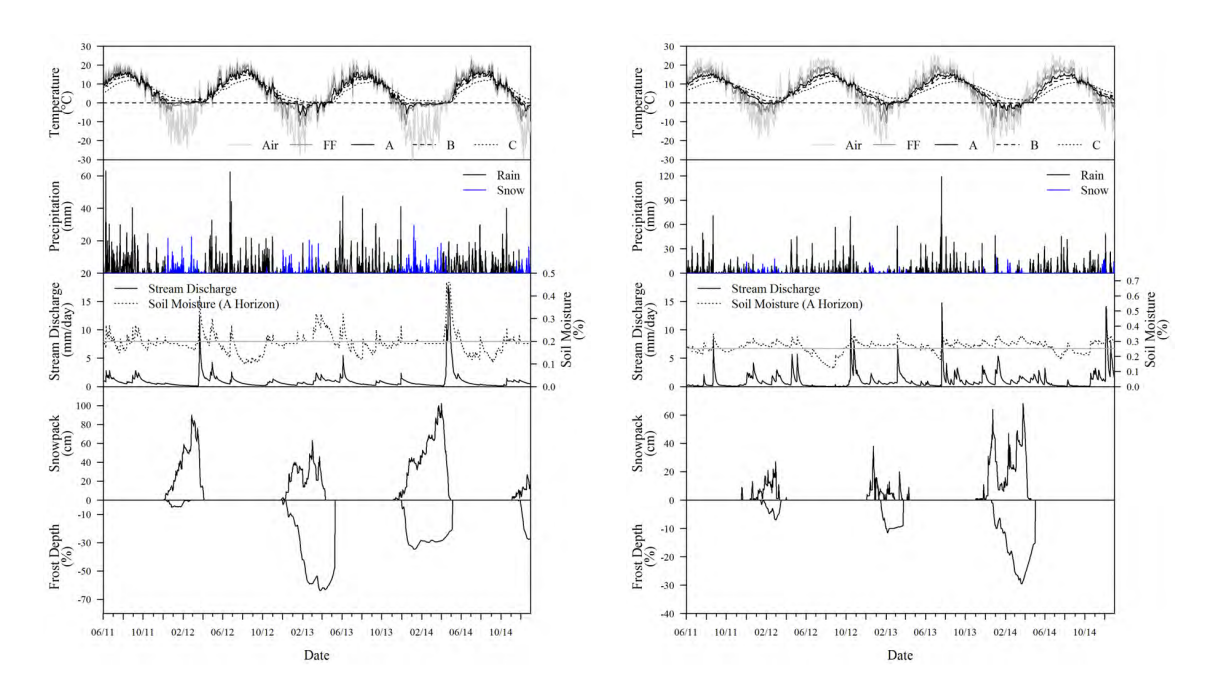


Figure 4.11: Daily variations in Block 1 (left) and Block 9 (right) for air temperature and precipitation (ForHyM input) and stream discharge, MC_{PS} for top 15 cm of mineral soil, estimated field capacity, snowpack depth, and frost depth (ForHyM output; (Jones *et al.*, 2018)).

Table 4.5: Mean block-specific soil property values including soil moisture content at ridge top (MC_{PSO}) and minimum upslope open-channel flow initiation area FIA.

g cm ⁻³ % % % 1 0.92 27.1 6.5 11.6 42.4 3 2 0.91 16.7 6.8 11.4 52.3 3 3 0.96 25.5 5.4 10.3 48.2 3		_
2 0.91 16.7 6.8 11.4 52.3 3 3 0.96 25.5 5.4 10.3 48.2 3	MC _{PSO} FIA ha	
3 0.96 25.5 5.4 10.3 48.2 3	31.9 1	
	34.1 8	
4 0.98 25.5 3.4 9.4 52.5 2	31.5 1	
	28.9 8	
5 0.91 8.6 2.2 12.5 72.5 2	29.6 8	
6 0.90 22.5 7.1 14.6 44.8 4	42.0 1	
7 0.99 30.1 4.7 9.0 44.7	42.0 1	
8 1.09 32.5 5.3 7.3 44.9 3	36.2 4	
9 0.79 33.6 4.4 24.1 28.9	44.9 0.25	
10 0.85 10.8 5.5 14.4 60.5	47.4 8	
11 0.85 9.4 4.9 21.2 61.9	40.0 16	

MC_{PS} regression results listed in **Table 4.6**, and to Eq. 4.14:

$$MC_{PS} = 32.18 - 1.49 \times log_{10}DTW_{FIA,1ha} + 0.27 \times MC_{PS,DTW} + 42.56 \times D_b$$
$$-0.10 \times Elevation + 13.09 \times HW + 3.93 \times Track$$
$$R^2 = 0.61$$
 (4.14)

The corresponding best-fitted MC_V results, also listed in **Table 4.6**, led to Eq. 4.15:

$$MC_V = 35.25 - 1.33 \times log_{10}DTW_{FIA,1ha} + 0.19 \times MC_{PS,DTW} + 13.37 \times D_b$$

$$-0.07 \times Elevation + 9.38 \times HW + 2.43 \times Track$$

$$R^2 = 0.51$$
(4.15)

Based on the t-value entries in **Table 4.6**, one determines that the significance contributions of all the MC_{PS} and MC_V predictor variables follow these sequences:

$$\begin{split} &\text{for MC}_{PS}\text{: }D_b\approx MC_{PS,DWT}\approx \text{Elevation}\approx HW>&\text{log}_{10}\text{DTW}_{FIA,1ha}>&\text{Tracks}>&\text{Sand}>CF;\\ &\text{for MC}_{V}\text{: }MC_{PS,DWT}\approx \text{Elevation}\approx HW>&\text{log}_{10}\text{DTW}_{FIA,1ha}>&\text{Sand}>&\text{Tracks}>D_b\approx CF. \end{split}$$

As to be noted, there is a high to low D_b regression coefficient and significance change from MC_{PS} (Eq. 4.14) to MC_V (Eq. 4.15) due to the greater dependence of MC_{PS} on D_b via Eqs.4.5 and 4.6 while the significance levels for the predictor variables remain about the same. Also note that the best-fitted R^2 and RMSE drop from MC_{PS} to MC_V due to the narrower MC_V data range.

The + and - signs for the regression coefficients in Eqs. 4.14 and 4.15 follow expected trends for MC, namely:

- i. MC decreases with increasing DTW but increases as MC_{PSO} % (and therefore $MC_{PS,DWT}$ %) increase, as to be expected,
- ii. MC decreases towards higher and generally steeper elevations,

Table 4.6: Best-fitted MC_{PS} % and MC_V % models based on using plot-generated (Eqs. 4.14, 4.15; top) versus plot-projected (Eqs. 4.16, 4.17; bottom), listing significant regression variables and their coefficients, standard error estimates, and t- and p-values, together with R^2 , RMSE values and sample size (n).

Regression optimization	Dependent variables	Intercept & predictor variables	Regr. coeff.	±SE	t-value	p-value	R ²	RMSE	n
Using	MC _{PS} %	Intercept	48.396	6.131	7.894	< 0.0001	0.61	10.11	394
plot-specific	Eq. 4.14	$MC_{PS,DTW}$	0.212	0.063	3.357	0.0009			
determinations		log ₁₀ DTW _{1ha}	-2.178	0.813	-2.680	0.0077			
for each block		Sand	-0.144	0.046	-3.014	0.0018			
DIOCK		CF	-0.075	0.287	-2.624	0.0090			
		D_b	41.537	3.407	12.189	< 0.0001			
		Elevation	-0.107	0.010	-10.499	< 0.0001			
		HW Blocks	12.190	1.541	7.909	< 0.0001			
		Tracks	3.899	1.026	3.800	0.0001			
	MC _V %	Intercept	42.748	4.309	9.921	< 0.0001	0.51	7.49	394
	Eq. 4.15	$MC_{PS,DTW}$	0.155	0.047	3.304	0.0010			
		log ₁₀ DTW _{1ha}	-1.854	0.606	-3.057	0.0024			
		D_b	14.437	2.438	5.920	< 0.0001			
		Elevation	-0.077	0.008	-10.308	< 0.0001			
		HW Blocks	9.012	1.146	7.862	< 0.0001			
		Tracks	2.378	0.766	3.104	0.0021			
Using	MC _{PS} %	Intercept	70.883	6.326	11.205	< 0.0001	0.46	9.45	394
regionally	Eq. 4.16	$MC_{PS,DTW}$	0.264	0.073	3.589	0.0003			
available		$log_{10}DTW_{1ha}$	-2.764	0.926	-2.986	0.0003			
DEM, DSM, DTW layers		OM_{DSM}	-0.981	0.278	-3.529	0.0005			
together		Elevation	-0.091	0.013	-6.937	< 0.0001			
with forest		HW Blocks	10.224	2.136	4.788	< 0.0001			
cover and		Tracks	4.090	1.233	3.316	0.0010			
plot/weather- specific FIA	MC _V %	Intercept	49.018	4.096	11.968	< 0.0001	0.48	7.72	394
assignments	Eq. 4.17	$MC_{PS,DTW}$	0.186	0.047	3.932	< 0.0001			
		log ₁₀ DTW _{1ha}	-1.665	0.599	-2.927	0.0057			
		OM_{DSM}	-0.421	0.180	-2.338	0.0199			
		Elevation	-0.073	0.008	-8.650	< 0.0001			
		HW Blocks	9.000	1.383	6.509	< 0.0001			
		Tracks	2.449	0.798	3.067	0.0023			

- iii. MC is higher inside than outside soil tracks,
- iv. Soils under hardwood cover tend to be moisture than elsewhere, in part due to deeper rooting and higher top-soil OM accumulation.
- v. Contributions of sand and CF (both negative) to MC were also found to be significant, but only marginally s0: excluding these from the analysis changed R^2 for MC_V from 0.51 to 0.50, and for MC_{PS} from 0.63 to 0.60 (details not shown).

The best-fitted MC_{PS} and MC_V equations - obtained from substituting the plot-generated values for $MC_{PS,DTW}$ % with the block-assessed FIA values and with plot-level Eq. 4.3 estimates for OM generated from the digital soil layers for OM % (labelled OM_{DSM}) - are as follows (**Table 4.6**):

$$\begin{split} MC_{PS} &= 60.80 + 0.26 \times MC_{PS,DTW} - 1.84 \times log_{10}DTW_{1ha} - 0.74 \times FIA \\ &+ 0.14 \times Sand_{DSM} - 0.10 \times Elevation + 9.96 \times HW + 4.32 \times Tracks \end{split} \tag{4.16}$$

$$R^2 &= 0.46$$

$$MC_V = 45.22 + 0.18 \times MC_{PS,DTW} - 1.75 \times log_{10}DTW_{1ha} + 0.13 \times Sand_{DSM} \\ &- 0.54 \times OM_{DSM} - 0.07 \times Elevation + 8.48 \times HW + 2.53 \times Track \end{split} \tag{4.17}$$

$$R^2 = 0.46$$

The corresponding actual versus best-fitted scatterplots associated with MC_{PS} via Eqs. 4.12, 4.13, 4.14 and 4.16 are shown in **Figure 4.12**.

Using Eq. 4.14 produced the block-by- block presentation in **Figure 4.7**, which also shows the field-determined MC_{PS} plot values for the top 15 cm of soil outside and inside the tracks. Visually, there is a general agreement between the off-track field determinations and the corresponding projection, with off-track MC_{PS} generally higher than inside track.

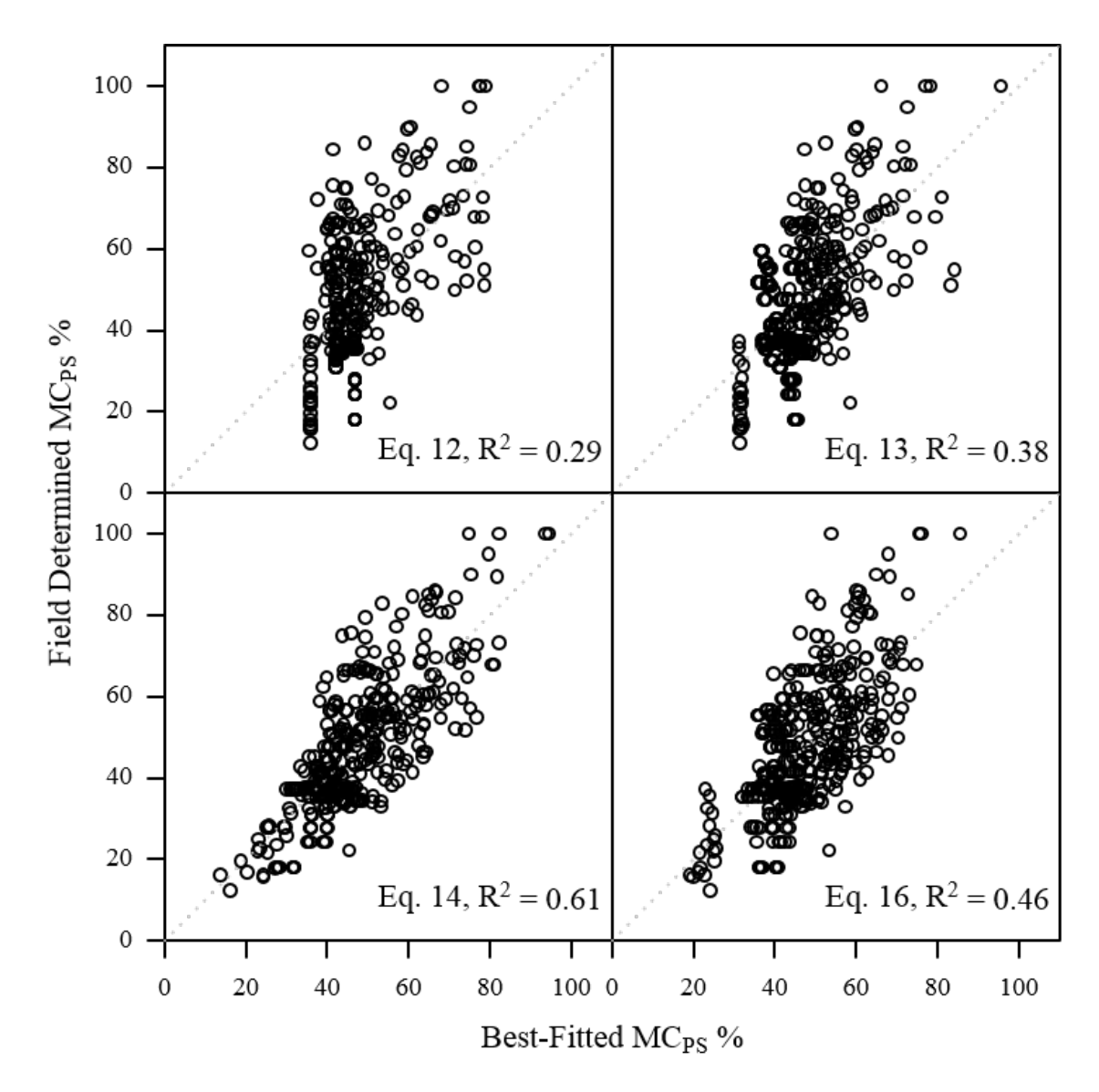


Figure 4.12: Scatterplots of actual versus best-fitted MC_{PS} scatterplots. Eq. 4.12 demonstrates the influence of block-generated DTW mapping on MC_{PS} alone. Eq. 4.13 demonstrates the improvements generated by way of block- and weather-influenced DTW mapping. Eq. 4.14 demonstrates the additional improvements obtained by adding variables describing forest cover type, elevation, soil density and track versus non-tracked specifications to the MC_{PS} regression analysis. Eq. 4.15 demonstrates that MC_{PS} can also be emulated using block-specific estimates for upslope soil- and weather-dependent flow-channel initiation (FIA) and organic matter estimates (OM_{DSM}) based of digital soil mapping (DSM).

Grouping the off- and in-track projections and corresponding field determinations into 10 % MC_{PS} classes produced the MC_{PS} confusion matrix and associated MC_{PS} cumulative conformance plots in **Figure 4.13**. In summary, the \pm 5 % MC_{PS} conformance level so found amounts to 34 % across the 20 <MC_{PS} <100 % range, but increases to 81 and 96 % as the conformance uncertainty increases to Δ MC_{PS} increases to \pm 15 and \pm 25 %, respectively. The possibility of randomly achieving these conformance levels have kappa values of 0.26, 0.73 and 0.92, respectively. The kappa value for random chance agreements equals zero, by definition.

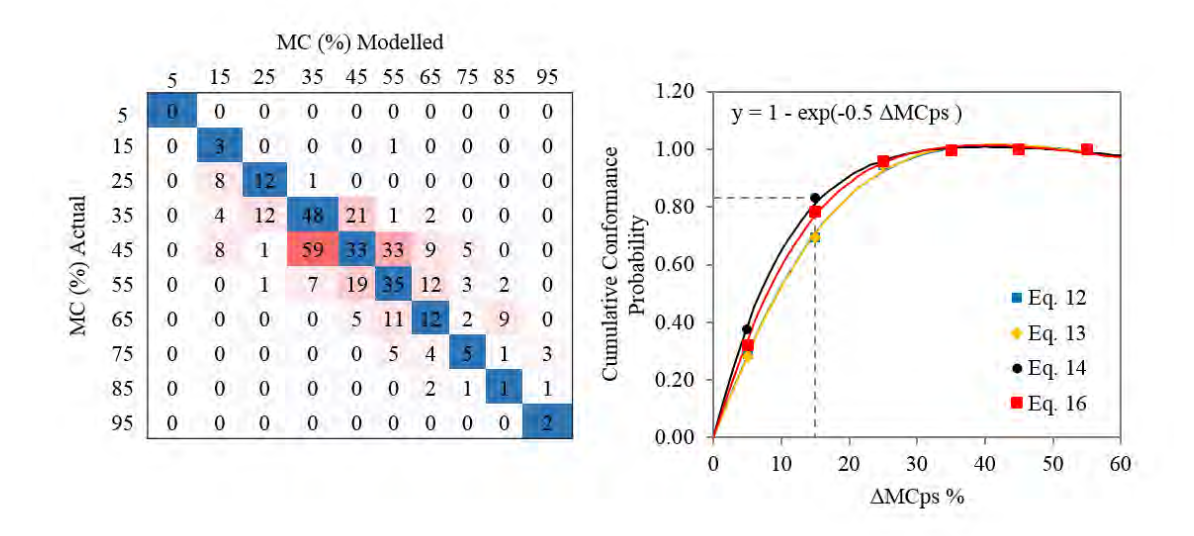


Figure 4.13: Confusion matrix for actual versus Eq. 4.14 projected MC_{PS} (left) and cumulative conformance probability for Eqs. 4.12, 4.13, 4.14, and 4.16 (right). Blue squares align 1 on 1 for the actual versus projected MC% classes, while the shades from dark to light red represent increasing projection differences.

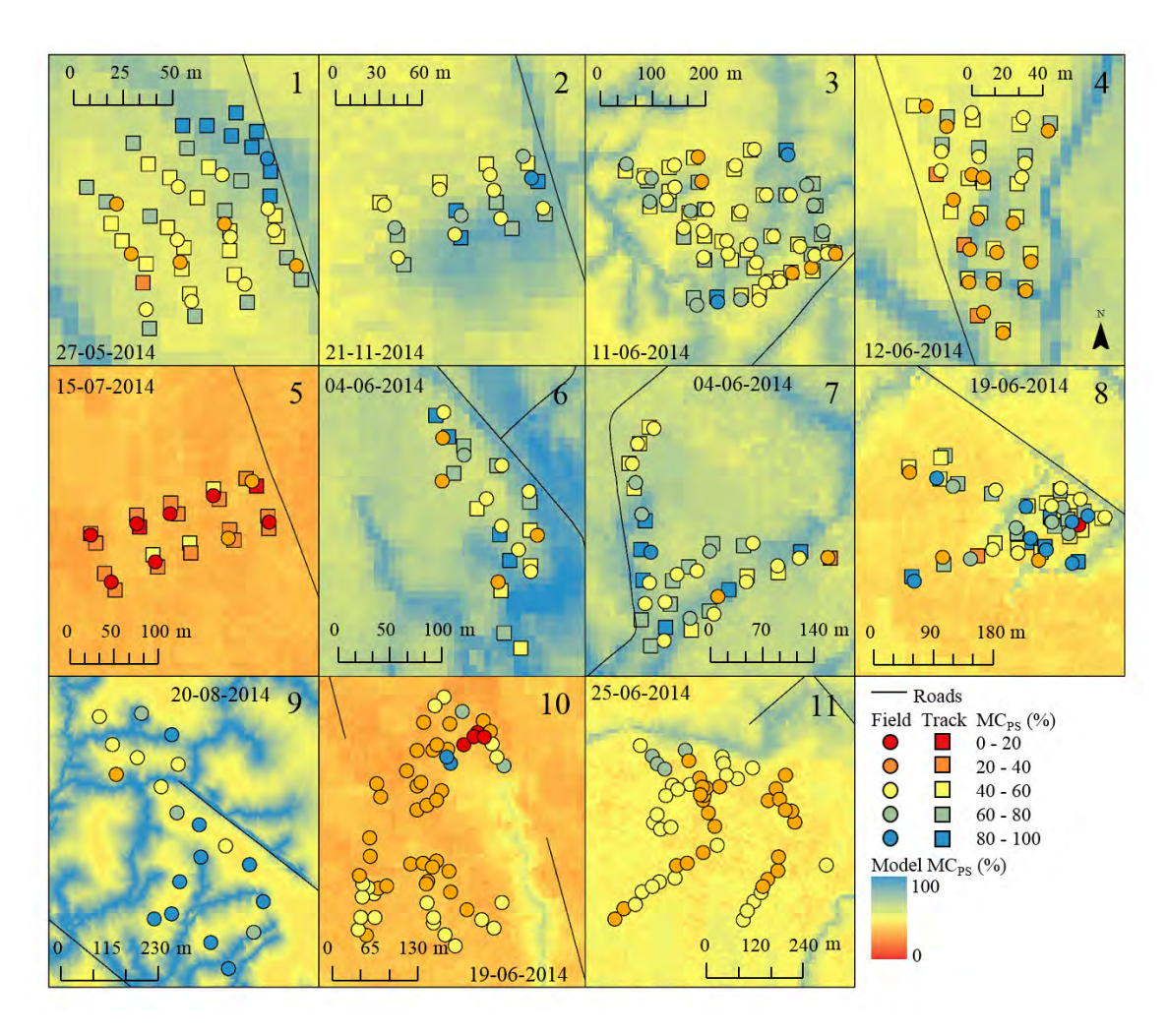


Figure 4.14: Overlay of field- and track- determined MC_{PS} on the Equation 4.16 generated MC_{PS} projections for Blocks 1 to 11 (blocks 9-11 have only field measured MC_{PS})

4.3.3 CI Derivation

The best-fitted CI results using plot-determined and plot-projected data are listed in **Table 4.7** and led to the following equations:

$$CI(plot-determined) = 1.60 - 0.01 \times MC_{PS} + 0.03 \times Depth +$$

$$0.76 \times Tracks + 0.40 \times SW$$

$$R^{2} = 0.41$$

$$CI(plot-projected) = 1.60 - 0.03 \times log_{10}DTW_{1ha} - 0.02 \times MC_{PS0} +$$

$$0.02 \times Depth + 0.64 \times Tracks + 0.32 \times SW$$

$$R^{2} = 0.39$$

$$(4.19)$$

where $0.03 \log_{10} DTW_{1ha}$ - $0.02 MC_{PS0}$ in Eq. 4.19 replaced -0.01 MC_{PS} in Eq. 4.18. These results affirm that the plot-determined CI values, as to be expected, increase with decreasing soil depth, are higher inside that than outside the tracks, are higher under softwood forest cover, decrease with increasing soil moisture content, and increase with increasing soil density. The associated significance levels vary as follows:

for Eq. 4.18: Track >Depth >MC_{PS} >SW >D_b for Eq. 4.19: Track >Depth >SW
$$\approx$$
 DTW_{1ha} >MC_{PSO}

Other variables such as Sand, Clay, CF and OM would also affect CI, but these variables were not found to make additionally significant CI contributions to the plot-determined or projected values. Quantitatively, Eq. 4.17 indicates that a change in MCPS from 0 to 100 % would lead to a change in CI by 3.1 MPa (all other conditions remaining the same). In comparison, CI would on average increase by 2.6 MPa from 0 to 1m soil depth. In comparison, CI values are about 0.7 MPa higher inside than outside tracks.

Table 4.7: Best-fitted CI models based on using plot-generated (Eq. 4.18) versus plot-projected (Eq. 4.19) and \log_{10} plot-generated CI (Eq. 4.20), listing significant regression variables and their coefficients, standard error estimates, and t- and p-values, together with R^2 , RMSE values and sample size (n).

Dependent variables	Intercept & Predictor variables	Regr. coeff.	±SE	t- value	p-value	R ²	RMSE	n
CI MPa	Intercept	1.599	0.159	10.06	< 0.0001	0.41	0.59	372
Eq. 4.18	MC_{PS}	-0.011	0.002	-5.98	< 0.0001			
	Depth	0.025	0.002	9.90	0.0583			
	Tracks	0.760	0.064	11.91	< 0.0001			
	SW Blocks	0.397	0.064	6.20	< 0.0001			
CI MPa	Intercept	1.604	0.367	4.37	<0.0001	0.39	0.60	376
Eq. 4.19	MC_{PSO}	-0.023	0.009	-2.53	0.0119			
	DTW_{1ha}	0.034	0.009	3.85	< 0.0001			
	Depth	0.022	0.002	8.87	< 0.0001			
	Tracks	0.644	0.067	9.62	< 0.0001			
	SW Blocks	0.319	0.087	3.66	0.0003			
log ₁₀ CI MPa	Intercept	0.152	0.039	3.90	< 0.0001	0.41	0.14	372
Eq. 4.20	MC_{PS}	0.002	0.001	-5.58	< 0.0001			
	Depth	0.006	0.001	10.03	< 0.0001			
	HW Blocks	0.091	0.016	5.84	< 0.0001			
	Tracks	0.189	0.015	12.11	< 0.0001			

The scatterplots associated with Eqs. 4.18 and 4.19 are presented in **Figure 4.15**. The scatterplot for the former is more heteroscedastic than the latter. Log-transforming CI the best-fitted results so obtained as listed in **Table 4.7** produces an even scatterplot in **Figure 4.15**, and the following equation:

$$log_{10}CI = 0.152 - 0.002 \times MC_{PS} + 0.006 \times Depth$$
$$+ 0.189 \times Tracks + 0.091 \times SW$$
(4.20)
$$R^{2} = 0.41$$

The overlays of the field-determined on the Eq. 4.18 projected CI values for the top 15 cm of soil are shown by Block in **Figure 4.15**, which also shows the corresponding values at 30, 45, and 60 cm depth for Block 3.

Grouping the field-determined and projected CI values into 0.25 MPa classes produced the CI confusion matrix and associated cumulative conformance plots in Figure 4.16. As shown, the CI confusion matrix has an actual with projected Δ CI \leq 0.25 MPa class conformance of 32 % across the 0.5 < CI < 4.5 MPa range. This conformance increases to 78 and 95 % as the uncertainty range for CI increases from \pm 0.5 and \pm 0.75 MPa, respectively. Achieving these agreements have kappa values equal to 0.23, 0.67 and 0.88, respectively. In comparison with the MC_{PS} kappa values, this suggests that the CI projections are slightly more random than the MC_{PS} projections.

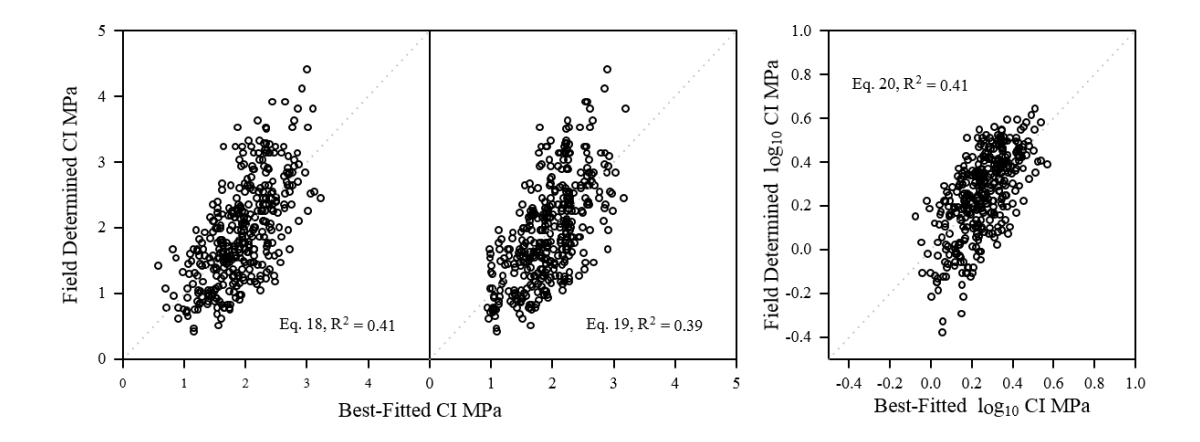


Figure 4.15: Scatterplots of actual versus best-fitted CI scatterplots. Eq. 4.18 demonstrates the additional improvements obtained by adding variables describing forest cover type, soil depth and track versus non-tracked specifications to the CI regression analysis. Eq. 4.19 demonstrates that CI can also be emulated using block-specific estimates for upslope soil- and weather-dependent ForHyM MC_{PSO} and depth-to-water. Eq. 4.20 demonstrates the log_{10} of CI.

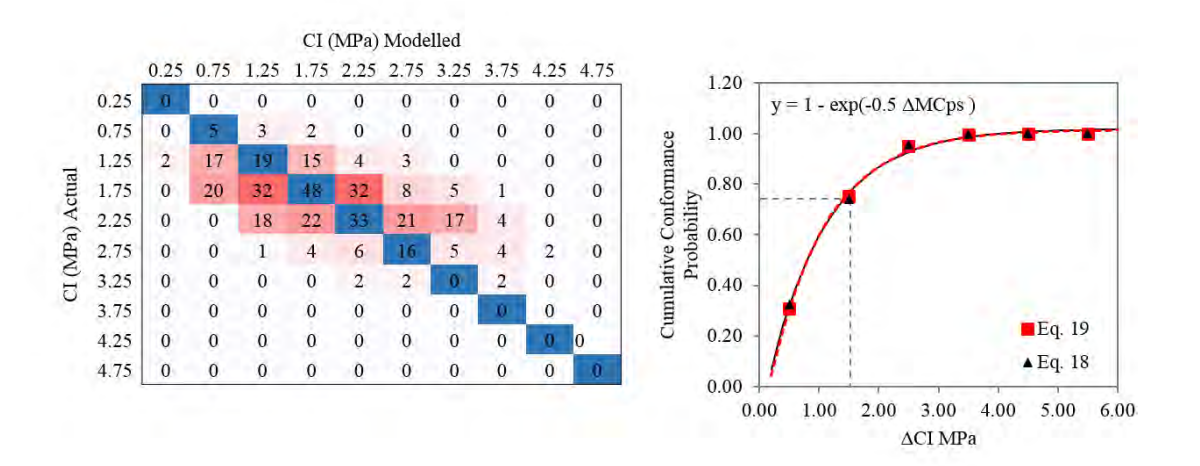


Figure 4.16: Confusion matrix for modelled vs Eq. 4.18 projected CI (left) and cumulative conformance probability for Eqs. 4.18 and 4.19 (right). Blue squares align 1 on 1 for the actual versus projected MC% classes, while the shades from dark to light red represent increasing projection differences.

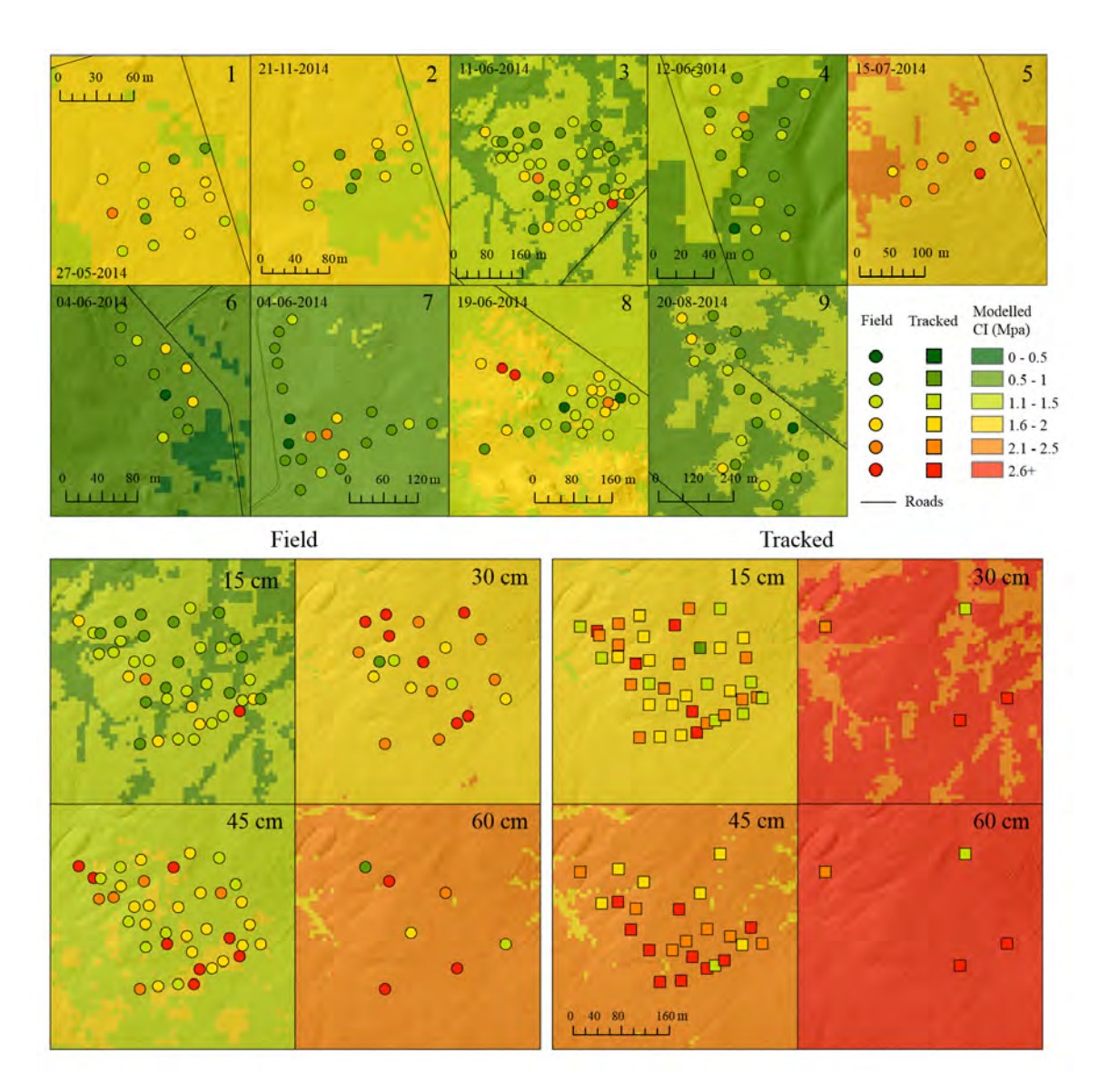


Figure 4.17: Eq. 4.18 generated CI projections at 15 cm depth for Blocks 1-9 outside wood-forwarding (top), and for 15, 30, 45 and 60 cm soil depths outside (left) and inside (right) the wood forwarding tracks for Block 3 (bottom).

4.3.4 Forecasting Block-specific Soil Moisture and Penetrability Conditions

The above results show that the combination of emulating layered soil properties and daily soil moisture simulations produces non-random soil moisture and cone penetrability projections across harvest blocks of varying topography, forest cover, geological substrates and weather conditions. To this effect, the extent of pore-filled moisture content can be predicted with a tolerance of 15 %, 8 times out of 10 within the 20 to 100 % soil moisture range. Similarly, the cone penetrability index can be predicted with a tolerance of ± 0.5 MPa, 8 times out of 10 within the 0.2 to 4.5 MPa range. In summary, generalizing similar results for the purpose of forecasting soil trafficability block-by-block requires:

- i. A 10 m resolution DEM layer with a tolerance of at least 2 m, 8 times of out
 10 (Furze et al., 2017);
- ii. A digital soil mapping process that emulates the required soil property layers at a general conformance level of 80 % (Furze, 2018);
- iii. An assessment of the season and weather dependent minimum upslope open-channel flow initiation area (FIA) as this could vary from 0.25 to 8 ha (Figure 4.4).
- iv. A forest hydrology model that can be used to estimate weather- and season-affected soil moisture content (MC_{PSO}) for ridge-top soils, to initiate, e.g., the Eq. 4.14 and 4.16 calculations (Jones and Arp, 2017), based on block-by-block elevation, slope, aspect, texture, $D_{\rm b}$, OM, CF, vegetation type and % canopy closure.

The MC and CI results so produce are projected in **Figure 4.18** for hardwood and softwood areas somewhat larger than Block 3 and Block 4. This was done for weather conditions that varied from essentially frozen in February to wet in May, dry in July, and moist in October. The blue shading in these plots suggests where rutting would occur on account of elevated MC and lowered CI values once wood-forwarding operations cross the areas so marked. For the most part, areas

prone to rutting would be aligned with the DEM-based flow-channel and associated DTW delineations as these vary by weather and season. Least rutting would have occurred in February (ground mostly frozen) and July (ground mostly dry), but would have been most extensive in May and later fall (ground mostly moist to wet).

4.3.5 Additional comments

While the above study provides a useful framework for delineating and evaluating soil trafficability restrictions on account of changes in soil moisture and soil penetrability, there is a need to validate the generality of this framework by:

- i. testing across all dominant and minor soil types within the same region;
- ii. application across other regions;
- iii. conducting sequential MC and CI determinations as ground conditions transit from wet to dry and from frozen to non-frozen.
- iv. advancing the digital soil property mapping process from coarse textured DEMs (Furze, 2018) to 1 m LiDAR-generated terrain elevation resolution. Doing so will likely increase the significance by which projected sand, clay, organic matter, coarse fragments and bulk density gain significance as MC and CI predictors.

Repeated topsoil moisture and density testing should ideally be done without probe insertions, i.e. via nuclear moisture-density gauge (Corns, 1988; Brown et al., 1998; Labelle and Jaeger, 2011). CI testing would benefit from hydraulic rather than manual testing (Hooks and Jansen, 1984; Herrick and Jones, 2002). Doing so would assist in reducing manually generated errors, inconsistencies, and biases, but would increase sampling expense.

There are other DEM-utilizing soil MC projection techniques. Most notably among these is the topographic wetness index (TWI; Beven and Kirkby (1979); Sørensen

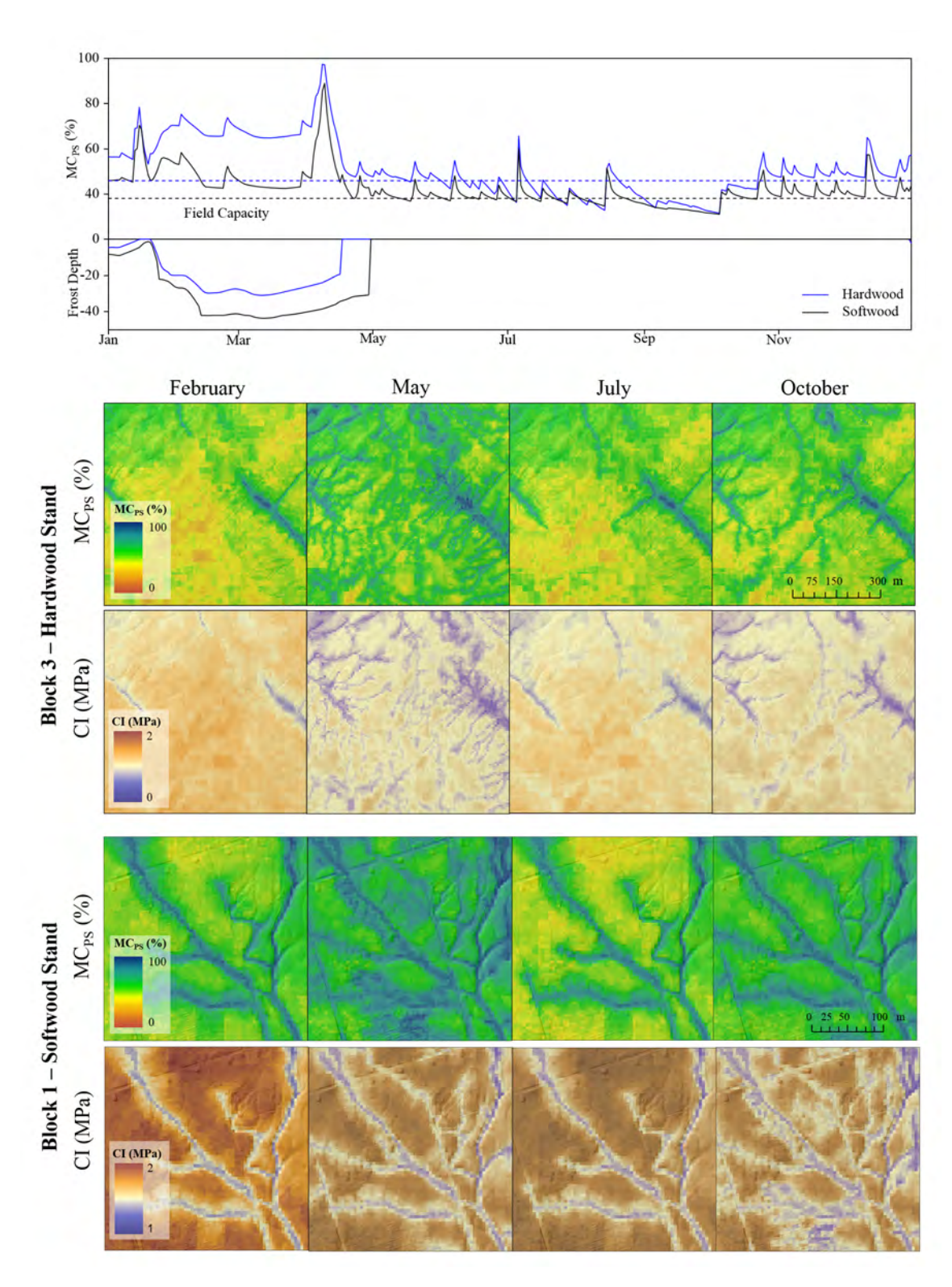


Figure 4.18: ForHyM modelled MC_{PS} for ice and water combined, in relation to soil moisture retention at field capacity (top) with spatially projected MC_{PS} (Eq. 4.14) and CI (Eq. 4.18) on block 3 (hardwood forest and soil conditions; middle) and block 4 (softwood forest and soil conditions; bottom).

et al. (2006)). This index emulates soil wetness to local upslope flow-accumulation areas and slopes, i.e., TWI = In (flow accumulation area / slope). Comparative studies revealed that TWI-inferred MC depends strongly on TWI-cell averaging (Murphy et al., 2009b; Ågren et al., 2014), while DTW-inferred MC can directly be related to field-based DTW measurements (Dobbie and Smith, 2006; Murphy et al., 2009b).

Optimal TWI-based MC interpretations are generated by filling noise-generated DEM pits, followed by changing the focal search radius for cell-centered mean elevation differences, slope and TWI (Southee *et al.*, 2012). The resulting MC correlations with TWI had R² values ranging from 0.06 to 0.36, with best-results obtained for the 5 to 10 m cell-size range. Attempts focused on analyzing soil moisture conditions from spectral surface images tend to produce mixed results, especially for soils covered by vegetation and vegetation litter (Njoku and Entekhabi, 1996; Das and Paul, 2015). Best results are generally observed for bare to open mineral soil surfaces (Jackson, 1993; Engman and Chauhan, 1995; Wang and Qu, 2009; Das and Paul, 2015).

Further digital soil property mapping improvements can likely be obtained using LiDAR-generated DEMs at 1 m resolution. Doing so would likely increase the significance by which projected sand, clay, organic matter, coarse fragments and bulk density gain significance as MC and CI predictors.

With reasonable soil- and weather-informed MC and CI projections, it is feasible to generate machine- and load-specific rut depth maps as affected by machine type, loads, tire dimensions, and number of wood-forwarding passes, as demonstrated by Vega-Nieva et al. (2009) and Jones et al. (2018). In turn, such projections can be used to evaluate existing traffic-induced soil disturbance impacts as demonstrated by Campbell et al. (2013).

4.4 Conclusion

The above soil MC and CI assessment is limited to forested areas within northwestern New Brunswick, Canada. The approach taken emulates block-specific soil MC and CI variations with $R^2 = 0.61$ and 0.40, respectively. The dominant predictor variable refers to daily soil moisture levels as affected by weather, DTW, sand, D_b, CF, soil depth, stand type (HW or SW) and sampling location, inside or away from harvest tracks). Other potentially important MC and/or CI contributing variables yet to be addressed refer to the presence and extent of stumps and roots, depth of local forest litter accumulations, local variations in micro-topography pertaining to mounds and pits, and the number of passes per track. Implicitly addressed are the variations in soil OM due to general association between OM, D_b and soil pore space via Equations 4.3 to 4.6. The effect of brush-matting on MC and CI was found to be too variable to make significant contributions to the best-fitted MC and CI regression results. The lack thereof is likely related to branch-specific soil compaction and displacement variations at the centimeter scale.

4.5 Acknowledgments

This research was supported by an NSERC-CRD supported Forest Trafficability project, with further support by J.D. Irving, limited. Special thanks go to the Forest Watershed Research Center at UNB for field sampling (Doug Hiltz, Mark Castonguay, Clara Ndekuringe Dennis, and Tanner Sagouspe).

Chapter 5

Soil Trafficability Forecasting

Marie-France Jones and Paul Arp

Faculty of Forestry and Environmental Management,

University of New Brunswick, Fredericton NB, Canada E3B 6C2

Email: arp2@unb.ca

Foreword:

The following chapter is a published article within the Open Journal of Forestry. It was submitted on July 10, 2019 and accepted for publication on July 23, 2019. Publication permission can be found in **Appendix D.1**.

Citation:

Jones, M.-F., Arp, P.A. (2019) Soil Trafficability Forecasting. *Open Journal of Forestry*. Approved for publication.

Abstract

This chapter introduces and evaluates a Soil Trafficability Model (STRAM) designed to estimate and forecast potential rutting depth on forest soils due to heavy machine traffic. This approach was developed within the wood-forwarding context of four harvest blocks in Northern and Central New Brunswick. Field measurements used for model calibration involved determining soil rut depths, volumetric moisture content, bulk density, soil resistance to cone penetration (referred to as cone index, or CI), and the dimensionless nominal soil cone index NCI defined by the ratio of CI over wheel foot print pressure. With STRAM, rut depth is inferred from: (i) machine dimensions pertaining to estimating foot print area and pressure; (ii) pore-filled soil moisture content and related CI projections guided by year-round daily weather records using the Forest Hydrology Model (ForHyM); (iii) accounting for within-block soil property variations using multiple and Random Forest regression techniques. Subsequent evaluations of projected soil moisture, CI and rut-depth values accounted for about 40 (multiple regression) and 80 (Random Forest) percent of the corresponding field measured values.

Keywords

Soil trafficability, forecasting, rutting, soil moisture, density, cone index, wood forwarding, regression comparisons, depth-to-water index.

5.1 Introduction

With the wide-spread use of modern mechanized harvest machinery, forest and agricultural planners have to deal with the effects of heavy machine loads on soil rutting, compaction, erosion, and subsequent reductions in crop yields (Brady and Weil, 2008). Increased soil compaction reduces soil porosity, increases soil runoff, damages and crushes roots, and leads to reduced root growth due to decreased soil oxygen levels (Grigal, 2000; Horn *et al.*, 2004; Bassett *et al.*, 2005; Singer and Munns, 2006; Chen and Weil, 2011). Rutting results from combined soil compaction and soil displacement. Soil displacement occurs when the soils within depressions and along slopes are moist to wet above field capacity (Raper, 2005; Naghdi *et al.*, 2009). Depending on their slope orientations, ruts can increase, decrease, or collect run-off (Sutherland, 2003; Antille and Godwin, 2013; Poltorak *et al.*, 2018).

A measure of soil strength, known as cone index (CI) is used to understand soil compaction and rutting. This strength and related CI measurements varies from weak to strong as soil moisture content decreases, and this is particularly so in fine-textured soils. In contrast, sandy soils remain friable from wet to dry (Earl, 1997; Vaz, 2003; a.R. Dexter *et al.*, 2007; Tekeste *et al.*, 2008; Vaz *et al.*, 2011; Kumar *et al.*, 2012; Jones and Arp, 2017).

To enhance compliances towards best forest management practices, various jurisdictions have established criteria as to what constitutes a rut. For example, the Province of British Columbia (Canada) classifies ruts >15 cm deep to be a hazardous disturbance. The Province of Alberta considers any soil disturbance track deeper than 10 cm as ruts (Alberta Forest Products Association, 1994; Van Rees, 2002). The Pacific Northwest region of the USA defines ruts to be at least 15 cm deep (Page-Dumroese *et al.*, 2000). Images of what constitutes minor to severe soil disturbances including rut depths are presented in **Table D.1**.

As summarized in **Table 5.1**, the earlier rut-depth prediction models by Maclaurin (1990) and Rantala (2001) focused on regression-related rut depth as caused by single wheel and single machine passes to the ratio of tire footprint pressure over soil resistance to penetration, also referred to as nominal cone index, or NCI. Scholander (1974) and Saarilahti (2002b) extended this approach towards multiple passes. Vega-Nieva *et al.* (2009) modified the NCI-based multi-pass regression model by examining the experimental wood-forwarding rut-depth data by Meek (1996) for a sandy and a clay loam soil at varying moisture content, and with a suggestion to correct for coarse fragment content. A recent study by Sirén *et al.* (2019a) also related rut depth to number of machine passes, volumetric soil moisture content, and Cl. All these studies, however, captured only a small portion of the field determined rut depth variations whether these were based on fixed or fixed plus random effects regression models.

Table 5.1: Historical rut depth model.

Rut Depth Parameter	Study Citation	Rut Depth Equation	R^2
First wheel pass	(Maclaurin, 1990)	$Z = d \times \frac{0.224}{NCI^{1.25}}$	0.10
First cycle pass	(Rantala, 2001)	$Z = -0.026 + \frac{0.629}{NCI}$	0.11
Multi-pass	(Scholander, 1974)	$Z = Z_1 \times n^{\frac{1}{a}}$	0.23
	(Saarilahti, 2002b)	$Z_n = (Z_{n-1}^{a_n} + Z_1^{a_b})^{\frac{1}{a_n}}$	0.10
	(Vega-Nieva <i>et al.,</i> 2009)	$Z_n^0 = \frac{r_1}{NCI_0} n^{\frac{1}{p_1(NCI_0)^{p_2}}} (1 - CF)^2$	0.25
	(Sirén <i>et al.</i> , 2019b)	$logZ = b_0 + b_1 \times M + b_2 \times MC_v + b_3 \times CI + u_{tm} + e_{tm}$	NR

z = rut depth; b_n = parameter coefficients; D = wheel diameter; Cl = cone index; n = number of passes; NCl = nominal cone index; CF = coarse fragment; MC_v = volumetric moisture content; M = cumulative machine mass; a = multi-pass coefficient (a=0.3 × CI; a= 1.5 × NCI^0 .7); p_1 , p_2 , and r_1 = site specific calibration parameters; utm = random line effect; etm = pass effect.

This chapter reports on the extent of improving wood-forwarding rut depth modelling based on:

- i. using field-determined data for soil density, texture, organic matter, coarse fragment and weather-inferred ridge-to-valley soil moisture, CI, and machine-specific NCI variations for the rut depth projection purpose;
- ii. employing fixed and random forest regression techniques for optimizing these projections;
- iii. selecting four of the eleven harvest blocks described in Jones and Arp (2019a) for this purpose; these blocks involved wood forwarding from shelterwood cutting (2) and from commercial thinning (2) in Northern and Central New Brunswick, Canada.

5.2 Materials and Methods

5.2.1 Block Descriptions

Details regarding the wood-forwarding operations within the four harvest blocks chosen for this study are presented **Figure 5.1** and **5.2** by location, and in **Table 5.2** by block-specific attributes. These blocks are a subset of the 11 blocks used by Jones and Arp (2019a) for their on- and off-track soil moisture and CI study.

Blocks 1 and 2 are within 1 km of each other, and share similar site characteristics. They are located within the Western reach of the Chaleaur uplands. Both Blocks are white spruce (*Picea glauca* (Moench) Voss) plantations. Block 2 covers a 2 ha area and block 3 covers 20.8 ha, but sampled in a 3.5 ha area. The region has an annual temperature of 3.8 °C, ranging between -11.5 °C and 18.2 °C in January and July averages, respectively. Mean precipitation is roughly 1110 mm with 300 mm as snow (Department of Environment and Climate Change Canada, 2016a). Surficial topography is mainly morainal sediment, including loamy lodgment tills, and is underlain by late Ordovician deep water marine clastics rocks.

Block 3 is a 20.9 ha shelterwood cut located in the southern reach of Notre Dame Mountains, within the Appalachians Mountain range. The area has a mean air temperature of 3.5 °C, ranging from -12.9 °C to 17.6 °C January and July averages, respectively. It has a mean precipitation of 1140 mm, with 310 mm as snow (Department of Environment and Climate Change Canada, 2016a). The block is composed moderate to intolerant hardwood/mixedwood rich in red maple (*Acer rubrum* L.), yellow birch (*Betula alleghaniensis* Britt.) and balsam fir (*Abies balsamea* L.). Geology of the area is later late Ordovician deep water marine clastics rocks, with topography ranging from gentle, rolling plateaus to steep valleys of hummocky ablation moraines.

Block 9 is a 25.5 ha shelterwood cut located in the Southern tip of the Miramichi highlands. It is roughly 50 km from the Fredericton, the provincial capital. The area has a mean air temperature of 5.5 °C, with a range of -9.4 to 19.4 °C, respectively for January and July, and roughly 1100 mm of annual precipitation, with 250 mm as snow (Department of Environment and Climate Change Canada, 2016a). The block is comprised of natural mixedwood and tolerant hardwood, including Eastern hemlock (*Tsuga canadensis* L. Carrire), yellow birch, sugar maples (*Acer Saccharum* Marsh.), beech (*Fagus grandifolia* Ehrh.), with some balsam fir, Eastern white cedar (*Thuja occidentalis* L.), and black spruce (*Picea mariana* Mill). The terrain of the region consists of morainal sediment (ablations and boulder tills) underlain by early Devonian mafic volcanic rock and late Ordovician deep water marine clastic rocks.

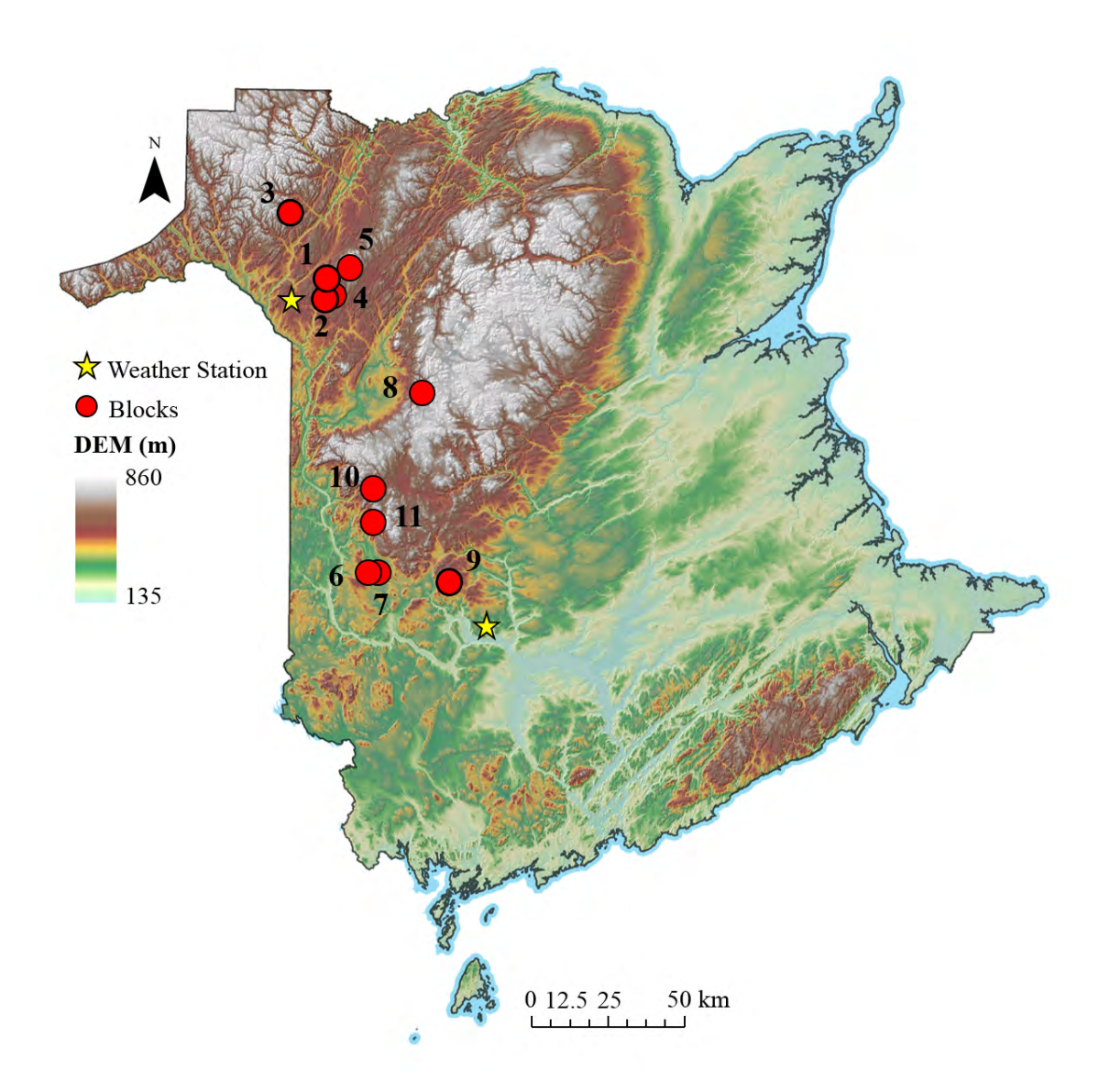


Figure 5.1: Map showing block locations (Blocks 1 to 11), with Blocks 1, 2, 3, and 9 selected for rut depth determinations following wood forwarding and a grapple skidder.

Table 5.2: Block description by geographical location, species specific forest type, block properties (elevation, slope, aspect), and soil association type, as well as plot counts for MC/CI, and rut field plots (highlighted in grey).

Rut Plots	29	40	75			1	1	1	63	,	
MC/CI Plots	28	28	80	46	33	56	43	2	24	147	159
Aspect (°)	158	112	189	127	149	148	158	140	182	185	214
Slope (°)	2.5	3.4	4.6	3.1	9.1	4.6	5.5	4.5	7	8.9	9.6
Elevation (m)	267	265	351	280	388	210	203	418	277	422	319
Soil Association	Victoria	Victoria	Glassville	McGee	Glassville	Jacquet River	Jacquet River	Juniper	Long Lake	Popple Depot	Kingston
Oper- ation ³	CI	C	SHW	00	C	SC	SC	SHW	00	SHW	SHW
Tree Species ²	WS	WS	BI/RM	BS	WS	EH/YB/M	EH/YB/M	SM/YB	SM/YB	SM/YB	SM/YB
Forest Type ¹	SWPL	SWPL	IntHW	SWPL	SWPL	Μ	Μ	TolHW	TolHW	TolHW	TolHW
Rut Sample Date	21/5/14	21/10/14	20/10/14			,	,	,	20/8/14	,	
MC/CI Sample Date	27/5/14	21/11/14	11/6/14	12/6/14	15/7/14	4/6/14	4/6/14	19/6/14	19/11/14	19/6/13	25/6/13
Oper- ation Date	5/14	6/14	6/14	5/14	7/14	6/14	6/14	6/14	10/14	9/12	10/12
Lat / Long Coord.	47°15′4.07″ N 67°37′27.10″ W	47°14′21.83″ N 67°37′26.92″ W	47°32′23.62″ N 67°47′46.29″ W	47°14′59.25″ N 67°37′18.82″ W	47°18′20.73″ N 67°31′42.64″ W	47°12′15.04″ N 67°14′17.55″ W	46°12′24.99″ N 67°15′55.07″ W	46°42′51.41″ N 67°3′38.87″ W	46°10′42.56″ N 66°56′30.53″ W	46°26′23.96″ N 67°15′24.66″ W	46°20′44.44″ N 67°15′1.28″ W
Block	_	2	က	4	5	9	7	∞	6	10	11

PL: plantation, INHW: intolerant hardwood, TOWH: tolerant hardwood, WS: white spruce, Bl: birch, RM: red maple, SM: sugar maple CT: commercial thinning,

CC: clear cut, SHW: Shelterwood



Figure 5.2: Plot specific location including machine tracks, field plot locations (top), and photos from within the blocks (bottom).

5.2.2 Wood Forwarding

Three GPS-tracking wood-forwarding machines were used: a John Deere 1510E forwarding Blocks 1 and 2, a John Deere 1110E forwarder in Block 3, and a Tigercat 635D in Block 4 (**Table 5.3**). The resulting GPS data were processed to determine the number of passes per same track using point buffering and overlapping tools (Buja, 2012). Studies have shown that the number of wood-forwarding passes affects soil structure, compaction, and rut depth (Eliasson, 2005; Ampoorter et al., 2007; Farzaneh et al., 2012; Jones et al., 2018). Some studies have looked at mitigating multiple-pass soil rutting using brushmats (McDonald and Sexias, 1997; Labelle et al., 2015). Brushmats were not found along the forwarding trails in Blocks 3 and 9, but were present to varying degree in Blocks 1 and 2 as part of the commercial thinning operation. Machine footprint is related to the amount of disturbance on a harvested site. Studies have shown that with increasing tire pressure there is a lower overall tire footprint which increases rutting (Raper et al., 1995; Saarilahti, 2002c; Jun et al., 2004; Affleck, 2005; Sakai et al., 2008). Lower pressured tires are used in wetter or sensitive areas for this reason.

Table 5.3: Machine specifications (Jones *et al.*, 2018).

Machine Specs	JD1	110E	JD1	510E	TC6	35D
wachine specs	Front	Rear	Front	Rear	Front	Rear
Vehicle Weight (ton)	16	.5	17	7.3	2	1.4
Full Load Weight (ton)	11	.0	12	2.0	1	5
Chassis Clearance (cm)	6	0	60).5	63	3.5
Wheel Rim (cm)	67	. .3	67	7.3	8	1.3
Number of Wheels	4	4	4	4	2	4
Tire Type	710/4	5-26.5	710/4	5-26.5	35.5Lx32	30.5Lx32
Accessories	Chains	Tracks	Tracks	Tracks	Chains	Tracks
Diameter (cm)	134	4.1	13	4.1	201.2	184.4
Section Height (cm)	33	.4	33	3.4	59.9	51.6
Width (cm)	71	.1	71	1.1	90.2	77.5
Pressure (max, psi)	3:	2	3	2	3	2

5.2.3 Data Sources

The data needed to process the temporal and spatial modelling of MC, CI, and soil rutting consists of:

- i. Daily precipitation (snow and rain) and mean air temperature data, needed for the hydrological soil moisture calculations for Blocks 1-3 and Block 9, were obtained from the airport weather station records at Saint Leonard and Fredericton, respectively (Department of Environment and Climate Change Canada, 2016a);
- ii. Hydrometric stream discharge data is needed to calibrate ForHyM from the nearby Black Brook Watershed group for Blocks 1-3 (Black Brook Watershed Research site, 2014), and Nashwaaksis stream data for Block 4 (Department of Environment and Climate Change Canada, 2016a);

- iii. LiDAR-generated bare-ground elevation data were downloaded from geoNBs website at 1 m resolution (GeoNB, 2015b);
- iv. Digital soil maps (DSM layers) for soil texture (sand, silt and clay content), bulk density, coarse fragments, and soil organic matter for top 30 cm of soil were downloaded from the Forest Watershed Research web-site server (Furze, 2019).
- v. GPS-recorded machine-clearance pattern spaced at 10 sec intervals along each wood-forwarding track (Jones *et al.*, 2018).

5.2.4 Field Measurements

Soil samples as well as volumetric soil moisture (MC $_{\rm v}$) and cone index (CI) readings were obtained from the top 15 cm layer of undisturbed mineral soil across Blocks 1 to 11, as described in Jones and Arp (2019a) in the Fall of 2014 after the wood-forwarding operations (**Table 5.2**). The samples were analyzed for texture (sand, silt and clay %), coarse fragments (%), organic matter content (%), and bulk density (g/cm 3). Wood-forwarding rut depths were determined at GPS-recorded intervals along the tracks. The number of passes along the tracks were obtained from the GPS-tracked wood-forwarding machine-clearance records (Jones *et al.*, 2018) through counting the number of passes per same track using digital point buffering and overlapping tools (Buja, 2012).

5.2.5 Soil Moisture Modelling

The Forest Hydrology Model ForHyM was used to estimate daily variations in pore-filled soil moisture content (MC_{PS}) on the well-drained soils in each block. The MC_{PS} output so generated then served to determine how MC_{PS} would have varied at the time of wood forwarding across the terrain of each block according to season- and weather- affected flow channel locations by way of

cartographic depth-to-water (DTW) modelling (Murphy *et al.*, 2009a; White *et al.*, 2012). This process is conceptualized and illustrated in **Figure 4.3** and **4.4**.

The cross-terrain MC_{PS} projections were originally based on Vega-Nieva *et al.* (2009) and Jones and Arp (2019a):

$$MC_{PS,DTW} = 100 - [100 - MC_{PS,top}] \times \left[\frac{1 - exp(-k_{mc} \times DTW)}{1 - exp(-k_{mc} \times DTW_{top})} \right]^{p_{mc}}$$
 (5.1)

where $MC_{PS,top}$ refers to the pore-filled soil moisture content, and DTW_{top} refers to at the DTW at highest elevation in each block. Also, k_{mc} and p_{mc} are block-specific calibration parameters (0.5 and 1.5), and $MC_{PS,DTW} = 100$ % along water-filled flow channels where DTW = 0 m by definition (**Table 5.4**). As indicated by Jones and Arp (2019a), the MC_{PS} projections were augmented via multiple regression analysis inside and outside wood-forwarding tracks to account for terrain changes in response to changes in elevation, forest cover type (hardwoods, softwood, open areas), and soil organic matter content (OM_{DSM}) as follows:

$$MC_{PS} = 70.88 + 0.26 \times MC_{PS,DTW} - 2.76 \times log_{10}DTW_{FIA} - 0.98 \times OM_{DSM}$$

 $-0.10 \times Elevation + 10.22 \times HW + 4.09 \times Track$ (5.2)
 $R^2 = 0.46$

with $log_{10}DTW_{FIA}$ referring to the logarithm of the rasterized depth-to-water index adjusted to the upslope flow initiation area (FIA) at the time of wood forwarding. In addition, OM_{DSM} is the digitally derived soil organic matter raster (Furze 2018; in %), DEM is elevation in meters, $logarithmath{Track} = 1$ for ruts and 0 otherwise, and $logarithmath{HW} = 1$ refers to locations dominated by hardwood, otherwise $logarithmath{HW} = 0$. The values of model parameters required for Eqs 1. and 2 are listed in **Table 5.4**.

Table 5.4: Model parameters for stands 1, 2, 3, and 9. MC_{PS} (%) refers to the ForHyM-modelled soil moisture content at highest elevation within each block at the time of wood forwarding.

Block	DTW _{FIA} (ha)	MC _{PS,top} (%)
1	1	39.9
2	16	35.3
3	1	39.4
9	0.25	26.4

5.2.6 Cone Index and Rut Depth Modelling

Rut locations and depths were GPS tracked and measured in the fall of 2014 immediately after the wood-forwarding operations, as listed in (**Table 5.2**). Volumetric soil moisture, bulk density (D_b) and cone penetration measurements were obtained prior to these operations (for details, see Jones and Arp, 2019). Once MC_{PS} was rasterized, CI (in MPa) and NCI version were emulated using the following expression (Jones and Arp, 2019a):

$$CI = 1.60 - 0.01 \times MC_{PS} + 0.03 \times Depth + 0.76 \times Track + 0.40 \times SW$$

$$R^{2} = 0.41$$
(5.3)

where Depth is the chosen soil depth (cm), Track = 1 signifies presence of track with Track = 0, is undisturbed soil, and SW = 1 signifies where softwoods are dominant, otherwise SW = 0.

The normalized cone index NCI (dimensionless) was derived from:

$$NCI_0 = \frac{(100 * CI * d * b)}{W} * \sqrt{\frac{\delta}{h}} * \frac{1}{(1 + 2 * d)}$$
 (5.4)

with d as tire diameter (m), b as tire width (m), W as total wheel load (kN) given by (machine weight + load) / number of tires, h as section height of the tire (m), and δ is tire deflection (m) given by 0.008 + 0.001 (0.365 + 170/p), with p is tire

inflation pressure (in kPa).

Machine-induced rut depths was estimated using multivariate regression by setting:

$$z = log_{10} Passes \times log_{10} NCI \times log_{10} DTW_{FIA}$$

$$R^{2} = 0.28$$
(5.5)

where z is the rut depth, NCI is Eq. 5.4, and DTW_{FIA} is the depth to water at the chosen FIA to accomodate seasonality. Further non-linear regression was used to develop:

$$z = \frac{40.8}{NCI_{adj}} \times Passes^{0.071 \times NCI_{adj}}$$
 (5.6)
$$R^2 = 0.32$$

where NCl_{adj} is Eq. 5.4 which has been adapted for increase proportional representation of DTW (NCI + 0.48 x DTW_{FIA}), and passes is the number of trail passes by machinery.

5.2.7 Statistical Analyses

All analyses were performed in R (R Core Team, 2015) after combining the rasterized data layers into a covariate stack. A correlation matrix was created to show the general association pattern between the covariates, and was evaluated by way of factor analysis to determine the general covariate association pattern. This was followed modelling MC_{PS} , CI, and z_n ($n_n = 1$) regression formulations (Breiman, 2001).

The multivariate regression (MR) formulation as detailed above by way of Eqs. 5.1 to 5.6 served to explore the extent of functional dependence of MC_{PS} , CI, and z_n on weather, season, machine-type, and digital soil mapping layers. This include a

non-linear DTW-based adjustment for Eq. 5.6. The Random Forest formulation served to explore the extent to which the field-determined MC_{PS} , CI, and z_n values could be replicated using the same specifications. The dataset for modelling MC_{PS} (n= 394) and CI (n = 372) included all top 15 cm soil sampling locations inside and outside the tracks in Blocks 1 to 11. The dataset for modelling rut depth (n = 207) applied to Blocks 1, 2, 3, and 9 only,

The required input for modelling MC_{PS} via Eq. 5.2 refers to $MC_{PS,DTW}$ (Eq. 5.1), $log_{10}DTW$, OM_{DSM} , DEM, HW=1 or 0, and Track=0 or 1. The required input for modelling CI via Eq. 5.3 refers to modelled MC_{PS} , Depth, SW=1 or 0, and Track=0 or 1. The required input for modelling rut depth via Eq. 5.4 refers to modelled NCI and number of passes.

The Random Forest analysis was conducted using k-fold cross validation of the entire dataset using the randomForest R package Liaw and Wiener (2002). The data training process was limited to optimizing the outcome of 10 fold validation with 10 replicates. Each analysis utilized optimized variables to decide on best-fitting MC_{PS} , CI, NCI and rut depth outcomes. Model performance was determined by evaluating the mean decreased accuracy and variable importance and then compared to linear regression using RMSE and R^2 for the MC_{PS} , CI, and rut depth evaluation outcomes.

5.2.8 Soil Trafficability Model (STRAM)

The information flow generated from modelling soil moisture, CI and rut depth via MR and RF was organized in the form of a Soil Trafficability Projection framework (STRAM), as represented by the flow chart in (**Figure 5.3**).

Applying STRAM involves:

- i. Initializing and calibrating ForHyM to determine MC_{PS} for specific weather conditions, by block and stand type.
- ii. Projecting MC_{PS} across the terrain based on digital elevation, DTW, and soil mapping techniques, by block, using Eq. 5.2.
- iii. Combining the weather-specific MC_{PS} projections with digitally generated soil property to generate the CI, NCI and rut depth data layers, by block, using Eqs. 5.3 to 5.5.
- iv. Optimizing these data layers through R-tool regression techniques (fixed effects, Random Forest) based on actual field observations where available.

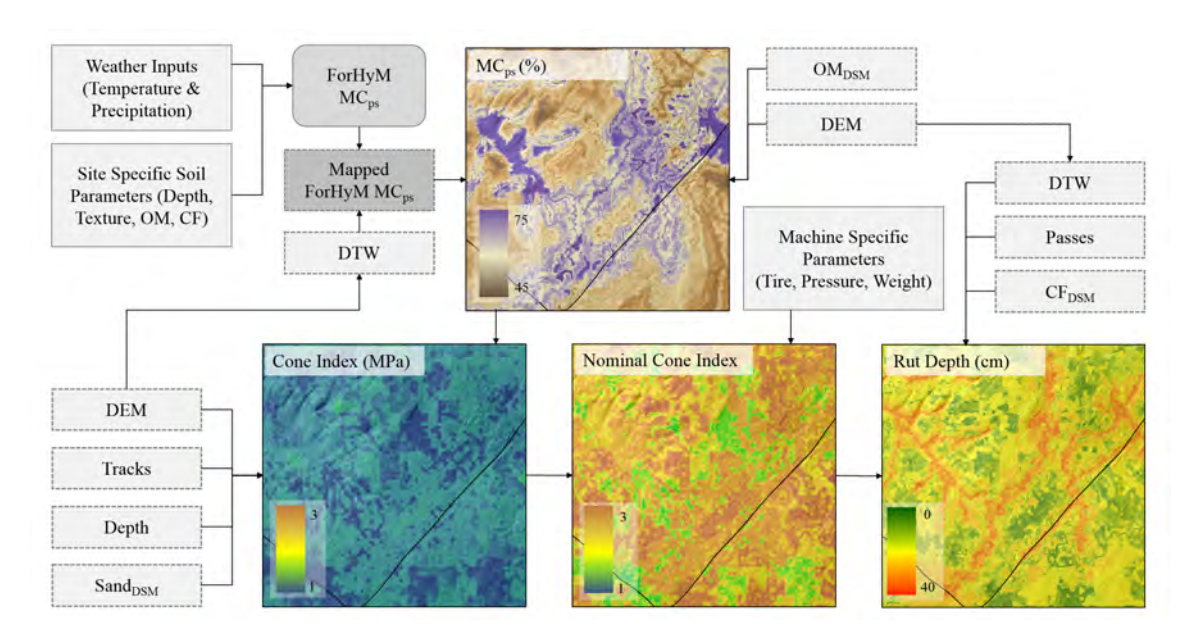


Figure 5.3: Flowchart for the soil trafficability model (STRAM): generating the rut depth raster for Block 3.

5.3 Results

The basic statistics of the plot-centered rut depth, MC_{PS} , CF_{DSM} , $Sand_{DSM}$, OM_{DSM} , $D_{b,DSM}$, C_{DSM} , elevation, DTW, CI, and NCI values are listed in **Table 5.5**. The

correlation coefficients and their non-zero significance levels between these variations in association with block location are compiled in **Table 5.6**, along with the corresponding factor analysis. Factor 1 indicates that the rut-depth determinations relate positively to number of wood-forwarding passes, to sand and organic matter content, and to soil depth (C_{DSM}), but negatively to NCI, as to be expected. In addition, rut depth is generally deeper in the hardwood blocks (Blocks 3 and 9). Factor 2 reflects that the hardwood blocks at the higher elevation and DTW locations had lower soil density and hence and lower soil resistance to penetration than the softwood blocks located at the lower elevations.

The MR-generated results revealed that MC_{PS} increased significantly with $MC_{PS,DTW}$ as influenced by wet weather and by decreasing DTW from ridge tops to low-lying areas next to water-filled flow channels. In addition, MC_{PS} was higher inside than outside the tracks, and higher under hardwood vegetation while decreasing towards the higher elevation blocks (**Table 5.7**). CI decreased with increasing pore-filled soil moisture content, but was noticeable higher within the softwood blocks and inside the tracks due to cumulative wheel-induced compaction. As per Eq. 5.5, rut depth increased significantly with number of forwarding passes ($log_{10}Passes$) and decreased significantly with increasing $log_{10}NCI$. The non-linear DTW-adjustment for Eq. 5.5 improved the MR regression results and related best-fitted scatterplot, but only to a small extent.

The RF regression process (**Table 5.7**) selected MC_{PS}, DTW, elevation (DEM) and OM_{DSM} as dominant MC_{PS} influencing predictors. For CI, RF selected elevation, MC_{PS}, Sand_{DSM}, Depth, and track location as dominant predictors. For rut depth, RF selected number of passes, NCI, DTW and CF as best predictors. Compared to MR, the best-fitted RF-generated R² values for MC_{PS}, CI and rut depth in **Table 5.7** were considerably higher. The scatterplots in **Figure 5.4** demonstrate the extent of MR versus FR generated goodness-of-fit: not only much less scatter and

Table 5.5: Soil physical properties and rut measurements.

Bloc	Block (n) Sand _D	Sand _{DSM} (%)	OM _{DSM} (%)	CF _{DSM} (%)	D _{b,DSM} (%)	C _{DSM}	Elevation (m)	DTW _{FIA}	MC _{PS, RF}	Cl _{RF} (MPa)	NCIRE	Passes (#)	Rut Depth (cm)
(29)	Mean	40.41	6.45	26.21	0.96	38.09	277.9	1.44	64.07	2.41	4.84	4.62	15.62
	Min	32.31	5.3	21.9	0.90	33.97	275.7	0.00	48.54	1.90	3.82	2.00	5.50
	Max	44.75	7.53	32.16	1.10	43.86	280.5	3.54	74.38	3.00	6.02	10.00	32.50
	SD	2.62	0.75	2.67	0.04	2.63	1.3	1.14	7.71	0.30	0.60	1.52	6.650
2 (40)	Mean	46.16	5.86	35.80	0.99	39.98	261.3	2.17	65.75	1.93	3.87	5.75	13.29
	Min	36.01	4.63	27.04	0.80	34.43	258.1	0.04	46.31	1.56	3.13	2.00	2.50
	Max	55.42	8.54	48.14	1.11	47.29	266.5	7.26	82.88	2.42	4.87	8.00	40.00
	SD	4.67	1.02	6.01	0.07	2.63	2.11	1.8	9.70	0.24	0.48	1.51	10.53
3 (75)	Mean	43.90	6.40	33.86	0.79	39.92	360.1	1.18	65.37	1.84	3.57	3.57	13.91
	Min	36.26	4.41	21.23	0.63	33.78	345.7	0.09	47.88	1.51	2.94	2.00	0.50
	Max	51.36	11.50	44.06	0.97	50.42	365.9	4.51	83.71	2.33	4.54	15.00	32.00
	SD	3.67	1.29	5.22	0.08	3.06	4.2	0.99	6.77	0.19	0.37	2.67	8.11
9 (63)	Mean	54.09	10.00	33.65	0.99	41.78	275.7	1.05	69.75	2.03	3.18	18.03	22.54
	Min	41.93	7.86	22.52	0.81	36.35	266.4	0.01	46.36	1.59	2.48	2.00	0.00
	Max	65.16	13.30	42.84	1.20	49.57	283.0	3.12	83.85	2.63	4.12	80.00	60.00
	SD	4.89	1.10	4.10	0.08	2.68	4.3	0.83	9.19	0.27	0.42	22.91	13.07

Table 5.6: Pearson's correlation matrix (non-shaded) with significance levels (shaded grey) for each variable pair, and Factor analysis showing plot results with oblique rotation.

Variable	Rut Depth	Passes	NCI	CF _{DSM}	Sand _{DSM}	ОМрѕм	D _{ь, DSM}	Срѕм	Elevation	DTW _{FIA}	HW Blocks	Factor 1	Factor 2
Rut Depth (cm)	1.000	<0.0001	<0.0001	0.6155	<0.0001	<0.0001	0.0061	0.2369	0.0171	0.0093	0.0247	0.536	-0.011
Passes (#)	0.470	1.000	0.0048	0.8253	<0.0001	<0.0001	<0.0001	0.0011	0.0011	0.0876	0.0189	0.622	-0.117
NO	-0.228	-0.195	1.000	<0.0001	<0.0001	<0.0001	0.5304	<0.0001	0.0845	0.0016	<0.0001	-0.682	-0.284
CF _{DSM} (%)	-0.035	-0.015	-0.321	1.000	<0.0001	0.0979	0.8540	0.0062	0.4404	0.5240	0.0147	0.298	0.234
Sand _{DSM} (%)	0.305	0.424	-0.596	0.228	1.000	<0.0001	<0.0001	<0.0001	<0.0001	0.0860	<0.0001	0.836	0.034
OM _{DSM} (%)	0.304	0.453	-0.389	0.115	0.569	1.000	<0.0001	<0.0001	<0.0001	0.0201	<0.0001	0.793	0.072
$D_{b,DSM}$ (g/cm ³)	0.190	0.321	0.044	0.013	0.365	0.312	1.000	0.0093	<0.0001	0.4840	<0.0001	0.347	-0.742
C _{DSM} (m)	0.083	0.225	-0.252	0.190	0.355	0.323	0.180	1.000	0.2901	0.6515	<0.0001	0.514	0.107
Elevation (m)	-0.166	-0.224	-0.120	0.054	-0.333	-0.301	-0.780	-0.074	1.000	0.0483	<0.0001	-0.208	0.873
DTW _{FIA} (m)	0.180	-0.011	0.217	0.045	-0.120	-0.160	0.049	0.032	-0.137	1.000	<0.0001	-0.312	-0.388
HW Block	0.156	0.163	-0.601	0.170	0.350	0.442	-0.367	0.247	0.585	-0.283	1.000	0.578	0.870

greater 1:1 conformance of actual versus fitted values generated with RF compared with MR for MC_{PS} , CI, and rut depth.

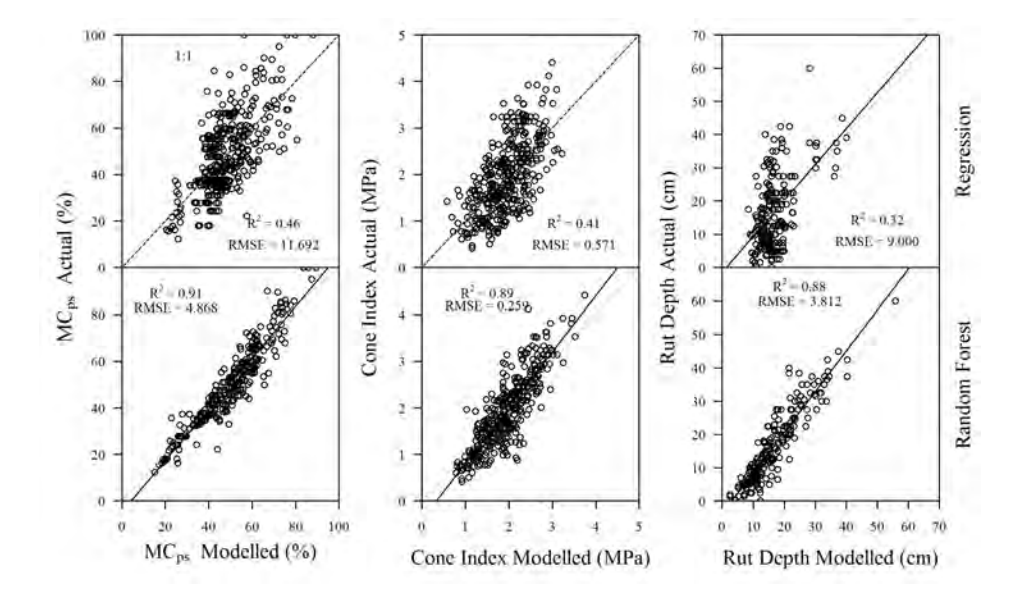


Figure 5.4: Comparison between modelled multiple linear regression and Random Forest for MC_{PS} , CI and rut depth.

The plots in **Figure 5.5** shows the conformance extent between actual and best-fitted STRAM-projected MC_{PS} , CI and rut depth values via MR and RF. In detail the eight-times-out-of-ten conformances within uncertainty brackets amounts to:

- i. \pm 14% for pore-filled moisture content, \pm 0.7 MPA for CI, and \pm 14 cm for rut depth via MR, and
- ii. \pm 4% for pore-filled moisture content, \pm 0.3 MPA for CI, and \pm 4 cm for rut depth via RF.

Inclusion of additional predictor variables increases the resulting best-fitted R^2 and RSME values for MC_{PS} , CI, and rut depth, but with diminishing gains following the inclusion of 4 or more variables. Using only one continuous predictor variable for MC_{PS} led to an RF- R^2 value of about 0.80, in comparison with $MR-R^2$ value of about 0.2. For CI and rut depth, MR and FR have about the same low R^2 values using the binary 0, 1 Track variable, and the grouped Passes variable,

Table 5.7: Regression results for MC_{PS} and CI from Jones and Arp (2019), regression results for rut depth and variable importance for Random Forest Model for MC_{PS} , CI and rut depth.

			Regr	ession Mo	odels				
Dependent Variables	Intercept & Predictor Variables	Para- meter #	Regr.	SE	t- value	p-value	R ²	RMSE	n
MC _{PS}	Intercept		70.883	6.326	11.205	< 0.0001	0.47	11.69	394
Eq. 5.2	Elevation	4	-0.091	0.013	-6.937	< 0.0001			
	HW Blocks	5	10.224	2.136	4.788	< 0.0001			
	$MC_{PS,DTW}$	1	0.262	0.073	3.589	0.0003			
	OM_{DSM}	3	-0.981	0.278	-3.529	0.0005			
	Tracks	6	4.090	1.233	3.316	0.0010			
	log ₁₀ DTW	2	-2.764	0.926	-2.986	0.0030			
Cl	Intercept		1.599	0.159	10.060	< 0.0001	0.41	0.571	372
Eq. 5.3	Tracks	3	0.760	0.064	11.910	< 0.0001			
	SW Blocks	4	0.397	0.064	6.200	< 0.0001			
	MC_{PS}	1	-0.011	0.002	-5.980	< 0.0001			
	Depth	2	0.025	0.002	9.900	0.0583			
Rut Depth	Intercept		18.880	6.592	2.864	< 0.0001	0.28	9.094	207
Eq. 5.5	log ₁₀ Passes	1	14.327	1.856	7.721	< 0.0001			
	log ₁₀ NCI	2	-22.213	10.625	-2.091	0.038			
	$log_{10}DTW_{FIA}$	3	-2.669	1.071	-2.492	0.014			
Eq. 5.6	a/NCl _{adj} x Passes ^{bNCl} adj						0.32	9.000	207
	а		40.886	3.275	12.728	< 0.0001			
	b		0.072	0.007	9.676	< 0.0001			
			Randor	n Forest M	/lodels				
Dependent Variables	Variables	Para- meter #	% M Decr Accu		Vario Import		R^2	RMSE	n
MC _{PS}	MC _{PS,DTW}	1	191	.04	5332.12		0.91	4.962	394
	Elevation	2	180).54	32079.21				
	OM_{DSM}	3	38	.17	16292	2.63			
CI	Tracks	1	0.2	224	33.2	20	0.88	0.263	372
	Depth	2	0.1	59	37.4	43			
	Elevation	3	0.1	08	49.2	27			
	$MC_{PS,RF}$	4	0.0		47.0				
	Sand _{DSM}	5	0.0)70	36.8	86			
Rut Depth	Passes	1	71	.77	7121	.22	0.84	4.307	207
	NCI_{RF}	2	24	.26	5744	1.51			
	DTW_{FIA}	3		.35	5971	.05			
	CF _{DSM}	4	0.0	65	3813	5.68			

respectively. While the predictive CI and rut-depth outcomes using these variables is low to modest, they serve in MR and especially so in RF to resolve the otherwise unresolved scatter associated with using the continuous predictor variables alone. The field-determined and projected MC_{PS}, CI, and rut depth were evaluated into cumulative conformance plots in **Figure 5.6**. 80 % conformance of the difference from actual to measured values ranged from 4 to 14 % for MC_{PS}, 0.4 to 0.7 MPa for CI, and 4 to 14 cm for rut depth, using RF and MR respectively.

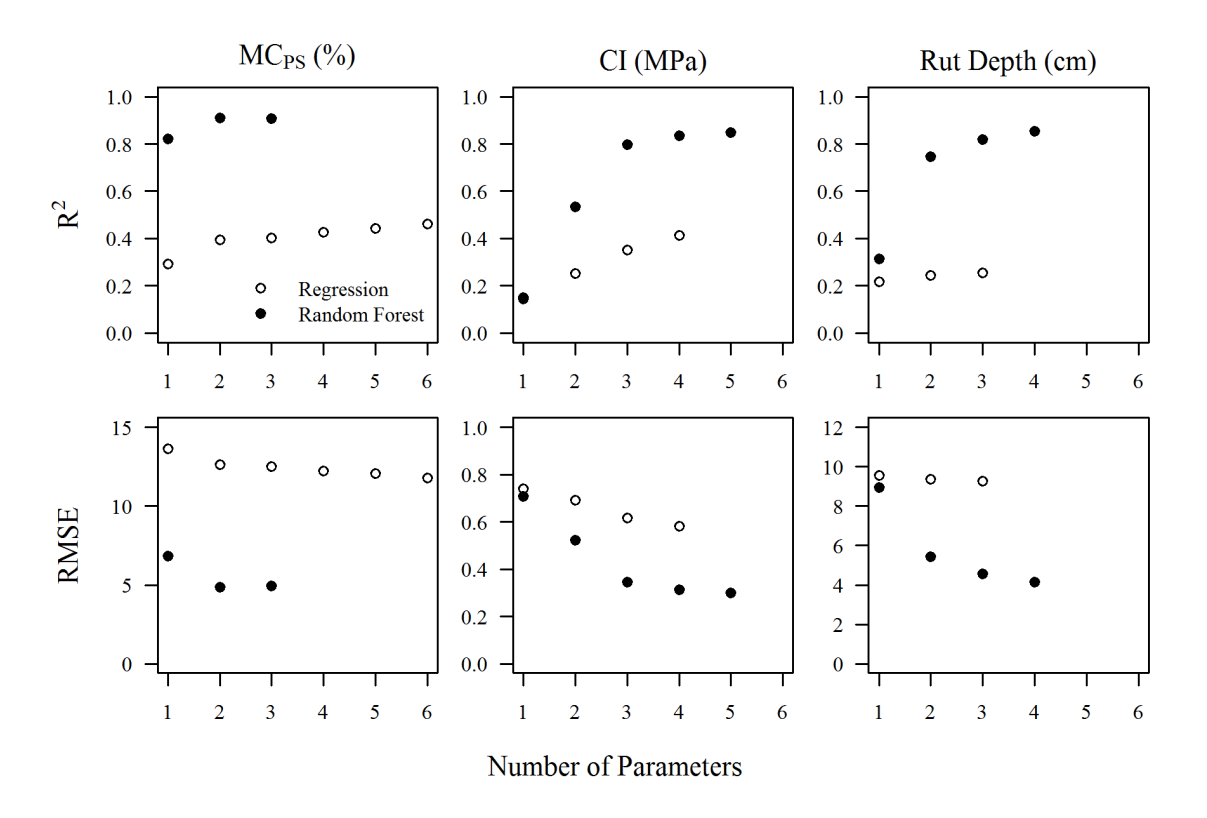


Figure 5.5: Best-fitted RF- and MR- R^2 and RSME value achieved using predictor variables in the order of decreasing numerical significance or influence.

The GPS-tracked wood forwarding tracks across Blocks 1, 2, 3, and 9 are overlaid on the delineated DTW <1m and hill-shaded DEM background, also showing the number of passes (top) and field-measured rut depths (bottom) at each location (**Figure 5.7**). Among these, Block 3 reveals a close association between deeper

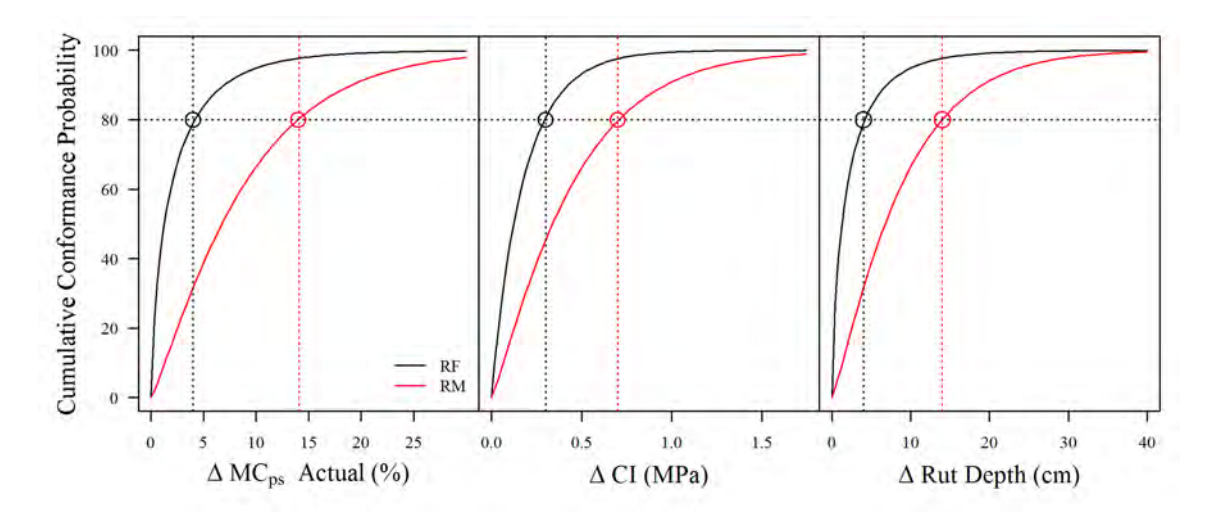


Figure 5.6: Cumulative conformance probability for differences in MC_{PS} , CI, and rut depth for RF and MR.

rut depths and DTW, followed by Block 9 and Block 2. Block 1 had no association between rut-depth and pass number. Rutting was deepest in Blocks 3 and 9 along multi-pass tracks across streams and wet-areas.

Figure 5.8 provides a closer look about the extent of track rutting in Block 9 in relation to the DTW <0.5 m delineation through overlay on the hillshaded-DEM(top) and the surface-image (bottom) backgrounds. This image was generated a year after the wood-forwarding operations. At this time, the extent of rutting had faded to some extent but remained prominent in the lower left corner of the block. Rutting >40 cm deep occurred along multiple pass tracks where DTW <0.5m.

5.3.1 MC_{PS}, CI, and rut-depth projections

Figure 5.9 presents the MR-and RF-generated projections and data points for MC_{PS} (top) and CI (bottom) for Blocks 1, 2, 3, and 9 with the latter more detailed than the former. In addition, there is also a considerably greater point to RF- than MR- projection conformance, as to be expected from the scatterplots in **Figure**

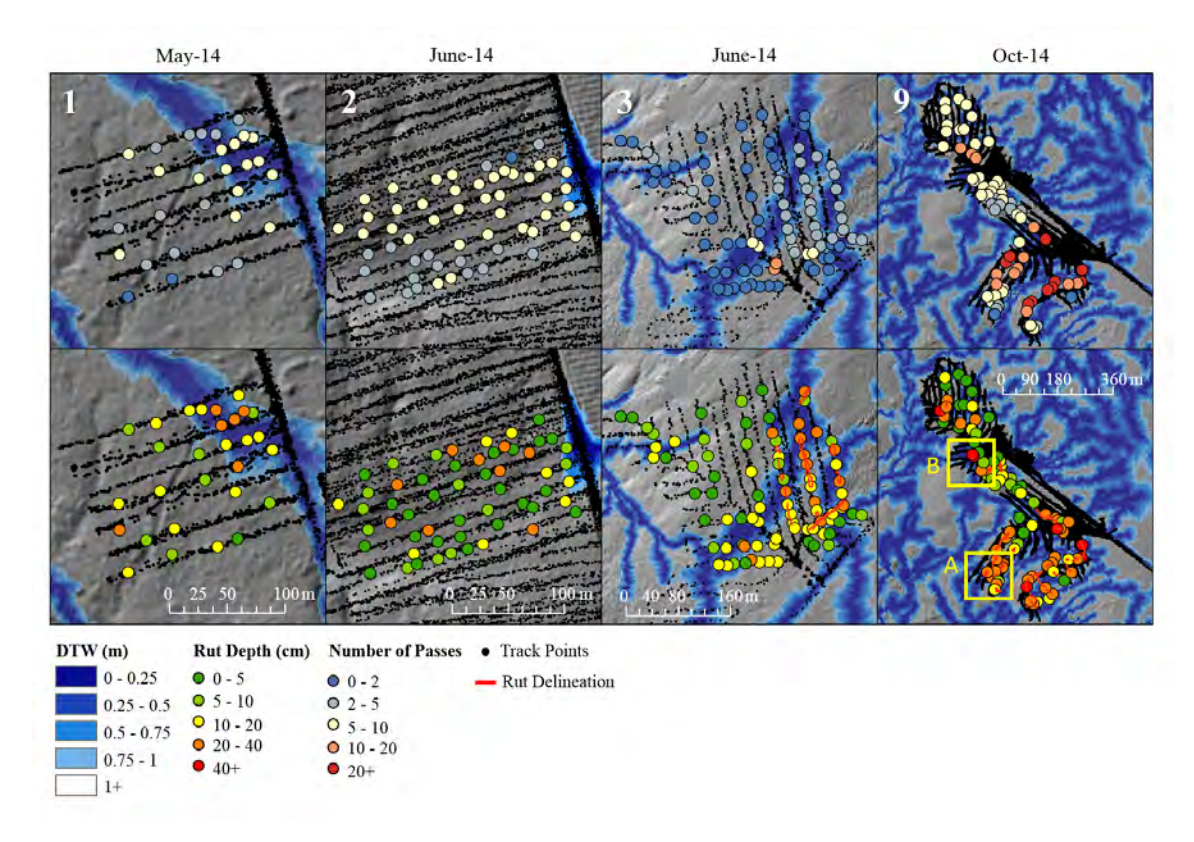


Figure 5.7: Field-measured rut-depth locations with number of passes along rut tracks (top) and rut depth (bottom) across Blocks 1, 2, 3 and 9, also showing the block-specific weather-affected DTW_{FIA} assignments, i.e. FIA = 1, 16, 1, 0.25, respectively. For A and B close-ups, see **Figure 5.8**.

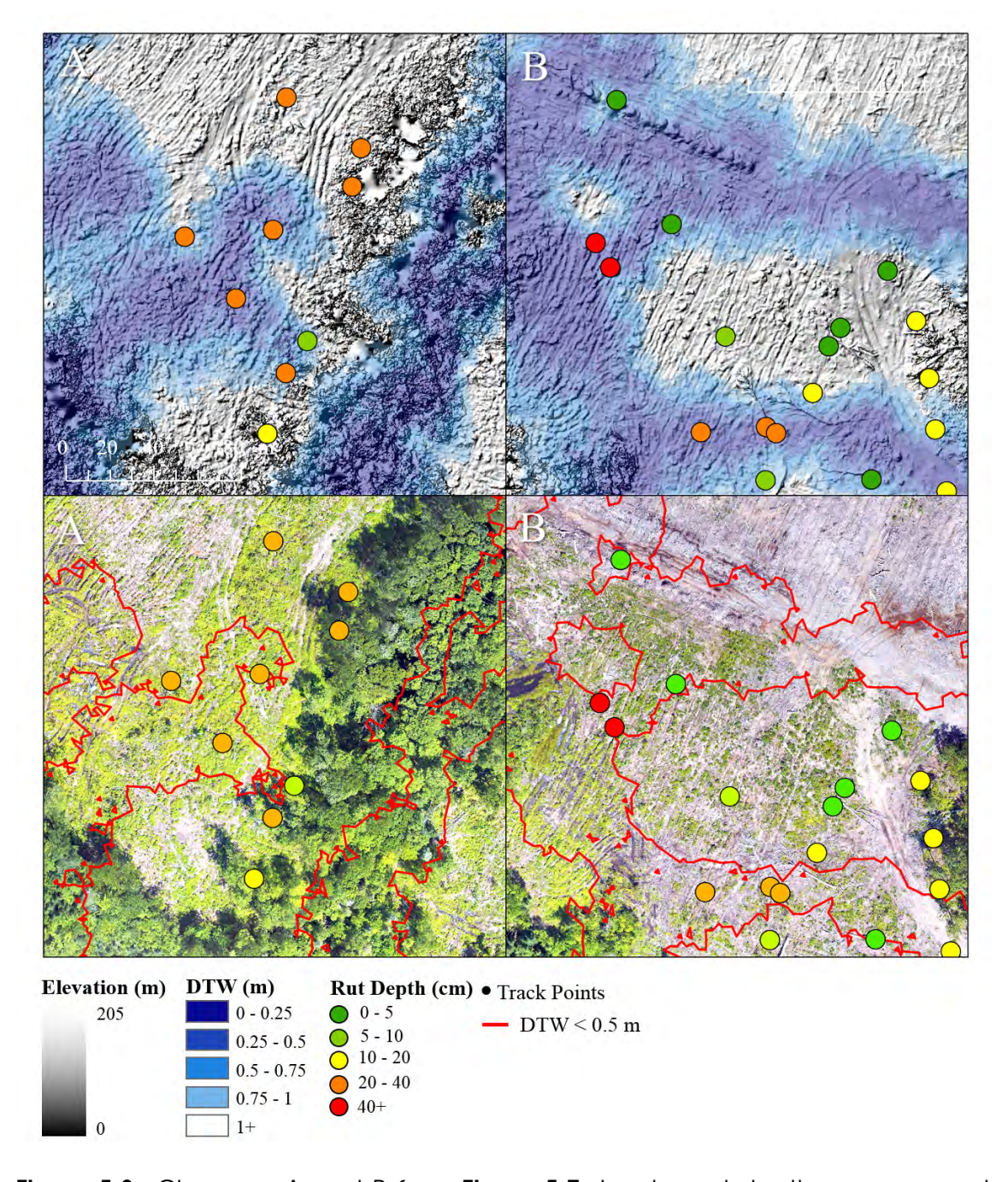


Figure 5.8: Close-ups A and B from **Figure 5.7** showing rut-depth measurement locations in Block 9 overlaid on a 10 cm resolution hill-shaded DEM and a high-resolution surface image one year after field operations. Also shown is the DEM-generated DTW 1 m extent (top; blue-shaded, 50% transparent) and its corresponding DTW = 0.5 m contour (bottom; red). The 10 cm DEM (top) was generated from scanned optical AUV surface images (bottom; Phantom 4)

5.4, and from the results listed in **Table 5.7**. Among them, Block 9 is shown to be the wettest, on account of 70 mm rain event two days before prior to the day of wood forwarding, and as reflected by the a consequential use of the DTW_{FIA} = 0.25 ha data layer as dominant MC_{PS} predictor in Eq. 5.4. In contrast, Block 1 was found to be excessively dry, such that the DTW_{FIA} = 16 ha projection was found to best representative of the field-determined MC_{PS} values for this block outside the tracks. For Blocks 2 and 3, the MC_{PS} were best presented using the DTW_{FIA} = 1 ha assignment to reflect the May and June soil moisture conditions at the time of wood forwarding. Although Blocks 2 and 3 use the same DTW_{FIA} = 1 ha assignment, they differed in terms of CI-measured soil strength which was weaker for the hardwood block (Block 3) than for the softwood softwood block (Block 2). Typically, shallow-rooting softwood forests are found on coarser and stonier soils with lower organic matter accumulations than deeper-rooting hardwood forests.

Figure 5.10 presents the overlay of rut depth points on the corresponding MR (top) and RF (bottom) projections for Blocks 1, 2, 3, and 9 after 1, 10 and 50 passes, with better and more resolved RF than MR data-to-projection conformances. These plots confirm that the spatial variations in soil moisture and increasing number of passes are important rut-depth predictor variables. Actual rut depth, however, also depend on machine weight/load and soil properties, and load as quantified by way CI and NCI in general and by the variables listed in **Table 5.7**.

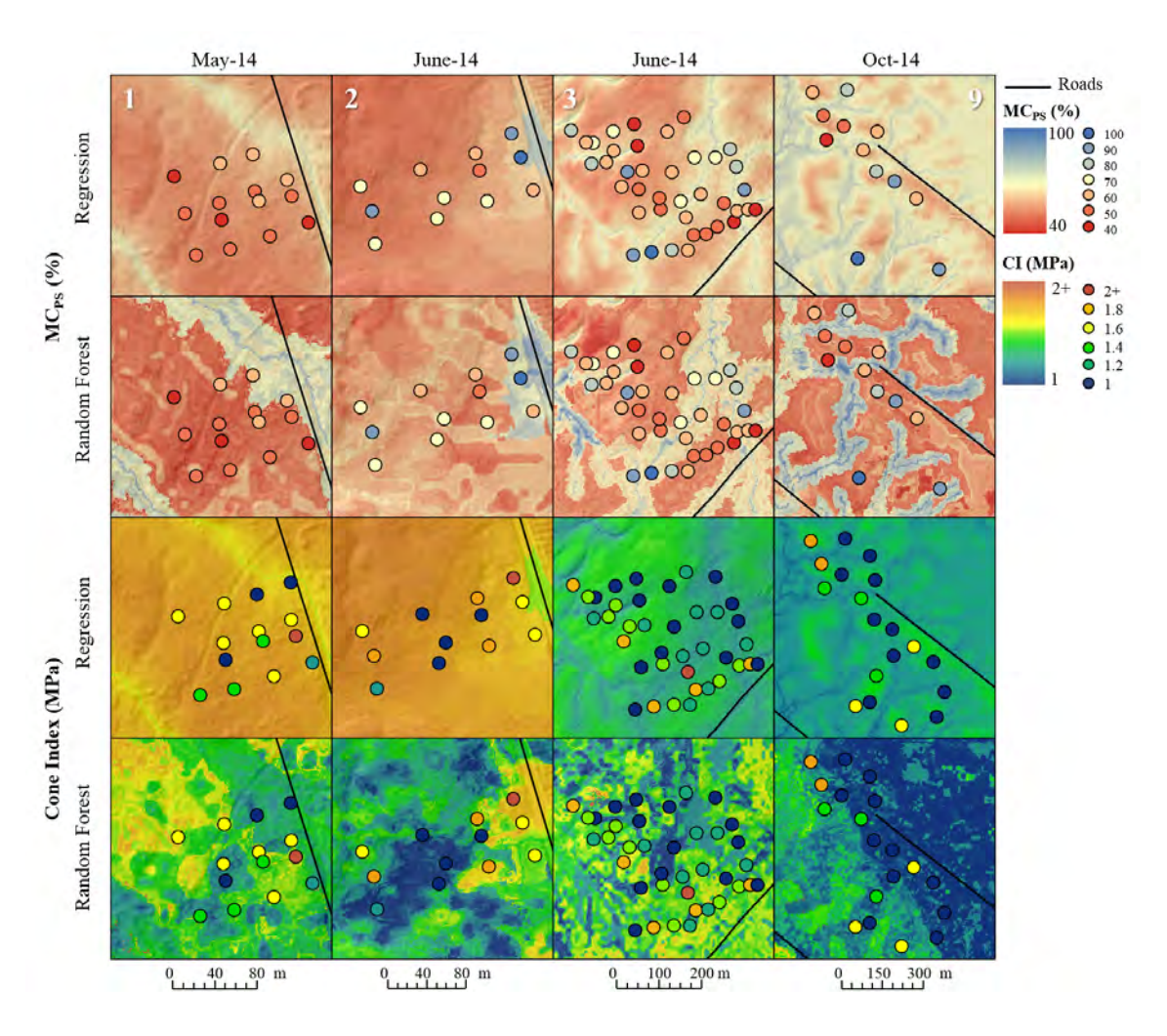


Figure 5.9: Measured MC_{PS} and CI values at 15 cm soil depth overlaid on the corresponding Eq. 5.2 and Eq. 5.3 map projections for Blocks 1, 2, 3 and 9, using FIA = 1, 16, 1, 0.25, respectively.

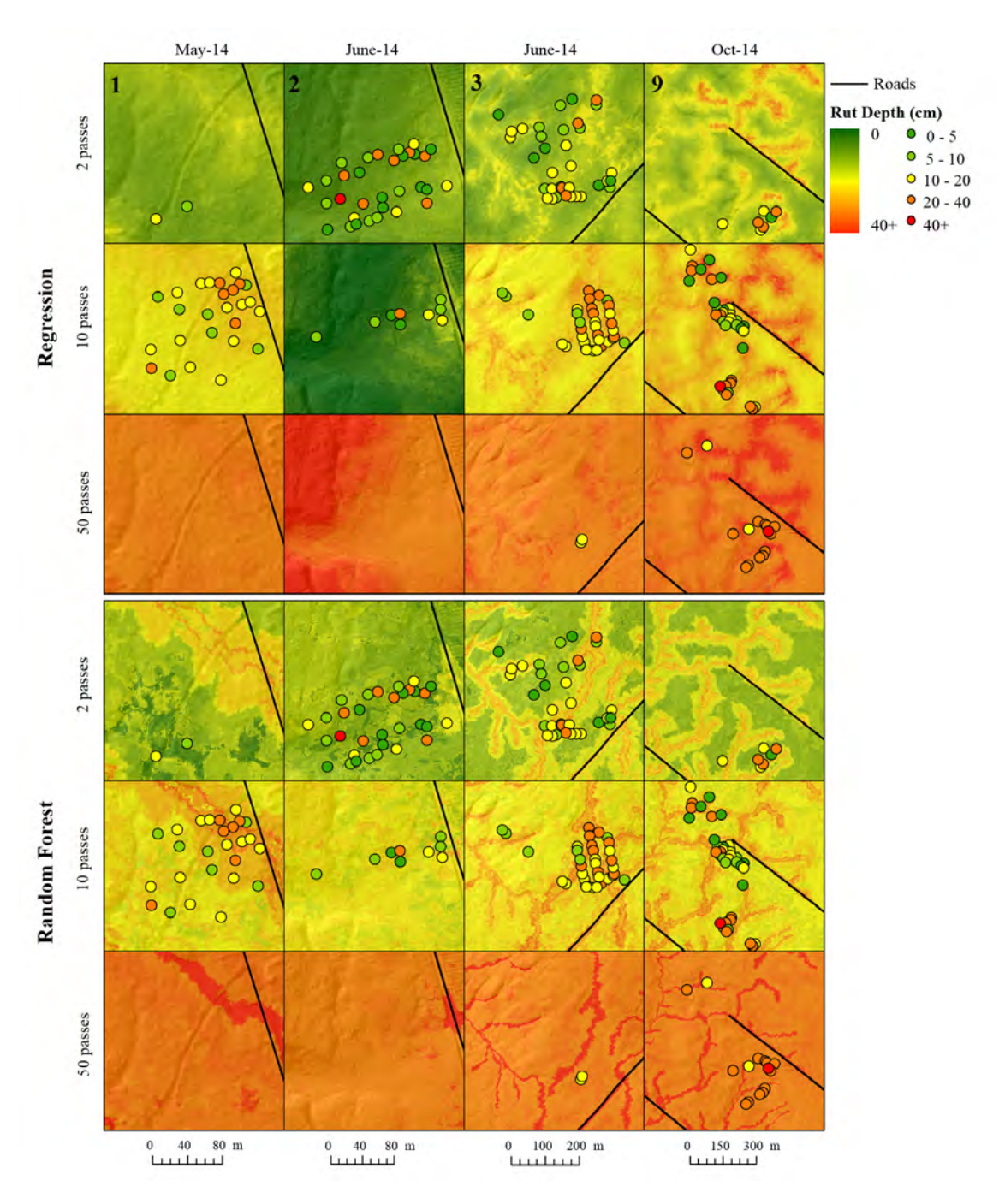


Figure 5.10: Random Forest modelled 2- and 10-pass rut depths for Blocks 1, 2, 3, 9 with machines carrying full loads, with the field plot results overlaid, using FIA = 1, 16, 1, 0.25, respectively.

5.4 Discussion

While RF produces a considerably better results between the field-measured values for MC_{PS}, CI and rut depth, it still needs literature- and theoretical MR-based guidance to interpret to results so generated. For example, moist to wet soils have lowered physical strength due to water filling pores and reducing particle cohesion (Kumar *et al.*, 2012), and many studies have shown that there is a correlation between soil disturbance and soil moisture (Sutherland, 2003; Han *et al.*, 2006; Nikooy *et al.*, 2016; Jones and Arp, 2017). To illustrate, Block 3 shows deeper ruts within the wetter DTW_{FIA} = 1 ha marked area next to a stream. Block 1 with no significant rut-depth observations was cut following dry weather conditions during mid-June of 2014, at which the overall soil moisture levels best conformed to a DTW_{FIA} - 16 ha flow-channel pattern, and rut depths remained low. In contrast, deep ruts were encountered across Block 9 due to field operations in October 2014 following a heavy rain event of 70 mm.

In terms of other soil properties, studies have shown that measured rut depth is also positively correlated to increased levels of OM in the soil (Sutherland, 2003; McFero Grace et al., 2006). For example, Block 9 due to its deeply rooting hardwood composition, positively correlated rut depth with OM as revealed by the factor analysis in **Table 5.6**. High sand content also contributes to low CI, NCI and therefore to increased rut depth, mainly due to low particle-to-particle cohesion (Balland et al., 2008; Brady and Weil, 2008; Kumar et al., 2012). In contrast, high coarse fragment content should increase CI and lower rut depth, but the overall CF variations within and across the blocks would not register this effect in a major way by way of MR, and only weakly so by RF. Typically, soils with high soil strength (high CI and NCI values) minimize soil disturbance (Antille and Godwin, 2013).

Significant and influential on the MR and RF results was the significant result (p = <0.0001) between rut depth and number of passes. This effect, however, decreases non-linearly due to gradually increasing soil compaction as quantified above via Eq. 5.6 and as reported by Eliasson (2005), Eliasson and Wästerlund (2007), Botta *et al.* (2009) and Jones *et al.* (2018). This is especially so for high traffic areas such a wood landing sites and tracks subject to hundred passes or more (Carter *et al.*, 2007; Taghavifar and Mardani, 2014; Jones *et al.*, 2018).

Given the above moderate (MR) to strong (FR) data-to-projection conformances across Blocks 1, 2, 3, and 9, it should be possible to forecast soil trafficability by way of the modeling flow chart in Figure 5.3. Fundamental for this effect is combining preceding and forecasted weather conditions with spatial soil property, drainage (DTW) and CI maps (Figure 5.9) to be informed about daily to seasonal variations in soil wetness as these may vary from year to year. Figure 5.11 presents an example of how trafficability affecting soil conditions would vary on average and by month in Block 1, summer through winter for a period of 14 years. Generally, soil trafficability conditions within this block would be best on solidly frozen ground, but worst during snow melt when soils tend to be equally wet across the land. In detail, April and November would be the wettest months. During spring, summer and fall, soil trafficability would vary on account monthly variations in precipitation and related extent of evapotranspiration as primarily affected by canopy leaf area. According to Figure 5.11, the driest summer occurred in 2005, while the wettest summer occurred in 2003. Soil trafficability would also have been poor during the essentially low snowpack and frost-free soil conditions in the winter of 2010.

A practical guide to forecast soil trafficability would establish whether the monthly soil conditions are frozen, partially thawed, wet, moist or dry. For the wet to dry conditions, it is important to decide likely block-specific upslope flow initiation areas as suggested in **Table 5.8**. To some extent, these suggestions

would need to be modified by soil texture, coarse fragment content: higher FIA numbers for well drained and rocky soils, and low FIA numbers for loamy and clayey soils. Extended droughts would also increase FIA, therefore increasing the areas available for off-road traffic. However, care needs to be given to not drive along or across established flow channels, because traffic induced disturbances in the channels would aggravate subsequent flooding effects by, e.g., accelerating stream bank erosion, and by partially compacting well aggregated soils that would reduce soil infiltration and hence increase soil erosion overall. An example of yearly soil trafficability forecasting by month and related weather-imposed DTW $_{\rm FIA}$ assignments following the flowchart in **Figure 5.3** is provided in **Figure 5.12**, with focus on 2 passes.

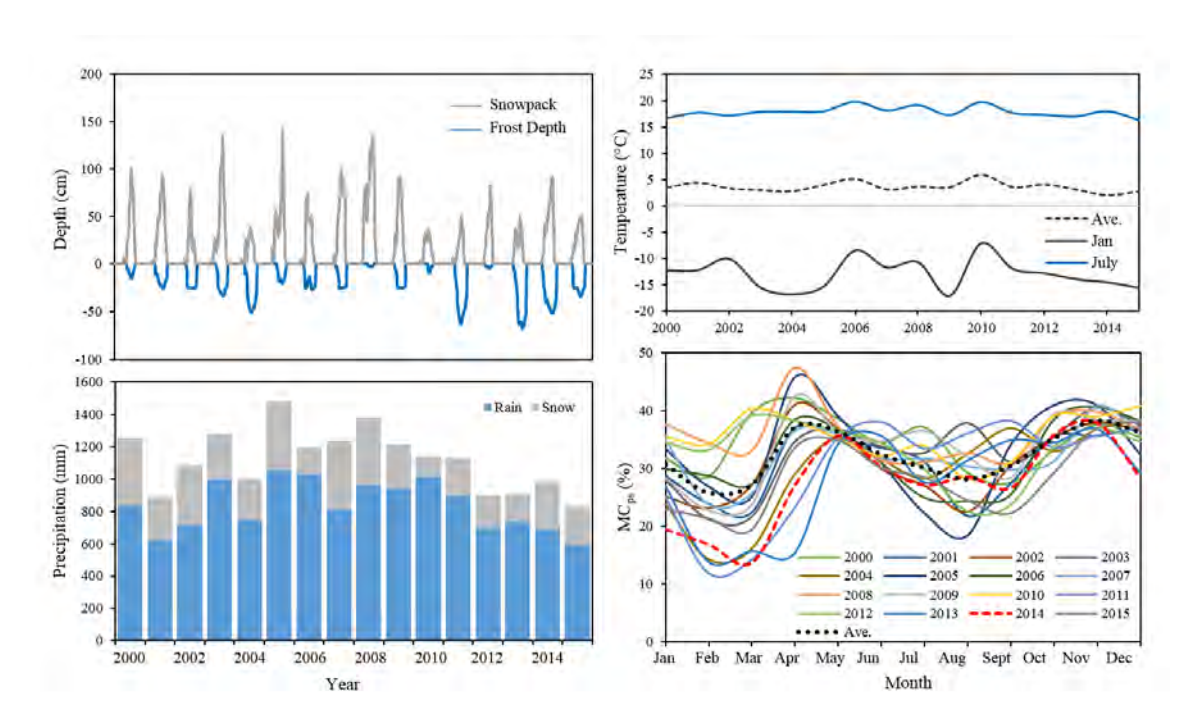


Figure 5.11: Historical weather for Block 1 from 2000 to 2015 showing cumulative precipitation (left-bottom), historical snowpack and modelled frost depth (left-top), and temperatures (right-top), as well as ForHyM-modelled weekly modelled average A & B horizon MC_{PS} (right-bottom).

Table 5.8: Monthly region-specific DTW $_{\text{FIA}}$ choices useful for forecasting soil trafficability across Blocks 1, 2, 3, and 9 and northwestern New Brunswick in general.

Month			FIA	
IIIOIIIII	16 ha	4 ha	1 ha	0.25 ha
January	Frozen	-	-	Partial Thaw
February	Frozen	-	-	Partial Thaw
March	Frozen	-	-	Partial Thaw
April	Frozen	-	-	Very Wet
May	Very Dry	Dry	-	Very Wet
June	Very Dry	Dry	Moist	Wet
July	Very Dry	Dry	Moist	Wet
August	Very Dry	Dry	Moist	Wet
September	Very Dry	Dry	Moist	Wet
October	-	Dry	Moist	Wet
November	-	Dry	Moist	Wet
December	Frozen	Dry	Moist	Wet

Soil trafficability: poor when soils are wet, and worst when partially thawed; intermediate when moist, and best when dry or very dry.

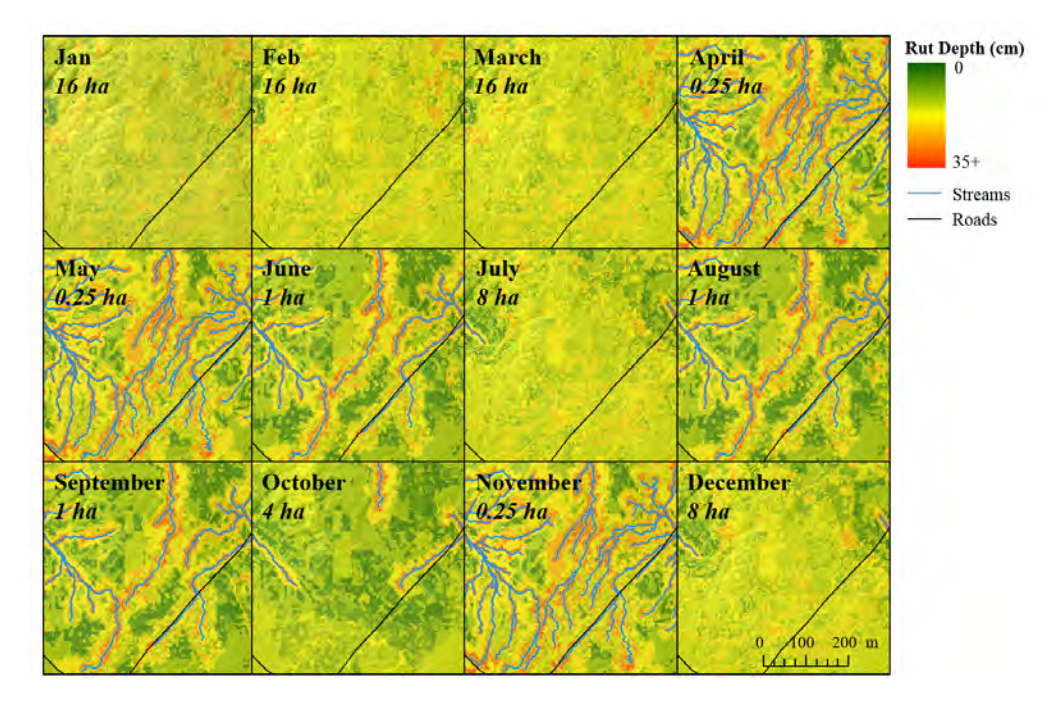


Figure 5.12: Year-round RF-generated soil trafficability projections by month for Block 1, with focus on 2 passes and 2014 weather-affected DTW $_{\text{FIA}}$ assignments.

5.5 Concluding Remarks

While this research has shown how soil trafficability can be assessed and forecasted based on coupling block-based soil surveys with temporal and spatial modelling techniques, there are ways by which this research can be improved. Traditional in-field data collection as done above is limited by high sampling costs. Area-systematic rut surveys can now be conducted by, e.g., equipping off-road vehicles with GPS-tracking LiDAR-based rut depth sensors (Salmivaara et al., 2018). Similarly, Giannetti et al. (2017) proposed terrestrial portable laser scanners and Haas et al. (2016), Pierzchała et al. (2016) and Launiainen et al. (2017) used unmanned airborne vehicles (UAVs) for stereo imaging and evaluating rut depth and length based on the underlying terrain conditions. In combination, advances in weather-affected digital soil property mapping will further assist soil trafficability forecasting, and the validity of these forecast can then be checked using systematically retrieved block post-operational rut depth data. In addition, the MR and RF techniques can be used to enable the overall soil trafficability forecasting from theoretical considerations and for numerical model validation. In this regard, MR-generated forecast would allow generalizing beyond the immediate survey areas, whereas the RF forecast, although more precise and accurate, would - for the most part - be restricted to the survey area.

5.6 Acknowledgment

This research was supported financially through an NSERC Collaborative Research Project with J.D. Irving Limited as industrial partner. Special thanks go to Forest watershed Research Centre at UNB, for facilitating this research, with additional support from Doug Hiltz for assistance with field sampling, and from Dr. Shane Furze for assistance in digital soil mapping and R statistical analyses.

Chapter 6

Conclusion

6.1 Thesis Summary

This chapter summarizes the main developments of this dissertation and creates a fluid connection between the published articles. Key findings are correlated to the STRAM model.

- i. **Chapter 2**: A 23 week field analysis was conducted, focusing on measuring the relationship between soil moisture (MC) and soil strength (cone index, CI). Site location, species composition and soil property variability were analyzed to model weather- and soil-dependent changes in soil moisture and penetrability conditions. The study focused on three locations across Fredericton, NB. The study results validated the use of ForHyM to predict MC and CI over time. By validating the predicted MC over time, ForHyM can be used to model temporal changes and then applied spatially through the use of the STRAM model introduced in Chapter 5. Without the ForHyM model, STRAM would only be a spatial trafficability model. Validated temporal soil MC (R² = 0.76) and CI (R² = 0.76), are the corner stone in modelling temporal effects of trafficability.
- ii. **Chapter 3**: Three heavy forest operation machines equipped with ultrasonic distance sensors and GPS trackers provided 4.2 million data points (at 10

second intervals across 54 harvest blocks) in an effort to understand how and where machines cause soil disturbances. It was found that the clearance data needed to be processed by block in order to isolate where single - to multiple-pass rutting occurred due to terrain and weather conditions. Machine clearance was primarily found to be an issue within the first pass and machine speed increased on drier sites over wet areas. The sensor data was used to help enumerate machine passes and overall effects on the blocks used in chapters 4 and 5. Number of passes was a significant factor in the STRAM model, given that understanding how many times a machine passes over a single area of land can signify greater soil disturbance. Given the issues (brushmat and general obstruction) with the clearance sensors, machine pass was the main output used for modelling.

- iii. **Chapter 4**: Inside and outside track measurements pertaining to soil moisture and penetrability were related to the terrain, soil and weather conditions at the time of wood forwarding operations by way of multivariate analyses. For continuity, the 11 harvest blocks monitored were from harvest blocks sampled in Chapter 3 for the machine sensor data. The multivariate analysis for soil MC was applied to field determined soil parameters (R²=0.51-0.61) as well as digitally derived DMS-based soil parameters (R²=0.46-0.48). Soil CI was similarly modelled with field-determined regression (R²=0.39) and DSM-based soil parameters (R²=0.41). It was found that the resulting expression would predict soil moisture and soil penetrability with an uncertainty range of 15 % and 1.5 % eight times out of 10.
- iv. **Chapter 5**: Due to the less than ideal performance of the regression results from Chapter 4, a new analysis was conducted in the form of machine learning algorithm Random Forest. This new model was applied to the soil MC and CI measurements across 11 harvest blocks, as well as the rut depth measurements from 4 blocks (2 hardwood and 2 softwood blocks). The MC RF model R² improved from 0.47 to 0.91, while CI improved from 0.44 to 0.88.

The soil moisture and penetrability results led to reasonable wood-forwarding rut depth projections by weather, block and machine specific Soil Trafficability Model (STRAM) projections. These projections captured 40 % and 80 % of the rut-depth variations when based on multivariate and Random Forest regression analysis, respectively.

Overall, the chapters outline a procedure created to validate temporal moisture and soil strength predictions, and extrapolate the temporal predictions spatially with rut depth through the use of machine learning algorithm Random Forest.

6.2 Original Contribution

6.2.1 Temporal Cone Index

This project developed an in-depth analysis of the importance of daily to seasonal soil moisture variation on soil strength. Using the results of a 23 week field analysis, relationships were solidified between soil strength (CI) and soil moisture, porosity, and coarse fragments. This analysis is a contribution to the understanding of temporal changes in soil moisture and strength over time, comparing results across the three research sites within Fredericton, NB. The validated model was then applied to operational blocks to help model rutting over time which can be used to better manage harvest operations in the future.

6.2.2 Sensor Analysis

GPS units and ultrasonic distant sensors were installed on 3 machines and their sensor readings helped support the connection between heavy forest machinery and soil displacement. The project provided valuable outputs to connect spatial terrain changes and temporal machine movement, especially in connection with high-resolution wet-areas mapping using the cartographic depth-to-water index, and how this would vary by antecedent to current weather conditions.

6.2.3 STRAM Model

The STRAM model is entirely original in its development and its function as soil trafficability projection tool. Through its multivariate formulation, this tool allows for area-wide generalizations based on generating a database of the model identified predictor variables. Its Random Forest formulation would use the same data base but would require further testing and training to achieve similar actual to prediction conformance as reported here.

6.3 Suggestions for Future Work

6.3.1 Machine Compressed Snowpack Module

The mitigating snowpack effect on machine-caused soil disturbance is not yet part of the STRAM formulation. With regard to snow pack accumulations, ForHyM quantifies (i) the progressive effects of changing winter weather conditions effect on snow density and snowmelt (Balland, 2002; Balland *et al.*, 2006) and (ii) the depth and thawing extent of soil frost based on variable snowpack depth. In general, snowpack-induced mitigation of soil disturbance impact is related to snowpack compaction and subsequent ice formation (Brun and Rey, 1986; Jellinek, 1957). Consequences of this formation refer reducing thawing delay and snowmelt infiltration into the soil (Singh *et al.*, 2000). Currently, STRAM projects zero soil penetrability when the top soil is partially to completely frozen.

6.3.2 Machine Mounted Sensors 2.0

Mounting an ultrasonic distance sensor and an inclinometer provided a useful insight on the effects of machinery on the terrain (**Chapter 3**). This research effort should be expanded by routinely tracking machine rutting through e.g., laser light scanning or stereo-scanning using optical or infra-red cameras to allow a clear digital ground conditions quantification and separation between ruts, displaced soil, rocks, stumps, and other woody debris. This scanning should be coupled with

machine location, speed, tire pressure, wheel rounds per minute, etc. The latter would inform about slippage-induced extent of soil displacement in wet areas and along slopes.

6.3.3 Integrating Real-Time Weather Forecasts

The STRAM formulations needs to be adapted to practical real-time application purposes by automatically incorporating antecedent weather reports and current forecasts, to allow for weather-informed soil trafficability update Glahn and Lowry (1972). In the absence thereof, STRAM can be used to assess overall changes insoil trafficability based on monthly weather assessments, as detailed in Chapter 5.

6.3.4 Model Adaptability: External Validation

The STRAM model has been calibrated for use within Northern and Central New Brunswick, Canada. It would be instructive to determine whether the model projections so generated are also applicable elsewhere, either directly, or through further calibrations.

6.3.5 Model Adaptability: Agriculture

Apart from the wood-forwarding application, STRAM can, in principle, be adapted to other off-road applications, whether this related to, e.g., forestry, gardening, or recreation, including trail building and maintenance. For example, agriculture machinery can cause similar damage to soil, with the added disadvantage of reduced root structures, coarse fragments, or brush piles (Hamza and Anderson, 2005; Chan *et al.*, 2006). Agriculture practices tend to create homogeneous soil profiles that are prone to erosion and susceptible to compaction (Gill, 1971). In detail, STRAM generated data layers for soil moisture, cone penetrability and potential rut depths could be useful to optimize crop placement and related yield expectations by way of in-field zonations.

References

- Ács, F., Breuer, H., and Szász, G. (2011). Estimation of actual evapotranspiration and soil water content in the growing season. *Agrokémia és Talajtan*, 60(2):57–74.
- Affleck, R. T. (2005). Disturbance Measurements from Off-Road Vehicles on Seasonal Terrain Cold Regions Research and Engineering Laboratory. Technical Report July.
- Ågren, a. M., Lidberg, W., Strömgren, M., Ogilvie, J., and Arp, P. a. (2014). Evaluating digital terrain indices for soil wetness mapping a Swedish case study. Hydrology and Earth System Sciences, 18(9):3623–3634.
- Akay, A., Sessions, J., and Aruga, K. (2007). Designing a forwarder operation considering tolerable soil disturbance and minimum total cost. *Journal of Terramechanics*, 44(2):187–195.
- Alberta Forest Products Association (1994). Forest Soils Conservation Guidelines. Technical report, Land & Forest Service.
- Alexander, L. and Skaggs, R. W. (1987). Predicting unsaturated hydraulic conductivity from soil texture. *Journal of Irrigation and Drainage Engineering*, 113(2):184–197.
- Allen, M. M. (1997). Soil compaction and disturbance following a thinning of second-growth Douglas-fir with a cut-to-length and Skyline system in the Oregon Cascades. Masters thesis, Oregon State University.

- Ampoorter, E., Goris, R., Cornelis, W., and Verheyen, K. (2007). Impact of mechanized logging on compaction status of sandy forest soils. *Forest Ecology and Management*, 241(1-3):162–174.
- Andersland, O. B. and Ladanyi, B. (1994). Mechanical Properties of Frozen Soil. In *An Introduction to Frozen Ground Engineering*, pages 121–150. Springer US.
- Antille, D. L. and Godwin, R. J. (2013). Soil Displacement and Soil Bulk Density Changes as Affected by Tire Size. *Transactions of the ASABE*, (May 2014):1683–1693.
- a.R. Dexter, Czyż, E., and Gae, O. (2007). A method for prediction of soil penetration resistance. *Soil and Tillage Research*, 93(2):412–419.
- Arnup, R. (1999). The Extent, Effects and Management of Forestry-related Soil Disturbance, with Reference to Implications for the Clay Belt: A Literature Review. Technical report, OMNR, Northeast Science & Technology. TR-037, Ontario, Canada.
- Arp, P. and Yin, X. (1992). Predicting water fluxes through forest from monthly precipitation and mean monthly air temperature record. *Canadian Journal of Forest Research*, 22:864–877.
- Ayers, P. (1994). Environmental damage from tracked vehicle operation. *Journal of Terramechanics*, 31(3):173–183.
- Baetens, J. M., Verbist, K., Cornells, W. M., Gabriels, D., and Soto, G. (2009). On the influence of coarse fragments on soil water retention. *Water Resources Research*, 45(7):1–14.
- Bagheri, I., Kalhori, S. B., Akef, M., and Khormali, F. (2012). Effect of Compaction on Physical and Micromorphological Properties of Forest Soils. *American Journal of Plant Sciences*, 03:159–163.

- Balland, V. (2002). Hydrogeological modeling of the flow of cations and anions in select watersheds of Eastern Canada with special focus on snowpack effects. Masters thesis, University of New Brunswick.
- Balland, V., Bhatti, J., Errington, R., Castonguay, M., and Arp, P. (2006). Modeling snowpack and soil temperature and moisture conditions in a jack pine, black spruce and aspen forest stand in central Saskatchewan (BOREAS SSA). *Canadian Journal of Soil Science*, 86(Special Issue):203–217.
- Balland, V., Pollacco, J. A., and Arp, P. A. (2008). Modeling soil hydraulic properties for a wide range of soil conditions. *Ecological Modelling*, 219:300–316.
- Bassett, I. E., Simcock, R. C., and Mitchell, N. D. (2005). Consequences of soil compaction for seedling establishment: Implications for natural regeneration and restoration. *Austral Ecology*, 30(8):827–833.
- Berisso, F., Schjønning, P., Keller, T., Lamandé, M., Etana, A., de Jonge, L., Iversen, B., Arvidsson, J., and Forkman, J. (2012). Persistent effects of subsoil compaction on pore size distribution and gas transport in a loamy soil. *Soil and Tillage Research*, 122:42–51.
- Beven, K. J. and Kirkby, M. J. (1979). A physically based, variable contributing area model of basin hydrology. *Hydrological Sciences*, 24:43–69.
- Black Brook Watershed Research site (2014). Black Brook Watershed stream disharge data.
- Blouin, V., Schmidt, M., Bulmer, C., and Krzic, M. (2004). Soil compaction and water content effects on lodgepole pine seedling growth in British Columbia. *SuperSoil Conf*, (December):5–9.
- Bonell, M., Purandara, B., Venkatesh, B., Krishnaswamy, J., Acharya, H., Singh, U., Jayakumar, R., and Chappell, N. (2010). The impact of forest use and reforestation on soil hydraulic conductivity in the Western Ghats of India:

- Implications for surface and sub-surface hydrology. *Journal of Hydrology*, 391(1-2):47–62.
- Botta, G. F., Becerra, A. T., and Tourn, F. B. (2009). Effect of the number of tractor passes on soil rut depth and compaction in two tillage regimes. *Soil and Tillage Research*, 103(2):381–386.
- Brady, N. C. and Weil, R. R. (2008). *The nature and properties of soils*. Prentic Hall, Upper Saddle River, N.J., 14th edition.
- Breiman, L. (2001). Random Forests. *Machine Learning*, 45:5–32.
- Bronick, C. J. and Lal, R. (2005). Soil structure and management: A review. *Geoderma*, 124(1-2):3–22.
- Brown, D. S. P.-D. R. E., Jurgensen, M. F., and Mroz, G. D. (1998). Comparison of Methods for Determining Bulk Densities of Rocky Forest Soils. *Soil Science Society of America Journal*, 63:379–383.
- Brun, E. and Rey, L. (1986). Field study on snow mechanical properties with special regard to liquid water content. *Davos Symposium, Avalanche Formation, Movement and Effects*, (162):183–193.
- Bryant, R., Doerr, S. H., Hunt, G., and Conan, S. (2007). Effects of compaction on soil surface water repellency. *Soil Use and Management*, 23(3):238–244.
- Buja, K. (2012). Finding Overlapping Features tool for ArcGIS.
- Busscher, W. J., Bauer, P. J., Camp, C. R., and Sojka, R. E. (1997). Correction of cone index for soil water content differences in a coastal plain soil. *Soil and Tillage Research*, 43(3-4):205–217.
- Busscher, W. J. and Sojka, R. E. (1987). Enhancement of subsoiling effects on soil strength by conservation tillage. *Transactions of the ASAE*, 30(4):888–892.
- Cambi, M., Certini, G., Neri, F., and Marchi, E. (2015). The impact of heavy traffic on forest soils: A review. *Forest Ecology and Management*, 338:124–138.

- Campbell, D. M. H. (2012). TRAIL: Optimizing trail locations by terrain conditions and other considerations, at high resolution. Msc thesis, MSc. Thesis. University of New Brunswick.
- Campbell, D. M. H., White, B., and Arp, P. A. (2013). Modeling and mapping soil resistance to penetration and rutting using LiDAR-derived digital elevation data. *Journal of Soil and Water Conservation*, 68(6):460–473.
- Carter, E., McDonald, T., and Torbert, J. (2000). Assessment of soil strength variability in a harvested loblolly pine plantation in the Piedmon region of Alabama, United States. *New Zealand Journal of Forestry Science*, 30(1/2):237–279.
- Carter, E. A., Aust, W. M., and Burger, J. A. (2007). Soil strength response of select soil disturbance classes on a wet pine flat in South Carolina. *Forest Ecology and Management*, 247(1-3):131–139.
- Chan, K. Y., Oates, A., Swan, A. D., Hayes, R. C., Dear, B. S., and Peoples, M. B. (2006). Agronomic consequences of tractor wheel compaction on a clay soil. *Soil and Tillage Research*, 89(1):13–21.
- Chen, G. and Weil, R. R. (2010). Penetration of cover crop roots through compacted soils. *Plant and Soil*, 331(1):31–43.
- Chen, G. and Weil, R. R. (2011). Root growth and yield of maize as affected by soil compaction and cover crops. *Soil and Tillage Research*, 117(2011):17–27.
- Chow, T. L., Rees, H. W., Monteith, J. O., Toner, P., and Lavoie, J. (2007). Effects of coarse fragment content on soil physical properties, soil erosion and potato production. *Canadian Journal of Soil Science*, 87(5):565–577.
- Corns, I. G. (1988). Compaction by forestry equipment and effects on coniferous seedling growth on four soils in the Alberta foothills. *Canadian Journal of Forest Research* 1, 18:75–84.

- Culley, J., Dow, B., Presant, E., and Maclean, A. (1981). Impacts of installation of an oil pipeline on the productivity of Ontario cropland Canad. Technical report.
- Czyz, E. A. (2004). Effects of traffic on soil aeration, bulk density and growth of spring barley. *Soil and Tillage Research*, 79(2 SPEC.ISS.):153–166.
- Das, K. and Paul, P. K. (2015). Present status of soil moisture estimation by microwave remote sensing. *Cogent Geoscience*, 1(1):1–21.
- Davies, D. B., Finney, J. B., and Richardson, S. J. (1973). Relative Effects of Tractor Weight and Wheel- Slip in Causing Soil Compaction. *European Journal of Soil Science*, 24(3):399–409.
- Department of Environment and Climate Change Canada (2016a). Historical Climate Data.
- Department of Environment and Climate Change Canada (2016b). Historical Hydrometric Data.
- Devore, J. L. (1999). *Probablity and Statistics for Engineering and the Sciences*. Duxbury Press, 5th edition.
- Dobbie, K. E. and Smith, K. A. (2006). The effect of water table depth on emissions of N 2 O from a grassland soil. *Soil Use and Management*, 22(March):22–28.
- Earl, R. (1997). Prediction of trafficability and workability from soil moisture deficit. Soil and Tillage Research, 40(3-4):155–168.
- Eichrodt, A. (2003). *Development of a spatial trafficability evaluation system.* vdf Hochschulverlag AG, Zurich.
- Eid, H. T. and Stark, T. D. (1998). Undrained shear strength fro cone penetration tests. In *Geotechnical Site Characterization*, pages 1021–1025. Robertson & Mayne (eds) Balkema, Rotterdam.

- Elbanna, E. B. and Witney, B. D. (1987). Cone penetration resistance equation as a function of the clay ratio, soil moisture content and specific weight. *Journal of Terramechanics*, 24(1):41–56.
- Eliasson, L. (2005). Effects of Forwarder Tyre Pressure on Rut Formation and Soil Compaction. *Silva Fennica Monographs*, 39(4):549–557.
- Eliasson, L. and Wästerlund, I. (2007). Effects of slash reinforcement of strip roads on rutting and soil compaction on a moist fine-grained soil. *Forest Ecology and Management*, 252(1-3):118–123.
- Elwaleed, A. K., Yahya, A., Zohadie, M., Ahmad, D., and Kheiralla, A. F. (2006). Effect of inflation pressure on motion resistance ratio of a high-lug agricultural tyre. *Journal of Terramechanics*, 43(2):69–84.
- Engman, E. T. and Chauhan, N. (1995). Status of microwave soil moisture measurements with remote sensing. *Remote Sensing of Environment*, 51(1):189–198.
- Ezzati, S., Najafi, A., Rab, M. A., and Zenner, E. K. (2012). Recovery of soil bulk density, porosity and rutting from ground skidding over a 20-year period after timber harvesting in Iran. *Silva Fennica*, 46(4):521–538.
- Farzaneh, B., Almassi, M., Sadeghi, M., and Minaei, S. (2012). Assessment of Soil Compaction Bulk Density Indices and Cone Index in Different Moistures and Depths for Application in Precise Tillage. *World Applied Sciences Journal*, 20(12):1704–1712.
- Fervers, C. (2004). Improved FEM simulation model for tiresoil interaction. *Journal of Terramechanics*, 41(2-3):87–100.
- Furze, S. (2018). A high-resolution digital soil mapping framework for New Brunswick, Canada. Phd dissertation, University of New Brunswick.
- Furze, S. (2019). Digital Soil Maps for New Brunswick.

- Furze, S., Ogilvie, J., and Arp, P. (2017). Fusing Digital Elevation Models to Improve Hydrological Interpretations. *Journal of Geographic Information System*, 09(05):558–575.
- Garcia, M., Özdogan, M., and Townsend, P. A. (2015). Impacts of forest harvest on cold season land surface conditions and land-atmosphere interactions in northern Great Lakes states. *Journal of Advances in Modeling Earth Systems*, 6(3):923–937.
- GeoNB (2015a). GIS Bare-earth digital elevation model. Technical report, Fredericton, NB.
- GeoNB (2015b). GIS Soils of New Brunswick. Technical report, Fredericton, NB.
- GeoNB (2018). GIS Ecological Land Classification. Technical report.
- Giannetti, F., Chirici, G., Travaglini, D., Bottalico, F., Marchi, E., and Cambi, M. (2017). Assessment of Soil Disturbance Caused by Forest Operations by Means of Portable Laser Scanner and Soil Physical Parameters. *Soil Science Society of America Journal*, (June):1–23.
- Gill, W. R. (1971). Economic Assessment of Soil Compaction. In *Compaction of Agricultural Soils*, pages 432–456. American Society of Agricultural Engineers, St. Joseph, Michigan.
- Glahn, H. R. and Lowry, D. a. (1972). The Use of Model Output Statistics (MOS) in Objective Weather Forecasting.
- Grady, T. R. (1982). The effects of snow compaction on water release and sediment yield. Masters thesis, Montana State University.
- Grahn, M. (1991). Prediction of sinkage and rolling resistance for off-the-road vehicles considering penetration velocity. *Journal of Terramechanics*, 28(4):339–347.

- Gregory, J., Dukes, M., Jones, P., and Miller, G. (2006). Effect of urban soil compaction on infiltration rate. *Journal of Soil and Water Conservation*, 61(3):117–124.
- Grigal, D. F. (2000). Effects of extensive forest management on soil productivity. Forest Ecology and Management, 138(1-3):167–185.
- Haas, J., Ellhöft, K. H., Schack-Kirchner, H., and Lang, F. (2016). Using photogrammetry to assess rutting caused by a forwarderA comparison of different tires and bogie tracks. *Soil and Tillage Research*, 163(14-20).
- Halvorson, J., McCool, D. K., King, L. G., and Gatto, L. W. (2001). Soil compaction and over-winter changes to tracked-vehicle ruts, Yakima Training Center, Washington. *Journal of Terramechanics*, 38:133–151.
- Hamza, M. and Anderson, W. (2005). Soil compaction in cropping systems. *Soil and Tillage Research*, 82(2):121–145.
- Han, H.-S., Page-Dumroese, D., and Han, S.-K. (2006). Effects of slash, machine passes, and soil moisture on penetration Resistance in a cut-to-length harvesting. *International Journal of Forest Engineering*, 17(2):11–24.
- Han, S.-K., Han, H.-S., Page-Dumroese, D. S., and Johnson, L. R. (2009). Soil compaction associated with cut-to-length and whole-tree harvesting of a coniferous forest. *Canadian Journal of Forest Research*, 39(5):976–989.
- Hausenbuilder, R. (1978). *Soil Science: Principles and Practices.* Wm. C. Brown Company, 2nd edition.
- Herrick, J. E. and Jones, T. L. (2002). A dynamic cone penetrometer for measuring soil penetration resistance. *Soil Science Society of America Journal*, 66(4):1320.
- Hooks, C. L. and Jansen, I. J. (1984). Recording cone penetrometer developed in reclamation research. *Soil Science Society of America Journal* 1, 50(1):10–12.

- Horn, R., Domżał, H., Słowińska-Jurkiewicz, A., and van Ouwerkerk, C. (1995). Soil compaction processes and their effects on the structure of arable soils and the environment. *Soil and Tillage Research*, 35:23–36.
- Horn, R., Vossbrink, J., and Becker, S. (2004). Modern forestry vehicles and their impacts on soil physical properties. *Soil and Tillage Research*, 79(2 SPEC.ISS.):207–219.
- Huntington, T. G. (2007). Available Water Capacity and Soil Organic Matter. In *Encyclopedia of Soil Science*, pages 139–143. Taylor & Francis, New York, 2nd editio edition.
- Jackson, T. (1993). Measuring surface soil moisture using passive microwave remote sensing. *Hydrological Processes*, 7(2):139–152.
- Jamshidi, R., Jaeger, D., Raafatnia, N., and Tabari, M. (2008). Influence of two ground-based skidding systems on soil compaction under different slope and gradient conditions. *International Journal of Forest Engineering*, 19(1):9–16.
- Jellinek, H. H. G. (1957). Compressive strength properties of snow. page 16.
- Jones, M.-F. and Arp, P. (2019a). Analyzing and Projecting Soil Moisture and Cone Penetrability Variations in Forest Soils. *Journal of Forestry*, 9:109–142.
- Jones, M.-F. and Arp, P. (2019b). Soil trafficability forecasting. *Open Journal of Forestry*, Submitted.
- Jones, M.-F. and Arp, P. A. (2017). Relating the cone penetration and rutting resistance of soils to variations in soil properties and daily moisture variations over time. *Open Journal of Soil Science*, 1(1):1.
- Jones, M.-F., Castonguay, M., Jaeger, D., and Arp, P. (2018). Track-monitoring and analyzing machine clearances during wood forwarding. *Open Journal of Forestry*, 8:297–327.

- Jun, H. G., Way, T. R., Löfgren, B., Landström, M., Bailey, A. C., Burt, E. C., and McDonald, T. P. (2004). Dynamic load and inflation pressure effects on contact pressures of a forestry forwarder tire. *Journal of Terramechanics*, 41(4):209–222.
- Jutras, M.-F. (2012). Modeling stream discharge in forest catchments across Canada: hydraulic conductivity calibrations. Masters thesis, University of New Brunswick.
- Jutras, M.-F. and Arp, P. (2010). Determining Hydraulic Conductivity from Soil Characteristics with Applications for Modelling Stream Discharge in Forest Catchments. In Elango, L., editor, *Hydraulic Conductivity Issues, Determination and Applications*, number ii, chapter 10, pages 189–202. InTech.
- Jutras, M.-F. and Arp, P. (2013). Role of Hydraulic Conductivity Uncertainties in Modeling Water Flow through Forest Watersheds. In Rodrigues da Silva, V., editor, *Hydraulic Conductivity*, chapter 2, pages 33–54. InTech.
- Kozlowski, T. (2008). Soil compaction and growth of woody plants. *Scandinavia Journal of Forest Resources*, 14:596–619.
- Krzic, M., Bulmer, C. E., Teste, F., Dampier, L., and Rahman, S. (2004). Soil properties influencing compactability of forest soils in British Columbia. *Canadian Journal of Soil Science*, 84(2):219–226.
- Kumar, A., Chen, Y., Sadek, A., and Rahman, S. (2012). Soil cone index in relation to soil texture, moisture content, and bulk density for no-tillage and conventional tillage. *Agriculture Engineering International: CIGR Journal*, 14(1):26–37.
- Labelle, E. R. (2008). Assessing Soil Disturbances Caused by Forest Machinery. Masters thesis, University of New Brunswick.
- Labelle, E. R. (2012). Effect of brush mats and machine characteristics on dynamic peak loads and surface contact pressure exerted by forest machinery. PhD thesis, PhD Thesis. University of New Brunswick.

- Labelle, E. R. and Jaeger, D. (2011). Soil compaction caused by cut-to-length forest operations and possible short-term natural rehabilitation of soil density. *Soil Science Society of America Journal*, 75(6):2314–2329.
- Labelle, E. R. and Jaeger, D. (2012). Quantifying the Use of Brush Mats in Reducing Forwarder Peak Loads and Surface Contact Pressure. *Croatian Journal of Forest Engineering*, 33(2):249–274.
- Labelle, E. R., Jaeger, D., and Poltorak, B. J. (2015). Assessing the Ability of Hardwood and Softwood Brush Mats to Distribute Applied Loads. *Croatian Journal of Forest Engineering*, 36(2):227–242.
- Launiainen, S., Ala-Ilomäki, J., Hiedanpää, J., Salmivaara, A., Finér, L., Nevalainen, P., Heikkonen, J., and Pahikkala, T. (2017). Estimating the Rut Depth by UAV Photogrammetry. *Remote Sensing*, 9(12):1279.
- Liaw, A. and Wiener, M. (2002). Classification and Regression by randomForest. *R news*, 2(December):18–22.
- Lin, J., Sun, Y., and Schulze Lammers, P. (2014). Evaluating model-based relationship of cone index, soil water content and bulk density using dual-sensor penetrometer data. *Soil and Tillage Research*, 138:9–16.
- Liu, K., Ayers, P., Howard, H., and Anderson, A. (2009). Influence of turning radius on wheeled military vehicle induced rut formation. *Journal of Terramechanics*, 46(2):49–55.
- Lowery, B. and Morrison, J. E. (2002). Soil Penetrometers and Penetrability. In *Methods of Soil Analysis, Part 4 Physical Methods*, pages 363–385. Soil Science Society of America, Inc., Madison, Wisconsin.
- Maclaurin, E. B. (1990). The use of mobility numbers to describe the in-field tractive performance of pneumatic tyres. In *Proceedings of the 10th International ISTVS Conference*, pages 177–186, Kobe, Japan.

- Manuwa, S. I. (2012). Evaluation of Shear Strength and Cone Penetration Resistance Behavior of Tropical Silt Loam Soil under Uni-Axial Compression. *Open Journal of Soil Science*, 02(02):95–99.
- McDonald, T. and Sexias, F. (1997). Effect of slash on forwarder soil compaction.

 International Journal of Forest Engineering, 8(2):15–26.
- McFero Grace, J., Skaggs, R. W., and Cassel, D. K. (2006). Soil Physical Changes Associated with Forest Harvesting Operations on an Organic Soil. *Soil Science Society of America Journal*, 70(2):503.
- McNabb, D., Startsev, A., and Nguyen, H. (2001). Soil wetness and traffic level effects on bulk density and air-filled porosity of compacted boreal forest soils. *Soil Science Society of America Journal*, 65:1238–1247.
- Meek, P. (1996). Effects of skidder traffic on two types of forest soils. Technical report, Forest Engineering Research Institute of Canada, Pointe-Claire, QC.
- Moehring, D. M. and Rawls, I. W. (1970). Detrimental effects of wet weather logging. *Journal of Forestry*, 68(1):166–167.
- Moroni, M. T., Carter, P. Q., and Ryan, D. A. J. (2009). Harvesting and slash piling affect soil respiration, soil temperature, and soil moisture regimes in Newfoundland boreal forests. *Canadian Journal of Soil Science*, 89:345–355.
- Muller, L. and Schindler, U. (1998). Wetness criteria for modelling trafficability and workability of cohesive arable soils. In *Proceedings of the Seventh Annual Drainage Symposium on Drainage in the 21st Century: Food Production and the Environment*, pages 472–479, Orlando, FL.
- Murphy, P., Castonguay, M., Ogilvie, J., Nasr, M., Hazlett, P., Bhatti, J. S., and Arp, P. (2009a). A geospatial and temporal framework for modeling gaseous N and other N losses from forest soils and basins, with application to the Turkey Lakes Watershed Project, in Ontario, Canada. Forest Ecology and Management, 258:2304–2317.

- Murphy, P., Ogilvie, J., and Arp, P. A. (2009b). Topographic modelling of soil moisture conditions: a comparison and verification of two models. *European Journal of Soil Science*, 60(1):94–109.
- Murphy, P., Ogilvie, J., Connor, K., and Arp, P. A. (2007). Mapping wetlands: A comparison of two different approaches for New Brunswick, Canada. *Wetlands*, 27(4):846–854.
- Murphy, P., Ogilvie, J., Meng, F.-R., White, B., Bhatti, J. S., and Arp, P. (2011). Modelling and mapping topographic variations in forest soils at high resolution: A case study. *Ecological Modelling*, 222(14):2314–2332.
- Naghdi, R., Bagheri, I., Lotfalian, M., and Setodeh, B. (2009). Rutting and soil displacement caused by 450c Timber Jack wheeled skidder (asalem forest northern Iran). *Journal of Forest Science*, 55(4):177–183.
- Nawaz, M. F., Bourrié, G., and Trolard, F. (2013). Soil compaction impact and modelling. A review. *Agronomy for Sustainable Development*, 33(2):291–309.
- Nikooy, M., Tsioras, P. A., Naghdi, R., Zenner, E. K., and Solgi, A. (2016). Soil disturbance caused by ground-based skidding at different soil moisture conditions in Northern Iran. *International Journal of Forest Engineering*, 27(3):169–178.
- Njoku, E. G. and Entekhabi, D. (1996). Passive microwave remote sensing of soil moisture. *Journal of Hydrology*, 184(1-2):101–129.
- Ogilvie, J. (2017). Flow-line and wet-areas conformance testing of wetland locations using LiDAR and SRTM elevation Data. Masters thesis, University of New Brunswick.
- Page-Dumroese, D., Jurgensen, M., Elliot, W., Rice, T., Nesser, J., Collins, T., and Meurisse, R. (2000). Soil quality standards and guidelines for forest sustainability in northwestern North America. *Forest Ecology and Management*, 138(1-3):445–462.

- Parkhurst, B. M., Aust, W. M., Bolding, M. C., Barrett, S. M., and Carter, E. A. (2018). Soil response to skidder trafficking and slash application. *International Journal of Forest Engineering*, 00(00):1–10.
- Pierzchała, M., Talbot, B., and Astrup, R. (2016). Measuring wheel ruts with close-range photogrammetry. *Forestry*, 89(4):383–391.
- Poesen, J. and Lavee, H. (1994). Rock fragments in top soils: significance and processes. *Catena*, 23(1-2):1–28.
- Poltorak, B. J., Labelle, E. R., and Jaeger, D. (2018). Soil displacement during ground-based mechanized forest operations using mixed-wood brush mats. *Soil and Tillage Research*, 179(August 2017):96–104.
- Porsinsky, T., Sraka, M., and Stankic, I. (2006). Comparison of two approaches to soil strength classifications. *Croatian Journal of Forest Engineering*, 27(1):17–26.
- Prakash, K. (2014). *Tire-soil interaction analysis of forest machines*. Masters thesis, KTH Royal Institute of Technology.
- Prose, D. V. (1985). Persisting effects of armored military maneuvers some soils of the Mojave desert. *Environmental Geology Water Sciences*, 7(3):163–170.
- R Core Team (2015). R: A Language and Environment for Statistical Computing. Technical report, R Foundation for Statistical Computing, Vienna, Austria.
- Rab, A., Bradshaw, J., Campbell, R., and Murphy, S. (2005). Review of Factors Affecting Disturbance, Compaction and Trafficability of Soils with Particular Reference to Timber Harvesting in the Forests of South-West Western Australia. Technical Report 2, Department of Conservation and Land Management, SFM Technical Report No. 2.
- Radford, B. J., Bridge, B. J., Davis, R. J., McGarry, D., Pillai, U. P., Rickman, J. F., Walsh, P. A., and Yule, D. F. (2000). Changes in the properties of a Vertisol and responses of wheat after compaction with harvester traffic. *Soil and Tillage Research*, 54(3-4):155–170.

- Raghavan, G. S. V., McKyes, E., and Chassé, M. (1977). Effect of wheel slip on soil compaction. *Journal of Agricultural Engineering Research*, 22(1):79–83.
- Rantala, M. (2001). Comparison of some measurement methods for predicting the site sensitivity (rut formation) in the practical harvesting of wood. *ECOWOOD*, pages 5–8.
- Raper, R. L. (2005). Agricultural traffic impacts on soil. *Journal of Terramechanics*, 42(3-4):259–280.
- Raper, R. L., Bailey, A. C., Burt, E. C., Way, T. R., and Liberati, P. (1995). The effects of reduced inflation pressure on soil-tire interface stresses and soil strength. *Journal of Terramechanics*, 32(1):43–51.
- Raven, P. H., Evert, R. F., and Eichgorn, S. E. (1999). *Biology of Plants*. W. H. Freeman, New York, New York, 6th edition.
- Roberts, S. D., Harrington, C. A., and Terry, T. A. (2005). Harvest residue and competing vegetation affect soil moisture, soil temperature, N availability, and Douglas-fir seedling growth. *Forest Ecology and Management*, 205(1-3):333–350.
- Robertson, P. K. (2016). Cone penetration test (CPT)-based soil behaviour type (SBT) classification system An update. *Canadian Geotechnical Journal*, 1927:1–18.
- Rohani, B. and Baladi, G. (1981). Correlation of mobility cone index with fundamental engineering properties of soil. Technical report, U.S. Army Engineer Waterways Expediment Station, Washington, DC.
- Rücknagel, J., Götze, P., Hofmann, B., Christen, O., and Marschall, K. (2013). The influence of soil gravel content on compaction behaviour and pre-compression stress. *Geoderma*, 209-210:226–232.
- Saarilahti, M. (2002a). Soil Interaction Model Development of a protocol for ecoefficient wood harvesting on sensitive sites (Ecowood) Appendix No. 8. Technical Report May.

- Saarilahti, M. (2002b). Soil Interaction Model Development of a protocol for ecoefficient wood harvesting on sensitive sites (Ecowood) Appendix No. 8 Forest soil properties. Technical Report May, University of Helsinki, Department of Forest Resource Management.
- Saarilahti, M. (2002c). Soil Interaction Model -Developement of a protocol for ecoefficient wood harvesting on sensitive sites (Ecowood) Appendix Report No 5. Technical Report May.
- Saarilahti, M. (2002d). Soil Interaction Model -Development of a protocol for ecoefficient wood harvesting on sensitive sites (Ecowood) Appendix No. 1. Technical Report May.
- Sakai, H., Nordfjell, T., Suadicani, K., Talbot, B., and Bøllehuus, E. (2008). Soil compaction on forest soils from different kinds of tires and tracks and possibility of accurate estimate. *Croatian Journal of Forest Engineering*, 29(1):15–27.
- Salmivaara, A., Miettinen, M., Finér, L., Launiainen, S., Korpunen, H., Tuominen, S., Heikkonen, J., Nevalainen, P., Sirén, M., Ala-Ilomäki, J., and Uusitalo, J. (2018). Wheel rut measurements by forest machine-mounted LiDAR sensors accuracy and potential for operational applications? *International Journal of Forest Engineering*, 00(00):1–12.
- Scholander, J. (1974). Bearing capacity of some forest soils for wheeled vehicles. Some technical aspects and consequences. Skogsmarks bärighet för hjulfordon. Några tekniska aspekter och konsekvenser. Specialnotiser från. Technical report.
- Shelrick, B. H. and Wang, C. (1993). Particle size distribution. In Carter, M. C., editor, *Soil Sampling and Methods of Analysis*, chapter 47, pages 499–518. Lewis Publishers, Boca Raton, FL.
- Shmulevich, I., Mussel, U., and Wolf, D. (1998). The effect of velocity on rigid wheel performance. *Journal of terramechanics*, 35:189–207.

- Shoop, S. A. (1989). Vehicle mobility on thawing soils. Technical Report September, Cold Region Research & Engineering Laboratory.
- Shoop, S. A. (1995). Vehicle bearing capacity of frozen ground over a soft substrate. *Canadian Geotechnical Journal*, 32:552–556.
- Singer, M. and Munns, D. (2006). *Soils: an introduction*. Pearson Prentice Hall, Columbus, Ohio, 6th edition.
- Singh, P., Kumar, N., and Arora, M. (2000). Degree-day factors for snow and ice for Dokriani Glacier, Garhwal Himalayas. *Journal of Hydrology*, 235(1-2):1–11.
- Sirén, M., Ala-Ilomäki, J., Lindeman, H., Uusitalo, J., Kiilo, K., Salmivaara, A., and Ryynänen, A. (2019a). Soil disturbance by cut-to-length machinery on midgrained soils. *Silva Fennica*, 53(2):1–24.
- Sirén, M., Salmivaara, A., Ala-Ilomäki, J., Launiainen, S., Lindeman, H., Uusitalo, J., Sutinen, R., and Hänninen, P. (2019b). Predicting forwarder rut formation on fine-grained mineral soils. *Scandinavian Journal of Forest Research*, 34(2):145–154.
- Smith, C. W., Johnston, M., and Lorentz, S. (1997). The effect of soil compaction and soil physical properties on the mechanical resistance of South African forestry soils. *Geoderma*, 78(1-2):93–111.
- Soane, B. and van Ouwerkerk, C. (1994). Soil compaction problems in world agriculture. In Soane, B. and van Ouwerkerk, C., editors, *Developments in Agricultural Engineering*, chapter 1, pages 1–21. Elsevier, Amsterdam.
- Solgi, A., Naghdi, R., Labelle, E. R., and Zenner, E. K. (2018). The effects of using soil protective mats of varying compositions and amounts on the intensity of soil disturbances caused by machine traffic. *International Journal of Forest Engineering*, 29(3):199–207.
- Sørensen, R., Zinko, U., and Seibert, J. (2006). On the calculation of the topographic wetness index: evaluation of different methods based on field observations. *Hydrology and Earth System Sciences*, 10(1):101–112.

- Southee, F. M., Treitz, P. M., and Scott, N. A. (2012). Application of Lidar Terrain Surfaces for Soil Moisture Modeling. *Photogrammetric Engineering & Remote Sensing*, 78(12):1241–1251.
- Startsev, A. and McNabb, D. (2000). Effects of skidding on forest soil infiltration in west-central Alberta. *Canadian Journal of Soil Science*, 80:617–624.
- Startsev, A. and McNabb, D. (2001). Skidder traffic effects on water retention, pore-size distribution, and van Genuchten parameters of boreal forest soils. *Soil Science Society of America Journal*, 65:224–231.
- Stobbe, P. C. (1940). Soil survey of Fredericton-Gagetown area. Technical report.
- Šušnjar, M., Horvat, D., and Šešelj, J. (2006). Soil compaction in timber skidding in winter conditions. *Croatian Journal of Forest Engineering*, 1:3–15.
- Sutherland, B. J. (2003). Preventing soil compaction and rutting in the boreal forest of Western Canada: A practical guide to operating timber-harvesting equipment. Technical report, Forest Engineering Research Institute of Canada (FERIC), Point-Claire, QC.
- Suvinen, A. (2006). A GIS-based simulation model for terrain tractability. *Journal of Terramechanics*, 43:427–449.
- Taghavifar, H. and Mardani, A. (2014). Effect of velocity, wheel load and multipass on soil compaction. *Journal of the Saudi Society of Agricultural Sciences*, 13(1):57–66.
- Taylor, J. H. and Burt, E. C. (1987). function of both surface unit pressure and the total load applied. The following formula from the Boussinesq equations was adapted to describe the pressures in the soil beneath a loaded circular plate:

 o , = Pro (1 - COS ` / Or) where a ~ Pm pressur. 24(3):179–186.
- Tekeste, M. Z., Raper, R. L., and Schwab, E. B. (2008). Soil Drying Effects on Soil Strength and Depth of Hardpan Layers as Determined from Cone Index Data. *Agricultural Engineering International: the CIGR Ejournal*, X:1–17.

- Towner, G. D. (1974). The assessment of soil texture from soil strength measurements. *Journal of Soil Science*, 25(3):298–306.
- Turnage, G. W. (1984). Prediction of in-sand tire and wheeled vehicle drawbar performance. In *Proceedings of the 8th International ISTVS Conference*, pages 121–150, Cambridge, UK.
- Van Rees, K. (2002). Regulations and guidelines for soil disturbance across Canada. Technical report, Department of Soil Science, University of Saskatchewan.
- Vaz, C. M. P. (2003). Use of a combined penetrometer-TDR moisture probe for soil compaction studies. Technical report.
- Vaz, C. M. P., Bassoi, L. H., and Hopmans, J. W. (2001). Contribution of water content and bulk density to field soil penetration resistance as measured by a combined cone penetrometer TDR probe. *Soil & Tillage Research*, 60:35–42.
- Vaz, C. M. P., Manieri, J. M., de Maria, I. C., and Tuller, M. (2011). Modeling and correction of soil penetration resistance for varying soil water content. *Geoderma*, 166(1):92–101.
- Vega-Nieva, D. J. D., Murphy, P. N. C., Castonguay, M., Ogilvie, J., and Arp, P. A. (2009). A modular terrain model for daily variations in machine-specific forest soil trafficability. *Canadian Journal of Soil Science*, 89(March 2008):93–109.
- Vogelmann, E. S., Reichert, J. M., Prevedello, J., and Awe, G. O. (2013). Hydro-physical processes and soil properties correlated with origin of soil hydrophobicity. *Ciencia Rural*, 43(9):1582–1589.
- Wang, L. and Qu, J. J. (2009). Satellite remote sensing applications for surface soil moisture monitoring: A review. *Frontiers of Earth Science in China*, 3(2):237–247.
- Wesseling, J. G., Stoof, C. R., Ritsema, C. J., Oostindie, K., and Dekker, L. W. (2009). The effect of soil texture and organic amendment on the hydrological behaviour of coarse-textured soils. *Soil Use and Management*, 25:274–283.

- White, B., Ogilvie, J., Campbell, D. M., Hiltz, D., Gauthier, B., Chisholm, H. K. H., Wen, H. K., Murphy, P. N., and Arp, P. A. (2012). Using the Cartographic Depth-to-Water Index to Locate Small Streams and Associated Wet Areas across Landscapes. *Canadian Water Resources Journal*, 37(4):333–347.
- Yin, X. and Arp, P. (1994). Fog Contributions to the Water Budget of Forested Watersheds in the Canadian Maritime Provinces: A Generalized Algorithm for Low Elevations. *Atmosphere-Ocean*, 32(3):553–566.
- Young, G. and Berlyn, R. (1968). Some variations in soil trafficability as measured with a cone penetrometer. Technical report, Pointe Claire, P.Q.
- Zhang, S., Grip, H., and Lövdahl, L. (2006). Effect of soil compaction on hydraulic properties of two loess soils in China. *Soil and Tillage Research*, 90:117–125.

Appendix A

Chapter 2 Appendices

A.1 Publication Copyright Permission: Chapter 2

Tue, Jul 18, 2017 at 2:51 AM

Subject: Thisesis Publication Permission

ojss@scirp.org <ojss@scirp.org>

To: "jones.mfn" < jones.mfn@gmail.com>

Cc: customer < customer@scirp.org >

Dear Dr. Marie-France Jones,

Nice to hear from you. You can use this part in your thesis. But you should add a footnote or a reference to explain its provenance. We expect to cooperate with you in the future.

Please feel free to contact me if you have any questions.

Best regards,

Ray WONG

Managing Editor of OJSS Editorial Office

http://www.scirp.org/journal/OJSS/

Email: ojss@scirp.org , feedback@scirp.org

Appendix B

Chapter 3 Appendices

B.1 Publication Copyright Permission: Chapter 3

Wed, Jul 18, 2018 at 9:23 PM

Subject: Thesis Publication Permission

Jenny Ran <papersubmission.ran@gmail.com >

To: "jones.mfn" < jones.mfn@gmail.com>

Dear Dr. Marie-France Jones,

Nice to hear from you. It is ok. You can use the paper within your PhD thesis. If you have new paper, you can send it to me via this email.

Wish everything goes on well with you.

Best regards

Jenny Ran (Editorial Assistant)

PaperSubmission.ran@gmail.com

B.2 Percent frequency of normalized clearance

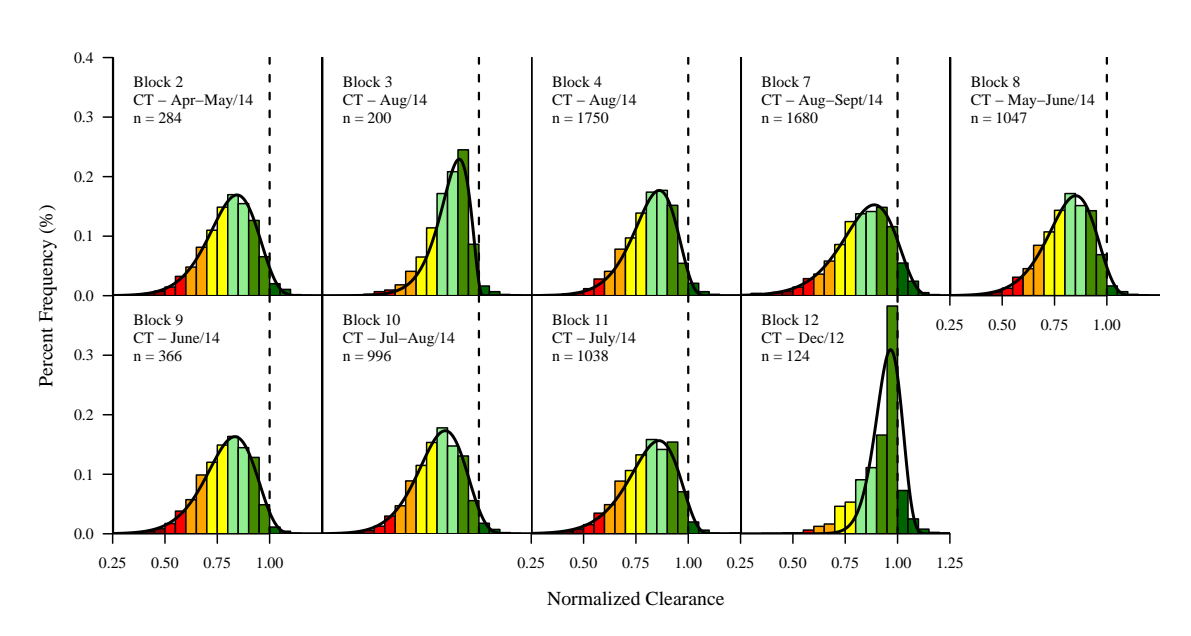


Figure B.1: Percent frequency of normalized clearance for the JD 1110E by block.

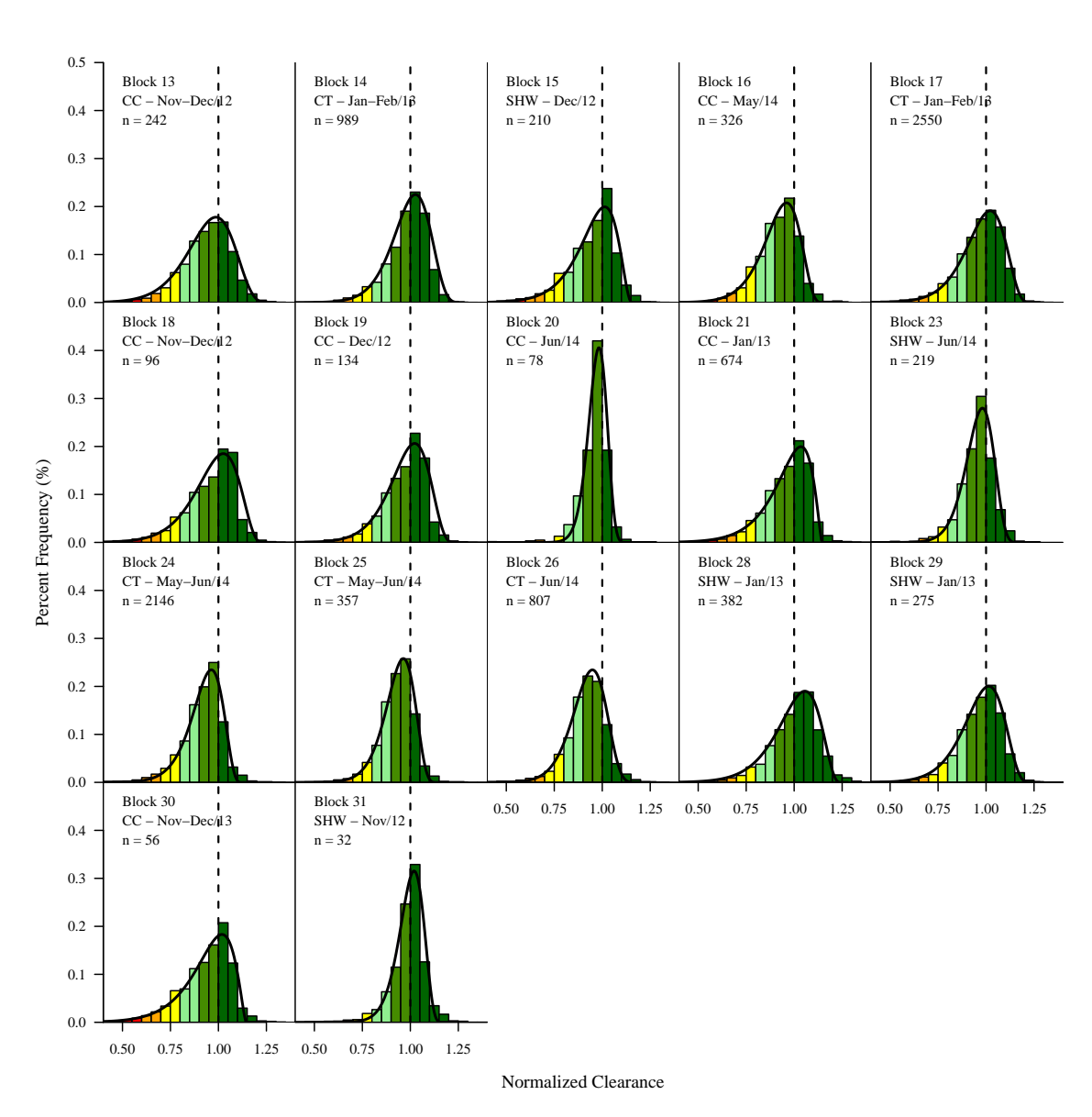


Figure B.2: Percent frequency of normalized clearance for the JD 1510E by block.

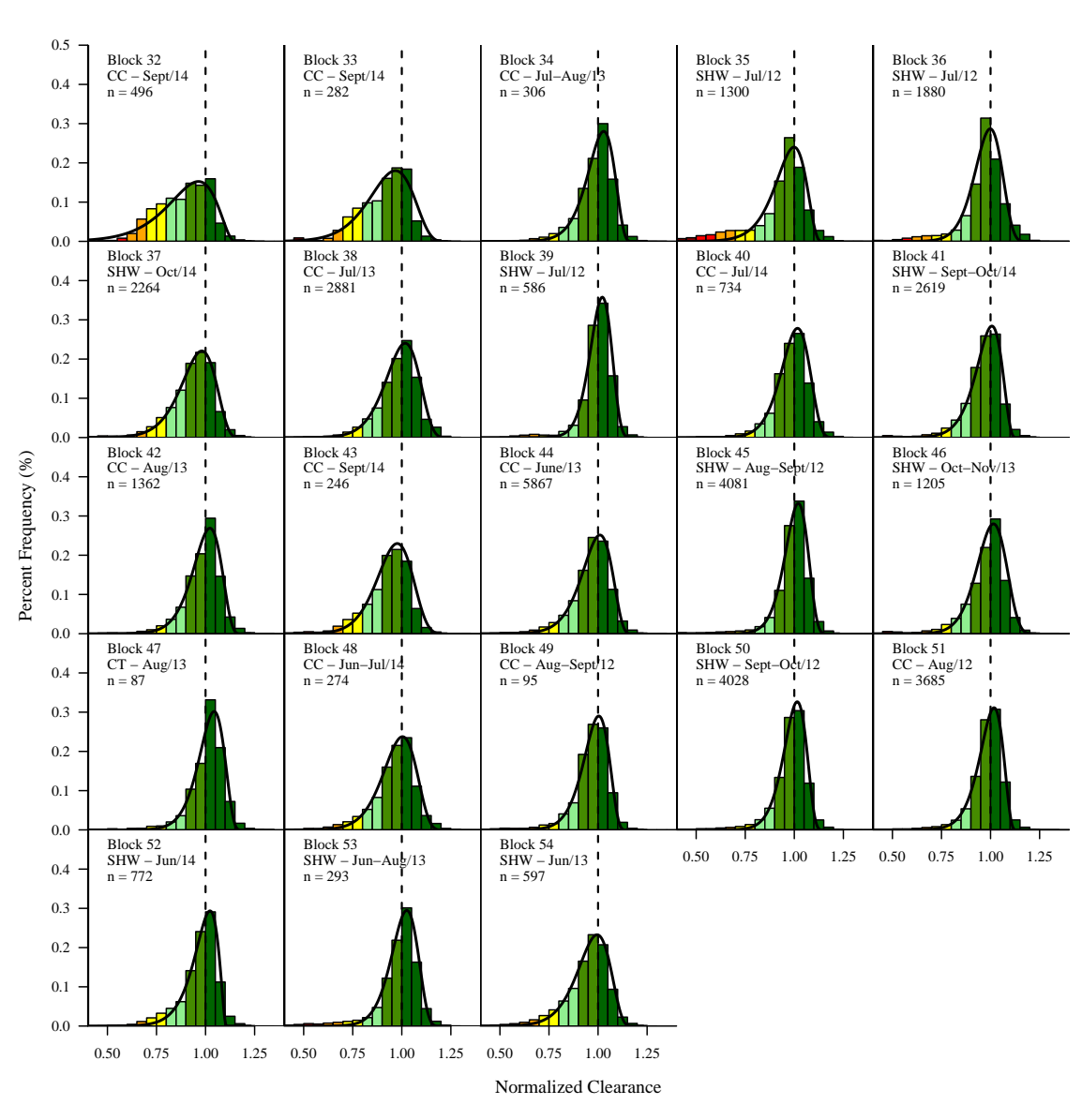


Figure B.3: Percent frequency of normalized clearance for the TC 635D by block.

B.3 Normalized Clearance by Block

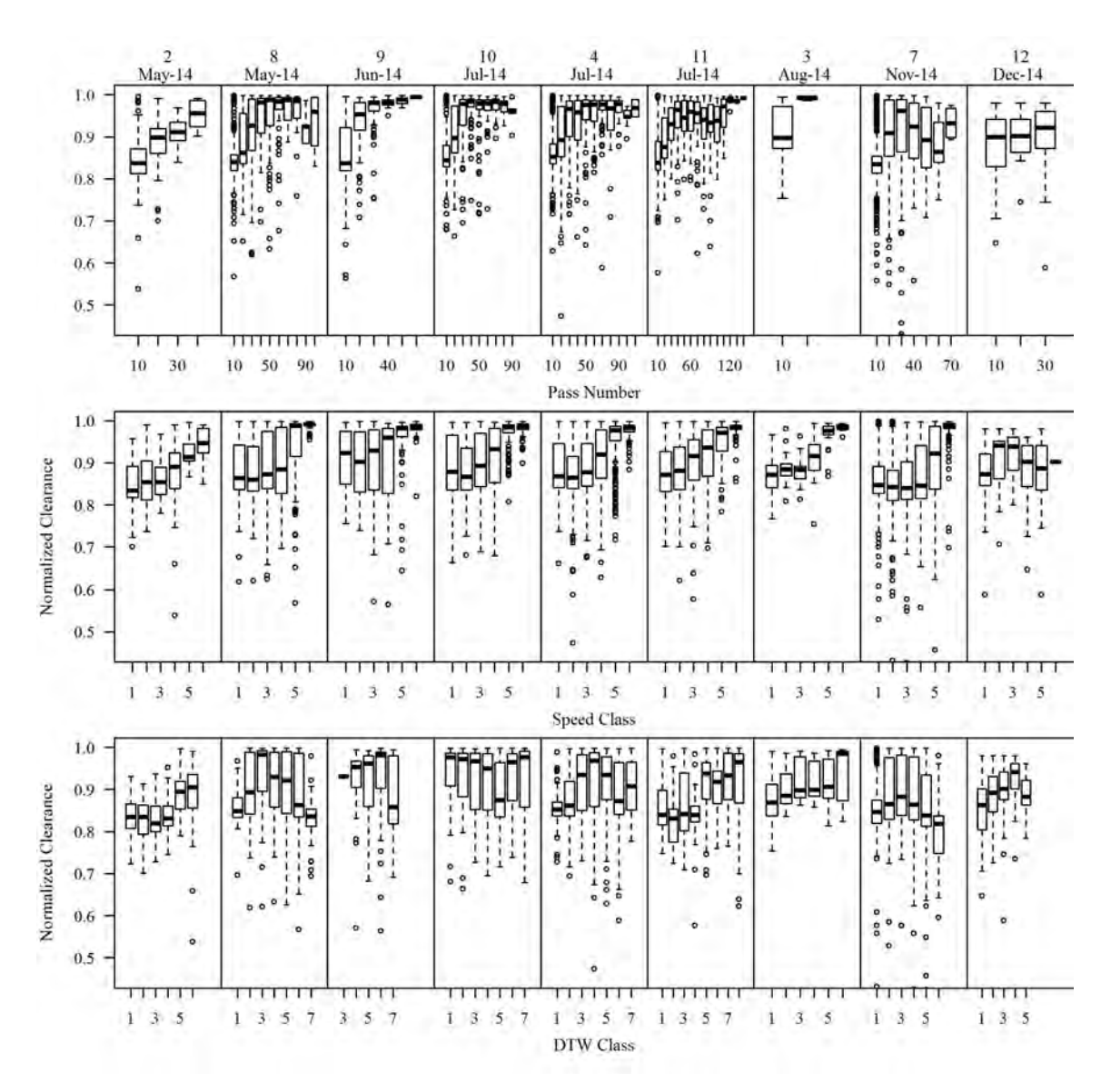


Figure B.4: Normalized Clearance by block for pass number, speed class, and DTW class for the JD 1110E.

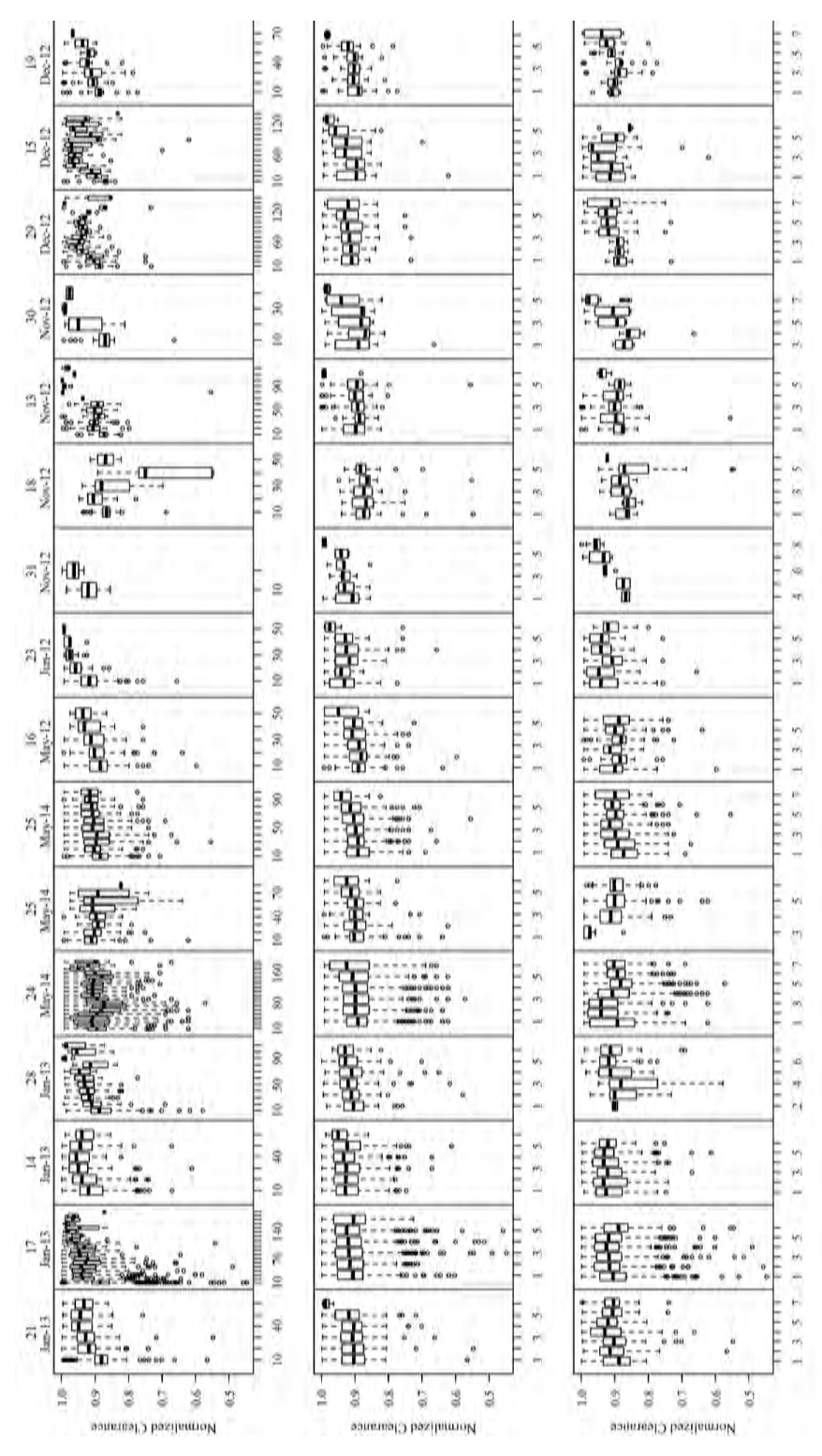


Figure B.5: Normalized Clearance by block for pass number, speed class, and DTW class for the JD 1510E.

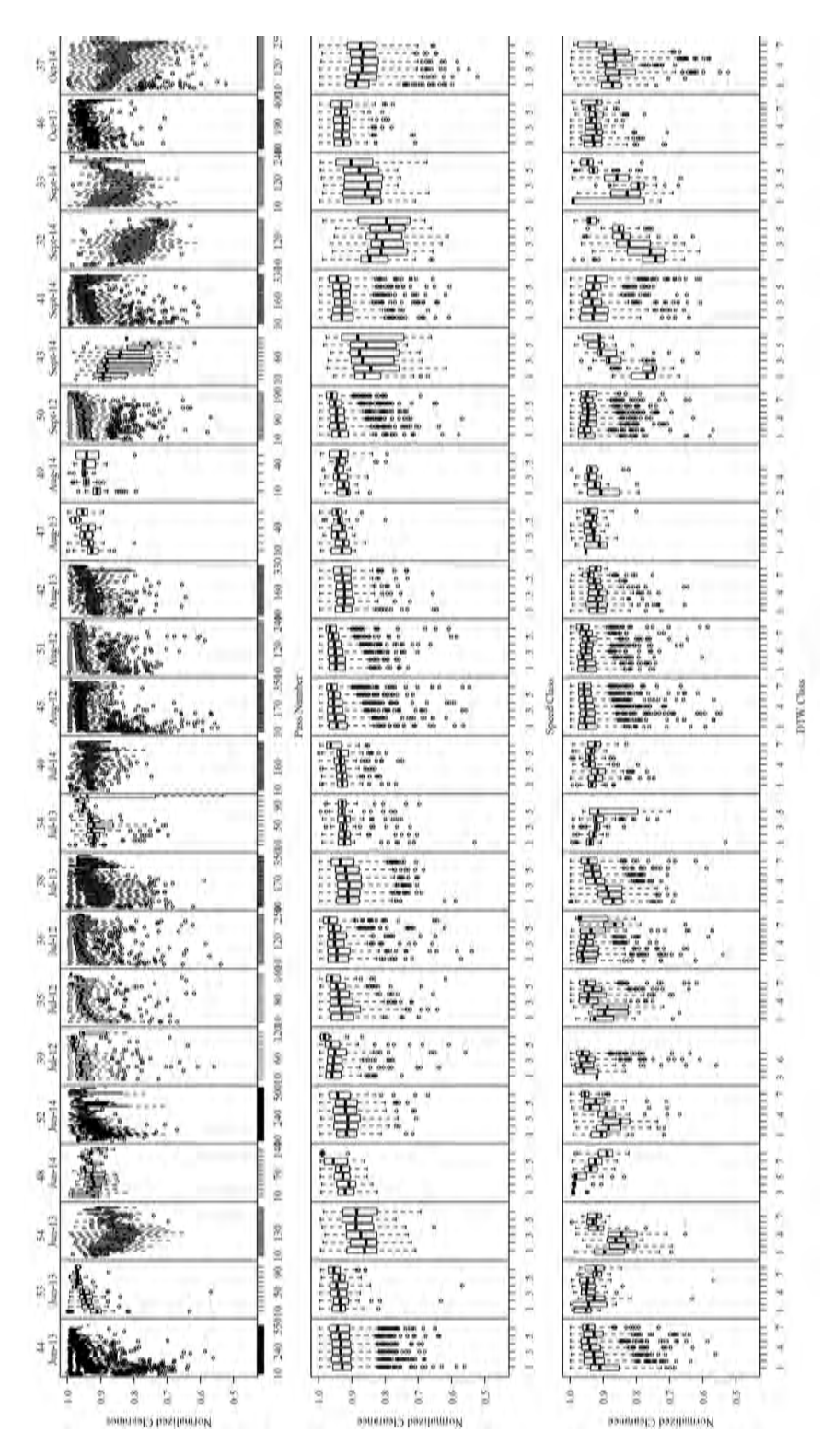


Figure B.6: Normalized Clearance by block for pass number, speed class, and DTW class for the TC 635D.

B.4 ForHyM Site Results

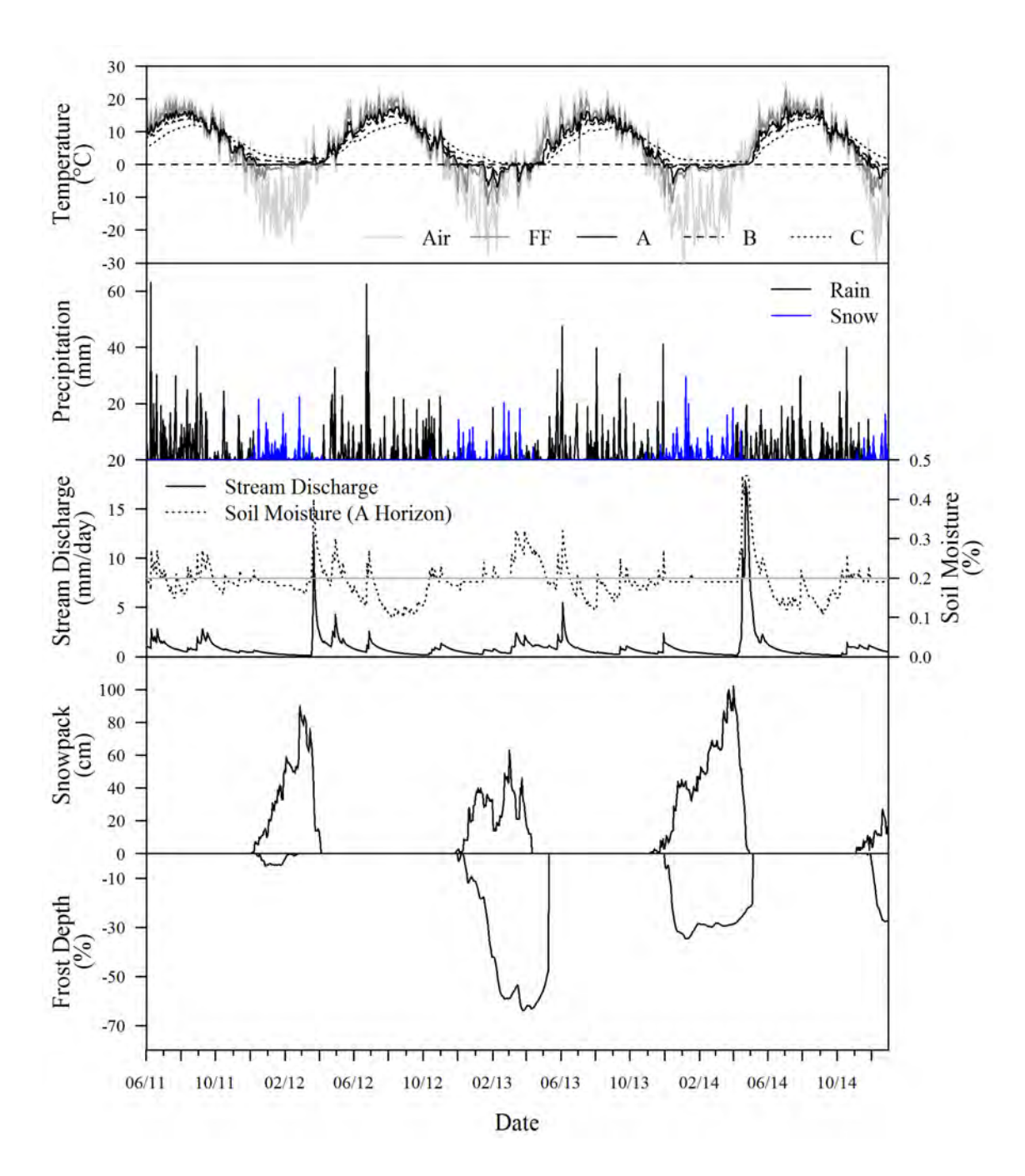


Figure B.7: Daily variations in air temperature and precipitation, with modelled stream discharge, volumetric soil moisture content including field capacities and snowpack depth, frost depth, and volumetric soil moisture content for the wider NWU areas.

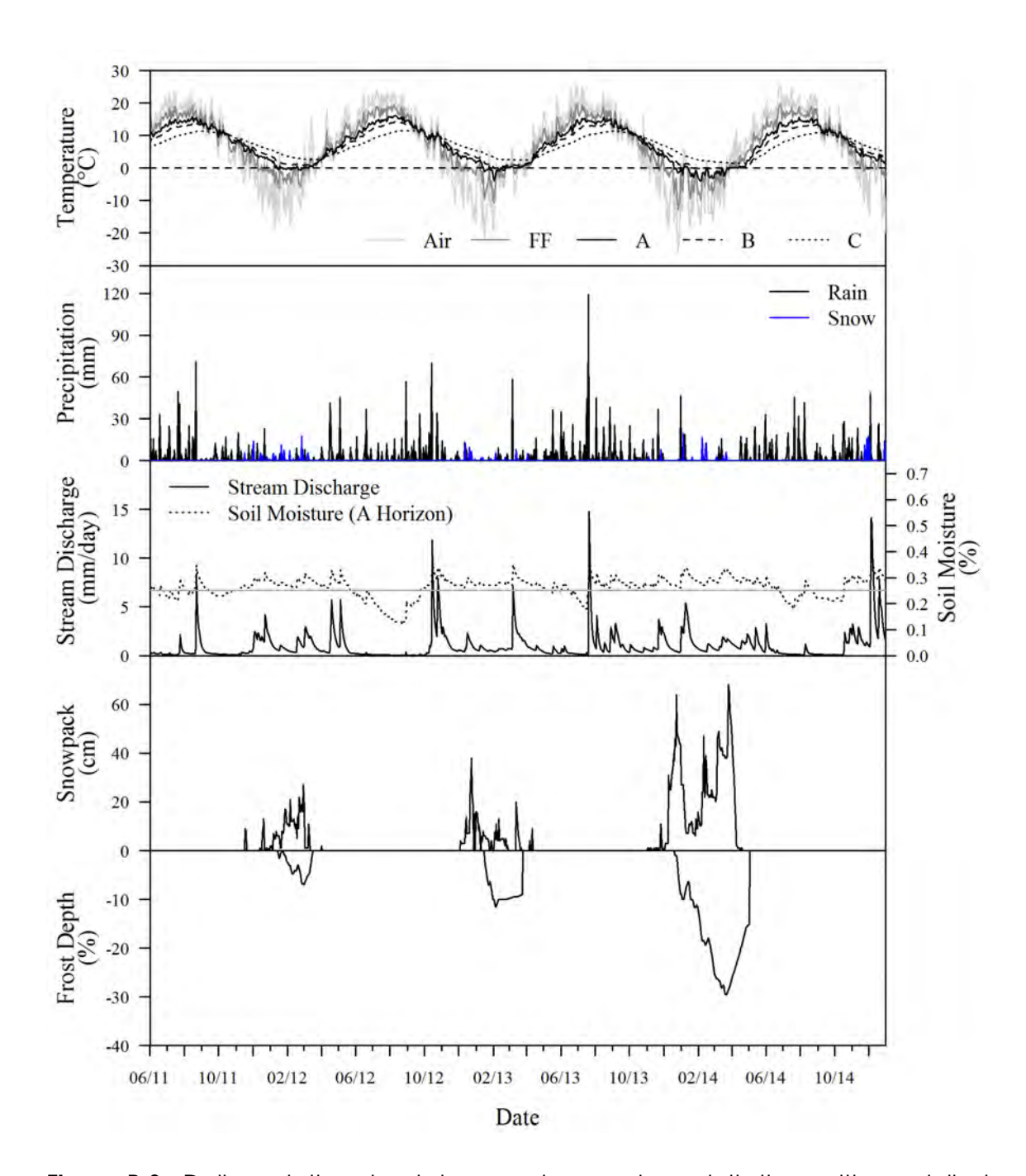


Figure B.8: Daily variations in air temperature and precipitation, with modelled stream discharge, volumetric soil moisture content including field capacities and snowpack depth, frost depth, and volumetric soil moisture content for the wider MWU+LL areas.

Appendix C

Chapter 4 Appendices

C.1 Publication Copyright Permission: Chapter 4

Tues, Feb 19, 2019 at 8:55 PM

Subject: Thesis Publication Permission

From: OJF Editorial Office < ojf@scirp.org>

To: "jones.mfn" < jones.mfn@gmail.com>

Dear Dr. Marie-France Jones,

Nice to hear from you. You can use this paper as a chapter. Please add a footnote or a reference in your thesis. I will publish your paper in March and provide DOI of this paper.

Please feel free to let me know if you have any question or need any assistance.

Best regards,

Ray WONG

Managing Editor

OJF Editorial Office

SKYPE: assistancewong@hotmail.com

QQ: 3384378078

C.2 Chapter 4 Appendices

Table C.1: Soil association, landform and lithology for blocks 1-11.

Landform	Lithology	Soil Association	Block # Associated
Colluvium and water re-worked till	Non-to weakly calcareous sandstone, shale, quartzite	Victoria	1, 2
	Metamorphosed non- to weakly- calcareous slate, quartzite, argillite, sandstone	McGee	4
Ablation till	Granite, quartzite, gneiss, argillite, volcanics and some sandstones	Juniper	8
	Metamorphosed rhyolite, andesite, schist, slate, granite	Jacquet River	6,7
Basal till	Mafic volcanics, gabbro, diorite	Kingston	11
	Metamorphosed rhyolite, andesite, schist, slate, granite	Popple Depot	10
	Strongly metamorphosed slate, quartzite, volcanics	Long Lake	9
Ablation/Basal till	Metamorphosed non- to weakly- calcareous slate, quartzite, argillite, sandstone	Glassville	3,5

Table C.2: Soil physical and moisture properties by block.

Bloc	ck (n)	Sand (%)	Silt (%)	Clay (%)	OM (%)	CF (%)	D _b (g/cm³)	PS (%)	MC _g (%)	MC _∨ (%)	MC _{ps} (%)	CI ¹ (MPa)
1 (56)	Min Max Mean SD	2.2 44.0 27.1 9.0	1.1 26.9 12.4 6.0	0.7 24.1 6.5 3.7	3.6 43.9 11.6 7.2	1.0 73.0 42.4 13.9	0.34 1.42 0.92 0.19	47 86 65 7	17.3 231.1 49.3 32.7	19.9 95.2 41.0 15.3	30.9 100.0 62.1 18.6	0.8 4.4 2.4 0.9
2 (28)	Min Max Mean SD	4.6 34.4 16.7 7.4	1.7 32.1 12.7 6.9	1.7 12.3 6.8 2.9	5.1 18.8 11.4 3.7	27.0 79.0 52.3 12.9	0.61 1.30 0.91 0.15	50 76 65 5	26.4 105.9 50.0 14.9	32.8 70.9 44.2 9.1	45.3 100.0 68.2 13.7	0.6 3.2 1.9 0.7
3 (80)	Min Max Mean SD	9.6 43.7 25.5 7.8	3.7 17.1 10.6 3.7	2.4 12.7 5.4 2.4	4.3 21.6 10.3 5.1	26.0 73.0 48.2 9.9	0.56 1.37 0.96 0.19	51 77 64 7	23.3 85.8 43.8 13.8	27.1 68.4 40.1 8.3	41.5 100.0 62.8 12.5	1.0 3.5 2.0 0.6
4 (46)	Min Max Mean SD	11.8 38.3 25.5 8.5	5.2 14.7 9.2 3.1	1.4 6.9 3.4 1.4	4.0 18.5 9.4 3.3	34.0 69.0 52.5 10.6	0.61 1.39 0.98 0.16	52 75 6 5	17.9 60.3 32.4 8.7	16.7 46.2 31.1 6.8	22.2 72.6 49.5 11.3	0.5 3.6 1.8 0.8
5 (33)	Min Max Mean SD	0.0 42.5 8.6 13.7	0.0 28.6 5.5 9.4	0.0 12.9 2.2 3.8	5.7 21.7 12.5 4.9	11.0 91.0 72.5 24.9	0.57 1.23 0.91 0.16	52 78 67 6	9.5 49.8 20.0 8.1	9.7 39.3 17.8 6.8	12.3 60.7 26.9 10.6	1.7 3.5 2.5 0.5
6 (26)	Min Max Mean SD	12.2 37.1 22.5 10.1	5.6 22.2 11.0 5.8	3.2 14.8 7.1 3.9	3.2 33.4 14.6 11.3	19.0 61.0 44.8 13.4	0.42 1.44 0.90 0.33	8 82 65 11	24.5 98.6 56.0 22.7	28.3 60.2 44.5 10.3	45.2 100.0 69.3 21.8	0.7 3.6 1.7 0.8
7 (43)	Min Max Mean SD	13.3 49.5 30.1 8.0	3.7 16.4 11.5 3.2	1.4 10.2 4.7 2.3	4.0 19.7 9.0 3.7	19.0 68.0 44.7 10.6	0.59 1.34 0.99 0.17	50 76 62 6	25.5 86.5 42.4 12.2	23.8 87.7 42.1 14.2	32.9 100.0 65.7 19.0	0.4 3.7 1.5 0.7
8 (54)	Min Max Mean SD	3.1 51.8 32.5 11.6	1.3 18.0 10.0 4.4	0.5 12.1 5.3 2.3	0.7 16.5 7.3 4.3	19.0 90.0 44.9 16.4	0.64 1.67 1.09 0.23	40 73 59 8	11.1 130.6 43.1 24.2	12.1 100.0 43.9 19.5	18.2 100.0 69.3 21.5	0.8 3.5 1.9 0.7
9 (24)	Min Max Mean SD	8.9 57.2 33.6 12.9	1.8 17.5 10.3 4.8	0.7 7.1 4.4 1.7	15.3 32.9 24.1 8.8	0.0 55.0 28.9 17.0	0.18 1.48 0.79 0.36	48 87 68 11	20.3 447.5 118.2 125.5	19.5 100.0 59.8 26.8	28.0 100.0 74.9 23.6	0.5 2.9 1.5 0.6
10 (147)	Min Max Mean SD	0.0 26.1 10.8 7.9	0.0 24.5 9.1 6.6	0.0 14.2 5.5 4.0	4.2 32.5 14.4 6.3	22.0 86.0 60.5 16.4	0.44 1.42 0.85 0.19	47 83 68 7	19.6 87.6 34.9 12.4	14.3 61.6 28.8 9.6	18.0 100.0 43.5 16.7	1.8 4.7 2.9 0.7
11 (159)	Min Max Mean SD	0.0 37.5 9.4 11.7	0.0 17.7 5.5 6.7	0.0 18.4 4.9 6.0	10.5 36.7 21.2 6.2	14.0 100.0 61.9 22.9	0.27 1.33 0.85 0.26	61 84 74 5	32.3 101.7 51.1 13.5	24.9 51.9 33.4 7.1	31.0 100.0 45.5 11.3	0.4 4.6 2.1 1.0

¹ Blocks 10 and 11 measured max CI per plot.

C.3 ForHyM Calibration Site Results

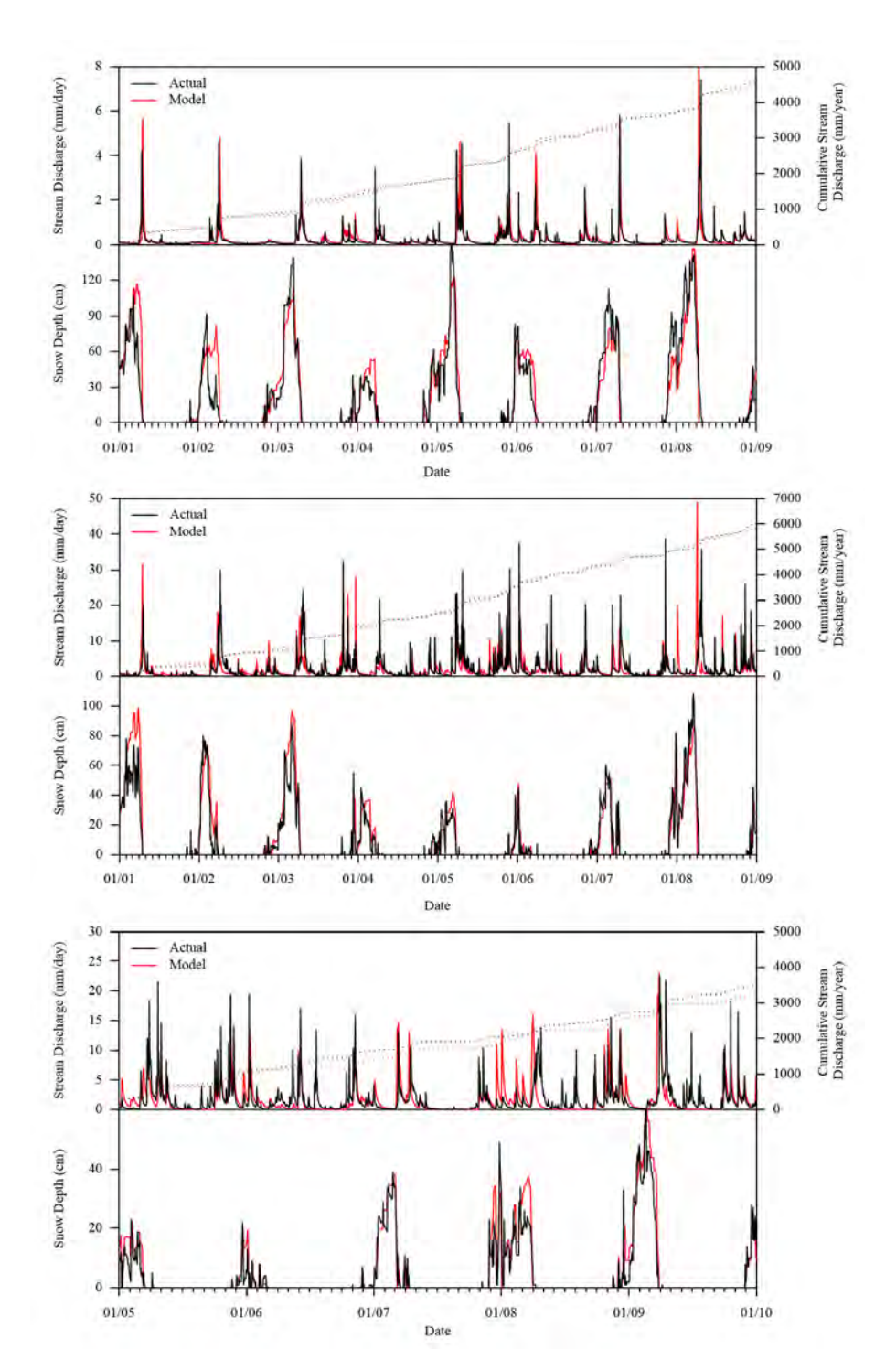


Figure C.1: Modelled vs measured ForHyM generated calibration outputs for snowpack and stream discharge for Northwestern Uplands (top), Midwestern Uplands (middle) and Lowlands (bottom).

Appendix D

Chapter 5 Appendices

D.1 Publication Copyright Permission: Chapter 5

Tue, August 4, 2019 at 7:40 AM

Subject: Thisesis Publication Permission

ojss@scirp.org <ojss@scirp.org>

To: "jones.mfn" < jones.mfn@gmail.com>

Cc: customer < customer@scirp.org >

Dear Dr. Marie-France Jones

Nice to hear from you.

Yes, you can use this paper in your thesis. But you should add a reference in it. After your paper is published, you can find the part of "How to cite" on our website.

Please feel free to let me know if you have any question or need any assistance.

Best Wishes

Ray WONG

Managing Editor of OJF Editorial Office

https://www.scirp.org/journal/ojf/

D.2 Rut Depth Severity Classes

Table D.1: Rut depth severity classes.

Description Photo Example Minimal ruts (0-5 cm): Minor surface abrasions, slight forest floor disturbance, little visible soil damage / root scuffing Shallow ruts (5-10 cm): Visible ruts, potential water retention, minimal effects on root and soil productivity Moderate ruts (10-20 cm): Visible soil disturbance, potential water retention, mineral soil exposed Deep ruts (20-40 cm ruts): Damage to roots, generally thick organic layers, exposed mineral soil Extreme ruts (40+ cm): Generally found in wet areas, high organic matter, machine loading zones

D.3 Temporal Soil Moisture Modelling

The Forest Hydrology Model (ForHyM) uses daily temperature and precipitation (rain and snow) data as well as block-specific area, vegetation, soil horizon texture, depth, OM, and CF (**Table D.2**) to predict soil moisture and temperature fluctuations through the soil (Arp and Yin, 1992; Yin and Arp, 1994; Jutras, 2012). Calibrating ForHyM consists of comparing actual snowpack and hydraulic flow to modelled outputs and adjusting the output parameters (**Table D.3**, **Figure D.1**).

Table D.2: ForHyM soil profile information used to initialize each stands.

Stand	Vegetation	Layer	Depth	Texture	OM (%)	CF (%)
1	INHW,	LFH	5	Organic	100	0
	deep	Α	25	SL	15	20
	rooted	В	50	SL	5	20
		С	100	SL	1	35
2	SW,	LFH	10	Organic	100	0
	shallow	Α	10	LS	2	20
	rooted	В	75	LS	10	24
		С	100	SL	1	35
3	SW,	LFH	10	Organic	100	0
	shallow	Α	10	LS	2	20
	rooted	В	75	LS	10	24
		С	100	SL	1	35
9	TOHW,	LFH	5	Organic	100	0
	deep	Α	55	LS	8	20
	rooted	В	55	LS	5	20
		С	150	SL	1	25

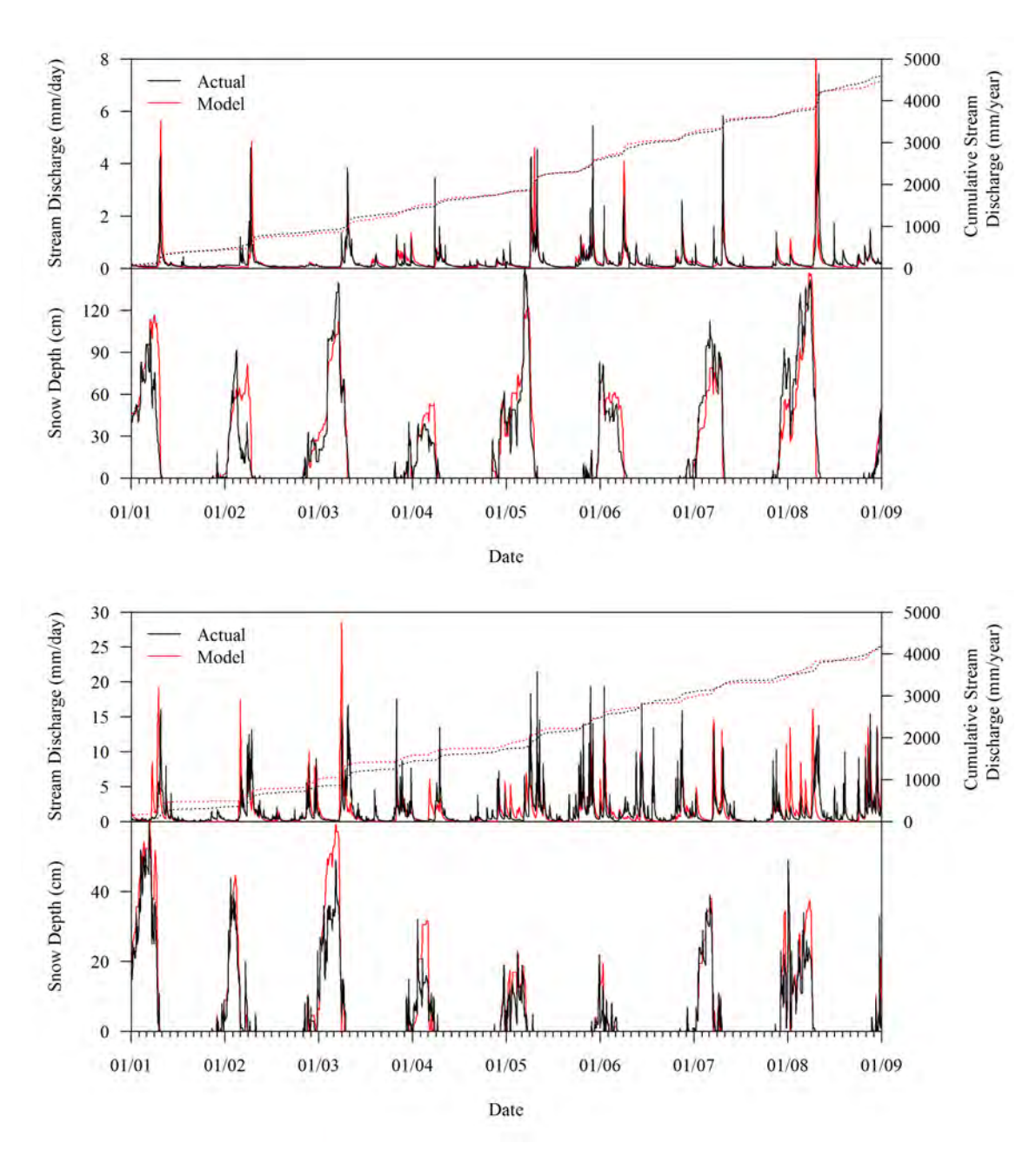


Figure D.1: Modelled vs measured ForHyM generated calibration outputs for snowpack and stream discharge for stands 1-3 (top), stand 4 (bottom).

Table D.3: ForHyM calibration variables for snowpack and saturated soil permeability.

	1-3	9	
Snowpack	Snow-to-air temperature gradient	0.16	0.2
	Density of fresh snow	0.16	0.2
Saturated	Surface runoff	1	1
Soil Permeability	Forest floor infiltration	1	1
	Forest floor interflow	0.01	0.01
	A&B horizon infiltration	1	1
	A&B horizon interflow	0.05	0.01
	C horizon infiltration	1	1
	C horizon interflow	0.1	0.1
	Deep water percolation	1	1

Vita

Candidate's Full Name:

Marie-France Noëlla (Jutras) Jones

Place and Date of Birth:

Cold Lake, Alberta; January 20th, 1986

Universities Attended:

University of New Brunswick, 2013-2019 Doctorate of Philosophy in Forestry

University of New Brunswick, June 2015 Diploma in University Teaching

University of New Brunswick, 2009-2012 Masters of Science in Forestry

University of Bangor, Wales, UK, 2006 Bachelor of Science in Forestry and Environmental Management (Study Abroad)

University of New Brunswick, 2004-2009 Bachelor of Science in Forestry and Environmental Management

Publications:

Jones, M.-F., Arp, P. 2019. Soil Trafficability Forecasting. *Open Journal of Forestry*. Approved for publication.

Jones, M.-F., Arp, P. 2019. Analyzing and Projecting Soil Moisture and Cone Penetrability Variations in Forest Soils. *Open Journal of Forestry*. 9:109-142.

Jones, M.-F., Castonguay, M., Jaeger, D., Arp, P. 2018. Track-monitoring and analyzing machine clearances during wood forwarding. *Open Journal of Forestry*. 8:1-25.

- **Jones, M.-F.**, Arp, P. 2017. Relating the cone penetration and rutting resistance to variations in forest soil properties and daily moisture fluctuations. *Open Journal of Soil Science*. 7(7):149-171.
- Nasr, M., **Jutras, M.-F.**, Arp, P. 2016. Mercury in Forest Soils and Vegetation, Including Mosses and Mushrooms A Case Study. Canadian Mercury Science Assessment, Summary of Key Results. Environment and Climate Change Canada. Pp 112-134.
- **Jones, M.-F.**, Castonguay M., Nasr, M., Ogilvie J., Bhatti J. S., Arp, P. 2014. Modeling and mapping hydrothermal regimes and potential impacts of climate change on permafrost within the South Mackenzie Plain, Northwest Territories, Canada. *Ecoscience*. 21 (1): 114.
- **Jutras, M.-F.**, Arp, P. 2013. Role of Hydraulic Conductivity Uncertainties in Modeling Water Flow through Forest Watersheds, Hydraulic Conductivity, Dr. Vanderlei Rodrigues Da Silva (Ed.), ISBN: 978-953-51-1208-2, InTech.
- **Jutras, M.-F.**, Arp, P. 2011. Determination of hydraulic conductivity from soil characteristics and its application for modelling stream discharge in forest catchment. Hydraulic Conductivity Book 1. Lakshmanan Elango (Ed.), ISBN: 978-953-307-288-3, InTech.
- **Jutras, M.-F.**, Nasr, M., Castonguay, M., Pit, C., Pomeroy, J., Smith, T.P., Zhang, C.-F., Ritchie, C.D., Meng, F.-R., Clair, T.A., Arp, P.A. 2011. Dissolved organic carbon concentrations and fluxes in forest catchments and streams: DOC-3 model. *Ecological Modelling*. 222(14):2291-2313 DOI: 10.1016 /j.ecolmodel.2011.03.035
- Bergeron M., Lacombe S., Bradley R., Whalen J., Cogliastro A., **Jutras M.-F.**, Arp P.A. 2011. Reduced soil nutrient leaching following the establishment of tree-based intercropping systems in eastern Canada. *Agroforestry Systems*. 83:321-330. DOI: 10.1007/s10457-011-9402-7

Honours and Awards:

- 2017 Canadian Forest Management Group Achievement Award by the Canadian Institute of Forestry.
- 2016 Esri Young Scholar Award. Translating weather records and forecasts into high-resolution soil trafficability maps.
- 2016 Esri Canada GIS Scholarship. Translating weather records and forecasts into high-resolution soil trafficability maps.

Conference Presentations:

Track-monitoring and quantifying ground clearance and machine speed during wood forwarding operations. UNB Graduate Research Conference. Fredericton, New Brunswick. March 23, 2018.

Translating weather records and soil moisture forecasts into high-resolution soil trafficability maps. ESRI Transforming Our World - User Conference. Fredericton, New Brunswick. October 25-26, 2016.

Mapping temporal and spatial soil hydrothermal and mechanical properties by way of the Soil Trafficability Prediction Model (STRAP). Soil Interfaces for sustainable development (ISMOM) Conference. Montreal, Quebec. July 5-10, 2015.

Mapping temporal and spatial soil hydrothermal and mechanical properties by way of the Soil Trafficability Prediction Model (STRAP). Science Atlantic Environment Conference. Halifax, Nova Scotia. March 13-14, 2015. Won first place for best graduate poster.

Modelling daily soil moisture changes by way of temporal hydrology modeling and spatial wet-areas-mapping. ESRI Transforming Our World - User Conference. Halifax, Nova Scotia. November 5-6, 2013.

Dissolved organic carbon concentrations and fluxes in forest catchments and streams: DOC-3 model. Paper presented at 65th Canadian Conference for Fisheries Research. Moncton, New Brunswick. 2012.

Dissolved organic carbon concentrations and fluxes in forest catchments and streams: DOC-3 model. Paper presented at the 10th International Conference on Mercury as a Global Pollutant. Halifax, Nova Scotia. 2011.

Calibrating hydraulic conductivity for modeling stream discharge in forest catchments of Eastern Canada, on varied bedrock formations. Poster presented at the Joint Aquaculture and Fisheries, Biology and Environmental Studies Conference. Halifax, Nova Scotia. Won second place graduate poster. 2011.